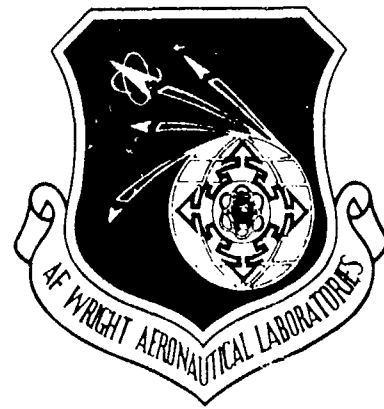AFWAL-TR-84-3080
VOLUME II

ADVANCED LIFE ANALYSIS

METHODS – Crack Growth

Analysis Methods for

Attachment Lugs

K. Kathiresan
T. M. Hsu

Lockheed-Georgia Company
Marietta, Georgia 30063

T. R. Brussat

Lockheed-California Company
Burbank, California 91520

September 1984

Flight Dynamics Laboratory
Air Force Wright Aeronautical Laboratories
Air Force Systems Command
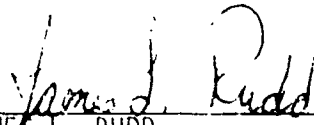Wright-Patterson Air Force Base, Ohio 45433
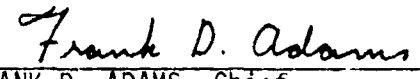
85   02   11   129

NOTICE

When Government drawings, specifications, or other data are used for any purpose other than in connection with a definitely related Government procurement operation, the United States Government thereby incurs no responsibility nor any obligation whatsoever; and the fact that the government may have formulated, furnished, or in any way supplied the said drawings, specifications, or other data, is not to be regarded by implication or otherwise as in any manner licensing the holder or any other person or corporation, or conveying any rights or permission to manufacture use, or sell any patented invention that may in any way be related thereto.
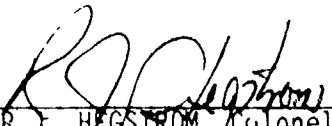
This report has been reviewed by the Office of Public Affairs (ASD/PA) and is releasable to the National Technical Information Service (NTIS). AT NTIS, it will be available to the general public, including foreig nations.

This technical report has been reviewed and is approved for publication.

JAMES L. RUDD
Project Engineer

FRANK D. ADAMS, Chief
Structural Integrity Branch
Structures & Dynamics Division

FOR THE COMMANDER

ROGER J. HEGSTROM, Colonel, USAF
Chief, Structures & Dynamics Division

"If your address has changed, if you wish to be removed from our mailing list, or if the addressee is no longer employed by your organization please notify AFWAL/FIBE, W-PAFB, OH 45433 to help us maintain a current mailing list".

Copies of this report should not be returned unless return is required by security considerations, contractual obligations, or notice on a specific document.

REPORT DOCUMENTATION PAGE

1a. REPORT SECURITY CLASSIFICATION	1b. RESTRICTIVE MARKINGS
Unclassified	

2a. SECURITY CLASSIFICATION AUTHORITY	3. DISTRIBUTION/AVAILABILITY OF REPORT
	Unclassified/Unlimited
2b. DECLASSIFICATION/DOWNGRADING SCHEDULE	

4. PERFORMING ORGANIZATION REPORT NUMBER(S)	5. MONITORING ORGANIZATION REPORT NUMBER(S)
LG82ER0117-II	AFWAL-TR-84-3080, Volume II

6a. NAME OF PERFORMING ORGANIZATION	6b. OFFICE SYMBOL (If applicable)	7a. NAME OF MONITORING ORGANIZATION
Lockheed-Georgia Company		Air Force Wright Aeronautical Laboratories (AFWAL/FIBEC)

6c. ADDRESS (City, State and ZIP Code)	7b. ADDRESS (City, State and ZIP Code)
86 South Cobb Drive Marietta, Georgia 30063	Wright-Patterson Air Force Base Ohio 45433

8a. NAME OF FUNDING/SPONSORING ORGANIZATION	8b. OFFICE SYMBOL (If applicable)	9. PROCUREMENT INSTRUMENT IDENTIFICATION NUMBER
AFWAL/FIBEC		F33615-80-C-3211

8c. ADDRESS (City, State and ZIP Code)	10. SOURCE OF FUNDING NOS.			
Wright-Patterson Air Force Base Ohio 45433	PROGRAM ELEMENT NO.	PROJECT NO.	TASK NO	WORK UNIT NO.

11. TITLE (Include Security Classification)				
See Reverse	62201F	2401	01	38

12. PERSONAL AUTHOR(S) Kathiresan, K., Hsu, T.M., Lockheed-Georgia Company, Marietta, Georgia Brussat, T.R., Lockheed-California Company, Burbank, California

13a. TYPE OF REPORT	13b. TIME COVERED	14. DATE OF REPORT (Yr., Mo., Day)	15. PAGE COUNT
Final Report	FROM Sept.80 TO Sept.84	84-9-17	189

16. SUPPLEMENTARY NOTATION

Cont'd

17.	COSATI CODES		18. SUBJECT TERMS (Continue on reverse if necessary and identify by block number)
FIELD	GROUP	SUB. GR.	Attachment Lugs, Cracking, Aircraft, Damage Tolerance,
1	3	1	Analysis Methods, Straight Lugs, Tapered Lugs, Stresses,
1	3	3	Stress Intensity Factors, Through-the-Thickness,

19. ABSTRACT (Continue on reverse if necessary and identify by block number)

Analysis procedures for the assessment of the damage tolerance of aircraft attachment lugs are developed and presented. Stress and fracture analyses are conducted for simple male straight shank lugs subjected to symmetric loading and tapered lugs subjected to symmetric and off-axis loadings. Solutions of stress distributions and stress intensity factors are obtained for various parameters. The parametric variations include lug outer-to-inner radius ratios (R_o/R_i), corner and through-the-thickness cracks, crack lengths and aspect ratios, with and without interference-fit bushing and loads above and below yield of the lugs. Methods of varying degree of sophistication are considered in the development of stress intensity factor solutions for cracks in attachment lugs. For through-the-thickness crack problems, simple compounding method, two-dimensional cracked finite element method, and the weight function method are used. In the case of corner cracks, solutions are obtained using simple compounding method,

20. DISTRIBUTION/AVAILABILITY OF ABSTRACT	21. ABSTRACT SECURITY CLASSIFICATION
UNCLASSIFIED/UNLIMITED ☒ SAME AS RPT. ☐ DTIC USERS ☐	Unclassified

22a. NAME OF RESPONSIBLE INDIVIDUAL	22b. TELEPHONE NUMBER (Include Area Code)	22c. OFFICE SYMBOL
J.L. Rudd	(513) 255-6104	AFWAL/FIBEC

DD FORM 1473, 83 APR EDITION OF 1 JAN 73 IS OBSOLETE.

11. T TLE

ADVANCED LIFE ANALYSIS METHODS - Crack Growth Analysis Methods for Attachment
Lugs (Unclassified)

18. Keywords
(Continued)

Corner, Interference-Fit Bushing, Elasto-Plastic Analysis, Crack Growth Analysis.

19. Abstract
(Continued)

weight function method and a rigorous three-dimensional hybrid displacement
cracked finite element method. The stress distributions and the stress intensity
factors are consolidated into a crack growth analysis procedure including several
crack growth models and spectrum retardation models to predict the fracture and
crack growth behaviors in attachment lugs. Originator furnished
Keywords include:

FOREWORD

This is Volume II of six final report volumes on Conrract F33615-80-C-3211, "Advanced Life Analysis Methods." The work reported herein was conducted jointly by Lockheed-Georgia Company and Lockheed-California Company under contract with Air Force Wright Aeronautical Laboratories, Wright-Patterson AFB. J. L. Rudd is the Air Force project leader.

TABLE OF CONTENTS

TABLE OF CONTENTS

(CONT'D.)

LIST OF FIGURES

LIST OF TABLES

SECTION I

PROGRAM SUMMARY

The objective of the program is to develop the design criteria and analytical methods necessary to ensure the damage tolerance of aircraft attachment lugs. As planned, the program proceeds logically from an extensive cracking data survey and nondestructive inspection (NDI) assessment, through method development and evaluation, to the preparation of damage tolerance design criteria for aircraft attachment lugs.

The program consists of three phases involving seven tasks. Phase I consists of Tasks I, II and III; Phase II consists of Tasks IV, V and VI; and Phase III consists of Task VII. A roadmap shown in Figure 1-1 summarizes the major activities by task, decision points and their interrelationships.

Task I involves a survey of structural cracking data such as the initial flaw size, shape and location which occur in aircraft attachment lugs. Sources for these data include open literature, available Lockheed data, and visits to the five Air Force Air Logistics Centers (ALCs). The types of aircraft structure used to obtain these data include service aircraft, full-scale test articles, component test articles, and coupon specimens.

Task II assesses the current NDI capability to find these flaws or cracks. This assessment is to be based upon information obtained from the open literature, available Lockheed NDI data and experience, and Air Force ALC data. The NDI techniques capable of finding flaws in attachment lugs and the flaw sizes these techniques are capable of finding are identified. Where possible, the probability of detecting a flaw of a particular size for the NDI technique involved is specified as well as the confidence level assigned to that probability. The results obtained from Tasks I and II will be used in the formulation of the initial flaw assumptions to be developed in Task VII as part of the damage tolerant design criteria for attachment lugs.

Task III involves three different levels of complexity and degrees of sophistication for determining stress intensity factors for single corner cracks and single through-the-thickness cracks in aircraft attachment lugs, and the development of crack growth analysis capable of
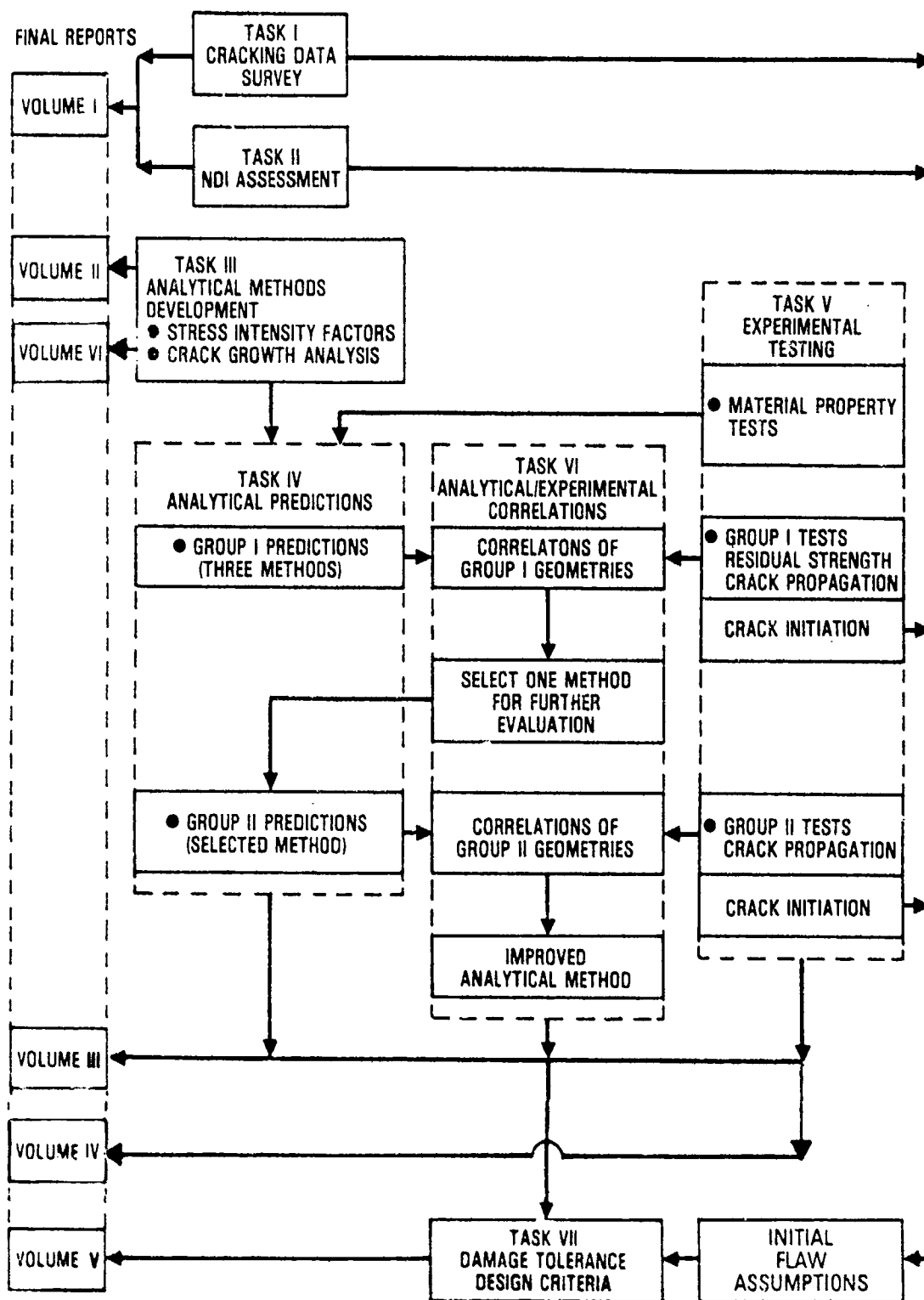
Figure 1-1. Roadmap of the Program

predicting the growth behavior of these cracks and residual strength of these lugs. These stress intensity factors and crack growth analyses are used in Task IV to predict the residual strength and the crack growth behavior for a number of different geometries and test conditions defined in the experimental program. These predictions are made prior to testing. Two groups of attachment lug geometries are tested and experimental test data are generated in Task V. The analytical methods developed in Task III are evaluated by correlating the analytical predictions made in Task IV with the Group I experimental test data (based upon accuracy and cost) for use in prediction of Group II tests. Further evaluation of the selected method is made by correlating the analytical predictions for the Group II tests (Task IV) with the experimental test results (Task V). These correlations indicate what improvements are necessary for the selected analytical method. The results are presented in parametric format useful to designers and analysts. Damage tolerant design criteria for aircraft attachment lugs are developed in Task VII. These criteria are similar in nature to those of Military Specification MIL-A-83444, and require crack growth analyses by the types of methods developed and verified in Tasks III through VI. The criteria include initial flaw assumptions (e.g., initial flaw type, shape, size, etc.) based upon the cracking data survey of Task I, NDI assessment of Task II, and crack initiation tests of Task V.

As Figure 1-1 shows, the following sequence of final report volumes is generated under this project:

Volume I. Cracking Data Survey and NDI Assessment for Attachment Lugs

Volume II. Crack Growth Analysis Methods for Attachment Lugs

Volume III. Experimental Evaluation of Crack Growth Analysis Methods for Attachment Lugs

Volume IV. Tabulated Test Data for Attachment Lugs

Volume V. Executive Summary and Damage Tolerance Criteria Recommendations for Attachment Lugs

Volume VI. User's Manual for "LUGRO" Computer Program to Predict Crack Growth in Attachment Lugs

This is Volume II on Crack Growth Analysis Methods for Attachment Lugs, which is the result of Task III efforts. It contains the developed analytical methodologies for determining the stress intensity factors for single corner cracks and single through-the-thickness cracks in aircraft attachment lugs, and for predicting the growth behavior of these cracks.

SECTION II

INTRODUCTION

In aircraft structures, lug-type joints are frequently used to connect major structural components or in linkage structure. The lug joint is normally connected by a single bolt or pin, creating a simple joint that is easy to assemble and disassemble. Since clamping of the joint is not normally allowed, the lug can act as a pivot. But the elastic gross section stress concentration for normal lugs is very high, resulting in a relatively short crack initiation and crack growth life. To improve the crack initiation life, the stress concentration factor can be effectively reduced by cold working the hole or by installing an interference-fit bushing prior to pin fitting. To minimize the wear in either the lug or the pin, most aircraft lugs have an oil fitting and/or lubrication provisions.

During the past decade, the influence of fracture mechanics on the design, manufacture, and maintenance of aircraft has steadily increased. Also, nondestructive inspection techniques have been improved significantly. However, some cracks still cannot be detected during routine maintenance inspection. Under service loading, such cracks will grow and fracture can occur if the crack length reaches a critical dimension before it can be detected and the part repaired or replaced. To assure aircraft safety, the U. S. Air Force has imposed damage-tolerance requirements (MIL-A-83444)[1] which include the prediction of fatigue crack growth life and residual strength of the structure by assuming that small initial flaws exist at critical locations of new structure due to various material and manufacturing and process operations. Assumptions regarding the initial size, shape, location, multiplicity, etc. for these flaws are specified in MIL-A-83444. However, these assumptions were established primarily for skin-stringer structure and may not be applicable for attachment lugs.

Attachment lugs are some of the most fracture critical components in aircraft structure, and the consequences of a structural lug failure can be very severe. Therefore, it is necessary to develop damage tolerance design requirements, similar to MIL-A-83444, for attachment lugs to ensure the safety of aircraft. The development of these damage tolerance requirements will be based upon actual cracking data for attachment lugs and current

nondestructive inspection capability. Once the damage tolerance design requirements for aircraft attachment lugs are established, the analytical methods necessary to satisfy the crack growth and residual strength requirements are needed. In particular, stress intensity factors for cracks in attachment lugs are needed. Such stress intensity factors will depend upon the complexities of structural configuration, crack geometry, applied loads, and the fit between the pin and the lug.

There are a number of different methods for determining the stress intensity factors, K, for cracks in aircraft attachment lugs. Schijve and Hoeymakers [2] and Wanhill [3] derived empirical K-solutions from the growth rate data for through cracks under constant amplitude loading using a back-tracking method such as that proposed by James and Anderson [4]. Analytically, Liu and Kan [5] and Kirkby and Rooke [6] used the simple compounded solution method which involves superimposing known solutions, such as in Reference [7] to estimate the stress intensity factors. Aberson and Anderson [8] used a special crack-tip singularity element to compute the stress intensity factors for a crack in a nonsymmetrical aft lug of an engine pylon. Pian et al [9] used the hybrid finite element method to compute the K-values for cracks oriented in various angles from the axial direction of straight lugs. Impellizzeri and Rich [10] modified the exact weight function derived by Bueckner [11], for an edge crack in a semi-infinite plate, to include a series of geometry correction factors. Then they computed the K-values using the weight function method. Except for Reference [8], all of these works made the assumption that the assumed or computed pin-bearing pressure distribution for an uncracked case remains unchanged even after the crack has initiated and propagated. Based on the parametric study conducted in Reference [9], it was found that, for any given crack length, the difference in the stress intensity factor computed using the uniform and cosine pin-bearing pressure distributions was as much as 30 percent. Therefore, it is salient that the correct representation of the pin-bearing pressure distribution during the crack growth process is essential to the calculation of accurate stress intensity factors. An analysis procedure using a finite element method with inclusion of a crack-tip singularity element for analyzing cracks in both straight and tapered lugs having a neat fit between the pin and the hole [12] has shown that it can accurately account for the change of pin-bearing pressure distribution with the change in crack length, and provide stress intensity factors which are in excellent agreement with the available data.

6

This approach was extended for the development of analytical methodology for analyzing cracks in attachment lugs with and without the presence of residual stress resulting from the installation of the interference-fit bushing [13]. The analytical procedure developed for computing the stress intensity factors for cracks in attachment lugs having residual stresses around the hole prior to the application of pin-bearing loads consists of two major steps. First, the effective unflawed stress distribution on the prospective crack surface was obtained by superimposing the residual hoop stresses due to the installation of an interference-fit bushing on the applied tangential stresses obtained due to the application of a pin loading. Second, a through crack was introduced in this stress field by removing the tractions on the crack faces and computing the corresponding stress intensity factor using the weight function approach.

This report describes the analytical methods and procedures for obtaining the stress intensity factors and for predicting the fatigue crack growth life for cracks at attachment lugs with and without the presence of residual stresses. Two types of attachment lugs are considered in the analysis. They are: (1) straight-shank male attachment lugs and (2) tapered male attachment lugs as shown in Figure 2-1. Three different outer-to-inner radius ratios, $R_o/R_i = 1.50$, 2.25 and 3.0, are considered in the analysis. The straight attachment lugs are subjected to axial pin loading only, while the tapered attachment lugs are subjected to axial, off-axis and transverse pin loadings. Types of cracks considered include single through-the-thickness crack and single corner crack as depicted in Figure 2-2.

For through-the-thickness cracks, the methods developed and described in this report include: (1) the compounding solution method which involves the superposition of known solutions for idealized cracked geometries; (2) the two-dimensional cracked finite element method which is capable of characterizing the crack-tip stress singularity internally; and (3) the weight function (also known as Green's function) method which computes the stress intensity factors from the knowledge of the unflawed stress distribution and the superposition technique. For corner cracks, the methods developed and described include: (1) the one parameter compounding method which assumes a constant crack shape and estimates the stress intensity factor at only one location on the crack front (at lug surface); (2) a two-dimensional approach which estimates the stress intensity factors along the crack front
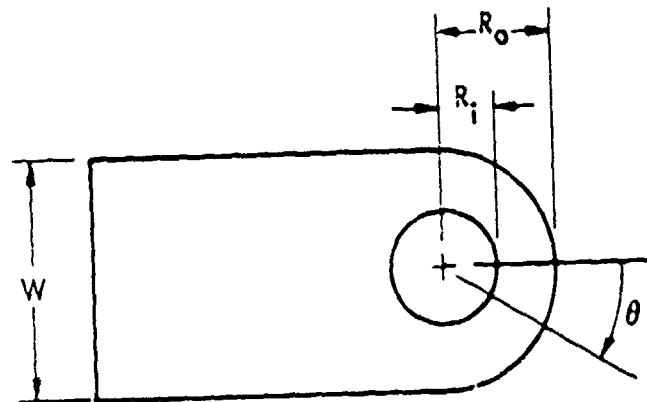
(a) STRAIGHT ATTACHMENT LUG
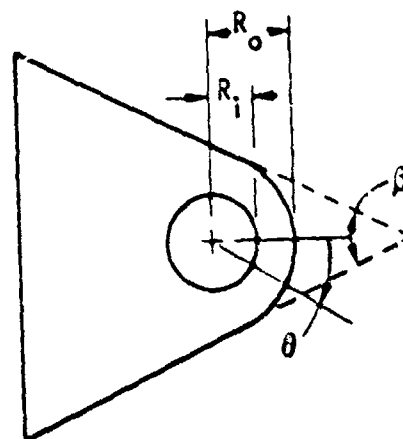
(b) TAPERED ATTACHMENT LUG

Figure 2-1. Types of Attachment Lugs
Considered in the Analysis
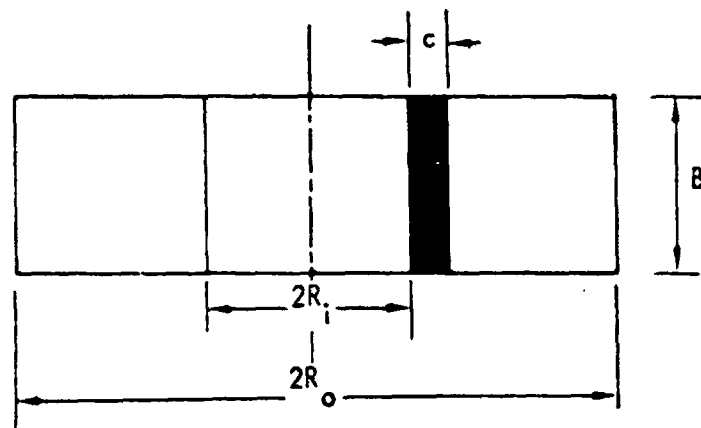
(a) SINGLE THROUGH CRACK
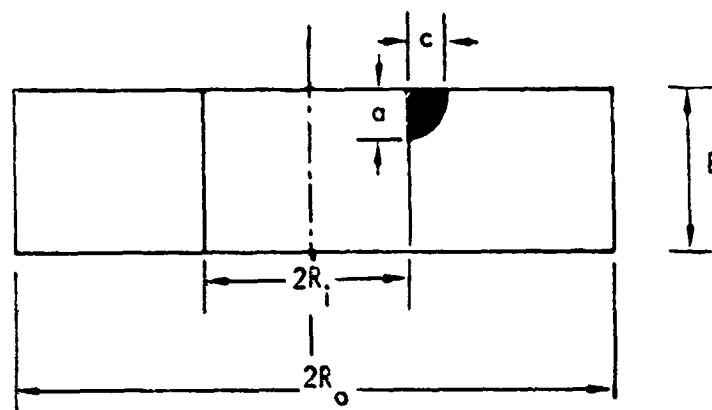
(b) SINGLE CORNER CRACK

Figure 2-2. Types of Cracks Considered
in the Attachment Lug Analysis

9

of a corner crack by modifying the Green's function for through-the-thickness crack solutions with appropriate hole curvature, flaw shape, front free surface and back surface correction factors; (3) the rigorous three-dimensional cracked finite element method, which was developed using a hybrid displacement finite element procedure.

After the stress intensity factor is determined as a function of crack length for a particular lug and loading condition, its range (ΔK) can be computed for the Nth cycle in a given load spectrum. Then a numerical integration of da/dN versus ΔK relation can be carried out to predict the crack growth characteristics. An automated computer program was developed utilizing the state-of-the-art fracture mechanics methodologies for the prediction of fatigue crack growth history under fatigue loading. The program is capable of predicting the crack growth behavior of single corner cracks and single through-the-thickness cracks in attachment lugs using block-by-block integration technique. In the case of corner crack problems, a transitional crack growth criterion from part-through crack to through-the-thickness crack was also developed and incorporated. Several load-interaction models were also included in the crack growth analysis program for spectrum loadings.

The prediction methods presented in this volume of the report are to be evaluated against fatigue crack growth test results. The test program consists of two parts. Group I tests consist of straight-shank male attachment lugs. Both constant amplitude and block spectrum loadings are considered in this group. Variational tests, such as different thickness and with residual stresses due to interference-fit bushings, are also included in Group I testing. Group II tests, performed later, encompass several additional lug configurations (tapered, dogbone, clevis and a simulated wing-pylon attach lug) and include both axial and off-axis loadings.

The stress intensity factor formulations prepared for Group I straight-shank male attachment lugs are described in Section III. A draft of Section III was completed prior to Group I testing. After Group I testing, these formulations are evaluated. Based on this evaluation, a stress intensity factor estimation methodology is selected for Group II testing. Section IV describes such a selected methodology for tapered attachment lugs. The crack growth prediction method which employs these stress intensity factor solutions is presented in Section V.

10

SECTION III

STRESS INTENSITY FACTORS FOR STRAIGHT ATTACHMENT LUGS

In this section, the analytical methodologies required for the development of stress intensity factors for cracks in simple straight-shank male attachment lugs are described. The stress intensity factor solutions are obtained for single through-the-thickness cracks and single quarter-elliptical corner cracks in attachment lugs. As mentioned previously, the following methods are used for through-the-thickness and corner cracks.

For through-the-thickness crack problems:

    (1)   Simple compounding method

    (2)   Two-dimensional cracked finite element procedure

    (3)   Weight function or Green's function method

For corner crack problems:

    (1)   Simple one parameter compounding method

    (2)   Two-dimensional Green's function solution modification

    (3)   Rigorous three-dimensional cracked finite element procedure

This section also describes the method for developing the stress intensity factor for problems with residual stresses (due to the installation of interference-fit bushings). A stress analysis of unflawed straight attachment lugs was also performed and is presented here. Note that all the specimens tested in the Group I test program are straight attachment lugs and the methodologies described in this section are evaluated using Group I test results.

1. STRESSES IN AN UNFLAWED STRAIGHT ATTACHMENT LUG

A primary item of interest in the analysis of cracked attachment lugs is the stress distribution in the uncracked state. This is important for at least three reasons. The location of the peak tangential stress determines the location of the most critical crack. The stress intensity factor for a very small crack is proportional to the stress concentration factor value. Finally, the weight function method of estimating stress intensity factors requires the stresses on the prospective crack surface in the uncracked lug.

11

The conventional displacement finite element method was used to obtain, for an uncracked straight lug, (1) the tangential stresses along the edge of the hole, (2) the stress distribution on the prospective crack surface, and (3) the pin-bearing pressure distribution along the contact surface between the pin and the lug. The rigidity ratio, E_{pin}/E_{lug}, is assumed to be 3.0 in the present analysis.

Figure 3-1 shows a typical model used in the analysis. Due to symmetry, only the upper half of the lug was modeled. The lug and the pin were represented by a set of constant-strain triangular and quadrilateral elements. To load the model, a concentrated force was applied at the center of the pin and reacted at the other end of the lug. Spring elements (S) were used to connect the pin and lug at each pair of nodes having identical nodal coordinates all around the periphery. The area of contact was determined iteratively by assigning a very high stiffness to spring elements which were in compression and a very low stiffness (essentially zero) to spring elements which were in tension. A neat-fit and no friction assumptions were made for the pin-to-lug assembly.

The calculated tangential stresses (normalized by the average bearing stress) along the edge of the hole for a pin loading applied in the $0°$ direction are shown in Figure 3-2 for R_o/R_i ratios of 1.50, 2.25 and 3.00. As anticipated, the maximum tangential stresses are located at about $90°$ away from the axis of the lug, and the minimum stresses (small amount in compression) are located at the $180°$ location.

The tangential stresses for pin loading applied in axial compression ($\theta = 180°$) are shown in Figure 3-3. As can be seen from this figure, the resulting stresses at $\theta = \pm 90°$ are small tensile stresses. Thus, reversing the loading direction does not cause a stress reversal at the critical $90°$ location. Furthermore, the tensile stresses produced are relatively small.

The unflawed elastic stress distributions on the prospective crack plane for axial tension applied in the $0°$ direction are presented in Figure 3-4. These values are also tabulated in Table 3-1. The tangential stresses along the x-axis shown in the figure are normalized by the average bearing stress. It is clear that the gradient of the stress distribution close to the edge of the hole is very steep, especially for a lug having a smaller R_o/R_i ratio. The corresponding elastic stress concentration factors at the edge of the hole, σ_{max}/σ_{br}, are plotted in Figure 3-5. The equation of the
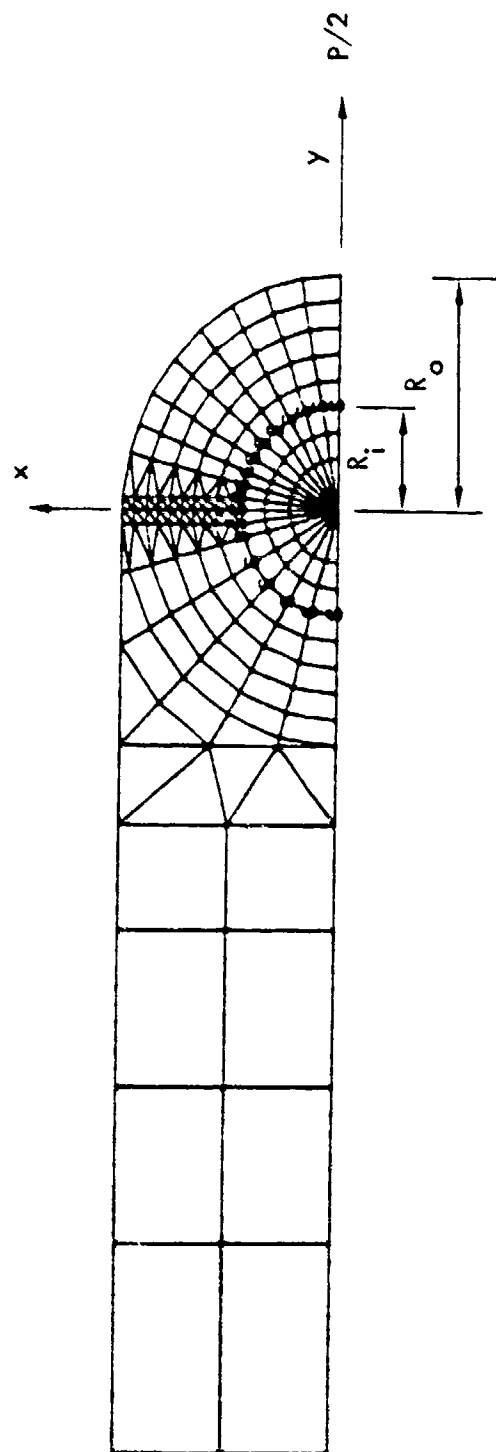
Figure 3-1. Typical Finite Element Model for Unflawed Stress Analysis
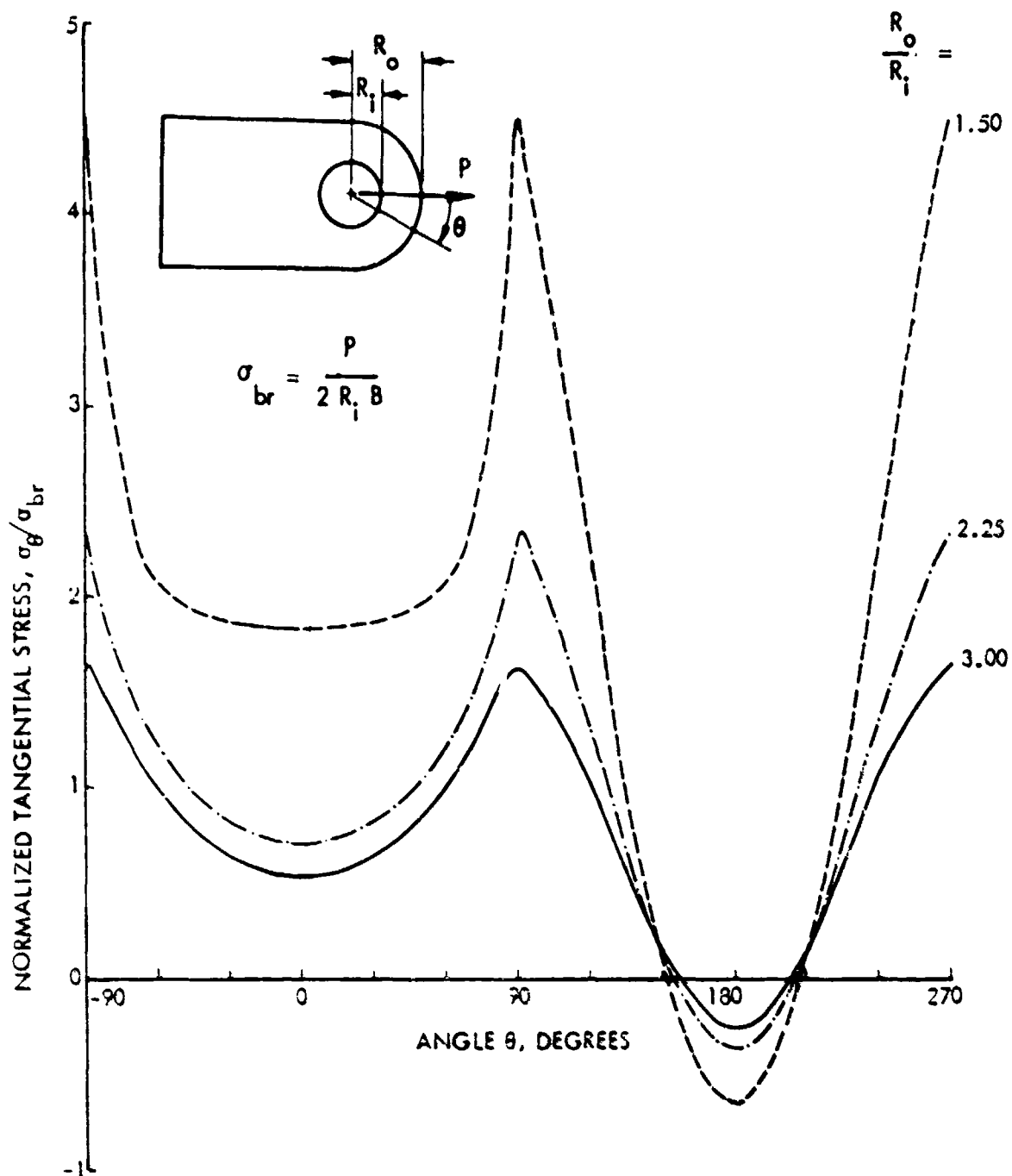
Figure 3-2. Tangential Stress Along the Edge of the Hole
for a Pin Loading Applied in $0°$ Direction
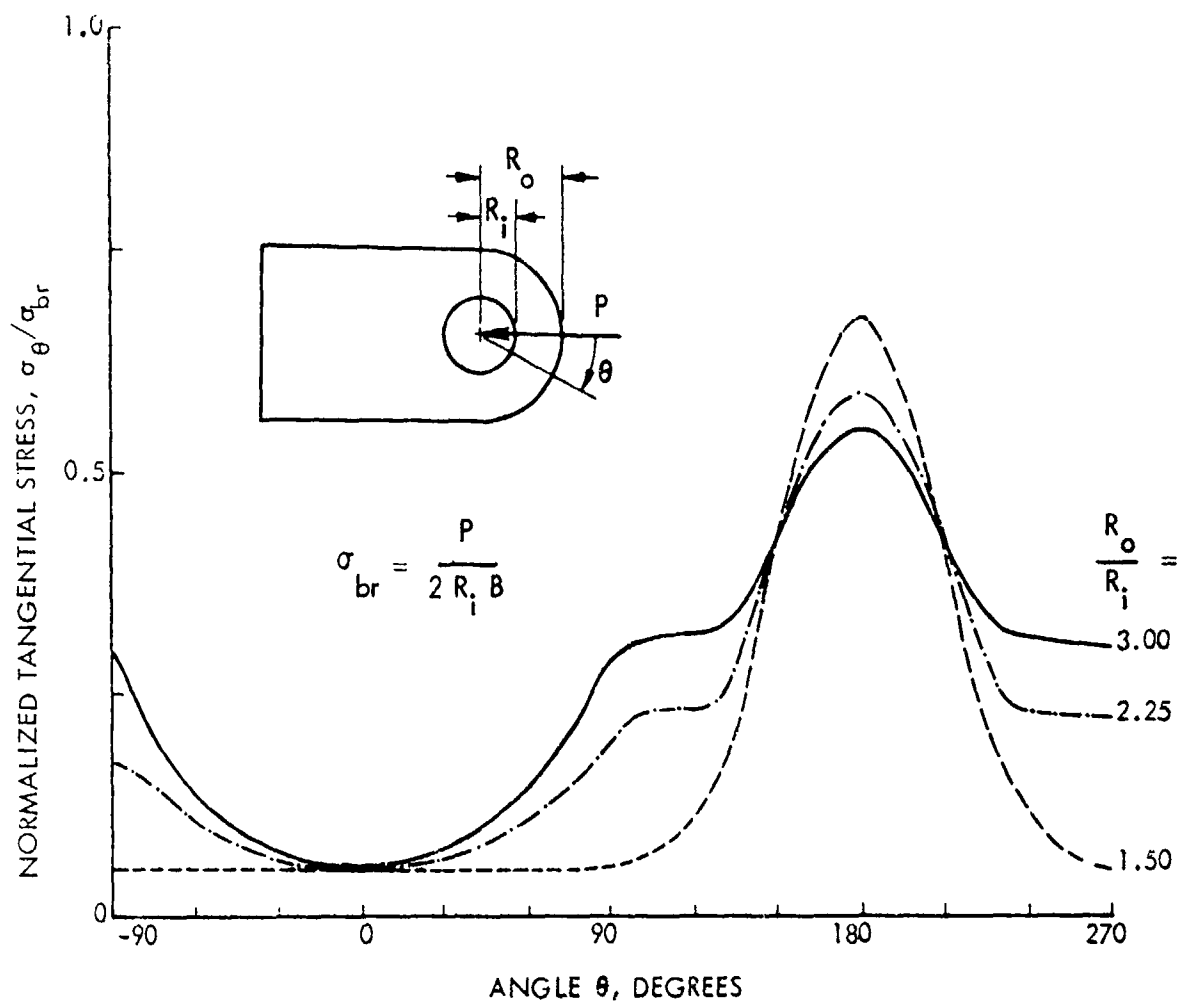
Figure 3-3. Tangential Stress Along the Edge of the Hole for a Pin Loading Applied in 180° Direction
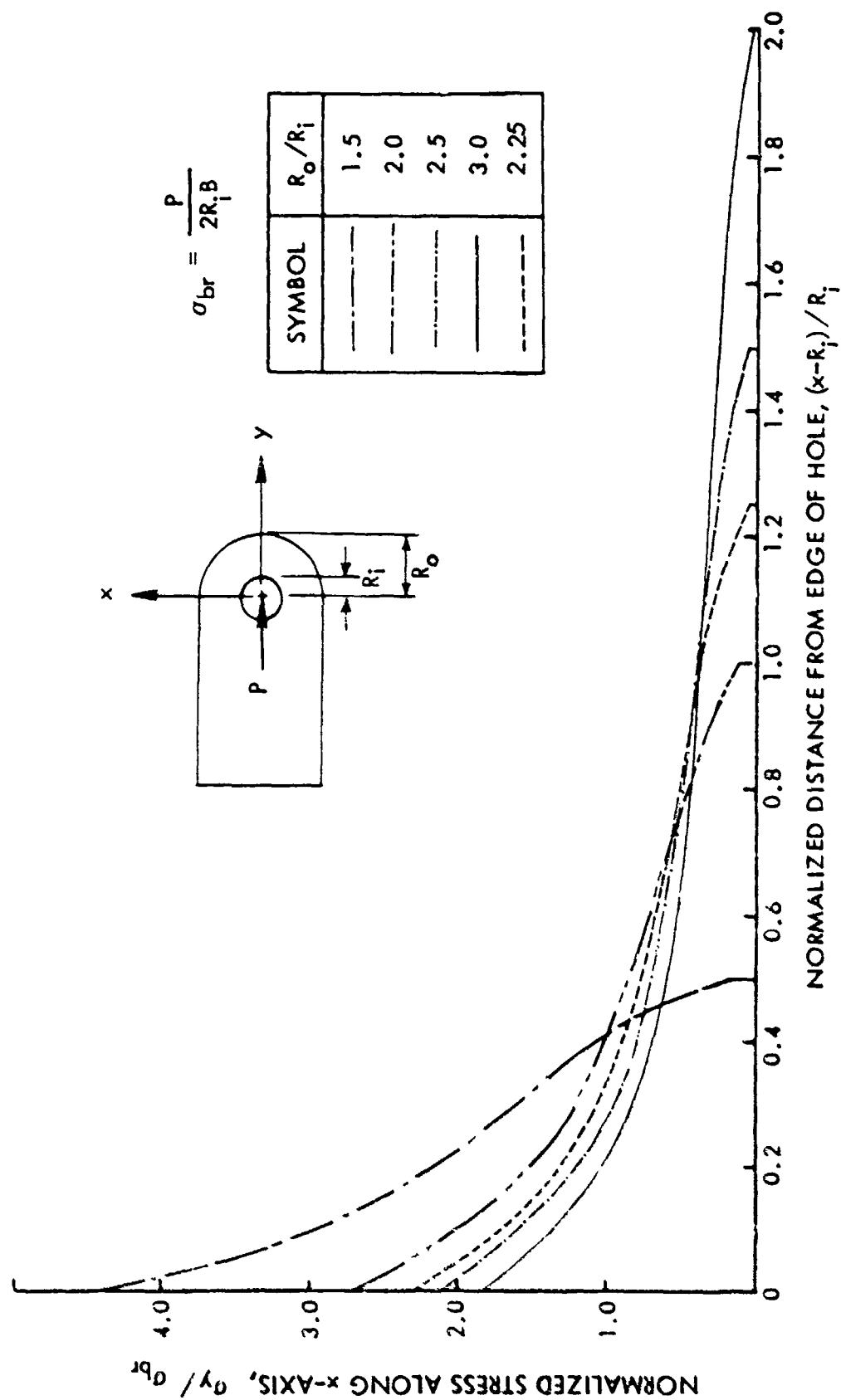
Figure 3-4. Unflawed Stress Distributions Along x-Axis for Straight Attachment Lugs Having Various R_o/R_i Ratios

TABLE 3-1. NORMALIZED UNFLAWED STRESS DISTRIBUTION ALONG x-AXIS FOR STRAIGHT ATTACHMENT LUGS

$\frac{x-R_i}{R_o-R_i}$ \ K_o/K_i	σ_y/σ_{br}					σ_y/σ_o				
	1.50	2.00	2.25	2.50	3.00	1.50	2.00	2.25	2.50	3.00
0.00*	4.389	2.737	2.364	2.100	1.715	6.584	5.474	5.319	5.250	5.145
0.05	3.903	2.313	1.884	1.739	1.367	5.855	4.626	4.239	4.348	4.101
0.15	3.219	1.728	1.375	1.167	0.878	4.829	3.456	3.094	2.918	2.634
0.25	2.677	1.333	1.044	0.842	0.618	4.016	2.666	2.349	2.105	1.854
0.35	2.319	1.105	0.862	0.692	0.499	3.479	2.210	1.940	1.730	1.497
0.45	1.990	0.925	0.723	0.578	0.416	2.985	1.850	1.627	1.445	1.248
0.55	1.736	0.788	0.620	0.493	0.355	2.604	1.576	1.395	1.233	1.065
0.65	1.464	0.651	0.520	0.410	0.299	2.196	1.302	1.170	1.025	0.897
0.75	1.218	0.529	0.432	0.334	0.248	1.827	1.058	0.972	0.835	0.744
0.85	0.894	0.376	0.320	0.242	0.186	1.341	0.752	0.720	0.605	0.558
0.95	0.487	0.213	0.181	0.147	0.111	0.731	0.426	0.407	0.368	0.333

*Extrapolated Values

17

R_o / R_i	σ_{max}/σ_{br}	
	FEM	EQUN
1.50	4.389	4.391
2.00	2.737	2.750
2.25	2.364	2.365
2.50	2.100	2.092
3.00	1.715	1.722

$$K_{tb} = 2.75 \left(\frac{R_o - R_i}{R_i}\right)^{-0.675}$$
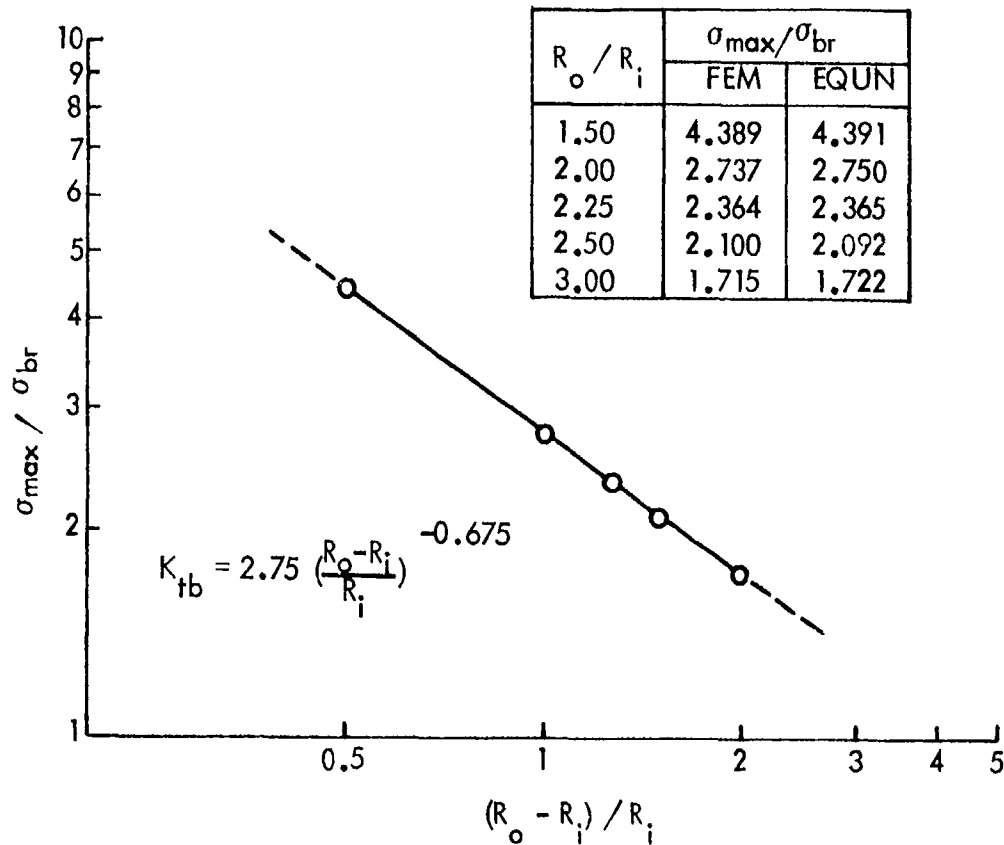
Figure 3-5. Elastic Stress Concentration Factors
for Straight Attachment Lugs

18

logarithmic straight line shown in this figure fits the computed values within 0.5 percent, as shown in the accompanying table.

The computed pin-bearing pressure distributions along the contact surface are shown in Figure 3-6. The figure shows that the shape of the distribution is close to uniform at the central portion of the contact surface. As the R_o/R_i ratio increases, the pressure decreases near $\theta = \pm 90°$ but increases near $\theta = 0°$.

2. STRESS INTENSITY FACTORS FOR THROUGH-THE-THICKNESS CRACKS

The development of stress intensity factor solutions for single through-the-thickness cracks in attachment lugs by various methods are described in this subsection. Also included in this subsection are the methods for analyzing attachment lugs with interference-fit bushings and elasto-plastic analysis for analyzing lugs which are loaded above yield.

2.1 COMPOUNDING METHOD APPROXIMATIONS

Stress intensity factors for an axially-loaded straight lug with a single through-the-thickness crack can be estimated by the compounding of known K solutions. The compounding method has been used for crack growth analysis of complex structure [14].

As Figure 3-7 shows, the actual lug configuration is approximated as an infinite strip of width $2R_o$ containing a central hole of radius R_i. A single through-the-thickness crack is assumed to be present at $\theta = 90°$ to the axis of the lug. The length of the crack is a_1, measured from the edge of the hole. The total pin load P is assumed to result from a uniform distribution of radial pressure from $\theta = -67.5°$ to $67.5°$, and to be reacted by a remote uniform stress $\sigma_o = P/(2R_o B)$, where B is the lug thickness.

The stress intensity factor for the configuration shown in Figure 3-7 can be approximated by combining a number of known K solutions. The basic solutions are for cracks emanating from holes in infinite plates. Multiplicative correction factors are used to modify these infinite plate solutions to account for the effects of finite width.

19
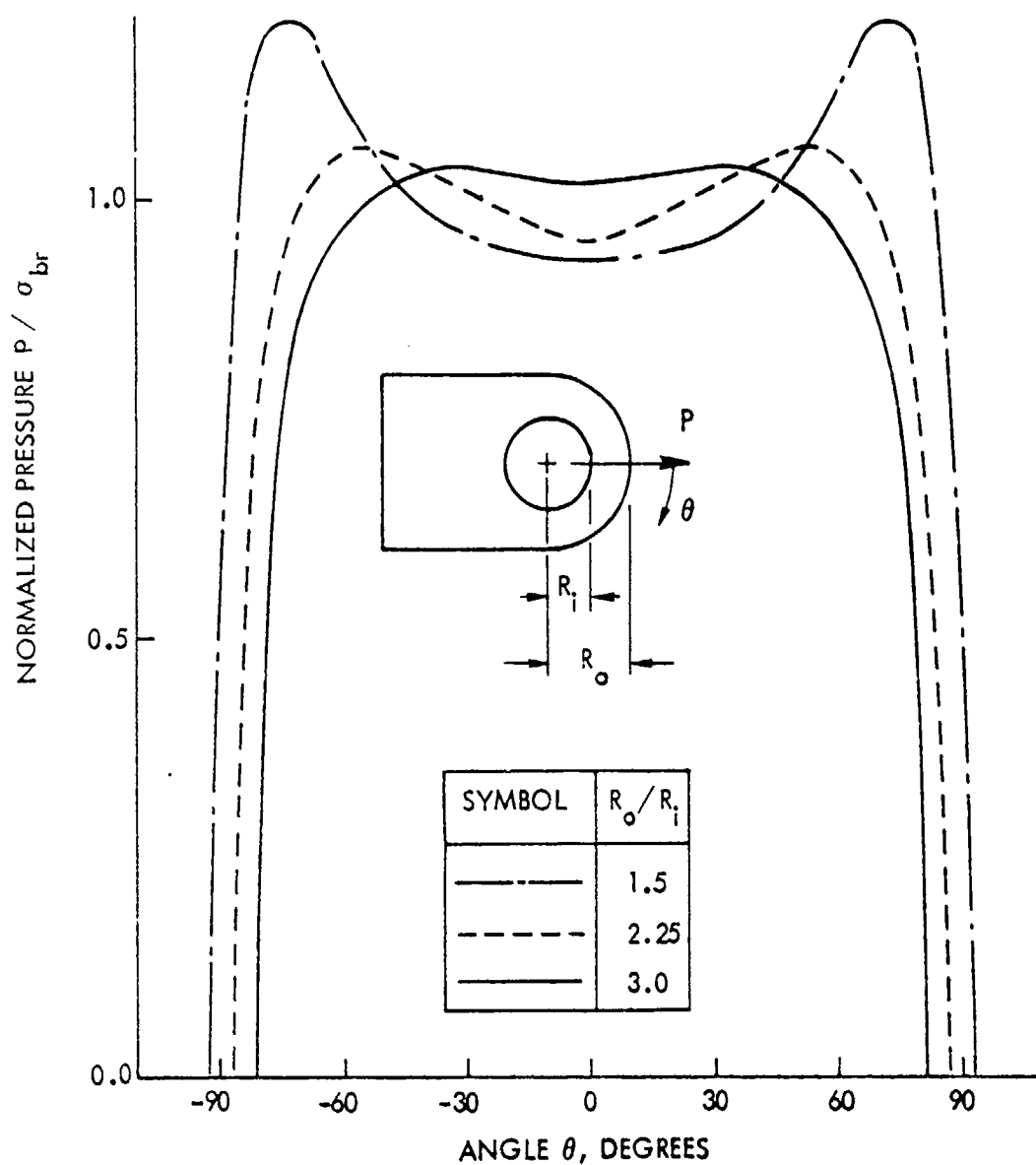
Figure 3-6. Pin-Bearing Pressure Distributions
Along the Contact Surface of Straight Lugs
Subjected to a Pin Loading Applied in
0° Direction
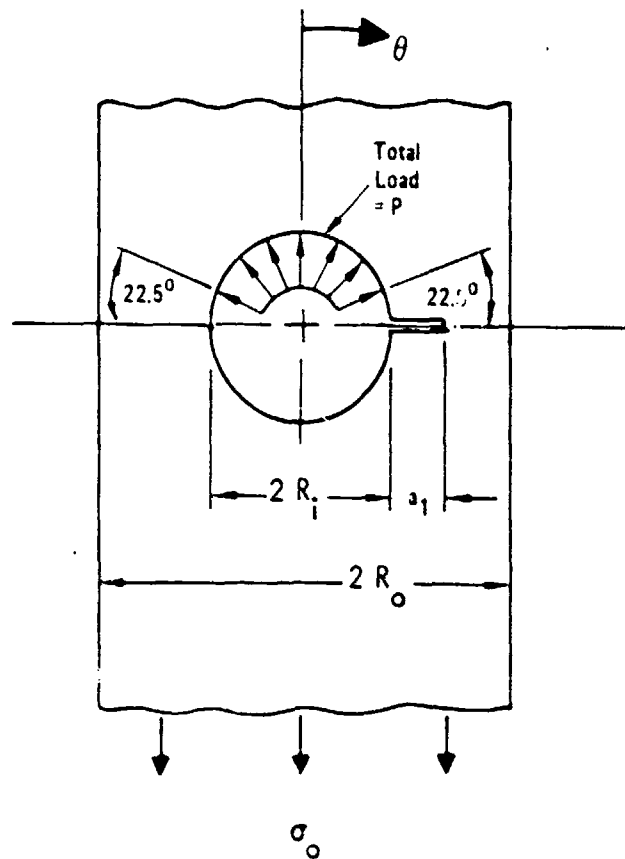
Figure 3-7. Approximation of Axially
Loaded Straight Lug

2.1.1 **Cracks at Holes in Infinite Plates** - The loading shown in Figure 3-7 consists of pin loading in one direction and remote loading in the other. Tweed and Rooke [15] have obtained the solution for a crack emanating from a circular hole in an infinite plate subjected to remote loading. This is Case 31 in the compendium given in Appendix A. The formula for K_{31} fits Tweed and Rooke's solution within 0.5 percent.

The general solution for the same geometry subjected to arbitrary radial loading at the hole is given in Reference[16]. Case 35 in Appendix A gives an equation which closely fits the special case of uniform radial pressure applied from $\theta = -67.5^\circ$ to $\theta = 67.5^\circ$, and from $(180^\circ - \theta) = -67.5^\circ$ to $(180^\circ - \theta) = 67.5^\circ$.

2.1.2 **Symmetrical Line Cracks in Strips** - The solution for a symmetrical line crack of length $2a_o$ in an infinite strip of width $2b$ under uniform tension stress σ_o is well known. It is given in Appendix A as Case 21. The function $\Phi_{21}(\lambda_o)$ is called the width correction factor, because it is applied multiplicatively to the infinite-plate K solution to give the correct solution for the strip.

Case 22 in Appendix A gives an approximate solution for the symmetrically-cracked strip subjected to concentrated splitting forces P applied to both surfaces of the crack at the centerline. This approximation is derived by the similarity method from three known K solutions, as follows:

Figure 3-8 shows the four similar configurations. In all four cases the crack lengths are the same and the shear stresses vanish along the lines $x = \pm b$. The unknown solution is K_{22}; the solutions for the other three cases shown are known in closed form. K_{19} is the well-known solution for periodic collinear cracks subjected to uniform loading [17]:

$$K_{19} = S\sqrt{\pi a_o} \ \sqrt{\frac{2b}{\pi a_o} \tan \frac{\pi a_o}{2b}} \tag{1}$$

The solution K_{20} for periodic collinear cracks subjected to central splitting forces on the crack surfaces is given by Tada, et al [18].

22
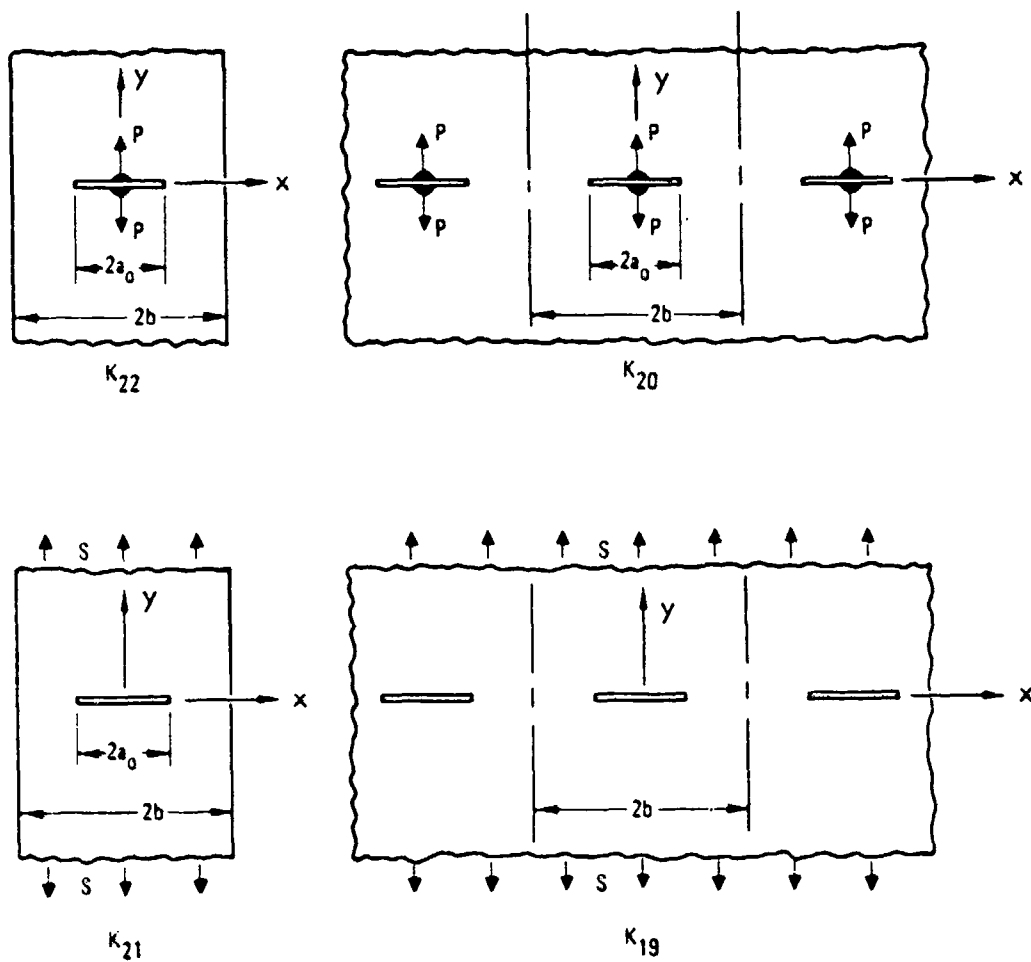
Figure 3-8.   Similarity Method for Approximating K_{22}

$$K_{20} = \frac{P}{B\sqrt{\pi a_o}} \sqrt{\frac{2b}{\pi a_o} \tan \frac{\pi a_o}{2b}} \quad \frac{\pi a_o/2b}{\sin(\pi a_o/2b)} \tag{2}$$

Notice in Figure 3-8 that Cases 21 and 22 are identical geometries, as are Cases 19 and 20. Furthermore, Cases 20 and 22 are identical in the applied loadings, as are Cases 19 and 21.

Thus, the correction factor approach can be applied in two alternative ways to estimate K_{22}. The ratio (K_{21}/K_{19}), a correction factor to account for the difference between a finite-width strip and a periodic crack array, can be multiplied times K_{20}, the solution for the periodic crack array with the Case 22 loading condition. Alternatively, the ratio (K_{20}/K_{19}), a correction factor to account for the difference between remote loading and point loading on the crack line, can be multiplied times K_{21}, the solution for remote loading of the Case 22 geometry. Either way, the resulting equation for K_{22} is the same:

$$K_{22} = \frac{K_{21} \, K_{20}}{K_{19}} \tag{3}$$

2.1.3 Effect of Eccentricity - The crack in the lug is eccentrically located, so eccentricity must be considered. Isida [19] has obtained the stress intensity solution for an unsymmetrical crack in a strip under uniform tension. Equations are given in Appendix A, Case 26, which fit Isida's numerical results within about 3 percent (within 1 percent for $a/b_n \leq 0.6$). There are two stress intensity formulas, $K_{26}^{(N)}$ for the crack tip nearest the edge and $K_{26}^{(F)}$ for the crack tip farthest from the edge. For the symmetrical crack both formulas reduce to the equation for K_{21}.

Case 27 in Appendix A gives an approximate solution for the unsymmetrical crack subjected to splitting forces on the crack surfaces at the strip centerline. This solution is obtained by the Similarity Method from the five known K solutions show... in Figure 3-9. (The solutions for Cases 12 and 13 are well known and are given in Reference [18].) There are two eccentricities in Case 27: the crack is not centered on the strip centerline, and the load is not centered on the crack centerline. Remove both eccentricities and Case 22 is obtained.

UNSYMMETRIC
CASES:

SYMMETRIC
CASES:

CASE 27

CASE 22

CASE 26

CASE 21

CASE 13

CASE 12
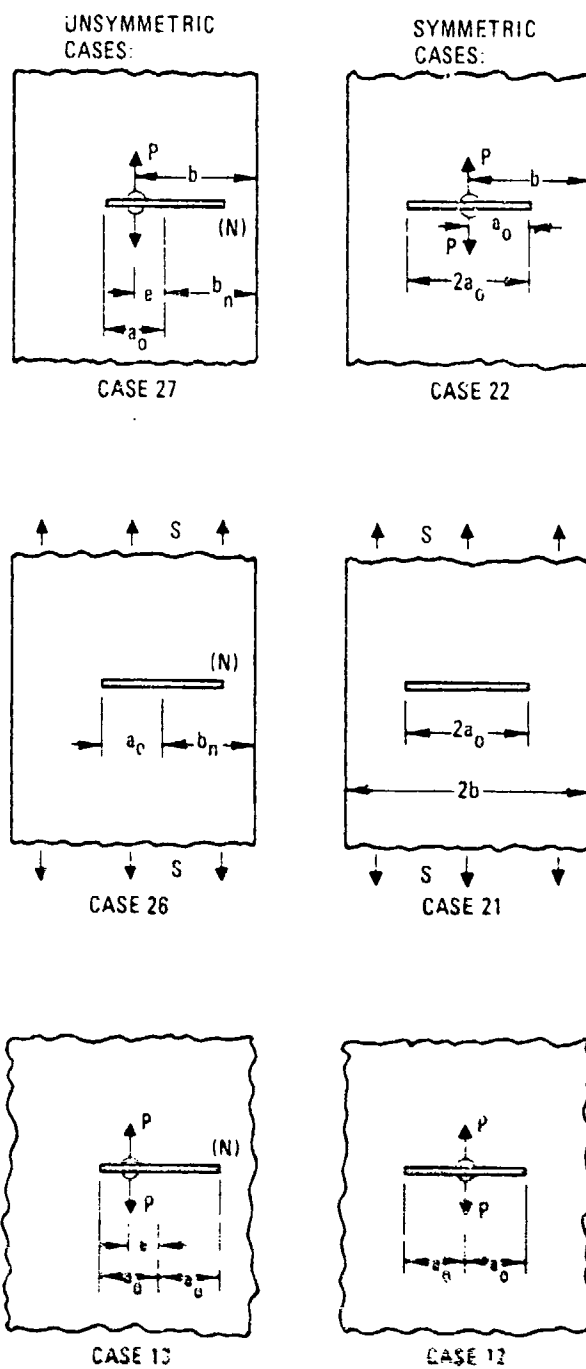
Figure 3-9. Similarity Method for
Approximating K_{27}

25

The crack is not centered on the strip in Case 26. Remove this eccentricity and Case 21 is obtained. Therefore, the correction factor to account for eccentricity between the crack and the strip is the ratio K_{26}/K_{21}.

The load is not centered on the crack in Case 13. Remove this eccentricity and Case 12 is obtained. Therefore, the correction factor to account for eccentricity between the loading point and the crack is the ratio K_{13}/K_{12}.

When both correction factors are applied to K_{22} the approximate formula for K_{27}, given in Appendix A, is obtained:

$$K_{27}^{(N)} = K_{22} \ \frac{K_{26}^{(N)}}{K_{21}} \ \frac{K_{13}^{(N)}}{K_{12}} \tag{4}$$

2.1.4 Cracks at Holes in Strips – The stress intensity solutions for cracks at holes in infinite plates and for line cracks in strips can be combined to obtain approximate K formulas for cracks at holes in strips. The resulting formulas can be superimposed to estimate K for a pin-loaded lug with a crack.

Case 41 in Appendix A gives an approximate solution for a uniformly loaded strip with a crack emanating from a central hole. Referring to Figure 3-10, one would expect the solution for K_{41} to be approximated by the product $K_{31} K_{26}/K_{11}$.

This product, however, does not account for the interaction between the hole and the edges of the strip. The gross area stress concentration factor given by Peterson [20] for a center hole in a strip can be approximated by the following formula:

$$k_t (r/b) = 3 \sec \left(\frac{\pi r}{2b}\right) = 3 \, \Phi_{21}^2 \ (r/b) \tag{5}$$

As the crack length a_1 approaches zero, K_{41} has a known asymptotic solution in terms of the stress concentration factor, i.e.

$$\lim_{a_1/r \to 0} (K_{41}) \to k_t \ (r/b) \ \frac{K_{31}}{3} \to \Phi_{21}^2 \ (r/b) \ K_{31} \tag{6}$$
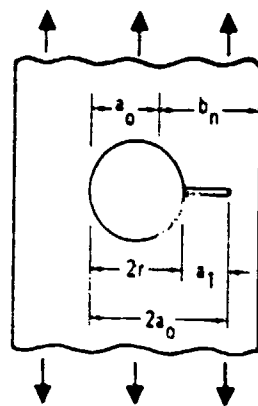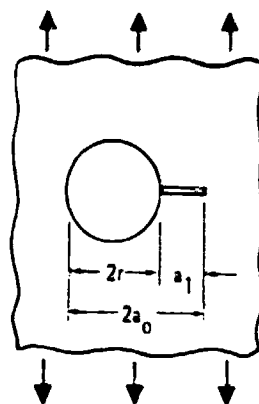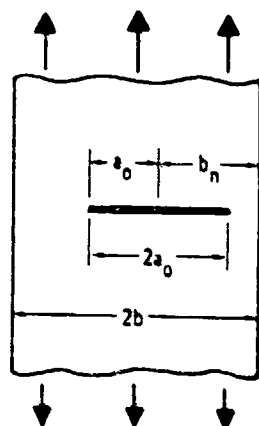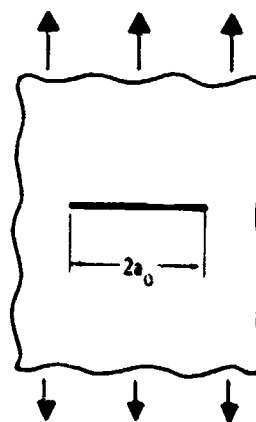
Figure 3-10. "Attempted" Similarity Method
for Approximating K_{41}

To satisfy Equation (6), a hole-strip width correction factor Φ_{21} (r/b) must be included, so that the approximate solution for Case 41 is

$$K_{41} = \frac{K_{31} \, K_{26}}{K_{11}} \, \Phi_{21} \, (r/b) \qquad (8)$$

Case 44 in Appendix A is an approximate solution for a strip with a crack at a central hole, loaded symmetrically at the hole. This solution is derived by the same approach used to derive K_{41}. In this case, however, the gross area stress concentration factor for the uncracked case is not known. Figure 3-5, obtained by finite element analysis, could have been used here to estimate the required k_t, but to do so would have compromised the independence of the solutions generated by the compounding and finite element methods. Based on engineering judgment, therefore, Φ_{21} (r/b) is appended to product solution obtained from Figure 3-11 to approximate K_{44}, just as was done for Case 41. Thus, K_{44} is approximated by the equation

$$K_{44} = \frac{K_{35} \, K_{27}}{K_{13}} \, \Phi_{21} \, (r/b) \qquad (9)$$

2.1.5 Cracked Lug – The final step in the derivation of a compounding method stress intensity factor for the pin-loaded straight lug is a simple superposition. As demonstrated in Figure 3-12, the result of superimposing Caes 41 and 44 is identical to the result of superimposing the lug approximation in Figure 3-7 with itself (oriented upside-down and backwards). Thus

$$K_{LUG} = \frac{1}{2} \, (K_{41} + K_{44}) \qquad (10)$$

Equation (10) was used to compute the stress intensity factors for R_o/R_i ratios of 1.50, 2.25 and 3.0, and the results are tabulated in Table 3-2.

2.2 TWO-DIMENSIONAL CRACKED FINITE ELEMENT METHOD

Because of the ease with which the finite-element method handles complex geometries and boundary conditions, this method has been used extensively to study fracture in complex structures. Two special crack-tip
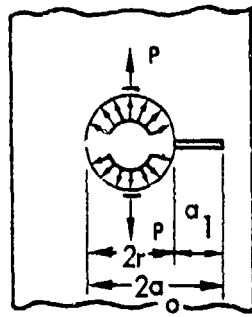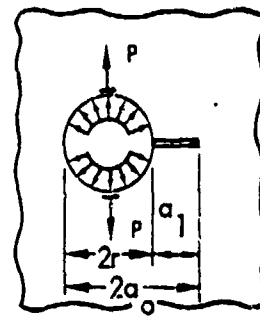
CASE 44   CASE 35
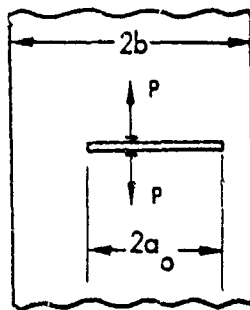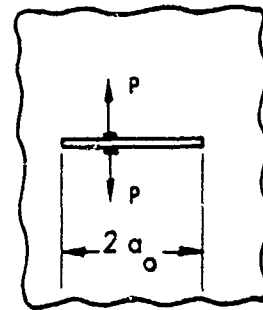
CASE 27   CASE 13

Figure 3-11. "Attempted" Similarity Method
for Approximating K_{44}
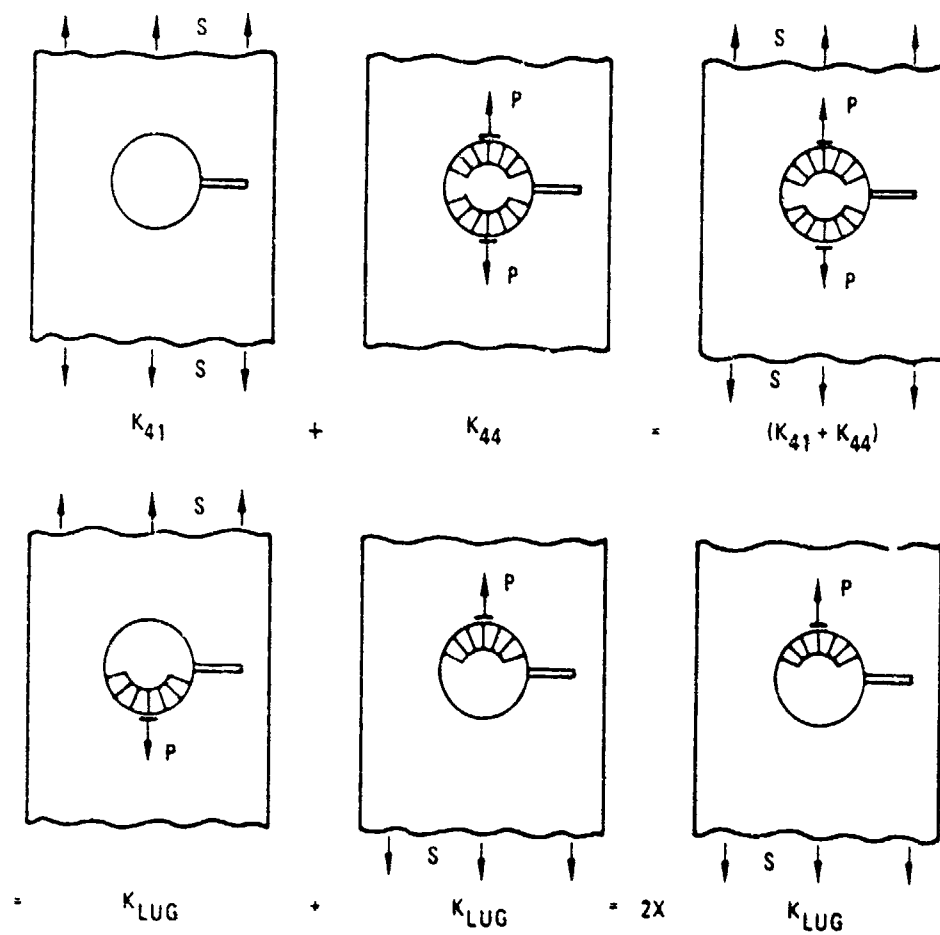
Figure 3-12.   Superposition of Cases 41 and 44

TABLE 3-2. NORMALIZED STRESS INTENSITY FACTORS FOR SINGLE THROUGH-THE-THICKNESS CRACKS IN STRAIGHT ATTACHMENT LUGS OBTAINED USING THE COMPOUNDING METHOD

$\dfrac{a_1}{(R_o-R_i)}$	$K/(\sigma_{br}\sqrt{\pi a_1})$, for R_o/R_i			$K/(\sigma_o\sqrt{\pi a_1})$, for R_o/R_i		
	1.50	2.25	3.00	1.50	2.25	3.00
0.0	4.472	2.283	1.762	6.708	5.136	5.286
0.1	4.134	1.752	1.146	6.201	3.942	3.438
0.2	3.899	1.449	0.866	5.848	3.260	2.599
0.3	3.751	1.267	0.719	5.626	2.851	2.156
0.4	3.683	1.159	0.635	5.525	2.607	1.906
0.5	3.702	1.103	0.592	5.553	2.482	1.775
0.6	3.827	1.094	0.577	5.741	2.461	1.732
0.7	4.115	1.138	0.594	6.172	2.561	1.782
0.8	4.721	1.273	0.658	7.082	2.864	1.974
0.9	6.287	1.659	0.851	9.431	3.733	2.553

singularity elements, usually referred to as cracked elements, developed at Lockheed-Georgia [8] have brought the power and flexibility of the finite-element method to bear much more effectively on fracture mechanics problems. This method has been used to analyze a crack in an unsymmetric lug of a C-5 engine pylon [8]. It has been modified slightly to accurately account for the change in pin-bearing pressure distribution for the change in crack length. The following discussion describes this method as it was used in the calculation of stress intensity factors for cracks at attachment lugs.

Figure 3-13 shows a typical finite element model used for a single crack emanating from a straight attachment lug. A 10-node high-order singularity element [8] was used at the crack tip region for computing the stress intensity factors. The remainder of the finite element modeling details was identical to those described in the stress analysis section for the uncracked lug, including the iterative determination of the contact area. The solution was obtained for several outer-to-inner radius ratios, R_o/R_i, and for a succession of cracks having normalized lengths, $c/(R_o - R_i)$ ranging from 0.1 to 0.9. As in the case of stress analysis, the rigidity ratio, E_{pin}/E_{lug}, of 3.0 is assumed in the fracture analysis.

The pin-bearing pressure distributions obtained for single cracks emanating from attachment lugs loaded by neat-fit pins are presented in Figures 3-14 through 3-16. These figures show the effect of crack length on the pin-bearing pressure distributions for a straight lug having R_o/R_i ratios of 1.5, 2.25 and 3.00, respectively. When there is no crack, the distribution is close to uniform at the central portion of the contact surface, unlike the cosine distribution commonly assumed in literature. There is no contact at the expected crack location, $\theta = -90°$. However, as soon as a crack appears, the contact spreads to one side ("upper lip") of the crack mouth. As the crack opens, the other side ("lower lip") of the crack mouth moves away from the pin resulting in no pin-bearing pressure on the lower lip. Figures 3-14 through 3-16 show that the longer the crack, the higher the pin-bearing pressure on the upper lip of the crack mouth, especially for a small R_o/R_i ratio. For example, for a R_o/R_i ratio of 1.5, the normalized pressure at the upper lip of the crack mouth increases from zero for $c/R_i = 0$ to more than twice the average pressure for $c/R_i \geq 0.3$. The pressure distribution elsewhere on the contact surface also changes with the crack length. For larger crack sizes, the pressure decreases from an initial
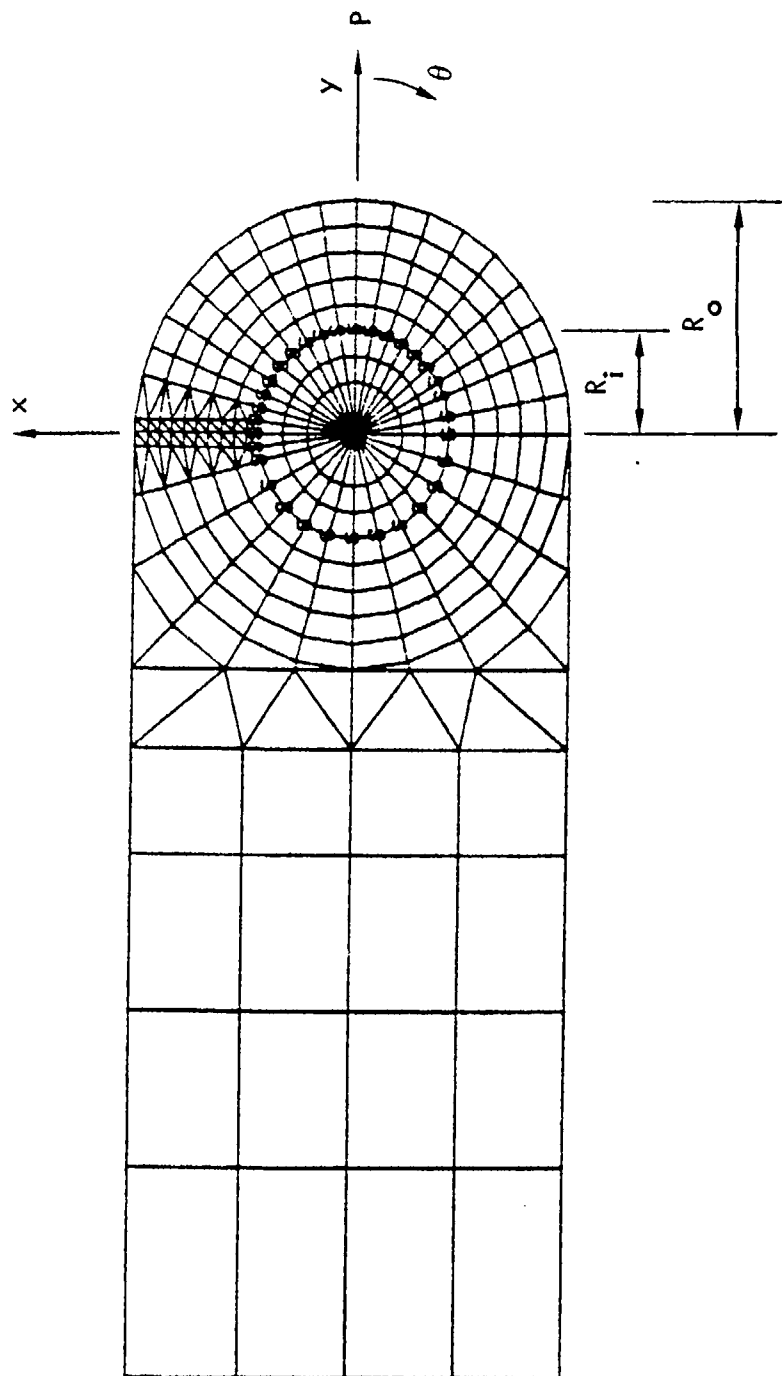
Figure 3-13. Typical Finite Element Model for Stress Intensity Factor Analysis
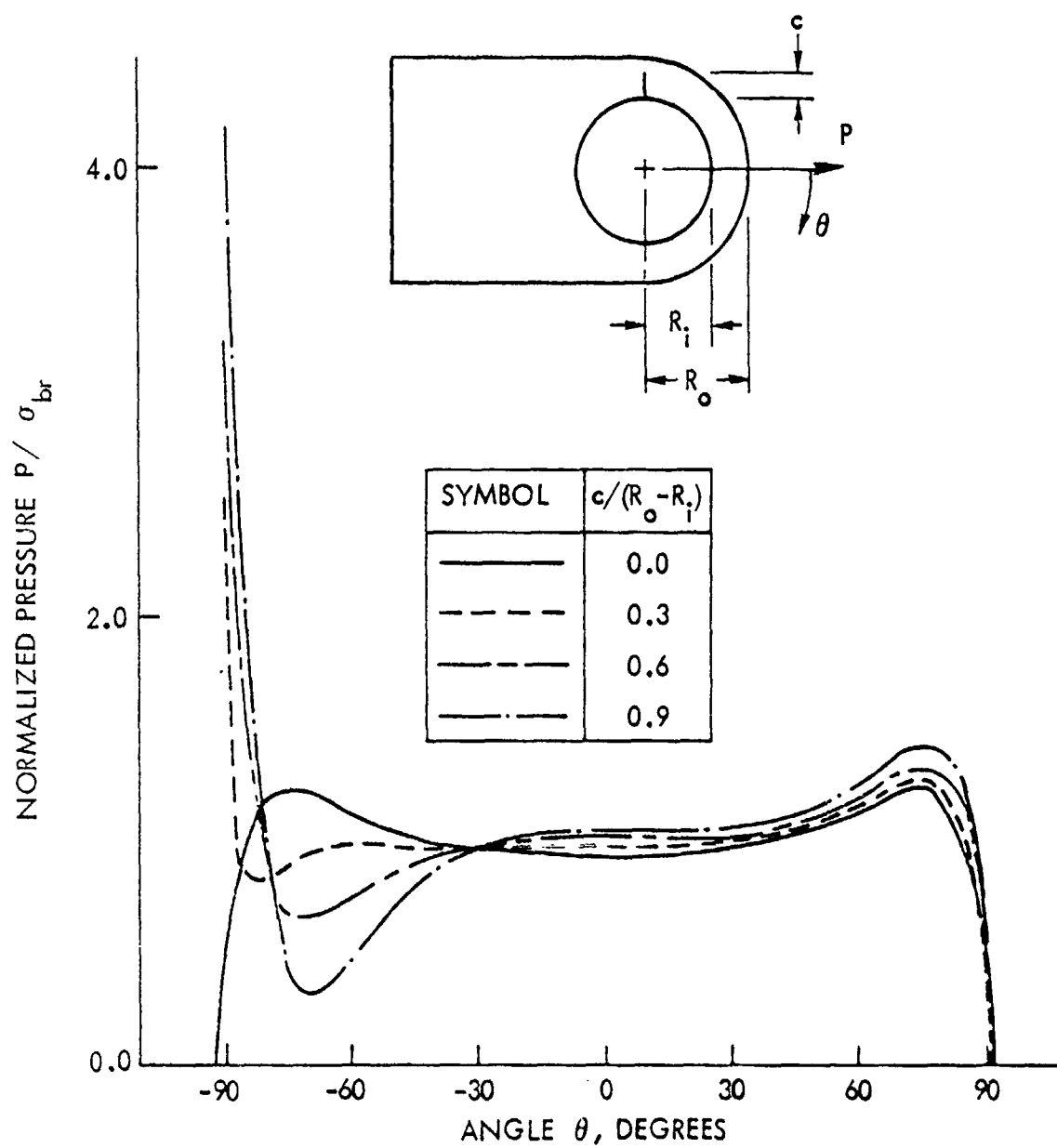
Figure 3-14. Pin-Bearing Pressure Distributions for Single Cracks at a Straight Attachment Lug Having a R_o/R_i Ratio of 1.50
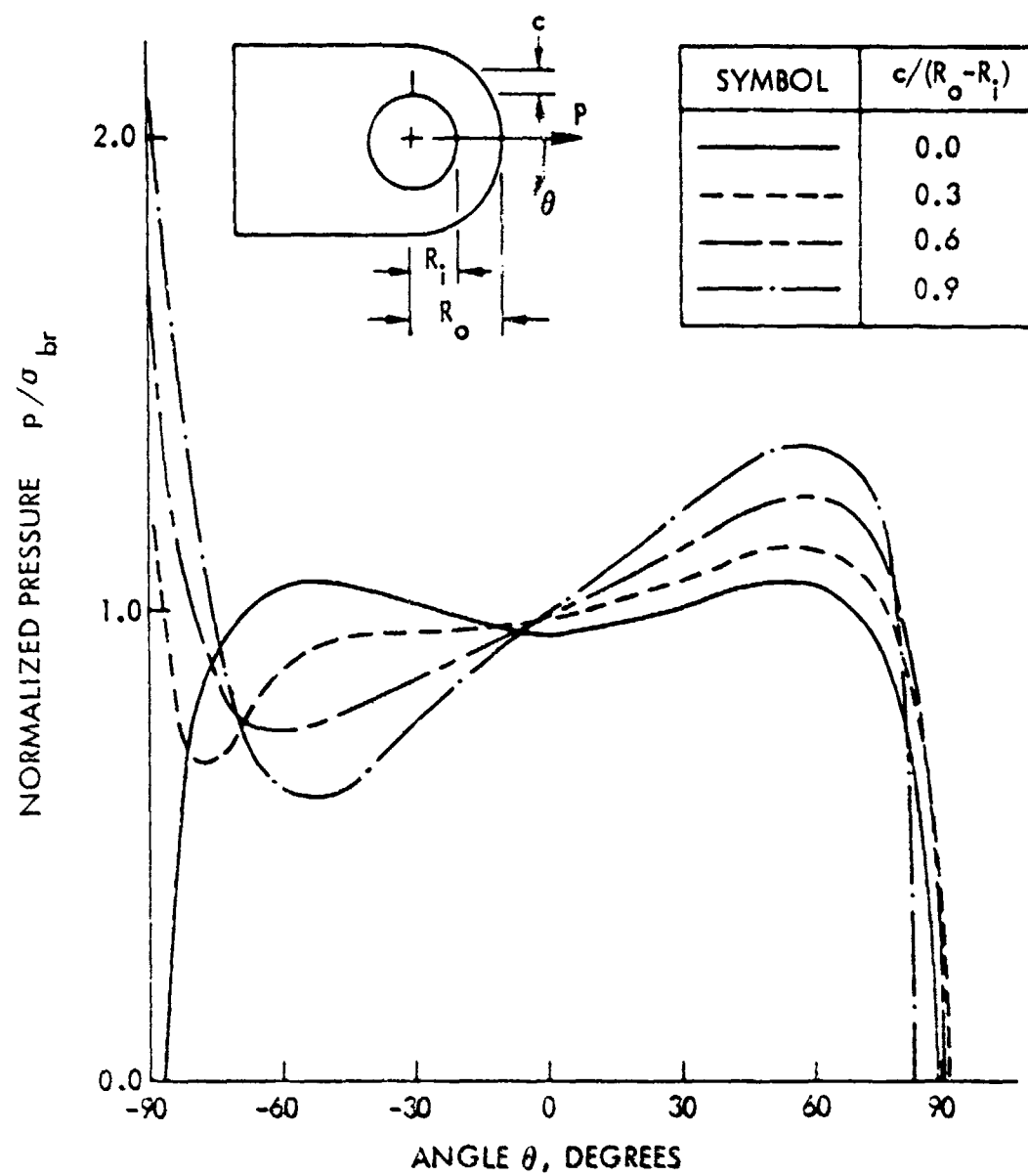
Figure 3-15.   Pin-Bearing Pressure Distributions for Single Cracks
at a Straight Attachment Lug Having a R_o/R_i Ratio of 2.25
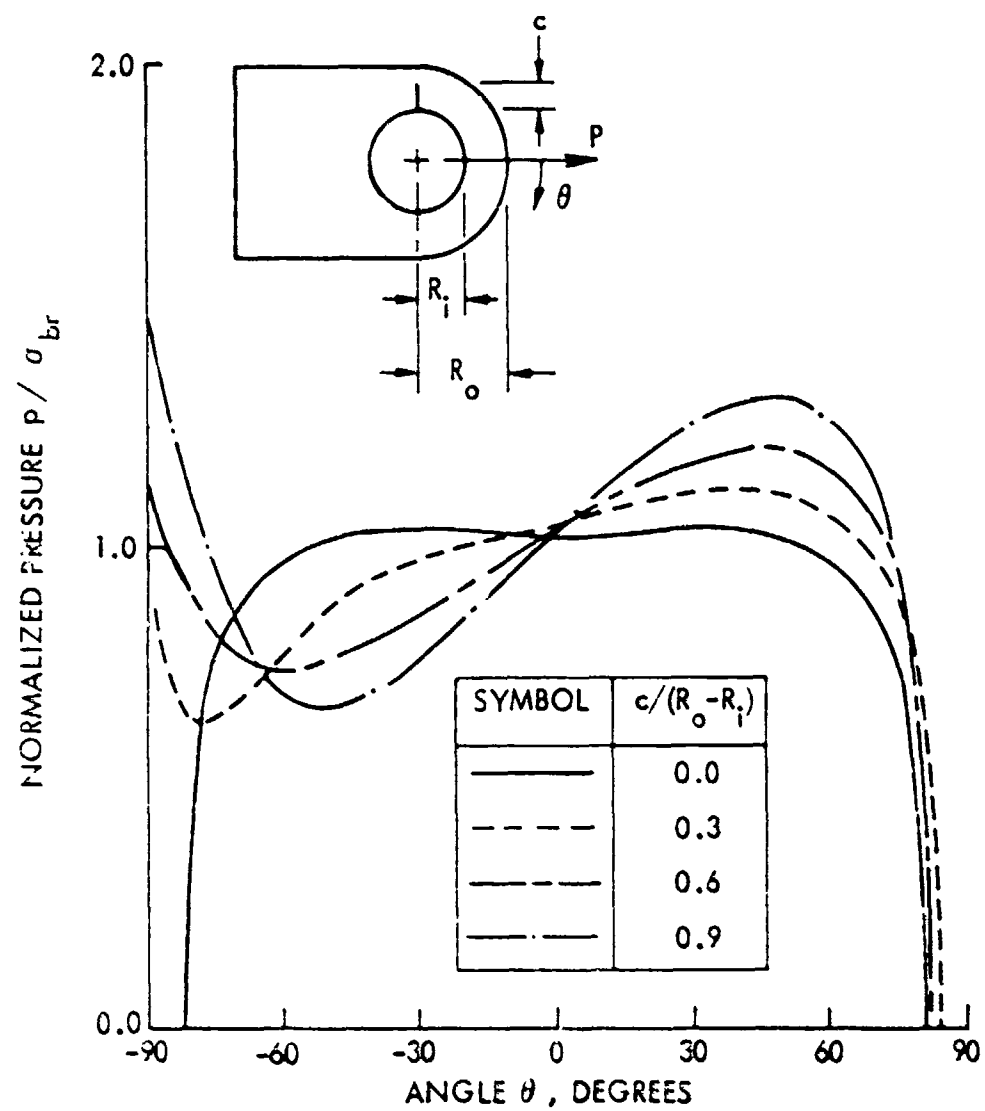
Figure 3-16. Pin-Bearing Pressure Distributions for Single Cracks at a Straight Attachment Lug Having a R_o/R_i Ratio of 3.00

maximum value at the crack mouth to a local minimum and then gradually increases again and approaches another maximum before decreasing to zero at the end of the contact surface.

The effect of pin-bearing pressure distributions on stress intensity factors is shown in Figure 3-17 for single cracks in a straight lug having a R_o/R_i ratio of 1.5. In Figure 3-17, the circle and triangle symbols are results obtained from Reference [9]*, where it is assumed tha: the pin-bearing pressure distributions are cosine and uniform distributions along the 180-degree contact surface, respectively, and that such distributions remain unchanged with the crack length. The square symbol represents the results obtained using the present analysis, which has properly accounted for the change in pressure distribution as the result of crack extension. As can be seen from this figure, when the crack is small ($c/R_i < 0.05$), the current computed K-value is practically the same as that obtained using a uniform pin-bearing pressure distribution. However, as the crack length increases, the current analysis gives a lower K-value than the others. This is because when the crack length increases, the pressure near $\theta = -90^o$ increases markedly and exceeds the average pin-bearing pressure (see Figure 3-14). This high pin-bearing pressure, when applied near $\theta = -90^o$ in the direction almost parallel to the crack orientation, tend to close the crack surfaces, hence reducing the stress intensity factor as discussed by Brussat [16].

The computed normalized opening mode stress intensity factors using a steel pin and an aluminum lug model are presented in Figure 3-18 as a function of normalized crack length (c/R_i) for single cracks emanating from the hole wall of straight attachment lugs with R_o/R_i ratios ranging from 1.5 to 3.0. In all cases, the computed sliding-mode stress intensity factors, K_{II}, are much smaller than those of the opening mode, K_I, so they are not presented in the figures. It should be noted that the K-values were normalized in terms of the average bearing stress, σ_{br}, instead of far-field gross section stress, σ_o. To convert these normalized factors in terms of σ_o, one can simply multiply these normalized factors by the corresponding ratio of R_o/R_i. For convenience, the computed K-values normalized in terms of the average far-field stress are tabulated in Table 3-3 as a function of

---

*The results are mislabeled in Reference [9]; uniform distribution results are labeled cosine distribution and vice versa.
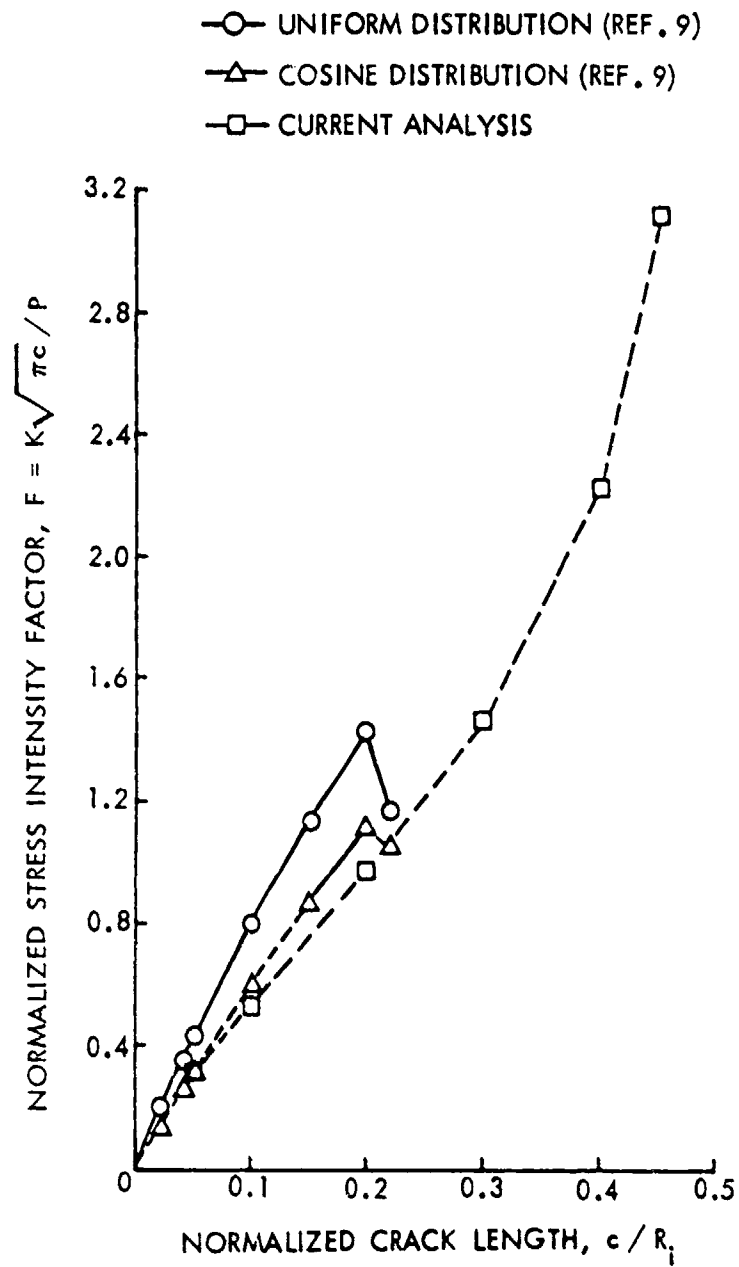
Figure 3-17. Sensitivity of Stress Intensity Factors
to Pressure Distributions (R_o/R_i = 1.50)
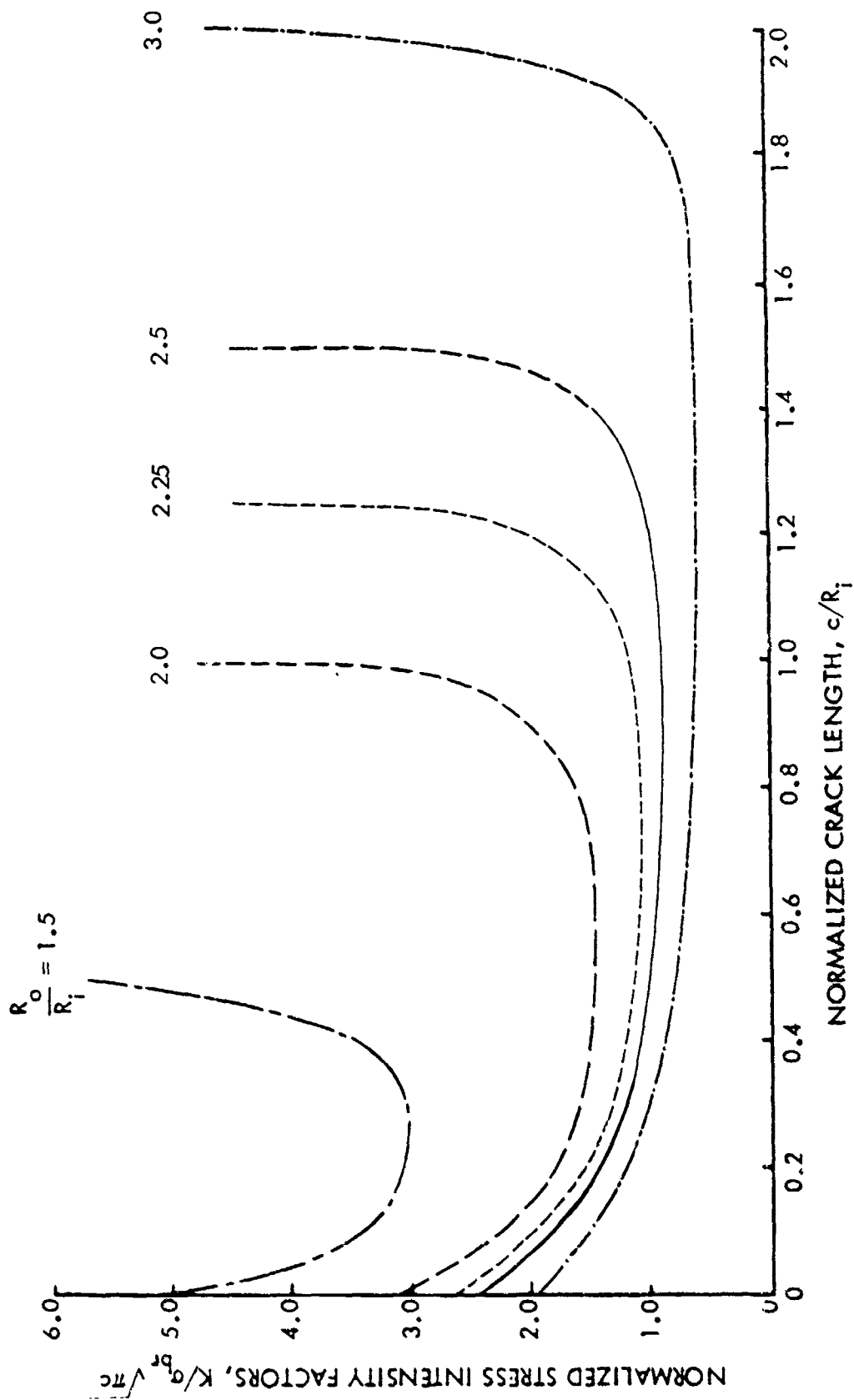
Figure 3-18. Normalized Stress Intensity Factor Solutions for Single Cracks at Attachment Lugs by Finite Element Method

39

TABLE 3-3. NORMALIZED STRESS INTENSITY FACTORS FOR SINGLE THROUGH-THE-THICKNESS CRACKS IN STRAIGHT ATTACHMENT LUGS USING CRACKED FINITE ELEMENT METHOD

$\dfrac{c}{(K_o-K_i)}$ \ K_o/K_i	$K/(\sigma_{br}\sqrt{\pi c})$					$K/(\sigma_o\sqrt{\pi c})$				
	1.50	2.00	2.25	2.50	3.00	1.50	2.00	2.25	2.50	3.00
0.0	4.916	3.066	2.648	2.352	1.921	7.374	6.131	5.957	5.880	5.762
0.1	3.580	2.237	1.733	1.524	1.153	5.370	4.474	3.899	3.809	3.460
0.2	3.110	1.789	1.389	1.185	0.869	4.665	3.578	3.126	2.963	2.607
0.3	2.945	1.639	1.246	1.060	0.749	4.423	3.277	2.804	2.650	2.246
0.4	2.816	1.506	1.111	0.954	0.657	4.224	3.012	2.500	2.385	1.971
0.5	2.820	1.472	1.076	0.917	0.624	4.230	2.943	2.422	2.293	1.872
0.6	2.824	1.442	1.051	0.892	0.603	4.236	2.884	2.364	2.230	1.810
0.7	2.981	1.509	1.095	0.922	0.620	4.472	3.017	2.463	2.306	1.860
0.8	3.219	1.619	1.176	0.985	0.659	4.828	3.238	2.646	2.463	1.977
0.9	4.080	2.044	1.470	1.246	0.812	6.120	4.088	3.308	3.115	2.436

normalized crack length (normalized by the net section). Note that
at the edge of the hole ($c/R_i = 0$), the normalized stress intensity factor
was obtained by multiplying the stress concentration factor determined
from unflawed stress analysis by 1.12, which was derived by Gross et al [21]
for a straight edge crack in a finite-plate specimen loaded in tension. Un-
flawed elastic distributions on the prospective crack plane and the corre-
sponding stress concentration factors at the edge of the hole have been given
in Figures 3-4 and 3-5, respectively.

Studies were also made to investigate the effects of a single crack
versus a symmetrical double crack and relative rigidity of the pin and the
lug (E_{pin}/E_{lug}). A typical comparison of K-values obtained for a single
crack and a symmetrical double crack in a straight aluminum lug loaded by a
steel pin ($E_{pin}/E_{lug} = 3.0$) is shown in Figure 3-19. As anticipated, the
computed K-values for a double crack are higher than those of a single crack,
and the difference increases with the crack length. It increases from less
than 1% for $c/R_i \leq 0.2$ to about 37% for $c/R_i = 0.9$. To study the effect
of the relative rigidity of the pin and the lug on the stress intensity
factors, the computed K-values for a single crack emanating from the hole
wall of a steel lug loaded by a steel pin ($E_{pin}/E_{lug} = 1.0$) is also included
in Figure 3-19. As presented in this figure, the K-values computed for a
combination of a steel pin and steel lug is slightly higher than that of the
steel pin and the aluminum lug. A comparison of stress distributions along the
$\theta = -90^\circ$ radial line for steel lug-steel pin and aluminum lug-steel pin
combinations is presented in Figure 3-20. These stresses can be used in
conjunction with Green's function to calculate the stress intensity factors
appropriately.

2.3 THE WEIGHT FUNCTION METHOD

The linear superposition method has been used frequently to obtain the
stress intensity factors for various types of crack problems. The principle
of superposition of linear elasticity implies that, for the purpose of cal-
culating stress intensity factors, loading the crack faces with $\sigma(x)$ is
equivalent to loading the cracked body with loads which produce $\sigma(x)$ on
the prospective crack faces in the absence of a crack.

Figure 3-21 shows the scheme of the linear superposition method. The
stress intensity factor of problem 3-21a is equivalent to the sum of that of
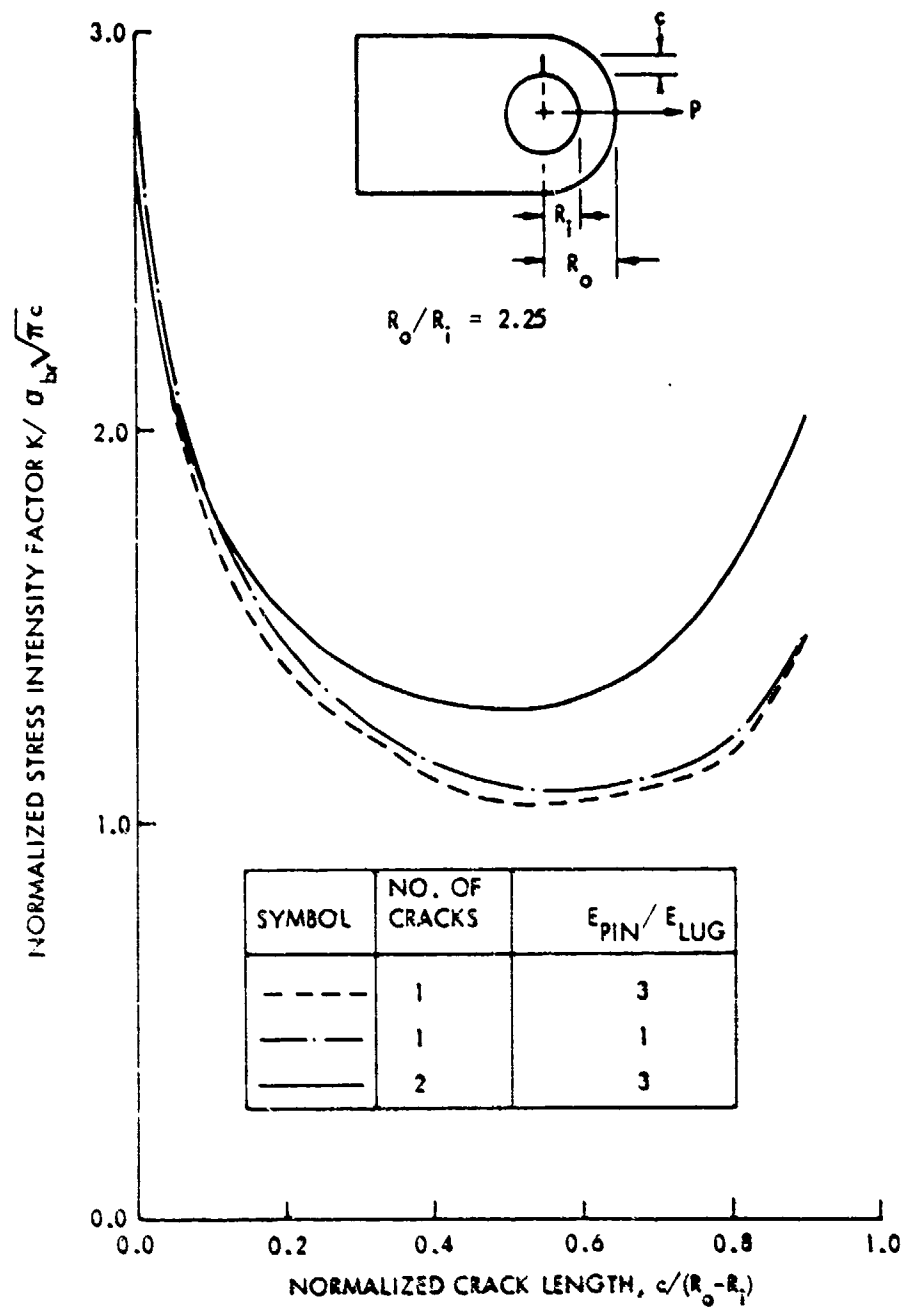
Figure 3-19. Normalized Stress Intensity Factors for Cracks Emanating from Straight Lugs for Single and Symmetric Cracks and for Various E_{pin}/E_{lug} Ratios $(R_o/R_i = 2.25)$

42
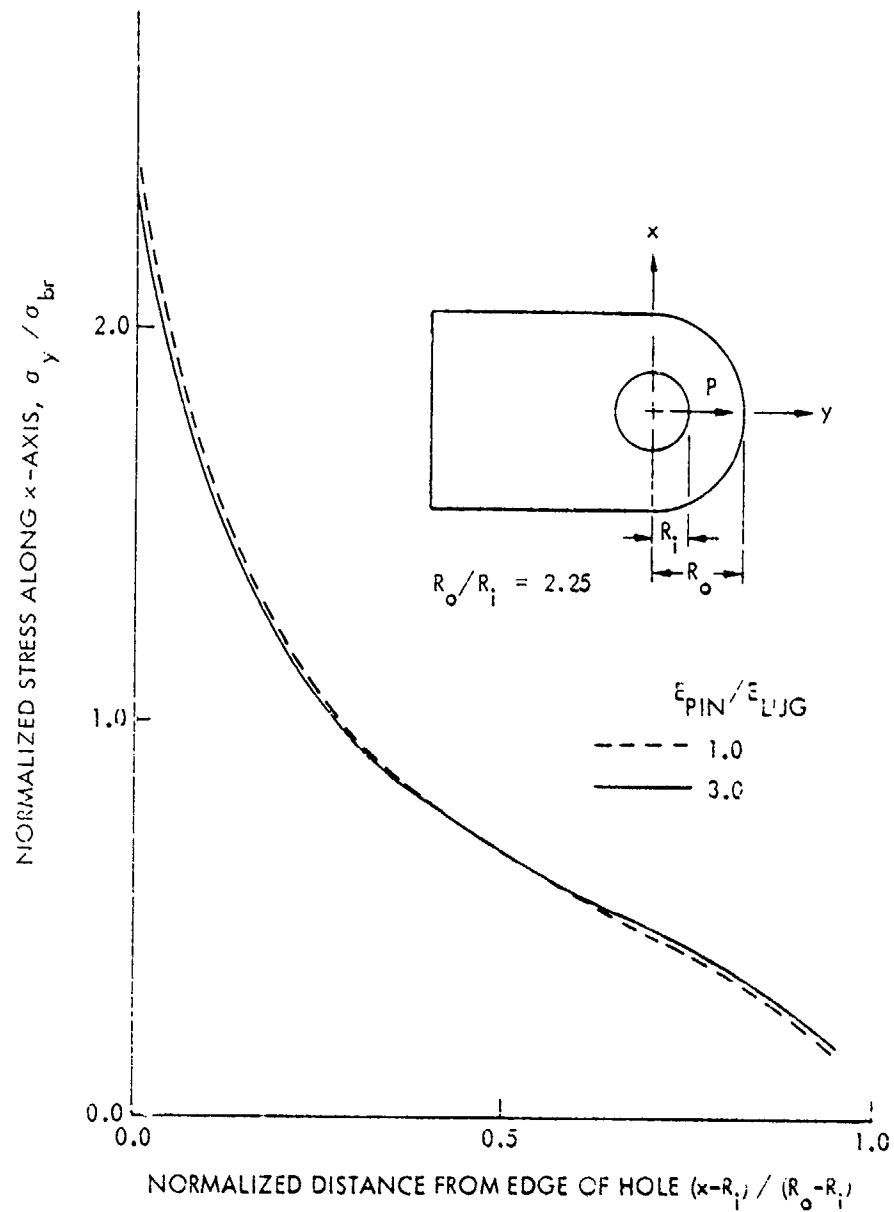
Figure 3-20. Unflawed Stress Distributions in Straight Attachment Lugs for Various E_{pin}/E_{lug} Ratios ($R_o/R_i = 2.25$)
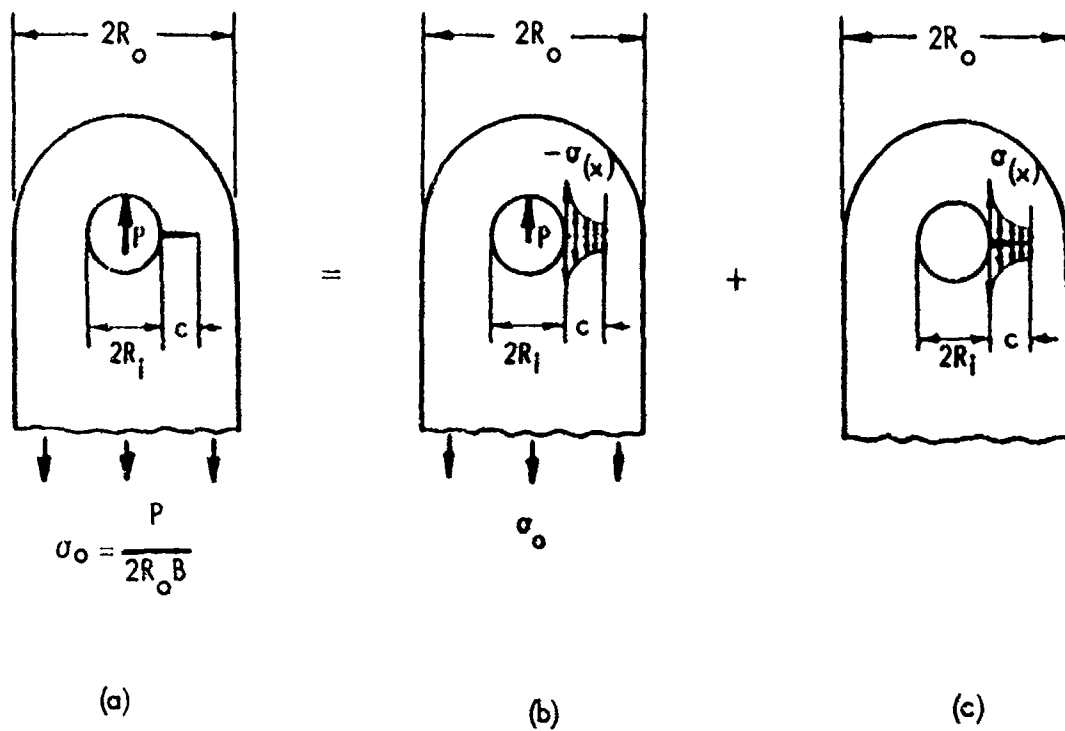
Figure 3-21. Schematic of Linear Superposition Method

problems 3-21b and 3-21c. Since problem 3-21b is crack free, the stress-intensity factor of problem 3-21a is equivalent to that of problem 3-21c. By idealizing the stress in problem 3-21c as N discrete loads, $P_1 \ldots, P_N$, then the stress-intensity factor, for a given crack length c, can be computed from the following equation

$$K(c) = \sum_{i=1}^{N} K_i = \sum_{i=1}^{N} k_i(x_i, c) \, P_i \, (x_i) \tag{11}$$

where $k_i(x_i, c)$ is the normalized stress-intensity factor due to the ith load, P_i, applied at location x_i. For arbitrary distributed stress, $\sigma(x)$, instead of discrete forces, P_i, Equation (11) becomes

$$K(c) = \int_{0}^{c} k(x, c) \cdot \sigma(x) \, dx \tag{12}$$

In Equation (12), $k(x, c)$ is the weight function (or Green's function). Bueckner [22] and Rice [23] defined the weight function as

$$k(x, c) = \frac{H}{2\bar{K}(c)} \cdot \frac{\partial u(x, c)}{\partial c} \tag{13}$$

for a symmetrical load system on a linearly elastic body containing a crack of length c. In the above equation, H is an appropriate elastic modulus: it is $E/(1-\nu^2)$ for plane strain and E for generalized plane stress. $\bar{K}(c)$ is the known stress intensity factor and $u(x, c)$ is the y-component of the crack surface displacement at x. The weight function was shown [22,23] to be unique for a given structural geometry and crack size regardless of the loading condition. Therefore, it can be developed for one load condition and then utilized to determine the stress-intensity factor for any other load condition.

The closed form expressions for the weight function for edge cracks [11,24], center cracks [25] and collinear cracks [26] in a wide panel are available. However, the closed form weight function for cracks emanating from a hole is not available. Therefore, the weight function for a straight center crack has sometimes been used to estimate the stress-intensity factor for radial cracks emanating from a circular hole [27-29], located in the

geometric center of a long plate. Impellizzeri and Rich [10] modified the weight function derived by Bueckner [11] for an edge crack in a semi-infinite plate to include the geometric correction factors for estimating the stress-intensity factor of a crack in an attachment lug. In order to establish the appropriate values of the derivative $\partial u/\partial c$, to be used in Equation (13), Grandt [30] supplemented Bowie's solutions [31] for a radially-cracked hole with a finite element analysis to obtain the corresponding crack-mouth opening displacements. Hsu and Rudd [32] developed the Green's function from the stress-intensity factors computed using the high-order singularity element for a double-radial crack emanating from an open hole and subjected to a pair of concentrated loads on and perpendicular to the crack surface. This approach is capable of accounting for the effect of hole curvature, finite width and the profile of the lug head. Therefore, it was used to develop the weight function for through-the-thickness cracks emanating from the hole of attachment lugs.

By defining the weight function $G = k(c/\pi)^{1/2}$ and $\xi = (x-R_i)/c$ and substituting them into Equation (12), one obtains

$$K(c) = \sigma_o \sqrt{\pi c} \int_o^1 G(c,\xi) \, \bar{\sigma} \, (\xi) \, d\xi \tag{14}$$

where σ_o is the uniform far-field stress and $\bar{\sigma} = \sigma/\sigma_o$ is the normalized unflawed stress distribution on the prospective crack surface.

The weight function G, for a single radial crack emanating from a circular hole of the lug and subjected to a pair of concentrated forces on the crack surfaces, as shown in Figure 3-22a, is obtained from the computed stress-intensity factor using 2-D cracked finite element analysis for various R_o/R_i ratios, crack lengths $c/(R_o-R_i)$, and $(x-R_i)/c$ ratios as follows:

$$G \left(\frac{c}{(R_o-R_i)} , \frac{x}{c} , \frac{R_o}{R_i} \right) = k(x,c) \, \sqrt{a/\pi} \tag{15}$$

Finite element methodology becomes difficult to employ when the concentrated forces are applied close to the crack tip, say $(x-R_i)/c > 0.9$. In this range the corresponding weight functions were obtained using the edge crack model as shown in Figure 3-22b. The weight function, G_1, for such edge cracks is available in Reference [18], and can be written as

46
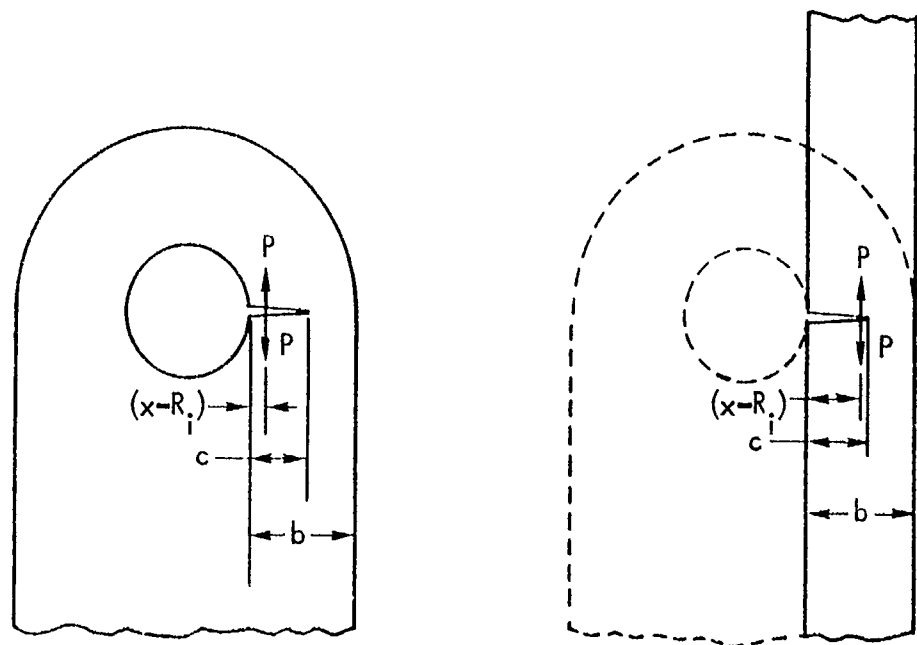
(a) FOR P APPLIED AWAY FROM
CRACK TIP

(b) FOR P APPLIED CLOSE TO
CRACK TIP

Figure 3-22. Model for Generating the Weight Functions

$$G_1 = \frac{2}{\pi} \left\{ \frac{3.52(1-(x-R_i)/c)}{(1 - c/2b)^{3/2}} - \frac{4.35 - 5.28 \ (x-R_i)/c}{(1 - \frac{c}{2b})^{1/2}} + \right.$$

$$\left. \left[\frac{1.30-0.30 \ ((x-R_i)/c)^{3/2}}{\sqrt{1 - ((x-R_i)/c)^2}} + 0.83-1.76 \ (x-R_i)/c \right] \left[1-(1-(x-R_i)/c) \frac{c}{b} \right] \right\} \quad (16)$$

In the conventional finite element method, the external force can only be applied at nodal points. When the crack length is small, it becomes cumbersome to refine the model such that there will be enough nodes along the crack faces for the purpose of computing the K and G values. Therefore, an alternate approach is used. For each crack length c, the K and G values were calculated at each available nodal point on the crack face, say $(x_i-R_i)/c$, using a finite element model for the configuration shown in Figure 3-22a and Equation (15). The weight function G_1 for an edge crack in a finite width strip (Figure 3-22b) was then calculated at the same locations, $(x_i-R_i)/c$, using Equation (16), and the ratio was obtained.

$$r \ ((x_j-R_i)/c) = G \ ((x_j-R_i)/c)/G_1 \ ((x_j-R_i)/c) \quad (17)$$

Assuming that r approaches 1 as $(x_i-R_i)/c$ approaches 1, a least squares polynomial fit is obtained.

$$r \ ((x-R_i)/c) = \sum_{j=1}^{M} C_j((x-R_i)/c)^{j-1} \quad (18)$$

The weight function at any location on the entire crack surface can then be computed using Equations (16) and (18) as

$$G \ ((x-R_i)/c) = r \ ((x-R_i)/c) \ G_1 \ ((x-R_i)/c) \quad (19)$$

The results obtained using the aforementioned procedure are shown in Figures 3-23 through 3-25 for R_0/R_i ratios of 1.50, 2.25, and 3.00, respectively. The symbols shown in these three figures are the discrete values obtained using the finite element method and the curves are obtained
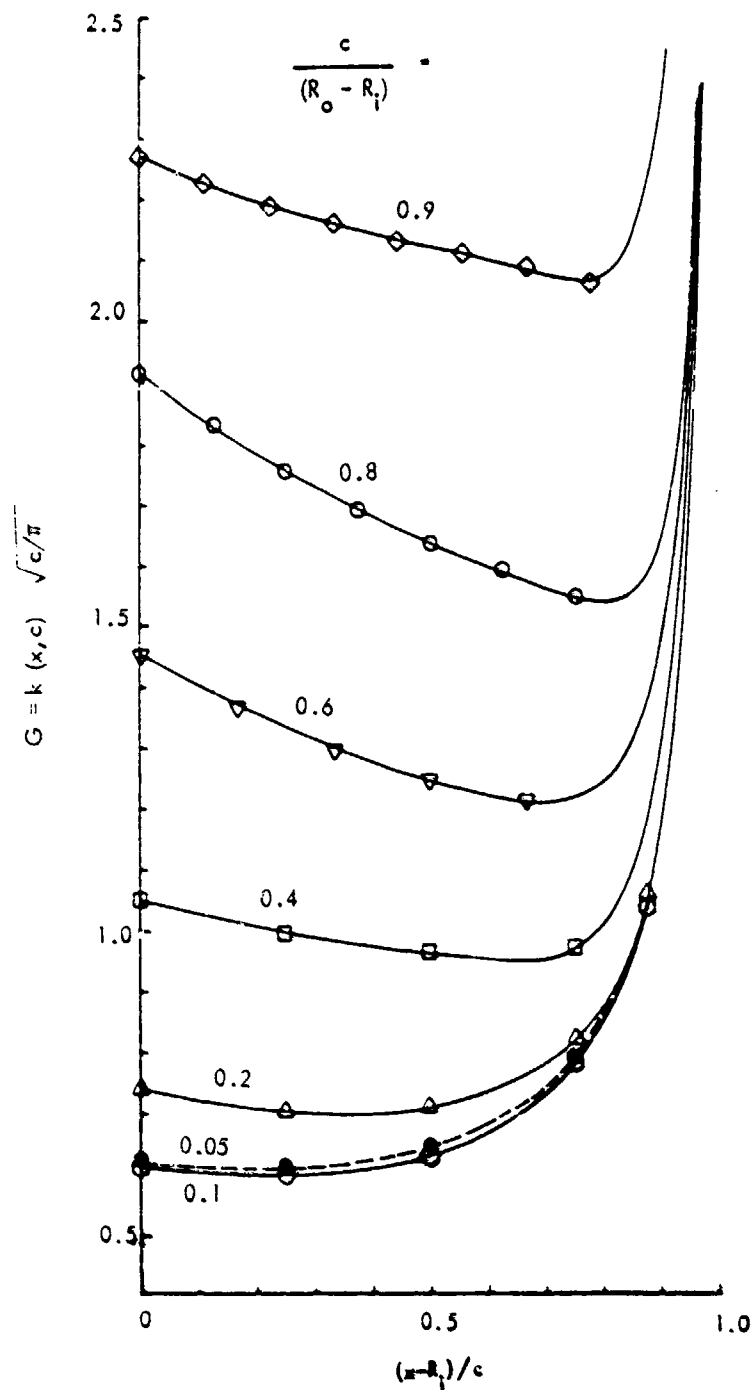
Figure 1-23. Original Height Functions for a Single Through-the-Thickness Crack at Straight Attachment Lug Having a R_o/R_i Ratio of 1.50

49
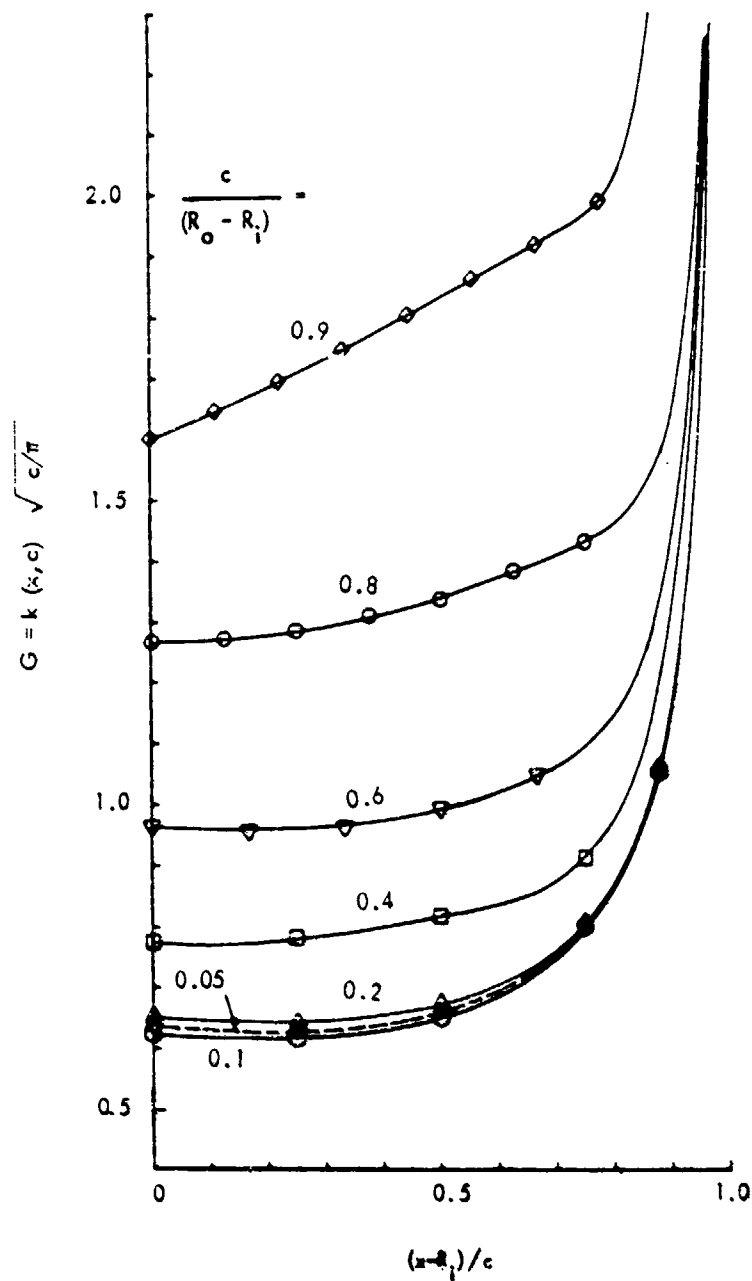
Figure 3-24.   Original Weight Functions for a Single
              Through-the-Thickness Crack at Straight
              Attachment Lug Having a R_o/R_i Ratio of 2.25
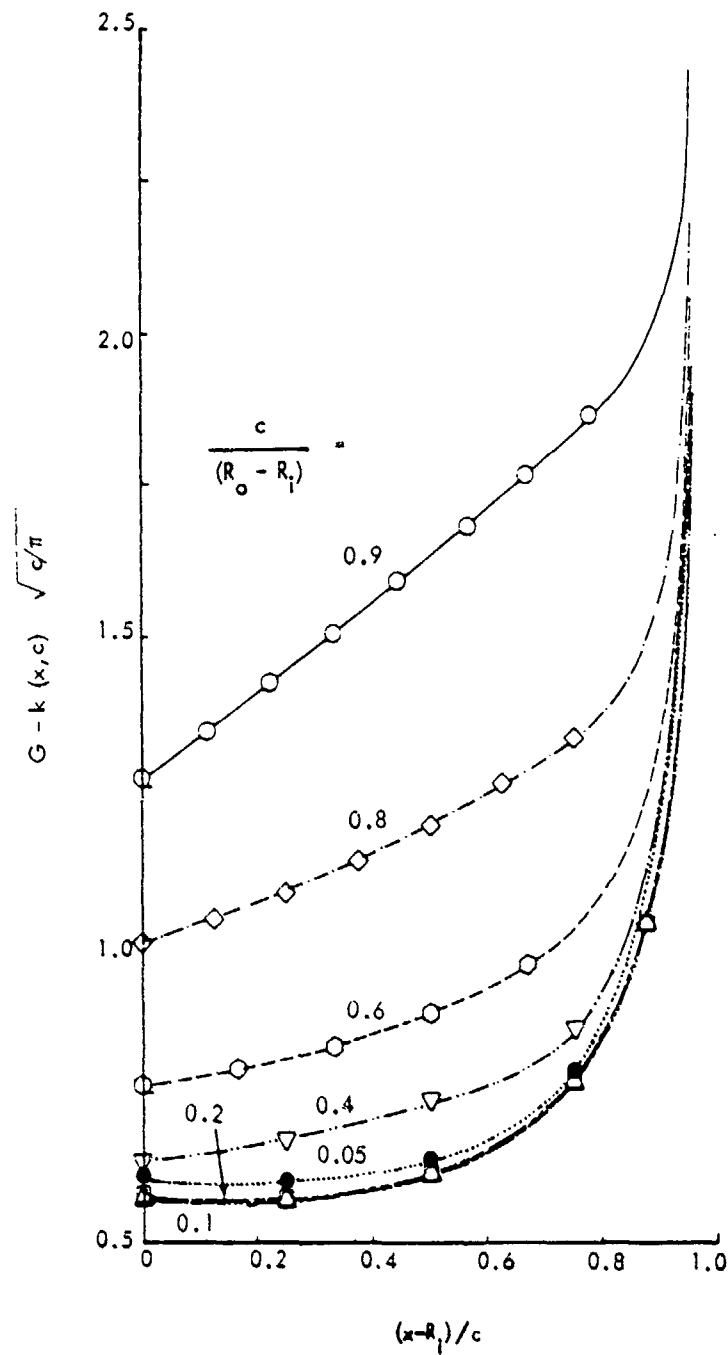
Figure 3-25. Original Weight Functions for a Single Through-the-Thickness Crack at Straight Attachment Lug Having a R_o/R_i Ratio of 3.00

using Equation (19). As seen from these figures, this alternate approach gives an excellent estimation of G-values at any desired location.

With a knowledge of the weight functions, G, and the unflawed stress, σ, on the prospective crack surface with the crack absent, one can numerically integrate in Equation (14) to obtain the corresponding stress-intensity factor for a radial crack in an attachment lug.

Integration of Equation (14) can be carried out accurately and efficiently by the Gaussian quadrature formula. In order to perform the Gaussian integration, the integral in Equation (14) needs to be transferred into the well-known Newton-Cotes quadrature formula for the range of integration between -1 and +1. This can be easily done by assuming that

$$\zeta = 2\xi - 1, \quad \text{or} \quad \xi = \frac{1}{2} (\zeta + 1), \tag{20}$$

and the integral of Equation (14) becomes

$$\int_0^1 \bar{\sigma}(\xi) G(c,\xi) d\xi = \int_{-1}^1 F(\zeta) d\zeta = \sum_{i=1}^n H_i F(\zeta_i) \tag{21}$$

where

$$F(\zeta) = \frac{1}{2} \bar{\sigma} \left(\frac{\zeta+1}{2}\right) G\left(c, \frac{\zeta+1}{2}\right) \tag{22}$$

The abscissae (ζ_i) and weight coefficients (H_i) of the Gaussian quadrature formula, Equation (21), for n up to 10 are given in Reference [33]. With this transformation, the stress-intensity factor can then be calculated from the following equation:

$$K = \sigma_0 \sqrt{\pi c} \sum_{i=1}^n H_i F(\zeta_i) \tag{23}$$

An evaluation was made on the calculation of the stress-intensity factor using Equation (23). It was found that, for n = 9, the computed K values using Gaussian integration are essentially the same as the ones obtained using trapezoidal rule numerical integration with 400 equal integration intervals.

Therefore, the more economical Gaussian integration was exclusively used in the K calculation using the weight function approach.

An important point on the development of the Green's function for attachment lugs is to be noted at this point. In the case of an attachment lug loaded by a pin, which is a contact problem, the pin bearing pressure distribution between the lug and the pin varies with the crack length (Figures 3-14 through 3-16). The pin bearing pressure distribution has a significant effect on the unflawed stress distribution (on the prospective crack surface) and on the stress-intensity factors (Figure 3-17). In the case of finite element analysis of cracked lugs, the pin bearing pressure distribution was taken into account in the analysis itself. In the case of the Green's function method, the pin bearing pressure distribution variation can be accounted for by two methods.

The first method is to use the Green's function developed above which should strictly be used only in conjunction with the correct unflawed stress distribution on the prospective crack surface for the varying pin bearing stress distribution as the crack length changes. The problem of calculating the pin bearing pressure distribution as the crack length changes is statically indeterminate, unless a fracture analysis, such as the finite element solution described before, is carried out. But, once a fracture analysis is made, then there is no need for the varying pin bearing pressure distribution, because the needed stress-intensity factors can be obtained from the fracture analysis. Thus, this method becomes redundant and is discarded.

The second method is to use available data of stress-intensity factors (from the finite element procedure, Figure 3-18) and the unflawed stress distribution on the prospective crack surface (Figure 3-4) to modify the Green's functions to account for the varying pin bearing pressure distribution. Such modifications have been made for the Green's function and are presented in Figures 3-26 through 3-28 for outer-to-inner radius ratios of 1.50, 2.25 and 3.00, respectively, whereas Figures 3-23 through 3-25 correspond to the original or unmodified Green's function. For calculating the stress-intensity factors in simple attachment lugs loaded by pins, the Green's functions in Figures 3-26 through 3-28 should be used. The Green's functions given in Figures 3-23 through 3-25 are still useful and needed in the analysis of attachment lugs where the unflawed stress distribution on the
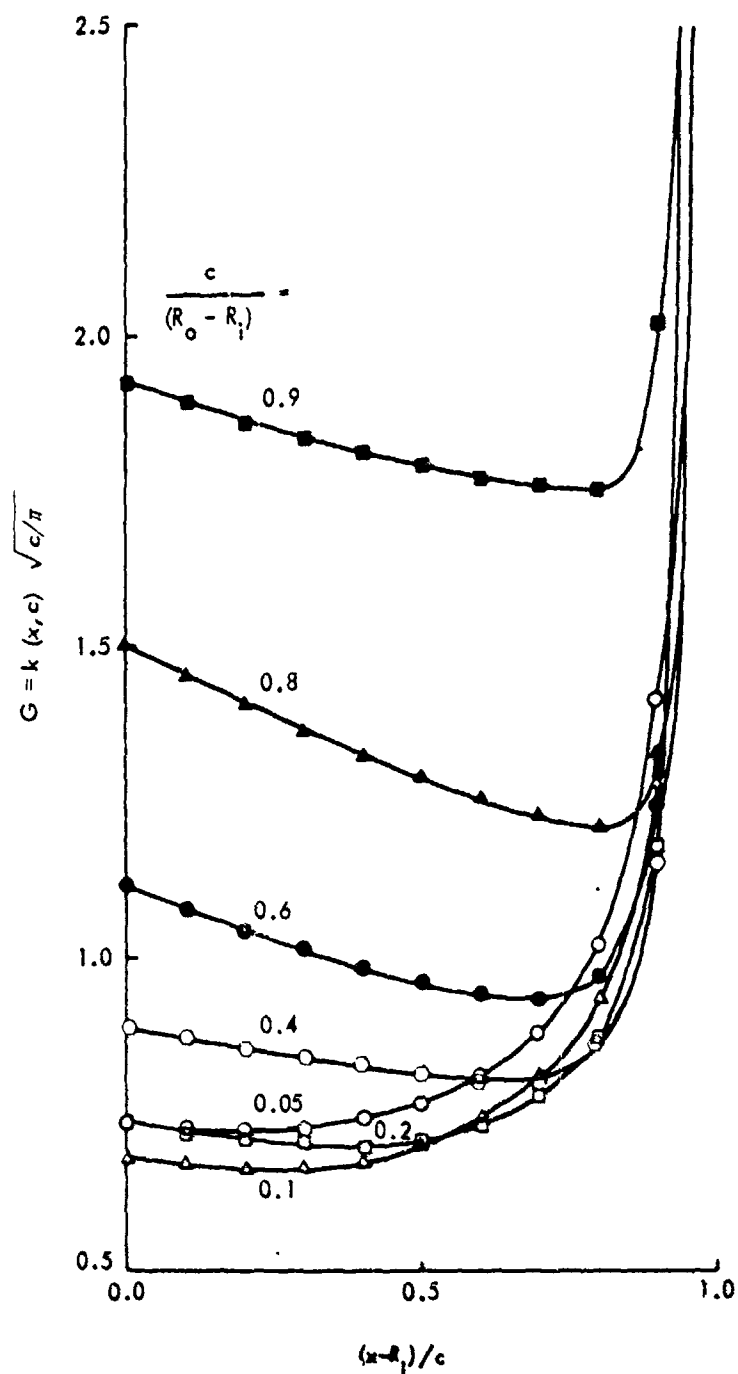
Figure 3-26.   Modified Weight Functions for a Single
Through-the-Thickness Crack at Straight
Attachment Lug Having a R_o/R_i Ratio of 1.50
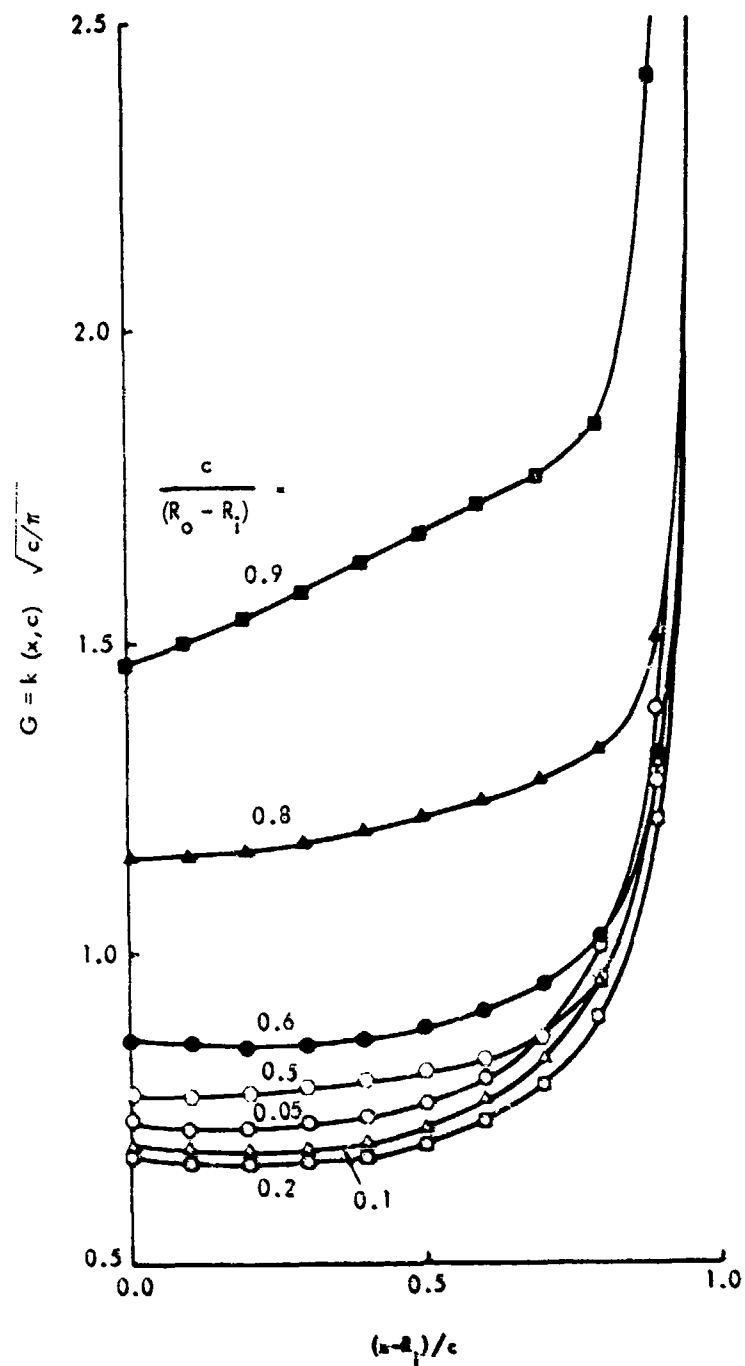
Figure 3-27. Modified Weight Functions for a Single
Through-the-Thickness Crack at Straight
Attachment Lug Having a R_o/R_i Ratio of 2.25
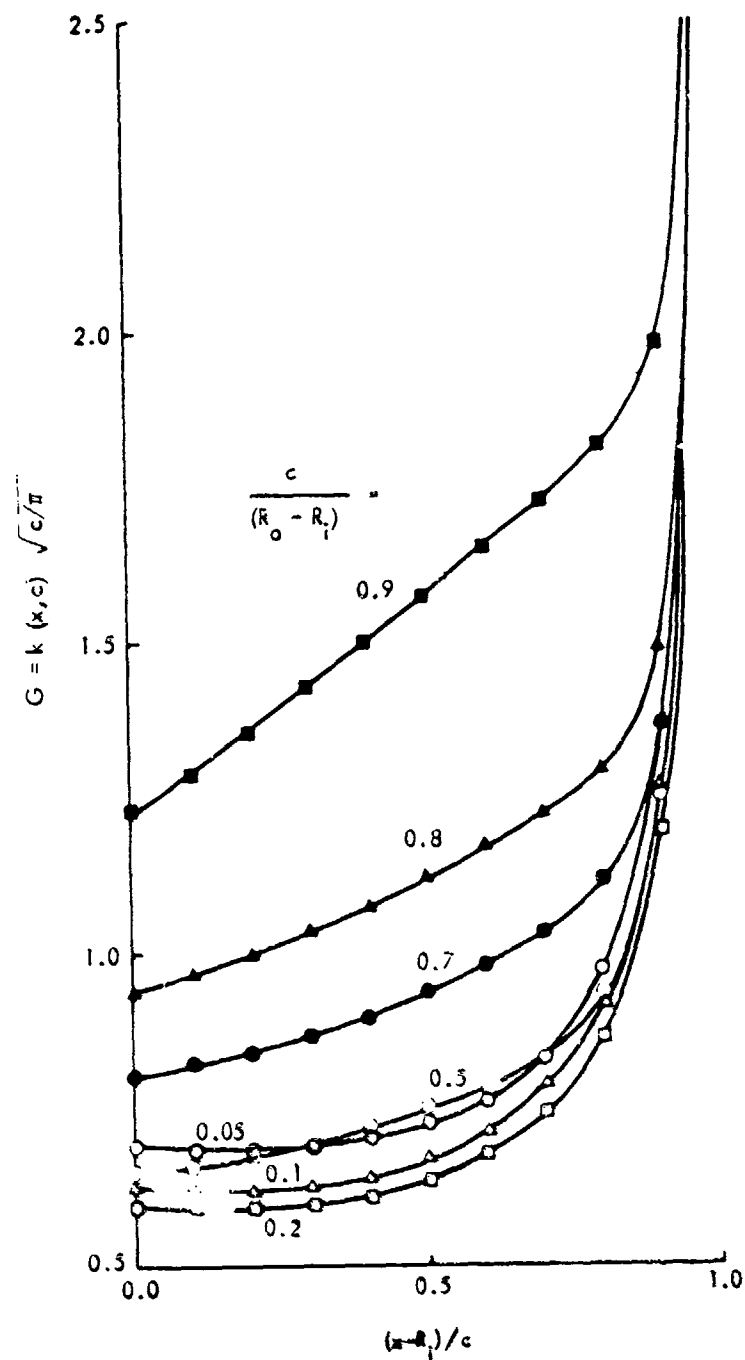
Figure 3-28. Modified Weight Functions for a Single Through-the-Thickness Crack at Straight Attachment Lug Having a R_o/R_i Ratio of 3.00

prospective crack surface does not depend on crack length, for example, residual stresses due to the installation of an interference-fit bushing. Tables 3-4 through 3-9 provide the original and modified Green's function values in a tabular form at several $(x-R_i)/c$ locations and different crack lengths for outer-to-inner radius ratios of 1.50, 2.25 and 3.00.

In order to put the results in perspective, Figure 3-29 compares the stress-intensity factors obtained by the compounding method, finite element method and original and modified Green's function methods. As can be seen from the figure, the results obtained by the modified Green's function method match the finite element solutions. The results of the original or unmodified Green's function method tend to be higher, especially for the R_o/R_i ratio of 1.50. The difference between the two Green's function methods essentially reflects the effect of pin bearing pressure distribution as the crack length changes.

Figure 3-29 also compares the compounding method solution to the other solutions. For R_o/R_i ratios of 2.25 and 3.00, the compounding solution gives excellent estimates of stress-intensity factors, except when the crack length is very small. The error at small crack lengths could be corrected by making proper use of the stress concentration factor values for the lugs, K_{tb}, given in Figure 3-5. However, for $R_o/R_i = 1.50$ the compounding solution tends to overestimate the stress-intensity factors, like the original Green's function method. This error may be partially due to the major differences between the true pin bearing pressure distribution and the idealized distribution used in the compounding method.

2.4 ANALYSIS OF LUGS WITH INTERFERENCE-FIT BUSHINGS

In order to improve the crack initiation and crack growth life, the concept of installing an interference-fit bushing to introduce beneficial residual stresses around the hole of the lug prior to pin fitting has been used in aircraft attachment lug design. For a given fatigue load cycle, the installation of an interference bushing can reduce the effective tangential stress range at the likely location of crack initiation, resulting in improvement in fatigue and crack growth life. It also reduces fretting damage of the hole wall of the lug.

57

TABLE 3–4. ORIGINAL WEIGHT FUNCTION FOR $R_o/R_i = 1.50$

$(x-R_i)/c$ \ $c/(R_o-R_i)$	0.0100	0.0500	0.1000	0.2000	0.4000	0.5000	0.6000	0.7000	0.8000	0.9000
0.0000	0.8341	0.6173	0.6091	0.7388	1.0495	1.2451	1.4503	1.6702	1.9145	2.2696
0.1000	0.8329	0.6115	0.6019	0.7179	1.0259	1.2099	1.4025	1.6096	1.8479	2.2321
0.2000	0.8349	0.6077	0.5981	0.7107	1.0046	1.1739	1.3520	1.5511	1.7874	2.1959
0.3000	0.8424	0.6114	0.5966	0.7025	0.9896	1.1451	1.3090	1.4981	1.7315	2.1698
0.4000	0.8579	0.6234	0.6053	0.6996	0.9781	1.1225	1.2749	1.4537	1.6822	2.1430
0.5000	0.8850	0.6444	0.6301	0.7100	0.9659	1.1022	1.2471	1.4165	1.6403	2.1214
0.6000	0.9303	0.6779	0.6728	0.7372	0.9535	1.0834	1.2236	1.3840	1.6032	2.1054
0.7000	1.0081	0.7375	0.7354	0.7844	0.9546	1.0769	1.2109	1.3580	1.5672	2.0801
0.8000	1.1564	0.8654	0.8439	0.8787	1.0150	1.1248	1.2447	1.3597	1.5429	2.0757
0.8250	1.2158	0.9209	0.8896	0.9212	1.0528	1.1583	1.2727	1.3731	1.5462	2.0987
0.8500	1.2912	0.9940	0.9507	0.9792	1.1082	1.2090	1.3168	1.3984	1.5595	2.1454
0.8750	1.3906	1.0934	1.0362	1.0617	1.1901	1.2856	1.3858	1.4431	1.5905	2.2300
0.9000	1.5282	1.2353	1.1624	1.1851	1.3151	1.4048	1.4963	1.5225	1.6543	2.3763
0.9250	1.7343	1.4526	1.3633	1.3837	1.5173	1.6009	1.6825	1.6691	1.7839	2.6285
0.9500	2.0872	1.8298	1.7264	1.7453	1.8838	1.9613	2.0324	1.9715	2.0692	3.0814
0.9750	2.8999	2.6953	2.5912	2.6107	2.7519	2.8243	2.8869	2.7874	2.8732	4.0337
0.9900	4.5359	4.3996	4.3203	4.3439	4.4783	4.5494	4.6137	4.5433	4.6415	5.7071

TABLE 3-5. ORIGINAL WEIGHT FUNCTION FOR $R_o/R_i = 2.25$

$c/(R_o-R_i)$ $(x-R_i)/c$	0.0100	0.0500	0.1000	0.2000	0.4000	0.5060	0.6000	0.7000	0.8000	0.9000
0.0000	0.8341	0.6336	0.6231	0.5499	0.7716	0.8609	0.9616	1.0950	1.2663	1.6029
0.1000	0.8329	0.6188	0.6143	0.6425	0.7651	0.8563	0.9594	1.0935	1.2708	1.6421
0.2000	0.8349	0.6192	0.6133	0.6405	0.7725	0.8581	0.9557	1.0938	1.2806	1.6825
0.3000	0.8424	0.6272	0.6136	0.6401	0.7861	0.8663	0.9583	1.0989	1.2946	1.7318
0.4000	0.8579	0.6391	0.6223	0.6476	0.8009	0.8795	0.9699	1.1120	1.3139	1.7795
0.5000	0.8850	0.6559	0.6462	0.6691	0.8152	0.8966	0.9906	1.1333	1.3396	1.8307
0.6000	0.9303	0.6848	0.6876	0.7066	0.8337	0.9195	1.0194	1.1620	1.3715	1.8869
0.7000	1.0081	0.7436	0.7485	0.7627	0.8722	0.9590	1.0606	1.2004	1.4087	1.9339
0.8000	1.1564	0.8772	0.8544	0.8644	0.9757	1.0536	1.1443	1.2646	1.4613	2.0228
0.8250	1.2158	0.9353	0.8953	0.9084	1.0250	1.0985	1.1834	1.2915	1.4836	2.0846
0.8500	1.2912	1.0114	0.9597	0.9679	1.0920	1.1601	1.2378	1.3283	1.5156	2.1861
0.8750	1.3906	1.1143	1.0443	1.0519	1.1857	1.2475	1.3165	1.3815	1.5647	2.3538
0.9000	1.5282	1.2598	1.1695	1.1767	1.3224	1.3771	1.4359	1.4640	1.6456	2.6352
0.9250	1.7343	1.4806	1.3695	1.3767	1.5361	1.5834	1.6307	1.6050	1.7914	3.1200
0.9500	2.0872	1.8601	1.7315	1.7397	1.9128	1.9533	1.9893	1.8877	2.0915	3.9658
0.9750	2.8999	2.7241	2.5948	2.6069	2.7859	2.8242	2.8546	2.6836	2.9071	5.3068
0.9900	4.5359	4.4213	4.3226	4.3415	4.5066	4.5520	4.5922	4.4683	4.6746	6.6985

TABLE 3-6. ORIGINAL WEIGHT FUNCTION FOR $R_o/R_i = 3.00$

$(x-R_i)/c$ \ $c/(R_o-R_i)$	0.0100	0.0500	0.1000	0.2000	0.4000	0.5000	0.6000	0.7000	0.8000	0.9000
0.0000	0.8341	0.6075	0.5687	0.5745	0.6332	0.6912	0.7601	0.8604	0.9933	1.2663
0.1000	0.8329	0.6035	0.5650	0.5688	0.6398	0.7021	0.7754	0.8802	1.0232	1.3341
0.2000	0.8349	0.5993	0.5653	0.5705	0.6581	0.7188	0.7907	0.9024	1.0582	1.4055
0.3000	0.8424	0.6025	0.5683	0.5746	0.6822	0.7414	0.8117	0.9294	1.0969	1.4802
0.4000	0.8579	0.6150	0.5810	0.5866	0.7078	0.7689	0.8410	0.9629	1.1397	1.5567
0.5000	0.8850	0.6371	0.6091	0.6124	0.7332	0.8001	0.8787	1.0038	1.1877	1.6342
0.6000	0.9303	0.6719	0.6548	0.6554	0.7619	0.8362	0.9236	1.0513	1.2409	1.7127
0.7000	1.0081	0.7323	0.7207	0.7196	0.8087	0.8865	0.9788	1.1062	1.2988	1.7937
0.8000	1.1564	0.8597	0.8326	0.8311	0.9181	0.9886	1.0724	1.1870	1.3710	1.8832
0.8250	1.2158	0.9149	0.8791	0.8775	0.9684	1.0348	1.1132	1.2203	1.3978	1.9103
0.8500	1.2912	0.9875	0.9410	0.9393	1.0363	1.0974	1.1689	1.2661	1.4341	1.9425
0.8750	1.3906	1.0865	1.0272	1.0254	1.1310	1.1857	1.2486	1.3326	1.4872	1.9847
0.9000	1.5282	1.2278	1.1540	1.1522	1.2688	1.3162	1.3690	1.4361	1.5718	2.0470
0.9250	1.7343	1.4447	1.3556	1.3540	1.4842	1.5237	1.5648	1.6109	1.7209	2.1546
0.9500	2.0872	1.8217	1.7195	1.7191	1.8641	1.8965	1.9260	1.9483	2.0244	2.3829
0.9750	2.8999	2.6880	2.5855	2.5896	2.7452	2.7755	2.7991	2.8058	2.8463	3.0752
0.9900	4.5359	4.3942	4.3162	4.3290	4.4779	4.5170	4.5514	4.5790	4.6265	4.7832

TABLE 3-7. MODIFIED WEIGHT FUNCTION FOR $R_o/R_i = 1.50$

$c/(R_o-R_i)$ $(x-R_i)/c$	0.0100	0.0500	0.1000	0.2000	0.4000	0.5000	0.6000	0.7000	0.8000	0.9000
0.0000	0.8341	0.7366	0.6768	0.7388	0.8909	0.9981	1.1199	1.2895	1.5063	1.9234
0.1000	0.8329	0.7296	0.6692	0.7179	0.8709	0.9703	1.0833	1.2426	1.4538	1.8916
0.2000	0.8349	0.7253	0.6641	0.7107	0.8527	0.9414	1.0439	1.1970	1.4064	1.8609
0.3000	0.8424	0.7293	0.6635	0.7025	0.8403	0.9188	1.0107	1.1558	1.3623	1.8388
0.4000	0.8579	0.7433	0.6738	0.6996	0.8308	0.9012	0.9846	1.1213	1.3235	1.8161
0.5000	0.8850	0.7690	0.7001	0.7100	0.8199	0.8846	0.9630	1.0924	1.2906	1.7978
0.6000	0.9303	0.8110	0.7454	0.7372	0.8081	0.8686	0.9445	1.0669	1.2614	1.7843
0.7000	1.0081	0.8828	0.8152	0.7844	0.8087	0.8639	0.9361	1.0473	1.2327	1.7628
0.8000	1.1564	1.0248	0.9400	0.8787	0.8662	0.9117	0.9732	1.0551	1.2159	1.7592
0.8250	1.2158	1.0835	0.9915	0.9212	0.9026	0.9447	1.0017	1.0702	1.2210	1.7793
0.8500	1.2912	1.1593	1.0590	0.9792	0.9561	0.9943	1.0458	1.0968	1.2357	1.8201
0.8750	1.3906	1.2604	1.1513	1.0617	1.0358	1.0696	1.1146	1.1428	1.2674	1.8948
0.9000	1.5282	1.4021	1.2845	1.1851	1.1585	1.1875	1.2247	1.2230	1.3307	2.0259
0.9250	1.7343	1.6158	1.4916	1.3837	1.3591	1.3831	1.4116	1.3701	1.4577	2.2577
0.9500	2.0872	1.9823	1.8574	1.7453	1.7277	1.7479	1.7673	1.6739	1.7379	2.6937
0.9750	2.8999	2.8208	2.7119	2.6107	2.6119	2.6338	2.6490	2.5017	2.5437	3.6803
0.9900	4.5359	4.4870	4.4118	4.3439	4.3735	4.4074	4.4346	4.3048	4.3578	5.4679

TABLE 3-8. MODIFIED WEIGHT FUNCTION FOR $R_o/R_i = 2.25$

$(x-R_i)/c$ \ $c/(R_o-R_i)$	0.0100	0.0500	0.1000	0.2000	0.4000	0.5000	0.6000	0.7000	0.8000	0.9000
0.0000	0.8341	0.7325	0.6916	0.6721	0.7112	0.7750	0.8548	0.9833	1.1491	1.4638
0.1000	0.8329	0.7186	0.6822	0.6646	0.7043	0.7704	0.8528	0.9818	1.1531	1.4997
0.2000	0.8349	0.7173	0.6802	0.6623	0.7116	0.7723	0.8495	0.9822	1.1621	1.5365
0.3000	0.8424	0.7239	0.6816	0.6621	0.7249	0.7802	0.8518	0.9868	1.1748	1.5816
0.4000	0.8579	0.7370	0.6920	0.6701	0.7387	0.7923	0.8622	0.9985	1.1923	1.6251
0.5000	0.8850	0.7583	0.7172	0.6919	0.7513	0.8073	0.8805	1.0176	1.2156	1.6719
0.6000	0.9303	0.7947	0.7609	0.7301	0.7673	0.8272	0.9059	1.0432	1.2446	1.7232
0.7000	1.0081	0.8629	0.8288	0.7882	0.8027	0.8629	0.9432	1.0779	1.2782	1.7661
0.8000	1.1564	1.0059	0.9507	0.8946	0.9023	0.9533	1.0228	1.1384	1.3269	1.8474
0.8250	1.2158	1.0657	1.0013	0.9403	0.9506	0.9972	1.0610	1.1649	1.3484	1.9041
0.8500	1.2912	1.1430	1.0678	1.0017	1.0165	1.0576	1.1144	1.2012	1.3794	1.9977
0.8750	1.3906	1.2461	1.1590	1.0878	1.1093	1.1441	1.1922	1.2545	1.4276	2.1530
0.9000	1.5282	1.3901	1.2910	1.2149	1.2455	1.2731	1.3111	1.3377	1.5075	2.4157
0.9250	1.7343	1.6064	1.4969	1.4170	1.4596	1.4797	1.5062	1.4803	1.6523	2.8752
0.9500	2.0872	1.9759	1.8613	1.7814	1.8393	1.8529	1.8682	1.7659	1.9520	3.7044
0.9750	2.8999	2.8174	2.7142	2.6461	2.7229	2.7367	2.7474	2.5661	2.7736	5.1196
0.9900	4.5359	4.4854	4.4130	4.3718	4.4614	4.4882	4.5127	4.3692	4.5652	6.6282

TABLE 3-9. MODIFIED WEIGHT FUNCTION FOR $R_o/R_i = 3.00$.

$(x-R_i)/c$ \ $c/(R_o-R_i)$	0.0100	0.0500	0.1000	0.2000	0.4000	0.5000	0.6000	0.7000	0.8000	0.9000
0.0000	0.8341	0.6943	0.6263	0.5991	0.6054	0.6500	0.7084	0.8045	0.9371	1.2235
0.1000	0.8329	0.6896	0.6225	0.5932	0.6113	0.6600	0.7227	0.8231	0.9653	1.2890
0.2000	0.8349	0.6850	0.6223	0.5947	0.6290	0.6759	0.7369	0.8437	0.9983	1.3580
0.3000	0.8424	0.6884	0.6264	0.5994	0.6523	0.6974	0.7565	0.8689	1.0348	1.4301
0.4000	0.8579	0.7024	0.6409	0.6121	0.6770	0.7233	0.7838	0.9002	1.0752	1.5041
0.5000	0.8850	0.7281	0.6708	0.6386	0.7010	0.7525	0.8189	0.9384	1.1205	1.5789
0.6000	0.9303	0.7693	0.7193	0.6827	0.7279	0.7860	0.8607	0.9828	1.1707	1.6548
0.7000	1.0081	0.8388	0.7921	0.7497	0.7726	0.8335	0.9125	1.0342	1.2252	1.7330
0.8000	1.1564	0.9770	0.9191	0.8674	0.8793	0.9323	1.0027	1.1114	1.2939	1.8196
0.8250	1.2158	1.0347	0.9709	0.9161	0.9288	0.9775	1.0426	1.1439	1.3199	1.8459
0.8500	1.2912	1.1097	1.0387	0.9804	0.9960	1.0392	1.0975	1.1887	1.3552	1.8774
0.8750	1.3906	1.2104	1.1313	1.0692	1.0899	1.1265	1.1763	1.2543	1.4074	1.9188
0.9000	1.5282	1.3522	1.2647	1.1990	1.2272	1.2563	1.2959	1.3568	1.4910	1.9805
0.9250	1.7343	1.5672	1.4722	1.4038	1.4424	1.4635	1.4914	1.5309	1.6391	2.0876
0.9500	2.0872	1.9373	1.8390	1.7708	1.8236	1.8375	1.8537	1.8685	1.9418	2.3156
0.9750	2.8999	2.7843	2.6962	2.6386	2.7100	2.7233	2.7341	2.7310	2.7661	3.0091
0.9900	4.5359	4.4618	4.4005	4.3670	4.4523	4.4783	4.5025	4.5198	4.5601	4.7246
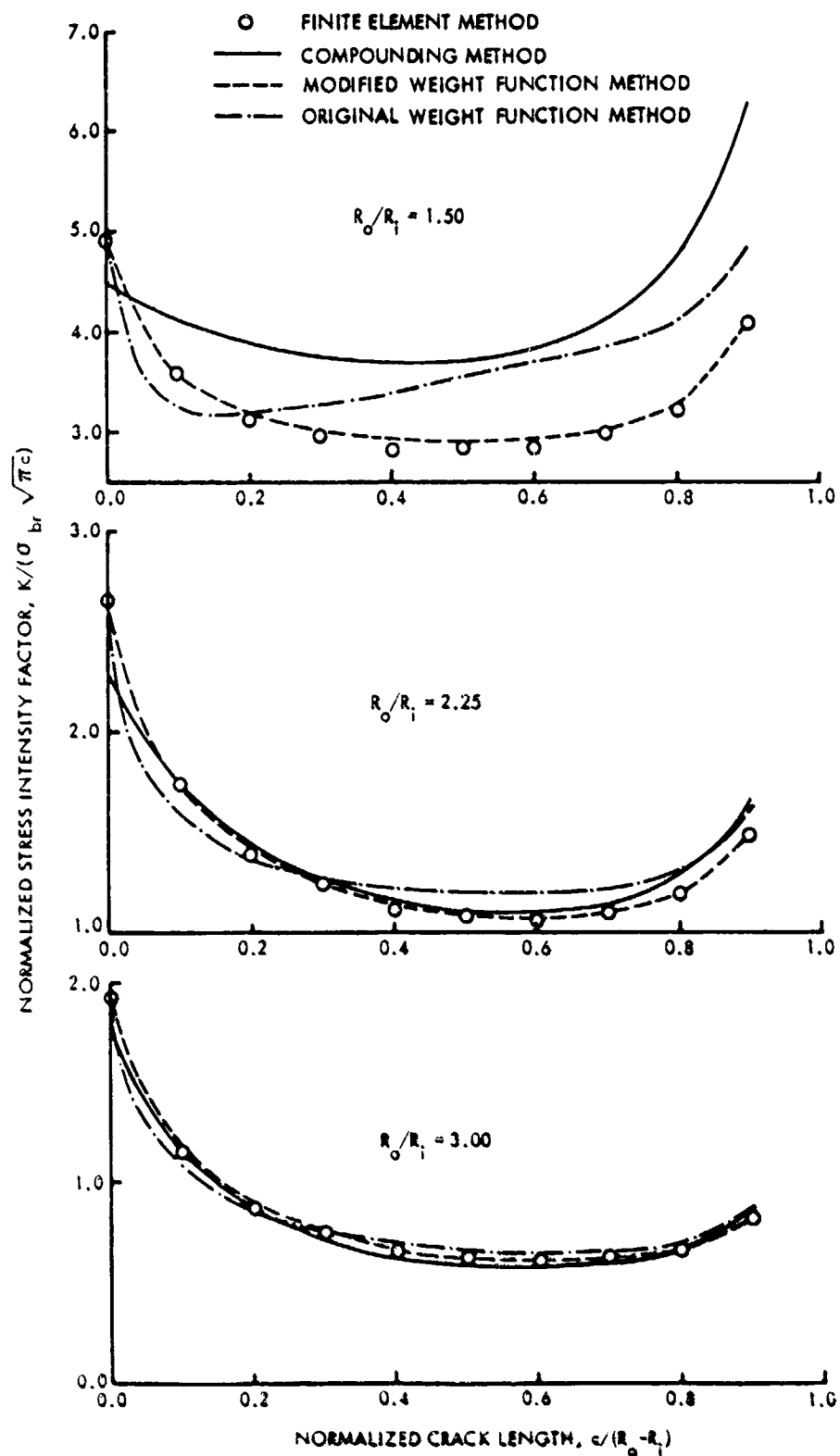
Figure 3-29. Comparison of Stress Intensity Factors Computed Using the Compounding, Weight Function and Cracked Finite Element Methods

64

The stress-intensity factors for a crack emanating from an attachment lug having an interference-fit bushing can be estimated using the weight function approach similar to the one reported in Reference [34]. The procedure consists of two major steps. First, the effective unflawed stress distribution on the prospective crack surface was obtained by superimposing the residual hoop stresses, σ_{re}, due to the installation of an intereference-fit bushing on the applied tangential stresses, σ_{ap}, obtained due to the application of a pin loading. Next, a crack was introduced in this stress field by removing the tractions on the crack faces and computing the corresponding effective stress-intensity factor using the developed weight function, G, and the following equation:

$$K = \sqrt{\pi c} \int_{0}^{1} (\sigma_{ap} + \sigma_{re}) \cdot G(c, \xi) d\xi \tag{24}$$

Unflawed Stress Analysis

The installation of an interference-fit bushing creates a compressive radial stress and a tensile hoop stress in the lug in a manner similar to a thick wall cylinder under internal pressure. On this basis, an approach similar to that of Seely and Smith [35] for a thick-wall cylinder under internal pressure is used to compute the residual stresses in the lug due to the installation of an interference-fit bushing. Before the residual stresses in the lug can be computed, the pressure, P_s, on the surface of contact between the bushing and the lug must be determined.

Let R_o and R_i denote outer and inner radii of the lug and r_o and r_i denote outer and inner radii of the bushing before the interference-fit installation, respectively. Let R_1 be the inner radius of the lug (and also the outer radius of the bushing) after installation, and let δ_R be the difference in these radii before installation.

$$\delta_R \quad r_o - R_i \tag{25}$$

After the installation of the bushing, the inner radius of the lug will be larger than its initial value by an amount, δ_1, which is related to the unknown contact pressure as

$$\delta_1 = \frac{P_s R_1}{E_L} \left(\frac{R_o^2 + R_1^2}{R_o^2 - R_1^2} + \mu_L \right) \tag{26}$$

where E_L and μ_L are the Young's modulus and Poisson's ratio of the lug. At the same time, the outer radius of the bushing will be changed (decreased) by an amount, δ_2, which is given by the following equation:

$$\delta_2 = \frac{P_s R_1}{E_B} \left(\frac{R_1^2 + r_i^2}{R_1^2 - r_i^2} - \mu_B \right) \tag{27}$$

where E_B and μ_B are the Young's modulus and Poisson's ratio of the bushing.

At the completion of the installation process, the difference in these original radii, δ_R, disappears as a result of the changes in the length δ_1 and δ_2. Therefore, the sum of the magnitudes of δ_1 and δ_2 is equal to δ_R i.e.,

$$\delta_R = \frac{P_s R_1}{E_L} \left[\left(\frac{R_o^2 + R_1^2}{R_o^2 - R_1^2} + \mu_L \right) + \frac{E_L}{E_B} \left(\frac{R_1^2 + r_i^2}{R_1^2 - r_i^2} - \mu_B \right) \right] \tag{28}$$

The contact pressure is obtained from the above equation as

$$P_s = \delta_R E_L \bigg/ R_1 \left[\left(\frac{R_o^2 + R_1^2}{R_o^2 - R_1^2} + \mu_L \right) + \frac{E_L}{E_B} \left(\frac{R_1^2 + r_i^2}{R_1^2 - r_i^2} - \mu_B \right) \right] \tag{29}$$

With contact pressure determined, the residual stresses in the lug due to the installation of an interference-fit bushing can be calculated using the following equations:

66

$$\sigma_\theta = \frac{P_s R_1^2}{R_o^2 - R_1^2} \left[\frac{R_o^2}{x^2} + 1 \right]$$

and $\qquad\qquad\qquad\qquad\qquad\qquad\qquad\qquad ; \quad x \geq R_i \qquad\qquad$ (30)

$$\sigma_r = \frac{P_s R_1^2}{R_o^2 - R_1^2} \left[\frac{R_o^2}{x^2} - 1 \right]$$

where x is the radial distance as shown in Figure 3-30.

Equation (30) can be used to compute the residual tangential stresses along the radial direction (x-axis) in attachment lugs due to the installation of interference-fit bushings. In the following discussion, results are presented for attachment lugs with lug outer radius to bushing inner radius ratio (R_o/r_i) of 2.25. The nondimensional parameters considered in the analysis are interference levels (δ_R/r_i), bushing-to-lug rigidity (E_B/E_L) and bushing thickness $t_B/r_i)$. The effects of these parameters on the stress distribution along the x-axis in attachment lugs are presented in Figures 3-30 through 3-32. Figure 3-30 shows the increase in residual stresses with increasing diametral interference for a bushing-to-lug rigidity ratio (E_B/E_L) of 3.0 and a bushing thickness (t_B/r_i) of 0.12. Figure 3-31 shows the increase in residual stresses with incrasing bushing-to-lug rigidity ratio (E_B/E_L) for a bushing thickness (t_B/r_i) of 0.12 and an interference level (δ_R/r_i) of 0.00533. Figure 3-32 shows the increase in residual stresses with increasing bushing thickness (t_B/r_i) for a bushing-to-lug rigidity ratio (E_B/E_L) of 3.0 and an interference level (δ_R/r_i) of 0.00533.

The tangential stresses along the x-axis due to the application of pin loading are then computed using the finite element method. In the analysis, it is assumed that the bushing and the lug remain in contact and that no slippage occurs along the hole wall surface during the application of the load. The computed tangential stress normalized by the far-field applied stress for a lug with a R_o/r_i of 2.25 are shown in Figures 3-33 and 3-34. Figure 3-33 depicts the decrease in stresses due to pin loading with increasing bushing-to-lug rigidity ratio (E_B/E_L) for a constant bushing thickness (t_B/r_i) of 0.12. Figure 3-34 presents the decrease in stresses due to pin loading with increasing bushing thickness (t_B/r_i) for a constant bushing-to-lug rigidity ratio (E_B/E_L) of 3.0
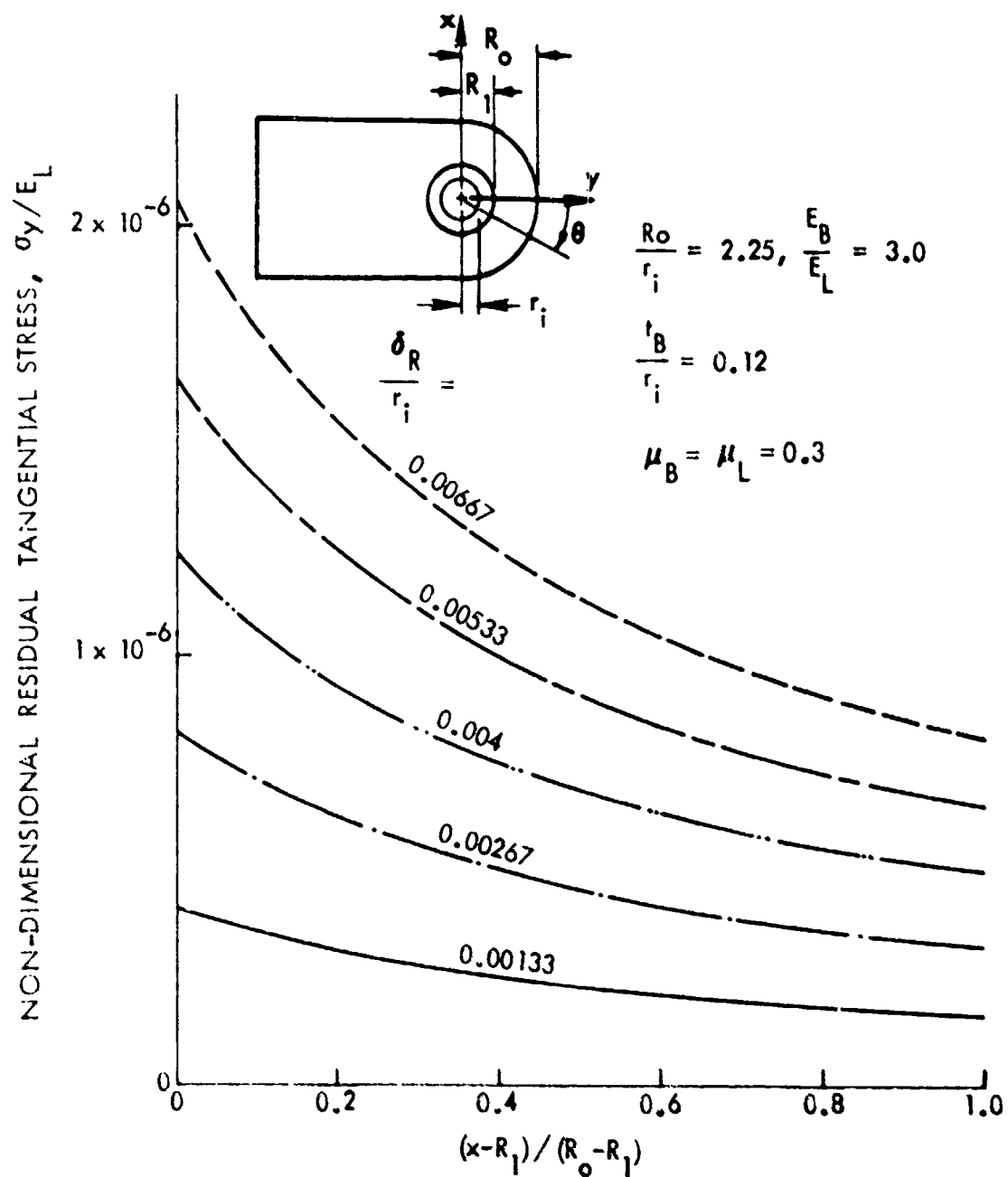
Figure 3-30. Stress Distributions Along x-Axis in an Attachment Lug With Bushing for Various Levels of Interference
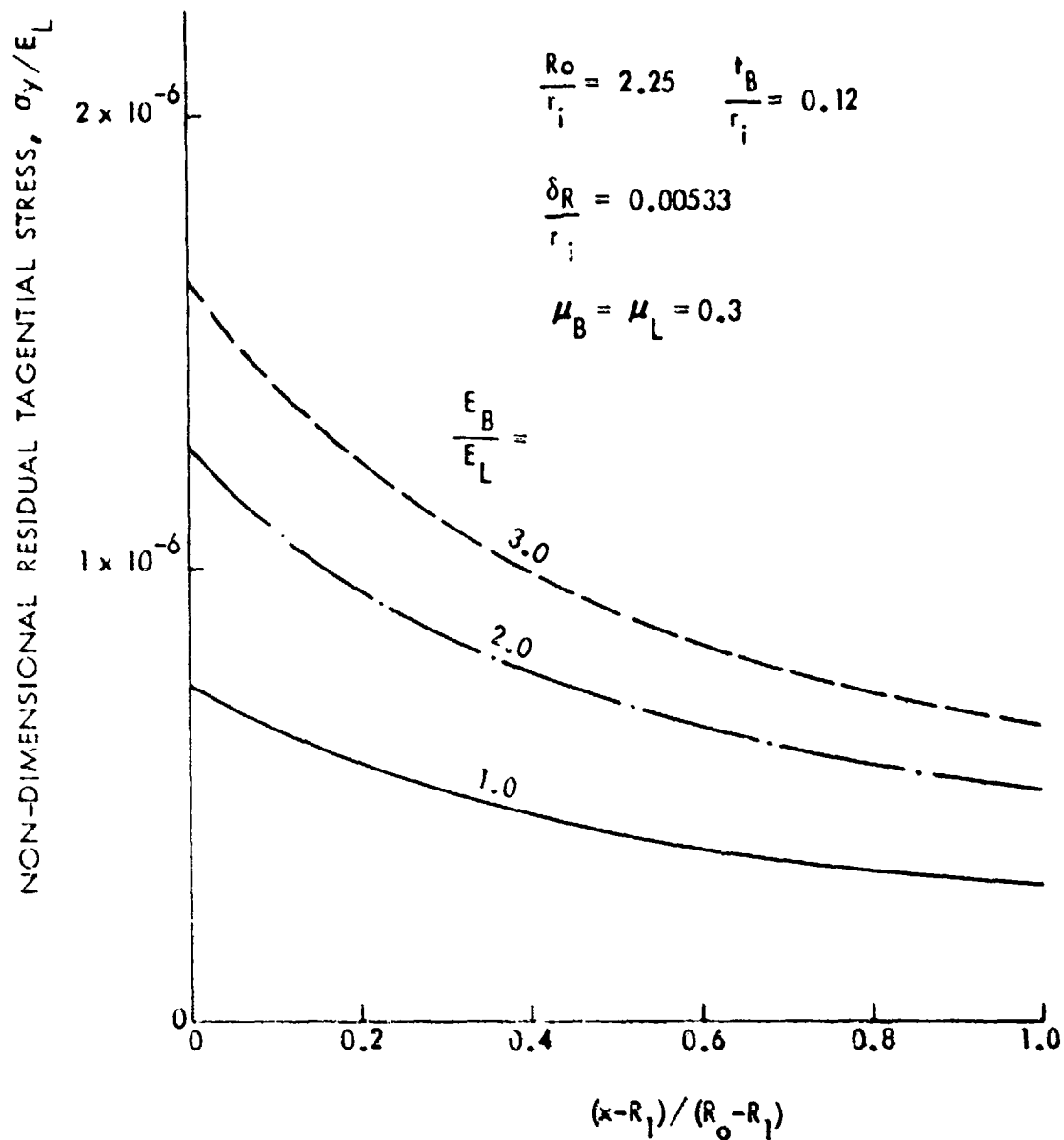
Figure 3-11. Stress Distributions Along x-Axis in an Attachment Lug With Bushing for Various Bushing-to-Lug Rigidity Ratios
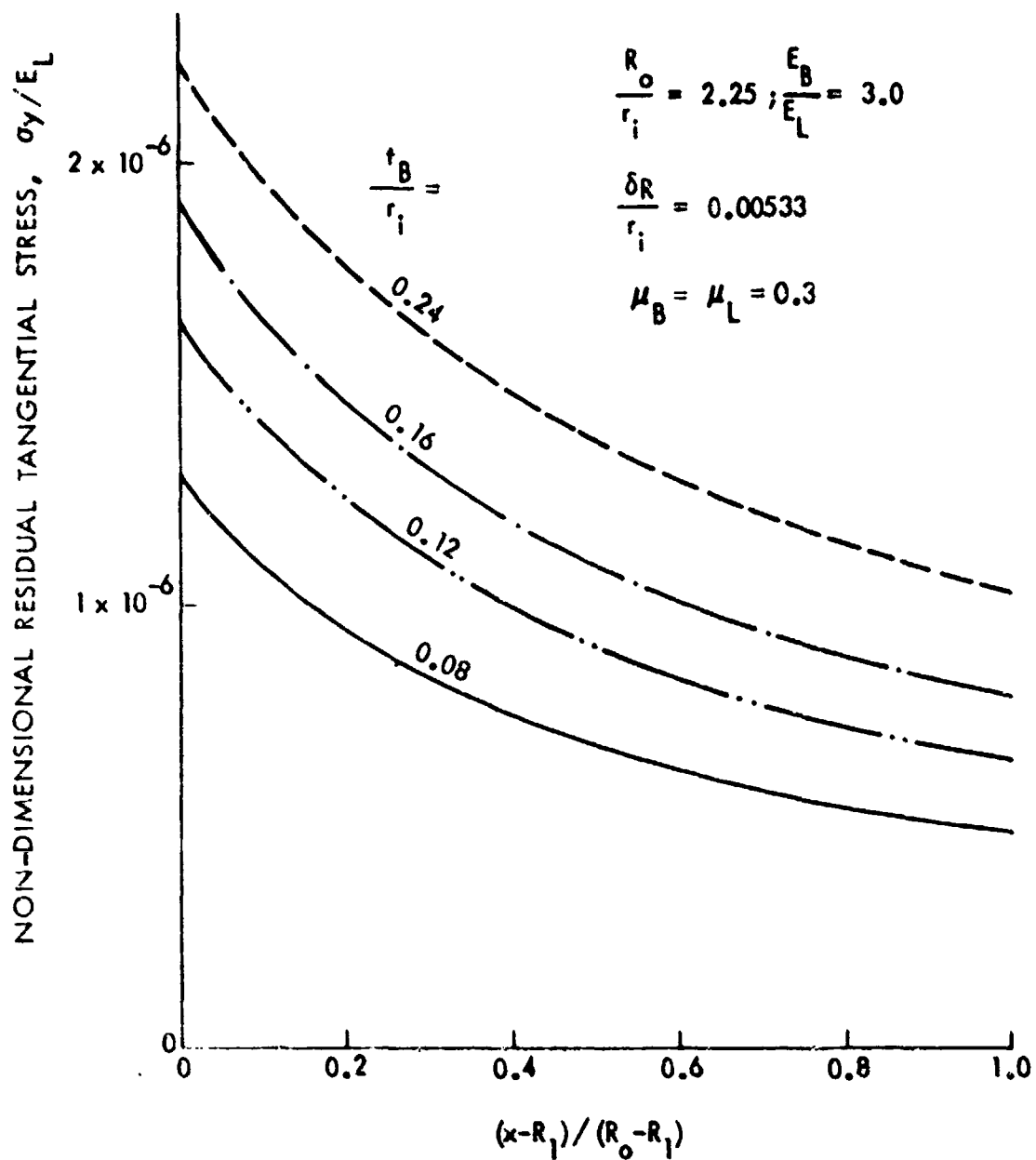
Figure 3-32. Stress Distributions Along x-Axis in an Attachment Lug
With Bushing for Various Bushing Thicknesses
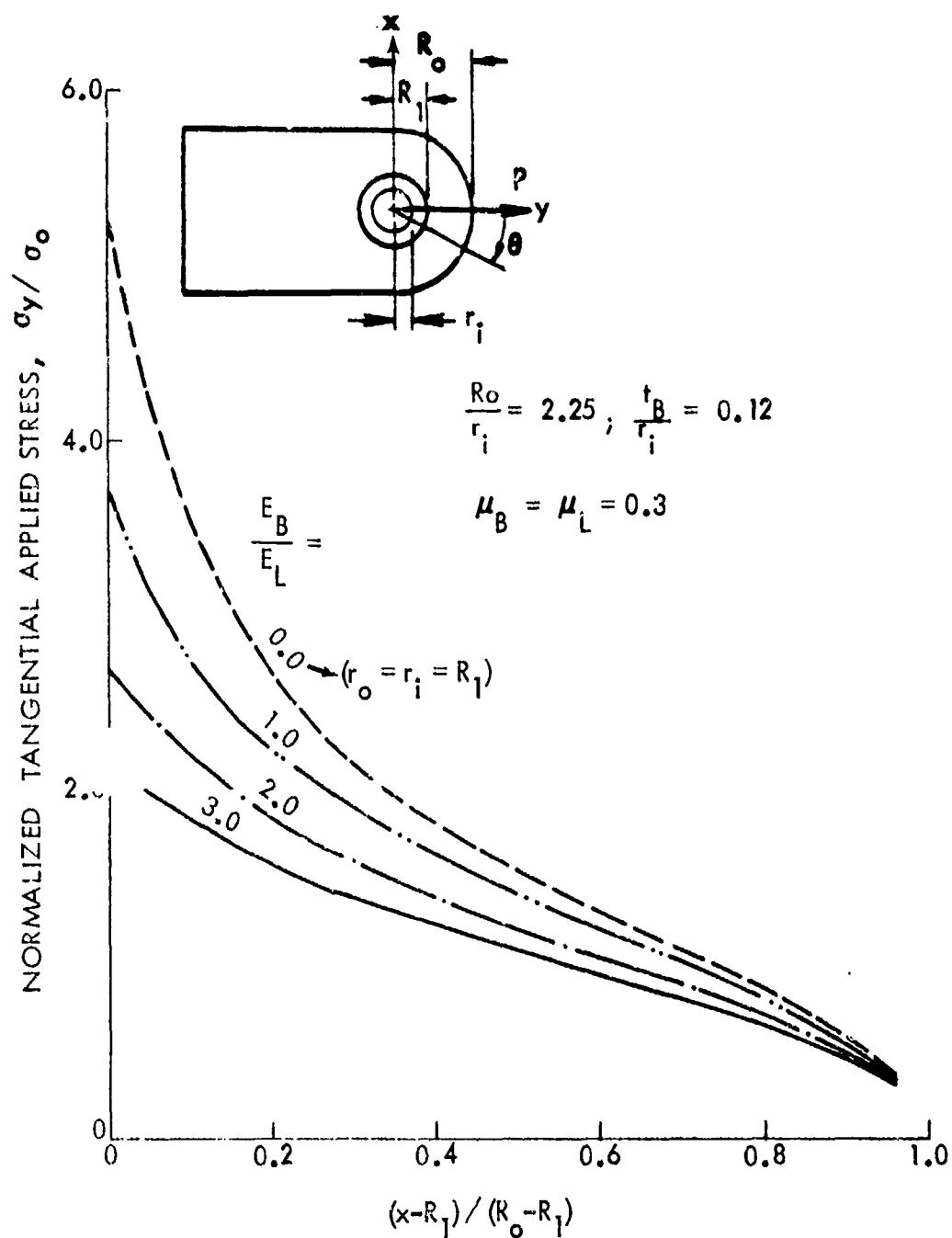
Figure 3-33. Stress Distributions Along x-Axis in an Attachment Lug
With Bushing Due to Pin Loading for Various
Bushing-to-Lug Rigidity Ratios
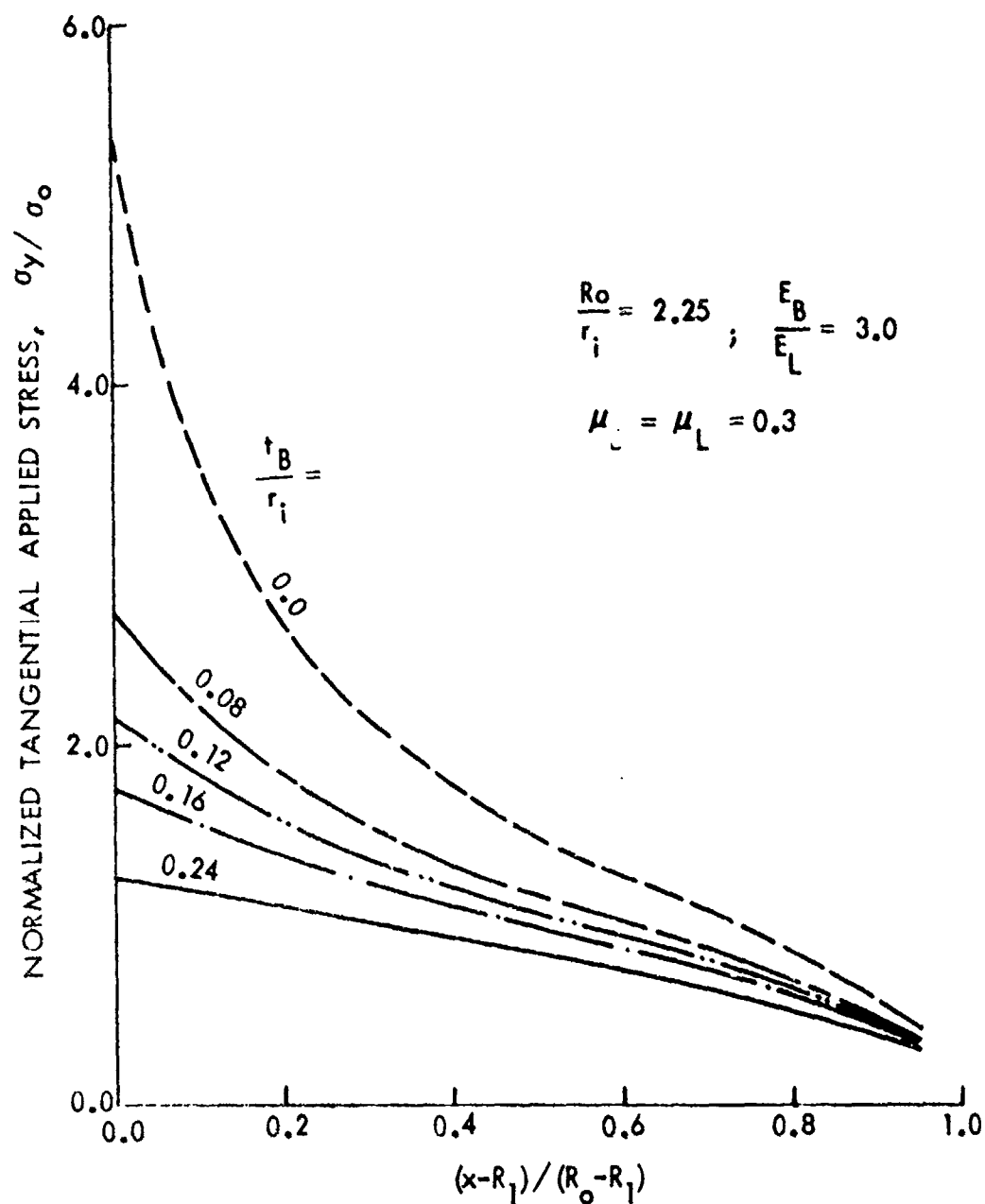
Figure 3-34. Stress Distributions Along x-Axis in an Attachment Lug
With Bushing Due to Pin Loading for Various
Bushing Thicknesses

The results presented in Figures 3-30 through 3-34 pertaining to the stress analysis of lugs with bushings should be used with caution in the sense that they can be used as long as the assumptions are not violated. In other words, these results can be used as long as there is sufficient interference to prevent separation between the bushing and the lug. When the interference level is small and/or when the crack length is large there will be separation, which again depends on the geometry and the magnitude of the applied loading. Also, the above results cannot be used when the total effective stress (residual stress plus applied stress) exceeds the material yield strength. If the total effective stress exceeds the material yield strength, a nonlinear elasto-plastic finite element analysis such as used in Reference [34] should be conducted to obtain the total effective stress. In the current study, only the linear analysis is performed. Once the total tangential stresses are obtained by superposing residual stresses and the applied stresses, then they can be used to calculate the stress intensity factors for a crack emanating from an attachment lug having an interference-fit bushing by using Equation (24) where $G(c,\xi)$ is the original or unmodified Green's function.

Stress-Intensity Factor Analysis

To study the effects of various parameters on actual (dimensional) stress-intensity factors rather than nondimensional, a physical lug having an outer radius of 1.6875 inches with a bushing inner radius of 0.75 inch ($R_o/r_i = 2.25$) subjected to a far field stress (σ_o) of 6 ksi and stress ratio (R_{far}) of 0.1 is considered in this discussion. For this lug configuration and loading, an effective stress ratio (R_{eff}) at the lug hole wall ($x = R_i$) as a function of interference levels can be computed and is presented in Figure 3-35a. Figure 3-35b shows the variation of R_{eff} along the x-axis of the lug for an interference level (δ_R/r_i) of 0.00533. It is seen from the figure that R_{eff} is constant almost throughout the net section (x-axis) except near the outer surface of the lug.

The stress-intensity factors were computed using Equation (24) and are presented in Figures 3-36 and 3-37. Figure 3-36 shows the effective stress-intensity factor range, ΔK, for various bushing-to-lug rigidities (E_B/E_L) for a given bushing thickness (t_B/r_i) of C.12. The data corresponding to $E_B/E_L = 0$ represent a simple lug with no bushing. It is clear from

73

(a)

$\frac{R_o}{r_i} = 2.25; E_B/E_L = 3.0$

$t_B/r_i = 0.12; x/R_1 = 1.0$

$\sigma_o = 6 \text{ KSI}; R = 0.1$

$r_i = 0.75 \text{ IN}$

(b)

$\frac{R_o}{r_i} = 2.25; \frac{E_B}{E_L} = 3.0$

$\frac{t_b}{r_i} = 0.12; \frac{\delta_R}{r_i} = 0.00267$

$\sigma_o = 6 \text{ KSI}; R = 0.1$

$r_i = 0.75 \text{ IN}$
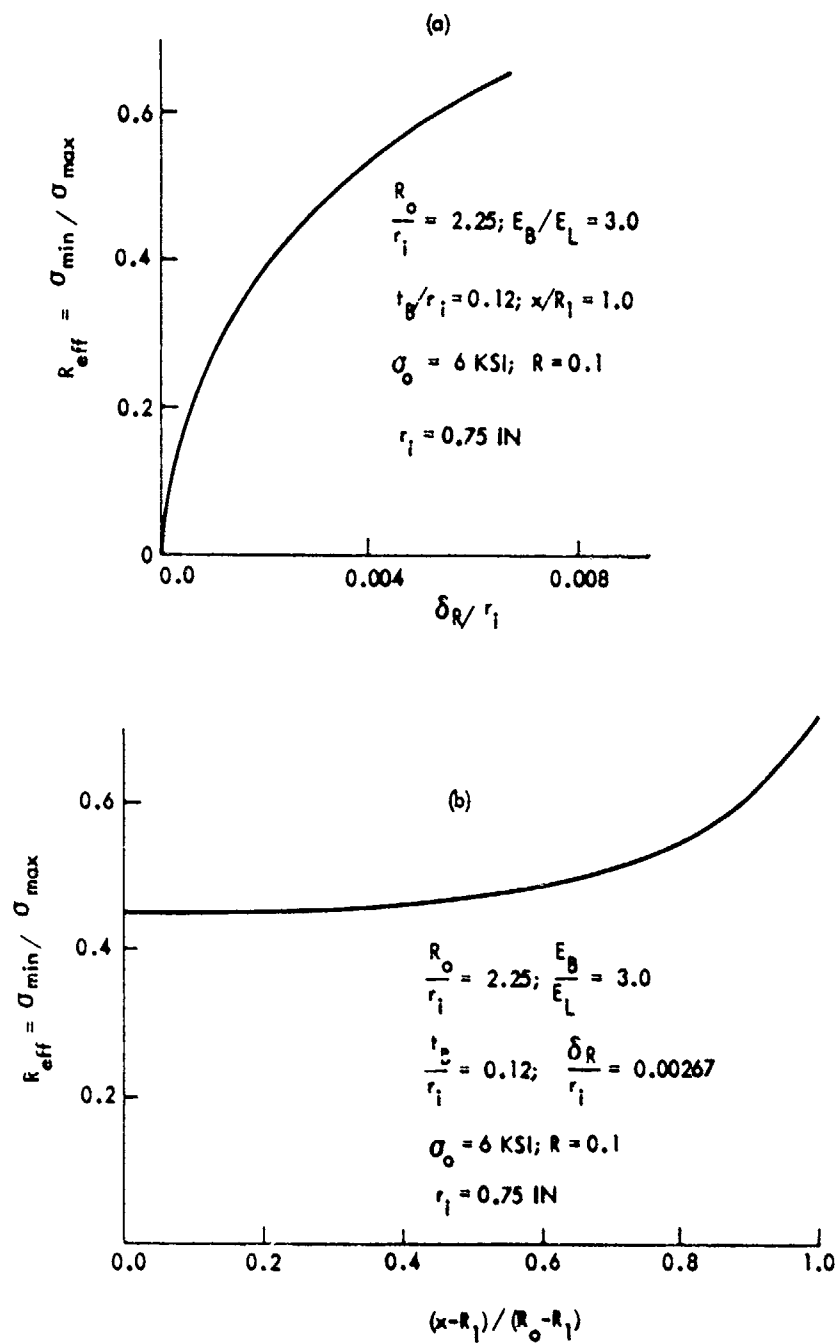
Figure 3-35.   Effective Stress Ratio in an Attachment Lug with Bushing for Various Interference Levels and Along x-Axis
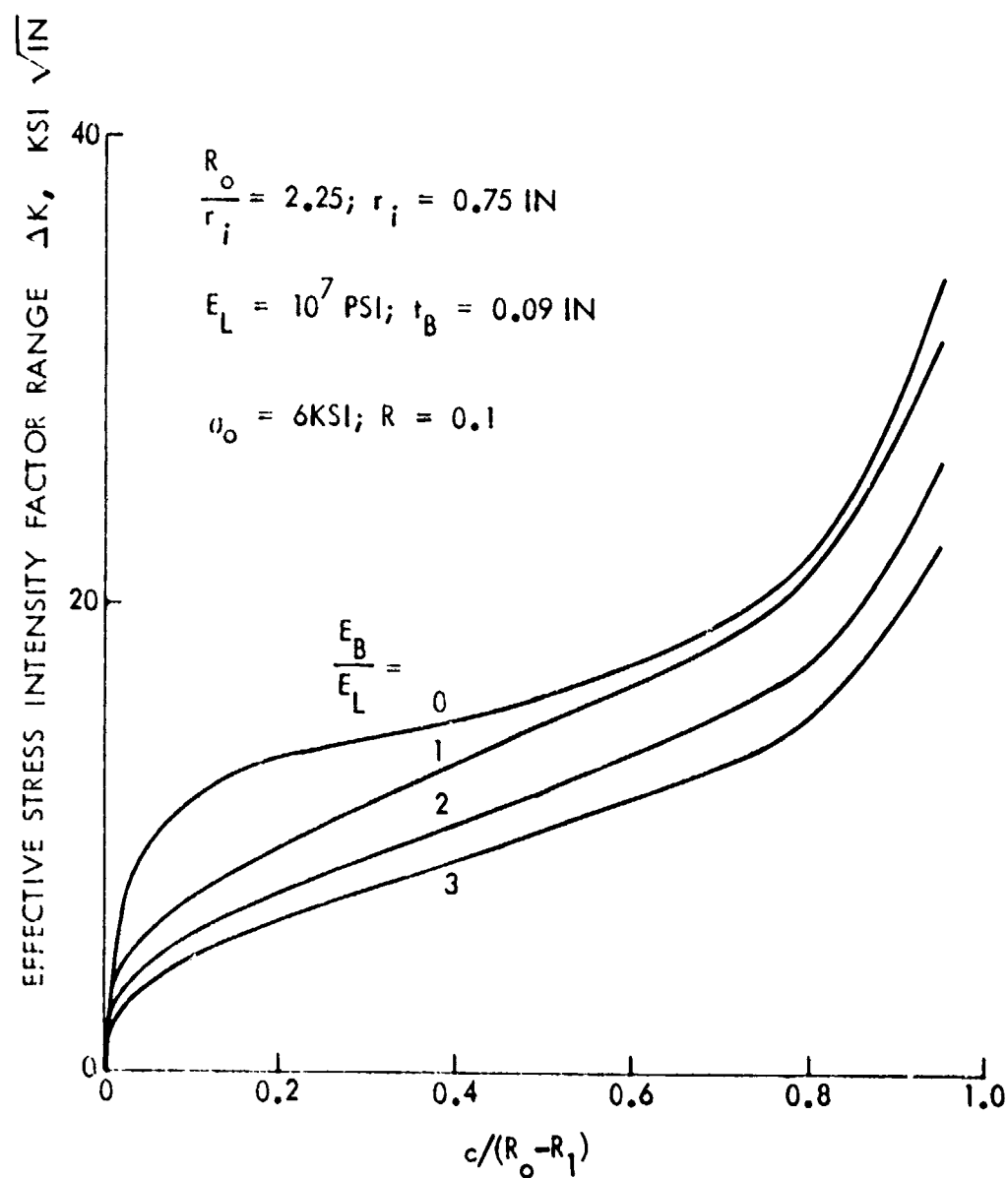
Figure 3-36. Stress Intensity Factor Ranges for Cracks
at an Attachment Lug for Various
Bushing-to-Lug Rigidity Ratios

75
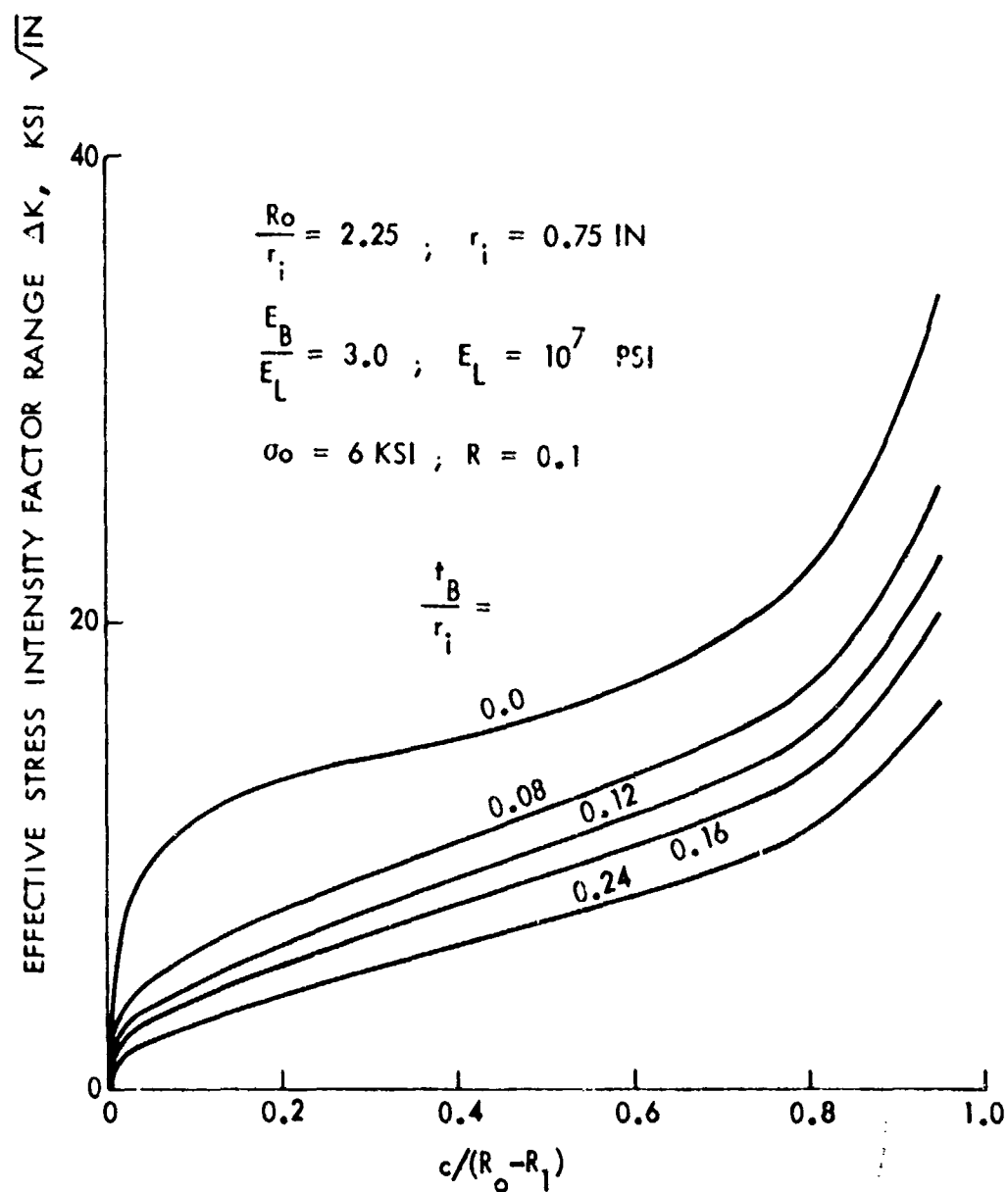
Figure 3-37. Stress Intensity Factor Ranges for Cracks
at an Attachment Lug With Bushing for
Various Bushing Thicknesses

Figures 3-35a and 3-36 that the installation of the interference-fit bushing causes an increase in the effective stress-intensity factor ratio, $R_{eff} = \sigma_{min}/\sigma_{max} = K_{min}/K_{max}$, but a significant decrease in the stress-intensity factor range, ΔK. This will result in the reduction of fatigue crack growth rate. The effects of bushing thickness (t_B/r_1) on the effective stress-intensity factor range, ΔK, are presented in Figure 3-37. Based on the results shown in Figures 3-36 and 3-37, it may be concluded that: (1) for constant bushing thickness, an increase in the bushing rigidity decreases the effective stress-intensity factor range; and (2) for constant bushing rigidity, an increase in bushing thickness decreases the effective stress-intensity factor range.

3. STRESS-INTENSITY FACTORS FOR CORNER CRACKS

One of the most common types of flaws for which there exists no closed form analytical solution is the corner crack at a circular hole. To date, several approximate methods have been proposed for computing the stress-intensity factors of a quarter-elliptical crack emanating from the corner of an open hole located in the geometric center of a plate. The methods range from an empirical equation which was developed using the fatigue crack growth method of calibrating the measured crack growth rate, da/dN, and the stress-intensity factor range, ΔK, to one- and two-dimensional compounded solutions, to the sophisticated three-dimensional finite element analysis. In this section, three methods in an increasing level of complexity and sophistication are presented for the determination of the stress-intensity factors for single corner cracks in aircraft attachment lugs.

3.1 ONE-PARAMETER COMPOUNDING APPROXIMATION

The corner crack is more difficult to analyze than the through-the-thickness crack because it has both surface length and bore depth dimensions and both must be considered in the crack growth analysis. One possible simplification is to assume a fixed relationship between crack depth "a" and surface length "c", so that only one crack length parameter is independent. This was the approach used in Reference [14] to analyze corner cracks at fastener holes. The following stress-intensity correction factor, governing the growth of the corner crack in the length direction, was verified empirically on open hole fatigue coupons in Reference [14]:

$$\Phi_{71}^{(c)} = 1 - \frac{0.2886}{1 + 2(\frac{a}{c})^2 (\frac{c}{B})^2} \tag{31}$$

This factor can be multiplied by the through-the-thickness crack solution, K_{LUG}, obtained by the compounding method and given in Equation (10).

$$K^{(c)} = K_{LUG} \, \Phi_{71}^{(c)} \tag{32}$$

Equation (32) provides a simple one-parameter K estimate for the point near the lug face. This factor can be used even after $a > B$, to smoothly change K as the corner crack becomes a through-the-thickness crack.

Equation (32) was used to estimate the stress-intensity factors for corner cracks at attachment lugs having R_o/R_i ratios of 1.50, 2.25, and 3.00. These results are tabulated in Tables 3-10 and 3-11 for $B/R_i = 2/3$ and 1/3, respectively. Note that, in the calculation, the depth-to-length ratio (a/c) was assumed to be constant and equal to 1.33, which was found experimentally by Schijve and Hoeymakers [2].

3.2 TWO-PARAMETER WEIGHT FUNCTION APPROXIMATION

In an earlier contractual program with the Flight Dynamics Laboratory, Hsu et al [36] developed a simple procedure for estimating the stress-intensity factors along the boundary of quarter-elliptical corner cracks emanating from fastener holes from corresponding through crack solutions. Correlation between the calculated stress-intensity factors and those deduced from the tests were good. A similar procedure can be used to estimate the stress-intensity factors along the periphery of a quarter-elliptical corner crack in an attachment lug.

The stress-intensity factor for a single through-the-thickness crack of length c in an attachment lug is given by

$$K(\frac{c}{R_i}) = \sigma_o \sqrt{\pi c} \, \beta_T \, (\frac{c}{R_i}) \tag{33}$$

where $\beta_T \, (c/R_i)$ is the through-the-thickness correction factor.

Then the corresponding stress-intensity factor for a single quarter-elliptical corner crack can be written as

TABLE 3-10. NORMALIZED STRESS INTENSITY FACTORS FOR SINGLE CORNER CRACKS IN STRAIGHT ATTACHMENT LUGS USING COMPOUNDING METHOD – $B/R_i = 2/3$, $a/c = 1.33$

$\dfrac{c}{(R_o - R_i)}$	$K/(\sigma_o \sqrt{\pi c})$ for $R_o/R_i =$			$K/(\sigma_{br} \sqrt{\pi c})$ for $R_o/R_i =$		
	1.50	2.25	3.00	1.50	2.25	3.00
0.0	4.772	3.654	3.761	3.181	1.624	1.254
0.1	4.446	2.930	2.685	2.964	1.302	0.895
0.2	4.285	2.632	2.269	2.857	1.170	0.756
0.3	4.249	2.463	1.995	2.833	1.095	0.665
0.4	4.316	2.356	1.816	2.877	1.047	0.605
0.5	4.483	2.308	1.718	2.989	1.026	0.573
0.6	4.776	2.332	1.692	3.184	1.036	0.564
0.7	5.271	2.457	1.751	3.514	1.092	0.584
0.8	6.183	2.771	1.948	4.122	1.232	0.649
0.9	8.389	3.636	2.526	5.593	1.616	0.842

TABLE 3-11. NORMALIZED STRESS INTENSITY FACTORS FOR SINGLE CORNER CRACKS IN STRAIGHT ATTACHMENT LUGS USING COMPOUNDING METHOD – $B/R_i = 1/3$, $a/c = 1.33$

$\dfrac{c}{(R_o-R_i)}$	$K/(\sigma_o \sqrt{\pi c})$ for $R_o/R_i =$			$K/(\sigma_{br} \sqrt{\pi c})$ for $R_o/R_i =$		
	1.50	2.25	3.00	1.50	2.25	3.00
0.0	4.772	3.654	3.761	3.181	1.624	1.254
0.1	4.543	3.182	3.002	3.029	1.414	1.001
0.2	4.568	2.946	2.476	3.045	1.309	0.825
0.3	4.680	2.701	2.106	3.120	1.200	0.702
0.4	4.824	2.524	1.881	3.216	1.122	0.627
0.5	5.017	2.429	1.759	3.345	1.080	0.586
0.6	5.312	2.424	1.722	3.541	1.077	0.574
0.7	5.809	2.532	1.774	3.873	1.125	0.591
0.8	6.747	2.839	1.967	4.498	1.262	0.656
0.9	9.065	3.707	2.546	6.043	1.648	0.849

$$K\left(\frac{a}{c},\, \alpha\right) = \sigma_0 \sqrt{\pi a}\;\; \beta_T\left(\frac{x-R_1}{R_1}\right) \frac{M_1'}{\phi}\left(\frac{a}{c},\, \alpha\right) M_C\left(\frac{c}{R_1},\, \frac{x-R_1}{c}\right) M_B\left(\frac{a}{c},\, \frac{a}{B}\right) \tag{34}$$

$$\text{for}\quad \frac{a}{c} \leq 1$$

and

$$K\left(\frac{c}{a},\, \alpha\right) = \sigma_0 \sqrt{\pi c}\;\; \beta_T\left(\frac{x-R_1}{R_1}\right) \frac{M_1'}{\phi}\left(\frac{c}{a},\, \alpha\right) M_C\left(\frac{c}{R_1},\, \frac{x-R_1}{c}\right) M_B\left(\frac{a}{c},\, \frac{a}{B}\right) \tag{35}$$

$$\text{for}\quad \frac{a}{c} > 1$$

where

$$M_C = F + \frac{x-R_1}{c}\;\;(1-F) \tag{36}$$

in which α is the elliptical angle measured from the hole wall, x is the distance from the center of the hole to the particular point of interest on the crack periphery, M_1'/ϕ is the combined front free surface and flaw shape factor, M_C is the wall curvature correction factor, and M_B is the back surface correction factor. The values of M_1'/ϕ and F, and M_B are presented in References [36] and [58], respectively. As in Reference [36], it is assumed that for a given number of applied load cycles, the extension of the quarter-elliptical crack border is controlled by the stress intensity factors at two points; namely. the intersections of the crack periphery with both the hole wall and plate surface (i.e., K_A and K_C). In general, the stress intensity factors at these two locations are different, resulting in different crack growth rates. Therefore, the new flaw shape aspect ratio after each crack growth increment differs from the preceding one. The new flaw shape aspect ratio is computed using the new crack lengths at both the hole wall and plate surface. All the correction factors have been reduced to simple equations for locations A and C, and the two-parameter corner crack stress intensity factor formulas are summarized in Figure 3-38.

In Reference [36], the above process was repeated until the crack length along the hole wall was equal to the plate thickness. At that time, the crack was assumed to be a through-the-thickness crack with length c. This assumption was based upon the experimental observation that after the crack penetrates the back surface and the cyclic load application continues, the back surface crack length increases much faster than that of the front surface until the front of the through-the-thickness crack becomes stable.

81

$$K_I^{(A)} = \sigma_0 \sqrt{\pi c} \; \beta_T(0) \sqrt{A_n} \; \frac{M'^{(A)}_1 F}{\sqrt{Q}} M_B$$

$$K_I^{(C)} = \sigma_0 \sqrt{\pi c} \; \beta_T\left(\frac{c}{R_i}\right) \sqrt{A_n} \; \frac{M'^{(C)}_1}{\sqrt{Q}}$$

. . . WHERE, IF

$$A_n \equiv MIN\ (a/c,\ 1.0)$$
$$C_n \equiv MIN\ (c/a,\ 1.0)$$

. . . THEN

$$\sigma_0 = P/(2\ R_0 B)$$

$$\beta_T = \frac{K_{THRU}}{\sigma_0 \sqrt{\pi c}}$$

$K_{THRU} = K_I$ FOR THROUGH-THICKNESS CRACK OF LENGTH c

$$Q = 1. + 1.464\ (A_n\ C_n)^{1.65}$$

$$M'^{(A)}_1 = [1. + 0.025\ C_n + 0.0965\ (1. - A_n)]\ \sqrt{C_n}$$

$$M'^{(C)}_1 = [1. + 0.214\ C_n - 0.0925\ (1. - A_n)]\ \sqrt{A_n}$$

$$F = 1. - 2.09\ S + 9.635\ S^2 - 23.37\ S^3 + 25.485\ S^4 - 10.403\ S^5$$

$$S = c/(c + R_i)$$

$$M_B = \begin{cases} 1.0, & a > c \\ 1.0 + (a/B)^{(1.8 + A_n)}\ (0.32 - 0.82\ A_n), & a < c \end{cases}$$

SECTION A-A
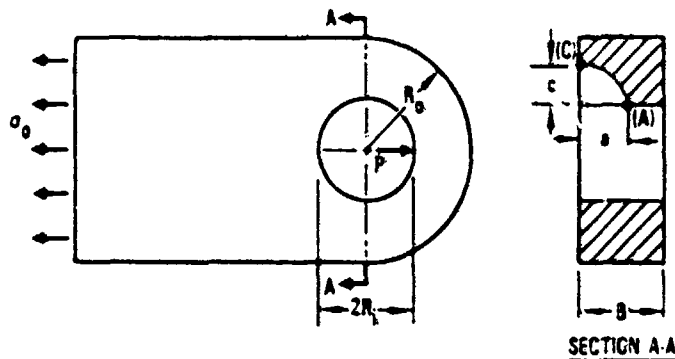
Figure 3-38. Two-Parameter Corner Crack Stress Intensity Factor Formulas

This transitional crack growth assumption is very reasonable for a crack at a fastener hole, since, at the time the crack grows through the thickness, the remaining net section is usually much larger than the surface crack length. However, for an attachment lug, when a part-through crack grows through the thickness, the remaining net section is usually small in comparison to the surface crack size. Therefore, a proper transitional crack growth criterion is needed for the transition period from the time the crack penetrates the back surface to the time the crack lengths are essentially equal on the front and back surfaces.

Figure 3-39 shows the transitional crack geometry, in which c_F and c_B are crack lengths on the front and back surfaces, respectively. Collipriest and Ehret [37] proposed a stress-intensity magnification factor for the crack tip at the back surface of a surface crack as

$$\alpha_t = \left[\frac{1}{1 - \sqrt{1 - \frac{c_B^2}{c_F^2}}} \right]^{1/2} \qquad \text{for} \quad c_B > 0 \tag{37}$$

When the back-side crack length equals the front-side crack length, the magnification is unity and the through crack has achieved a uniform front. This factor will be used to estimate the stress-intensity factor at the back surface of the transitional crack, i.e.

$$K_B = \sigma_0 \sqrt{\pi c_B} \; \beta_T \; (\frac{c_B}{R_i}) \cdot \alpha_t \tag{38}$$

The stress-intensity factor at the front surface will be calculated using Equation (35) and an imaginary crack length along the hole wall direction, a', i.e.

$$K_C = \sigma_0 \sqrt{\pi c_F} \; \beta_T \; (\frac{c_F}{R_i}) \; \frac{M_i'}{\Phi} \; (\frac{c_F}{a'}, 90^\circ) \tag{39}$$

An imaginary crack length a' can be determined by fitting an elliptical equation through points C and B, as
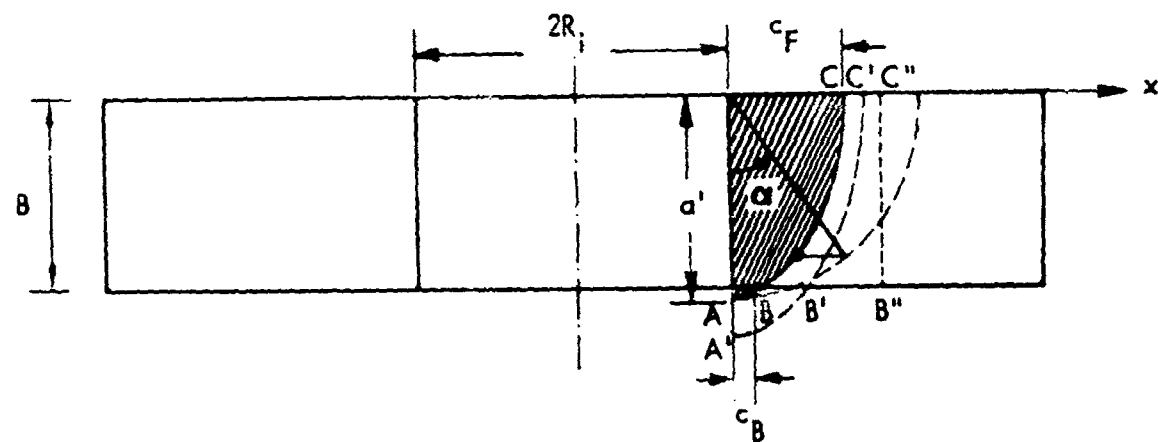
Figure 3-39. Transitional Crack Geometry

$$a' = B \left[1 - \left(\frac{c_B}{c_F} \right)^2 \right]^{-1/2} \tag{40}$$

When the back-side crack length, c_B, approaches that of the front side (i.e. B"C" as shown in Figure 3-38), the factor c_F/a' becomes very small and the corresponding M_l'/Φ ratio approaches unity. After that, the transitional crack becomes a through-the-thickness crack with a uniform front, i.e.

$$K_B = K_C = \sigma_o \sqrt{\pi c} \ \beta_T \left(\frac{c}{R_i} \right) \tag{41}$$

Equations (34) and (35) were used to compute the stress-intensity factors at the intersections of the crack periphery and the hole wall and plate surfaces. The 2-D finite element method solution results from Table 3-3 were used for the basic through-the-thickness crack solution, $K(c/R_i)$. The results are shown in Figures 3-40 through 3-42 for R_o/R_i ratios of 1.50, 2.25 and 3.0, respectively. In each plot, the flaw shape aspect ratio a/c was assumed as constant. It should be noted that the computed part-through crack stress-intensity factors are normalized by $\sigma_{br} \sqrt{\pi c}$. These solutions correspond to corner crack solutions for $a \leq B$. Figure 3-43 presents the normalized stress-intensity factors at the lug surface having a constant a/c ratio of 1.33 and a R_o/R_i ratio ranging from 1.5 to 3.0. In this figure, the solutions are presented even after the crack breaks through the back side, i.e. $a > B$. Corresponding normalized stress-intensity factors computed using the one-parameter compounding method are also shown in the figure for comparison.

3.3 THREE-DIMENSIONAL CRACKED FINITE ELEMENT METHOD

Numerical methods such as the slicing technique [38], the conventional three-dimensional (3-D) finite element method [39], the boundary integral equation approach [40], and the 3-D alternating technique [41] have been used to analyze corner-crack problems. To accurately depict the extreme stress gradient existing in the vicinity of a crack tip, the necessary computer effort in each case is considerable. In an attempt to minimize the economic problem of the conventional approach and to extract the stress-intensity factors directly, a 3-dimensional cracked finite element was used which is capable of characterizing the crack-tip stress singularity internally. The procedure used in the development of the 3-D cracked element is described in Reference [42] and summarized as follows.

85
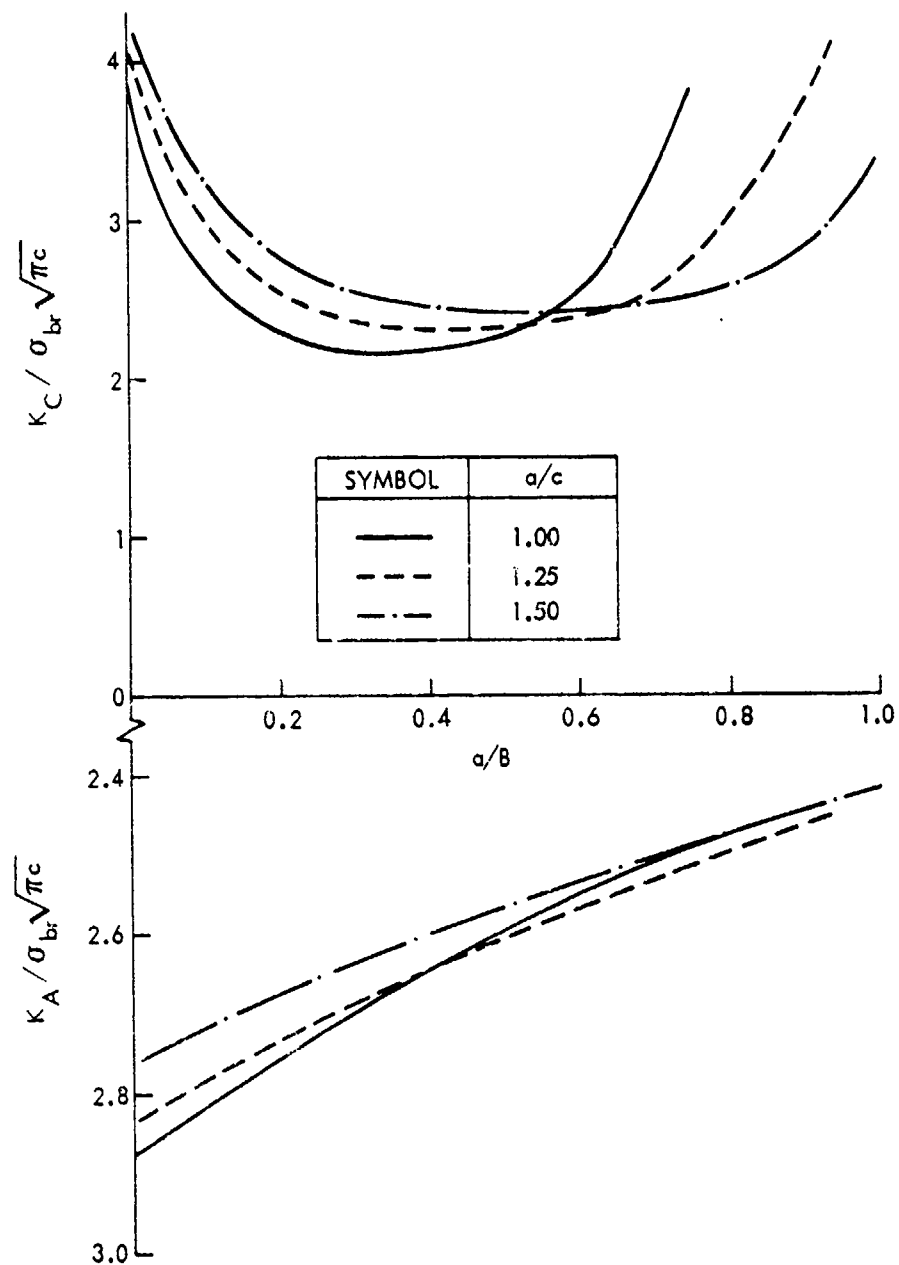
Figure 3-40. Normalized Stress Intensity Factors for Corner Cracks
in a Straight Attachment Lug Having a R_o/R_i Ratio of 1.50
and a B/R_i Ratio of 2/3
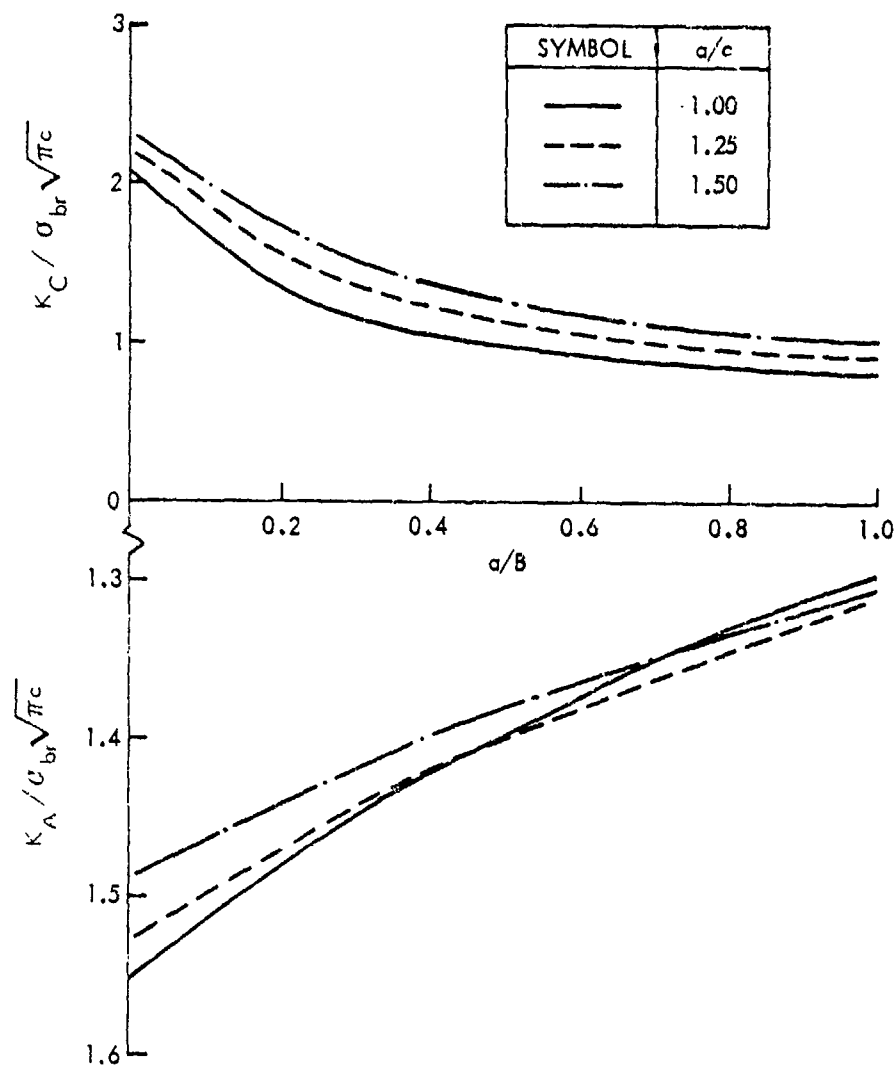
Figure 3-41. Normalized Stress Intensity Factors for Corner Cracks in a Straight Attachment Lug Having a R_o/R_i Ratio of 2.25 and a B/R_i Ratio of 2/3
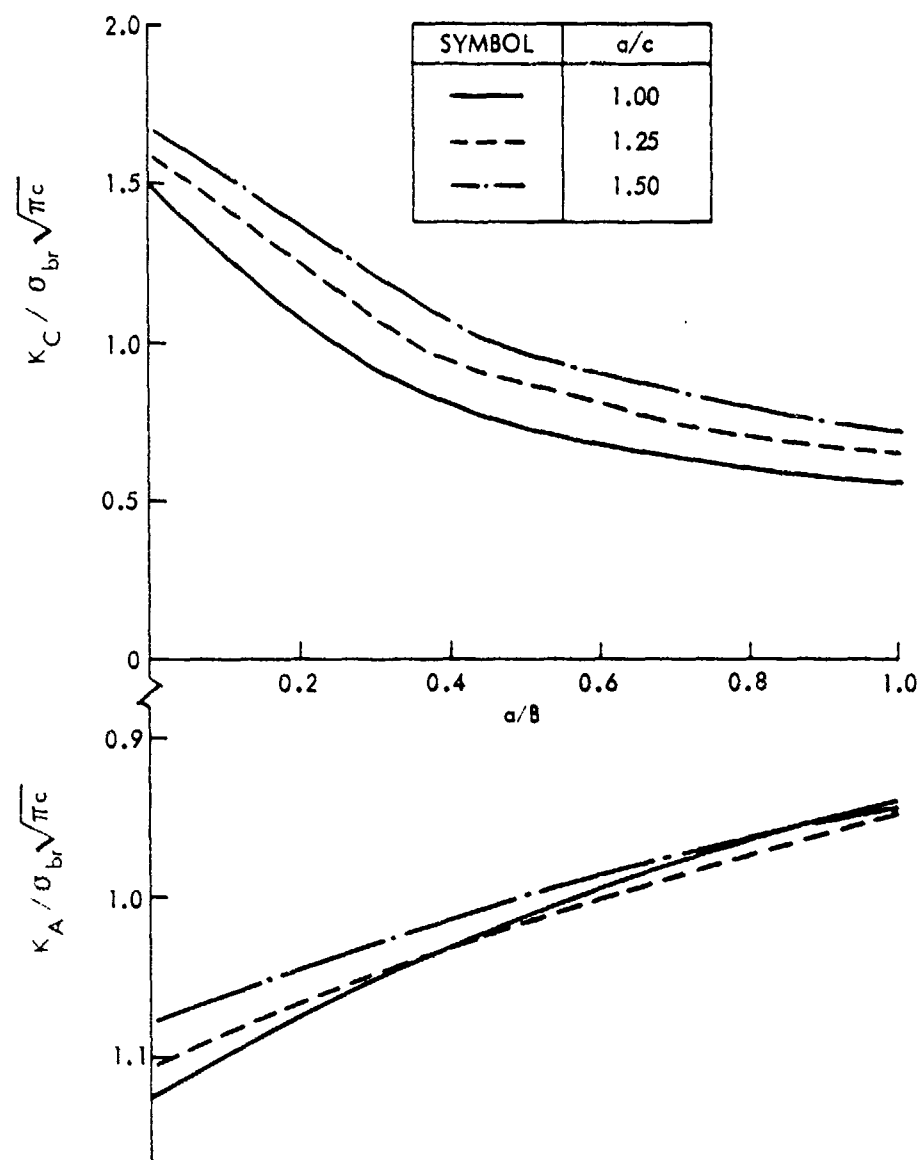
Figure 3-42. Normalized Stress Intensity Factors for Corner Cracks in a Straight Attachment Lug Having a R_o/R_i Ratio of 3.00 and a B/R_i Ratio of 2/3
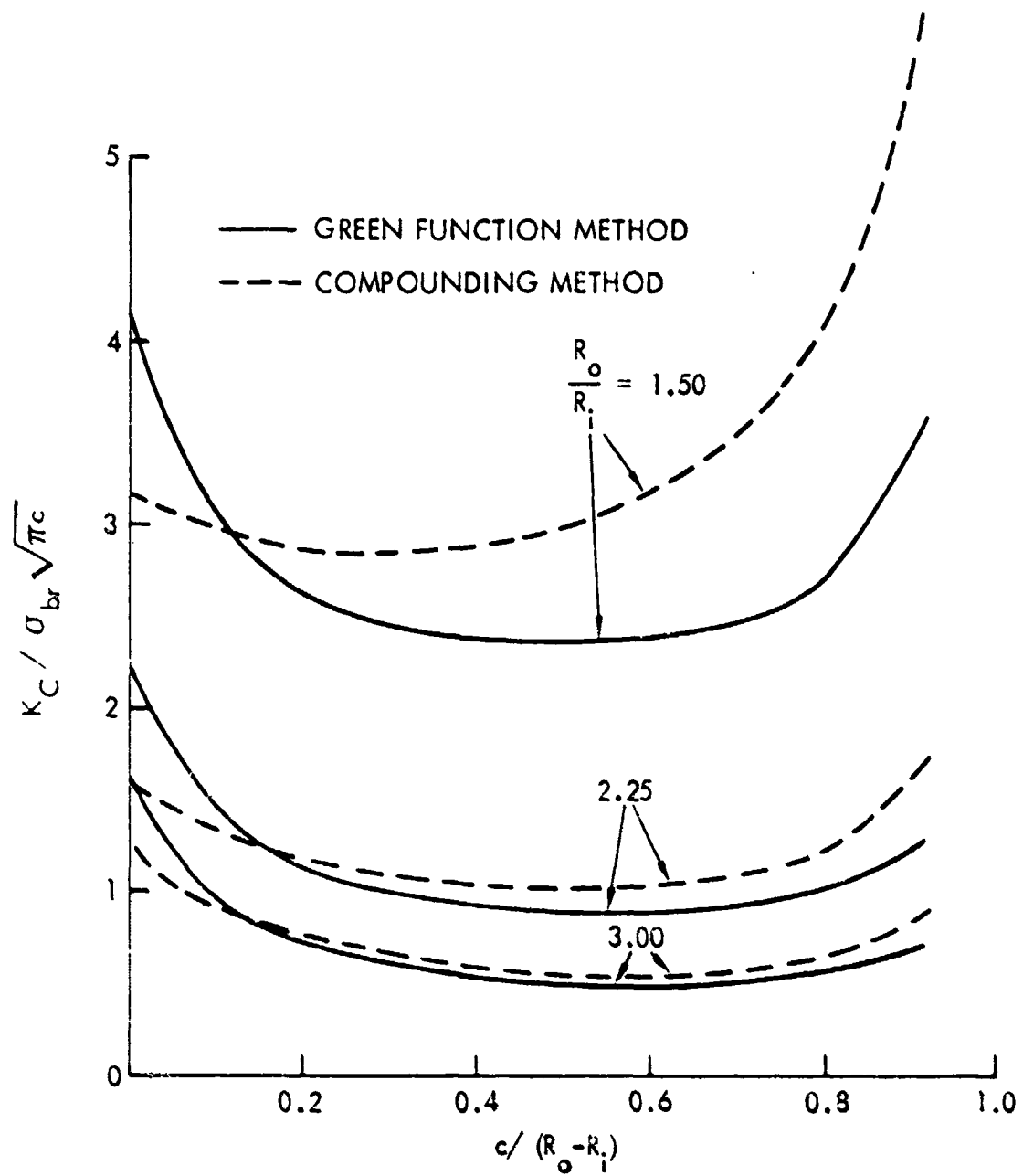
Figure 3-43. Normalized Stress Intensity Factors for Corner Cracks in Straight Attachment Lugs Having Constant Flaw Shape a/c of 1.33

Two types of 20-node 3-D cracked elements, as shown in Figure 3-44, were developed using a hybrid displacement finite element procedure. The variational principle which governs the assumed displacement hybrid finite element model is the stationary condition of a modified total potential energy functional with a relaxed requirement of interelement boundary displacement continuity, a priori. This variational principle is a three-field variable principle. The three field variables are the element interior displacements, element boundary displacements, and the Lagrange multipliers. The Lagrange multipliers are physically the interelement boundary tractions and are assumed to match the independently assumed element interior and boundary displacements at the interelement boundary. Three-dimensional asymptotic solutions for displacements ($\sqrt{r}$ – type) and stresses ($1/\sqrt{r}$ – type) near the crack front are embedded in this procedure. Apart from satisfying relevant field equations, the variational principle also enforces the conditions of displacement continuity and traction reciprocity at the interelement boundary a posteriori, assuring the convergence of the finite element procedure. The procedure is capable of analyzing mixed mode fracture problems (Modes I, II and III), and the three stress-intensity factors at various locations along the crack front are treated as unknowns along with the generalized nodal displacements of the structure. The final set of algebraic equations governing the global nodal displacements and the three stress-intensity factors at various locations along the crack front can be written as follows:

$$[K_1] \{q*\} + [K_2]^T \{K*\} = \{Q_1\} \tag{42}$$

$$[K_2] \{q*\} + [K_3] \{K*\} = \{Q_2\} \tag{43}$$

Where $\{q*\}$ are the structure's global nodal displacements, $\{K*\}$ are the mixed mode stress-inter.... factors at various locations along the crack front, $[K_1]$, $[K_2]$ and $[K_3]$ are the corresponding stiffness matrices (superscript T represents the transpose), and $\{Q_1\}$ and $\{Q_2\}$ are the corresponding nodal forces. It is evident from Equations (42) and (43) that the solution for stress-intensity factors can be obtained directly from the finite element solution procedure. This eliminates additional post-processing of displacement or stress solutions to obtain the stress-intensity factors through methods such as the crack opening displacement method, nodal force method, etc. A detailed description of the hybrid displacement procedure was documented in Reference [42].
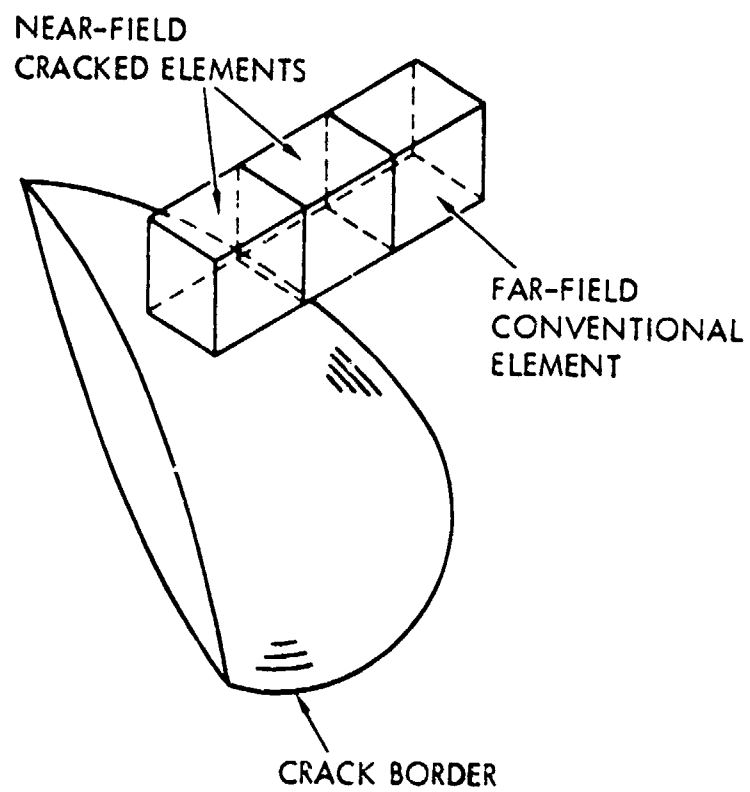
Figure 3-44. 20-Node Three-Dimensional Cracked Elements

The accuracy and convergence of the three-dimensional hybrid displacement finite element procedure have been tested and verified through the solution of several complex fracture problems of interest in aerospace structural components, nuclear pressure vessels and components, and solid rocket motor grain applications [43-45]. Raju and Newman [46], using Tracey's [39] wedge shaped distorted isoparametric crack elements, made a convergence study for the solution of semielliptical surface flaws in thin plates. A similar convergence study was also made using the present three-dimensional hybrid finite element procedure in Reference [44]. As discussed in Reference [44], the present solution with 4555 degrees of freedom has excellent agreement with that of Raju and Newman for their highest degrees of freedom, 6867.

The three-dimensional cracked element was used to compute the stress-intensity factors for single quarter-elliptical corner cracks at straight lugs. A total of eight problems of corner cracks in attachment lugs with various outer-to-inner radius ratios, crack aspect ratios, and crack depth-to-lug thickness ratios were considered for the present analysis. The geometry of an attachment lug with a corner crack is given in Figure 3-45(a), and the various parameters for the eight problems considered are defined in Table 3-12. The bearing pressure at the lug hole wall was assumed to be uniform and acts only on the right half of the hole as shown in Figure 3-45(a). This assumption of uniform bearing pressure over the right half of the lug hole wall was made due to the complexity involved in the generation of equivalent nodal forces corresponding to an actual pin-lug contact bearing pressure distribution in a three-dimensional case. Consequently, the solutions by the two-dimensional Green's function method generated for comparison purposes also correspond to the same bearing pressure. Also, the original Green's functions were used in the computation of two-dimensional solutions. The assumption of same bearing pressure in both cases is important, because the stress-intensity factor solutions vary significantly depending upon the bearing pressure distribution, namely, uniform, cosine and actual pin-lug pressure distributions.

A typical finite element breakdown, number of elements and total number of degrees of freedom for the present analysis are presented in Figure 3-45(b). In Figures 3-46 through 3-50, solutions of stress-intensity factor variations along the crack front by both two- and three-dimensional procedures are presented for problem numbers 1 and 2, 3, 4 and 5, 6 and 7, and 8, respectively.
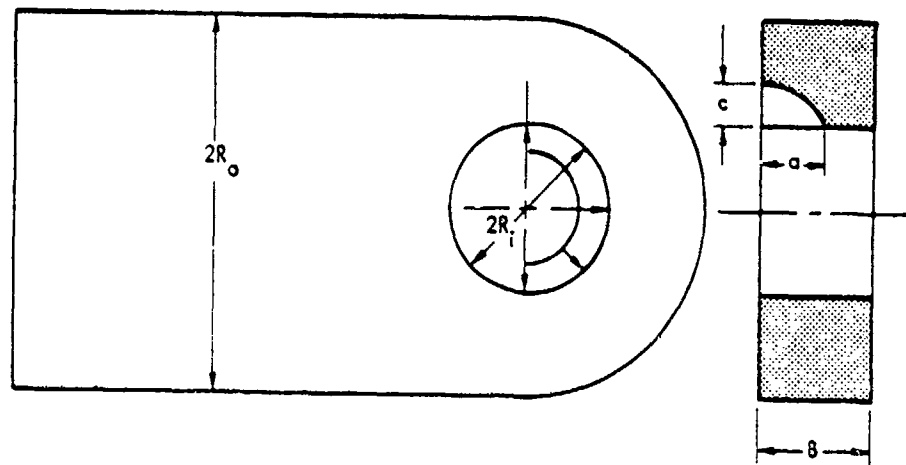
(a) Geometry
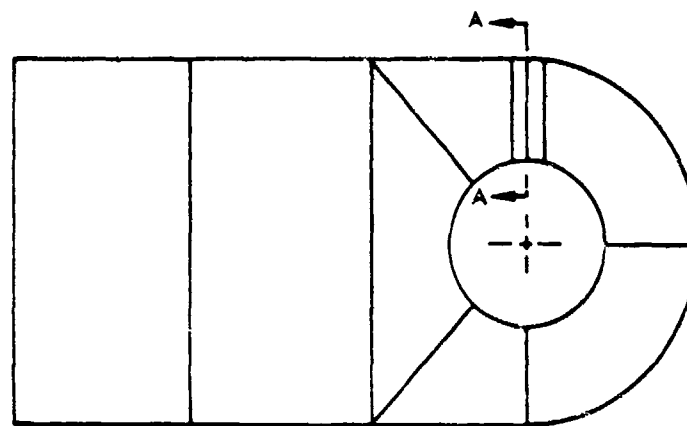
TOTAL NUMBER OF ELEMENTS = 333
TOTAL NUMBER OF D.O.F. = 5124
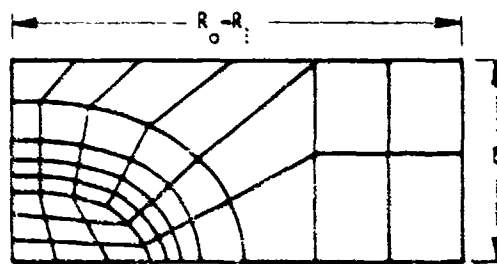
SECTION A-A

(b) Finite Element Breakdown

Figure 3-45. Geometry and Finite Element Breakdown of an Attachment Lug with a Corner Crack for Three-Dimensional Cracked Finite Element Analysis

TABLE 3-12. CORNER CRACK PROBLEMS ANALYZED
BY THREE-DIMENSIONAL CRACKED
FINITE ELEMENT PROCEDURE

PROBLEM NUMBER	R_o/R_1	a/c	a/B
1	1.50	1.0	0.50
2	1.50	1.5	0.50
3	2.25	1.0	0.1667
4	2.25	1.0	0.25
5	2.25	1.5	0.25
6	2.25	1.0	0.50
7	2.25	1.5	0.50
8	2.25	1.5	0.75
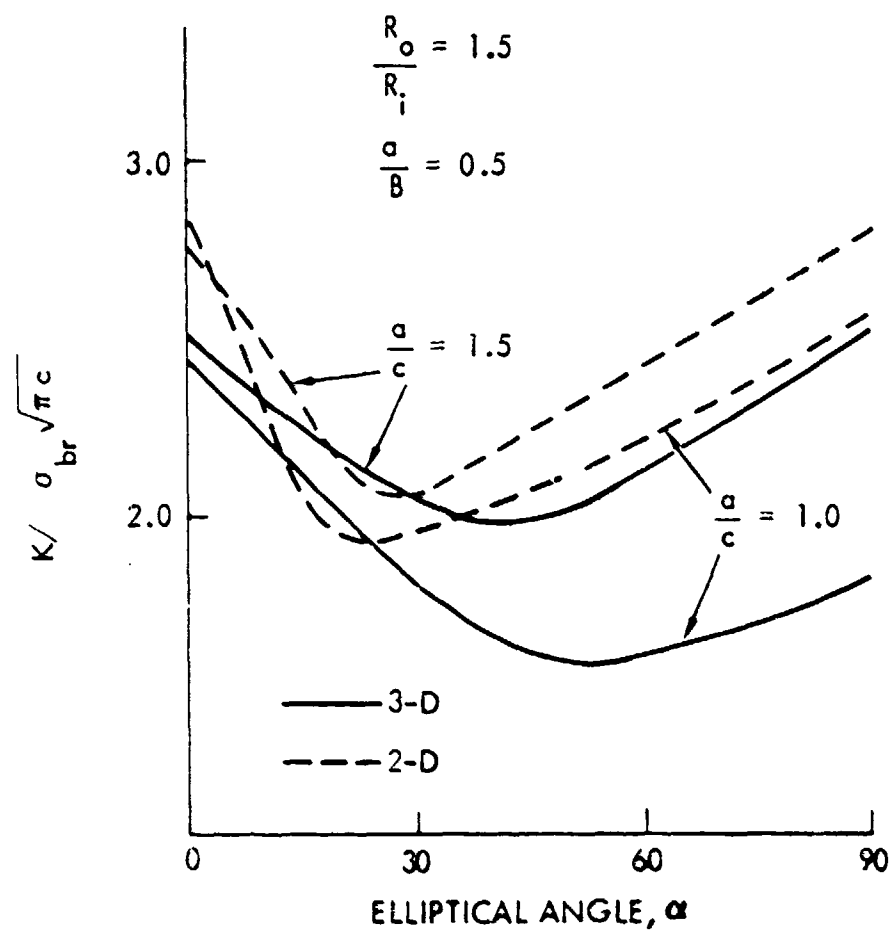
Figure 3-46. Normalized Stress Intensity Factors for Corner Cracks at a Straight Attachment Lug Having a R_o/R_i Ratio of 1.5 and an a/B Ratio of 0.5
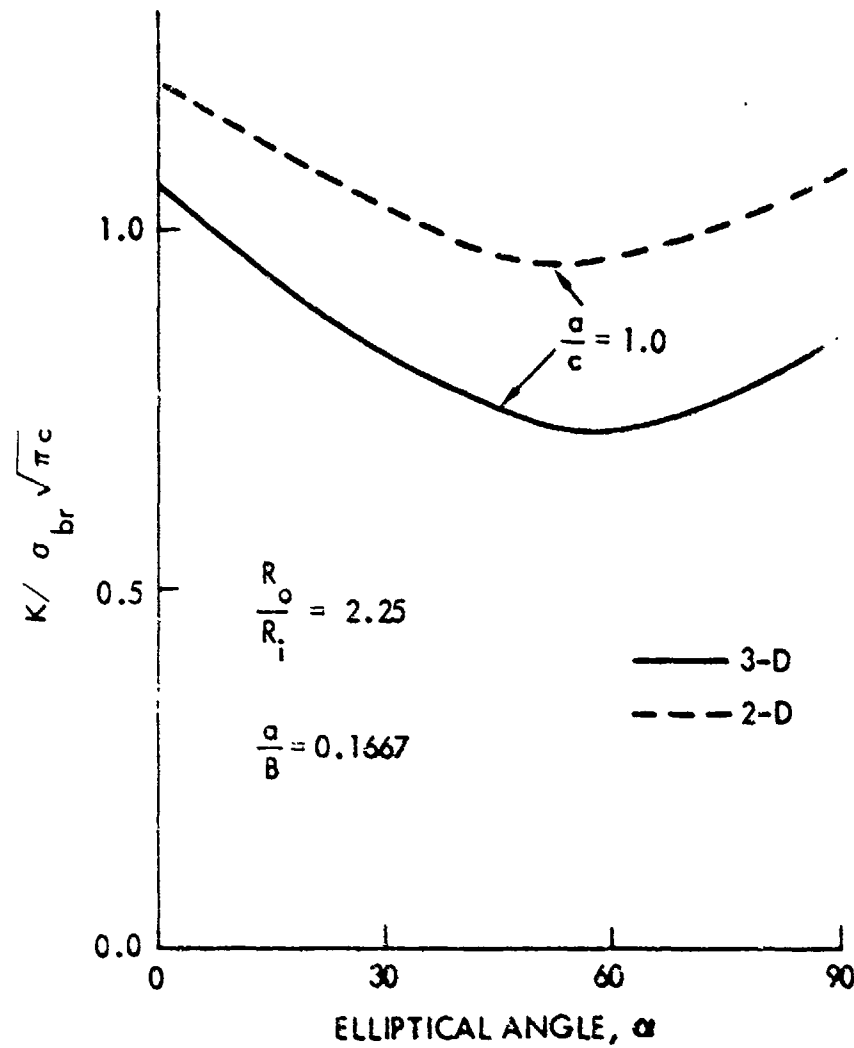
Figure 3-47. Normalized Stress Intensity Factors for Corner Cracks at a Straight Attachment Lug Having a R_o/R_i Ratio of 2.25 and an a/B Ratio of 0.1667
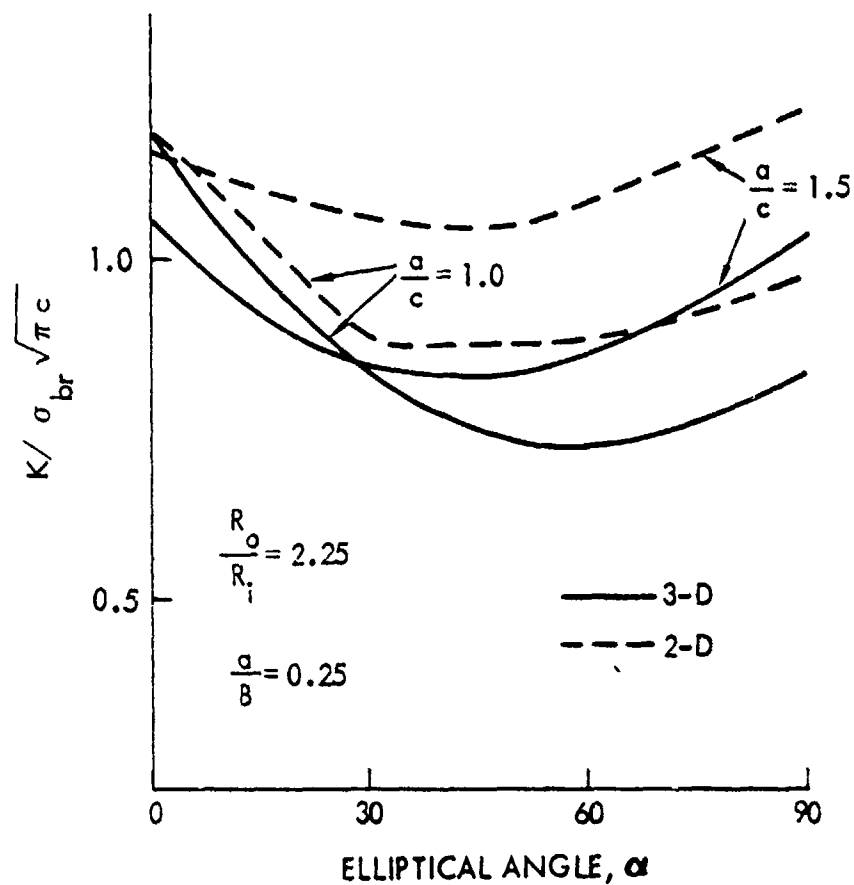
Figure 3-48. Normalized Stress Intensity Factors for Corner Cracks
at a Straight Attachment Lug Having a R_o/R_i Ratio of 2.25
and an a/B Ratio of 0.25
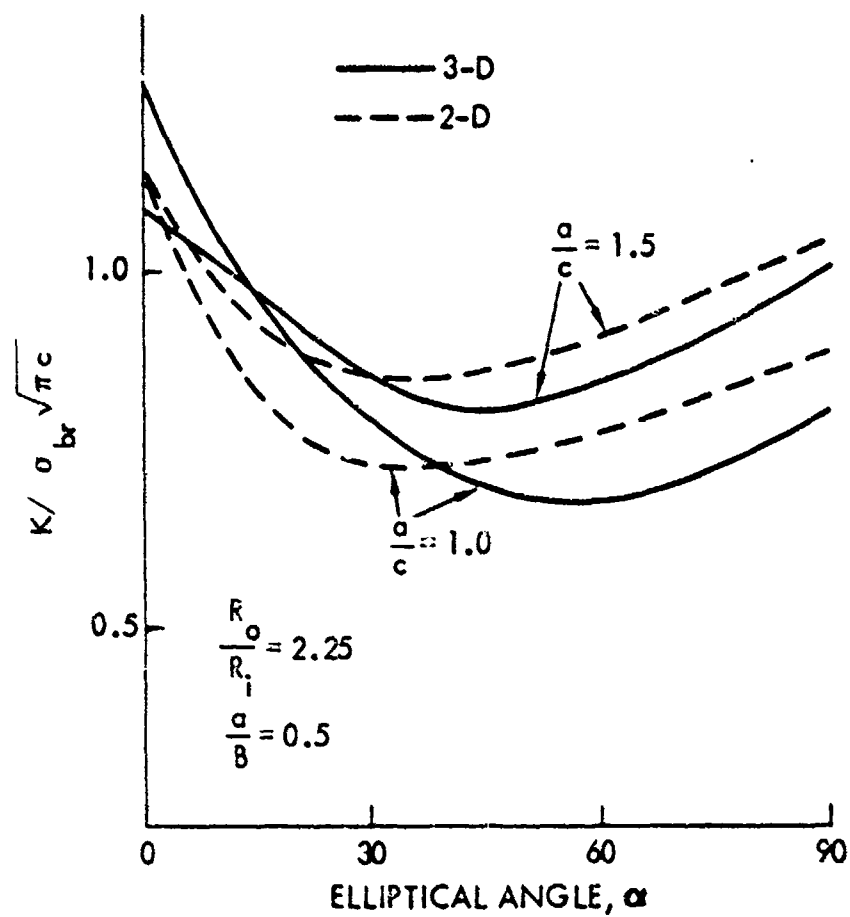
Figure 3-49. Normalized Stress Intensity Factors for Corner Cracks at a Straight Attachment Lug Having a R_o/R_i Ratio of 2.25 and an a/B Ratio of 0.5
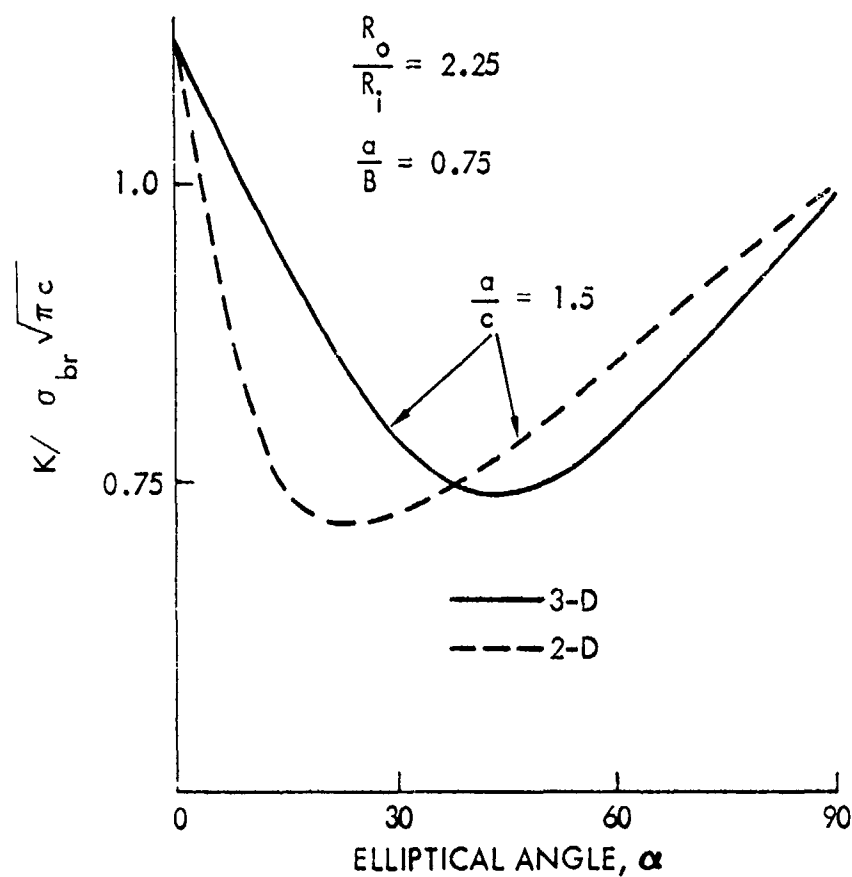
Figure 3-50. Normalized Stress Intensity Factors for Corner Cracks at a Straight Attachment Lug Having a R_o/R_i Ratio of 2.25 and an a/B Ratio of 0.75

The stress-intensity factor solutions are normalized by the exact solution of a through-the-thickness crack of length c in an infinite plate subjected to a crack pressure of σ_{br}. Elliptical angles (α) of 0° and 90° refer to the intersections of the crack front with the hole wall and lug surface, respectively.

A comparison of the results in Figures 3-46 through 3-50 reveals that the two solution procedures agree well at $\alpha = 0^O$, but significant differences exist near $\alpha = 90^O$. For lugs with an outer-to-inner radius ratio of 1.5, the maximum difference at $\alpha = 90^O$ is about 42 percent and the difference decreases as the aspect ratio of the crack (a/c) increases. For lugs with outer-to-inner radius ratio of 2.25, the maximum difference at $\alpha = 90^O$ is about 26 percent and the difference decreases as the aspect ratio of the crack (a/c) and the crack depth-to-thickness ratio (a/B) increase. The overall behavior of the differences in the solutions is that they decrease as the outer-to-inner radius ratio, crack aspect ratio and crack depth-to-thickness ratio increase. Also, the angle at which the normalized stress-intensity factor is minimum is lower for the two-dimensional procedure in almost all of the problems. Thus, from these results, the two-dimensional procedure seems to be consistently overestimating the stress-intensity factor solutions except for elliptical angles close to 0°.

The one-parameter compounding, two-parameter weight function and the three-dimensional cracked finite element solutions are compared in terms of corner crack correction factors at the lug surface in Figure 3-51. The corner crack correction factors are obtained by normalizing K_C with the stress intensity factor (by weight function method) of a through-the-thickness crack of length c and are expressed as a function of a/B.

4.   ELASTOPLASTIC ANALYSIS

Several analytical methods of varying complexities have been developed and discussed in previous sections for through-the-thickness and corner cracks in straight attachment lugs. These analyses are basically for linear fracture mechanics problems. However, attachment lugs may undergo substantial plastic yielding around the lug hole, depending on the specific application and/or design. For example, the concepts of cold-working of the hole or installation of an interference-fit bushing prior to pin fitting have been extensively used in actual aircraft attachment lug

100
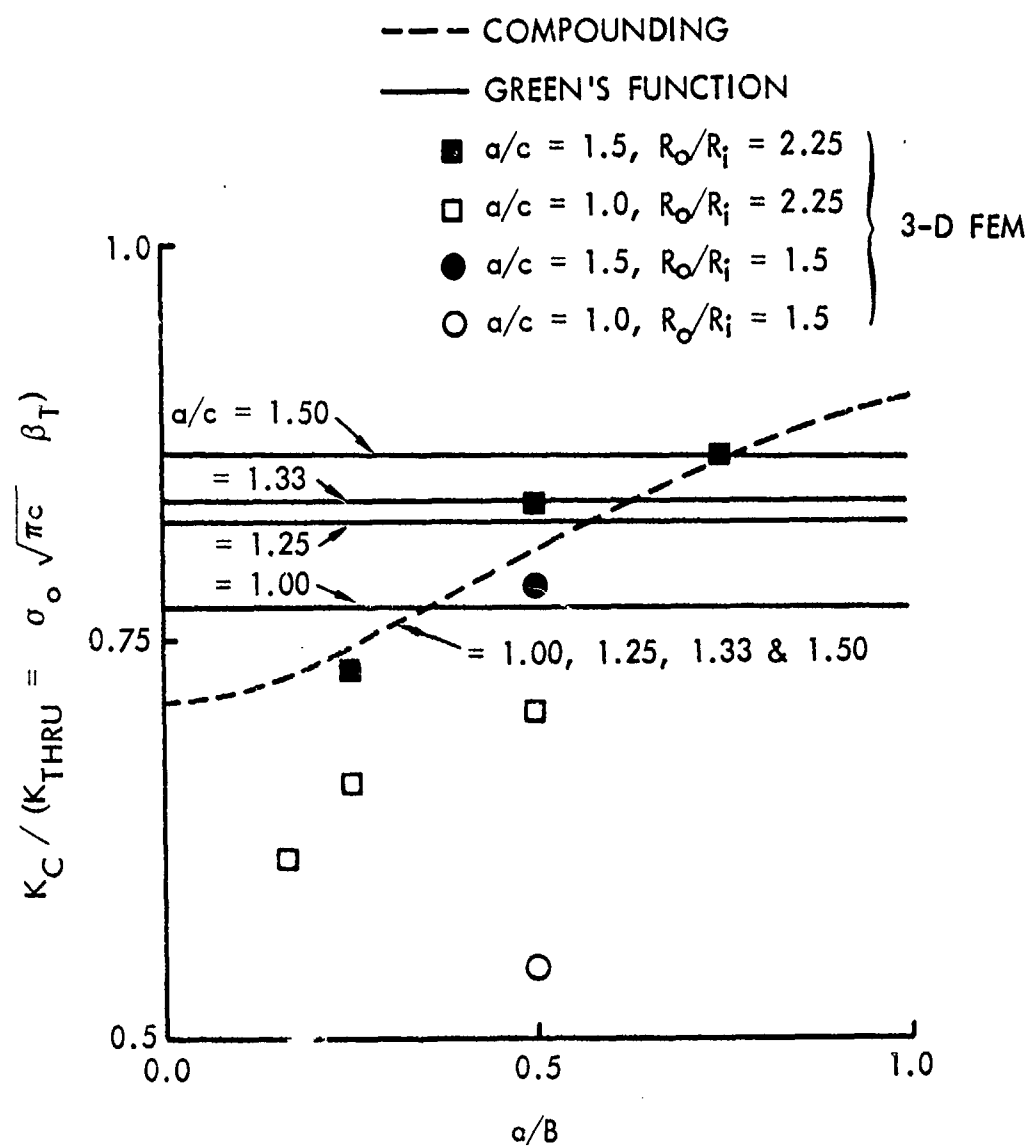
Figure 3-51. Comparison of Corner Crack Correction Factors at the Lug Surface by the Three Methods

design practices to improve the crack initiation life. These concepts are basically used to introduce fatigue-improving residual stresses around the hole of the lug. The lugs may also undergo plastic yielding due to the application of high pin loads. It is important to develop analytical procedures for analyzing such problems.

The analytical procedure is similar to that developed and verified for through-the-thickness cracks emanating from interference-fit and cold-worked fastener holes in infinite plates, under a previous Air Force contract (Reference [36]). The method involves an initial elasto-plastic stress analysis of attachment lugs to obtain the stress distribution on the prospective crack surface. These stresses are then used in conjunction with the Green's function to calculate the stress intensity factors for cracks emanating from lug holes. The Green's function developed for linear problems is also used for the elasto-plastic case.

The elasto-plastic stress analysis has been carried out for two materials, 4340 steel and 7075-T651 aluminum, which are being used for testing in the present contract work. These materials have been characterized and the nonlinear elasto-plastic stress-strain relationships were approximated by trilinear representation and are given in Figure 3-52. The unloading moduli have been assumed to be the same as the initial elastic moduli for both of the materials. The analysis was performed for lugs with outer-to-inner radius ratios, R_o/R_i, of 1.50, 2.25, and 3.00 and a constant lug inner radius of 0.75 inch. Far-field maximum stresses, σ_o, of 35 and 15 ksi were selected for steel and aluminum lugs, respectively. Isotropic hardening with the von Mises yield criterion was used in the elasto-plastic analysis. Steel pins were used in all cases, and it was also assumed that the pin did not yield.

The finite-element method was again used for the elasto-plastic stress analysis of attachment lugs. The finite element breakdown and the use of spring elements with high stiffness to simulate the pin-lug contact surface were similar to those in the linear stress analysis. The model was loaded by a single concentrated force at the center of the pin. In the nonlinear analysis, a loading was first applied to reach the yield point, followed by incremental loadings to reach the maximum far-field stresses listed above. The loadings were then reduced to give stress levels corresponding to far-field stress ratios, R, of 0.5 and 0.1.

102
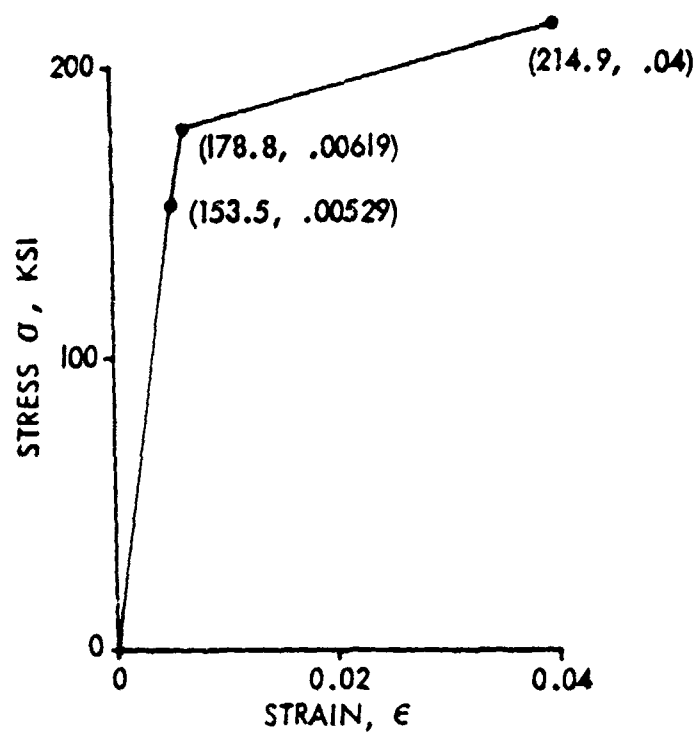
(a) STRESS-STRAIN CURVE FOR 4340 STEEL
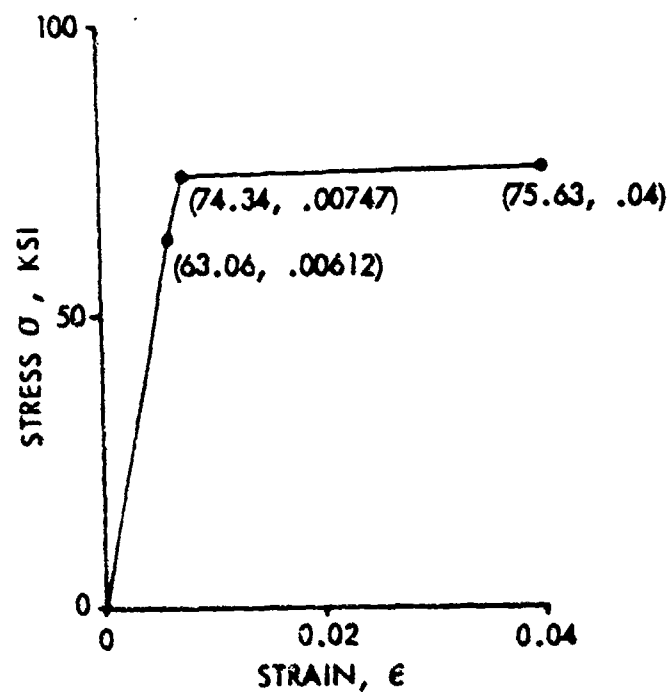
(b) STRESS-STRAIN CURVE FOR 7075-T651 ALUMINUM

Figure 3-52. Material Properties Used in
Elasto-Plastic Stress Analysis

In the plastic region, the following two convergence criteria were used in the analysis. A tolerance criterion of $\Delta E_{It}/\Delta E_{L.I} \leq 0.1$ was used in the analysis, where ΔE_{It}, $\Delta E_{L.I}$ are the energy changes for the iteration and the load increment, respectively. Regardless of the above tolerance criterion, the analysis was iterated at least twice for each load increment. In all the solutions presented here, the maximum value of $\Delta E_{It}/\Delta E_{L.I}$ was less than 0.035.

The unflawed stress distribution along the prospective crack surface, 90° away from the load line, obtained from the elasto-plastic finite element analysis for the far field stress levels given before are presented in Figures 3-53 through 3-55 for steel lugs and Figures 3-56 through 3-58 for aluminum lugs. These results are given in increasing order of R_o/R_i ratios of 1.50, 2.25 and 3.00.

For a steel lug with R_o/R_i of 1.50, the stresses (σ_{max}) corresponding to maximum far-field stress of 35 ksi and the stresses (σ_{min}, R = 0.5 and σ_{min}, R = 0.1) corresponding to minimum far-field stress for stress ratios of 0.5 and 0.1, respectively, are given in Figure 3-53. From these stresses, the difference between maximum and minimum stresses for stress ratios of 0.5 and 0.1, $\Delta\sigma_{R=0.5}$ and $\Delta\sigma_{R=0.1}$, respectively, can be obtained and are also included in the figure. At the maximum load, about 20 percent of the lug ligament has yielded. The effects of plastic yielding of the lug can also be seen in the distributions of $\sigma_{min, R=0.5}$ and $\sigma_{min, R=0.1}$. While unloading, due to plastic yielding, the stresses near the lug hole decrease at a higher rate than the rest of the ligament and become negative at the minimum stress corresponding to R = 0.1. If the loading was completely removed, significant negative residual stresses would exist near the lug hole. In calculations of crack growth any compressive minimum stresses near the lug hole are neglected due to crack closure, and $\Delta\sigma_{R=0.1}$ is assumed not to exceed σ_{max}. However, for illustration purposes, the actual difference in stresses near the lug hole is indicated in Figure 3-53 by a dotted line. Corresponding solutions for an aluminum lug with the same geometry are presented in Figure 3-56, and the results are qualitatively the same.

Similar analytical solutions for lugs with an R_o/R_i ratio of 2.25 are given in Figures 3-54 and 3-57 for steel and aluminum materials, respectively. In this case, for both the materials, the lugs yield only slightly;
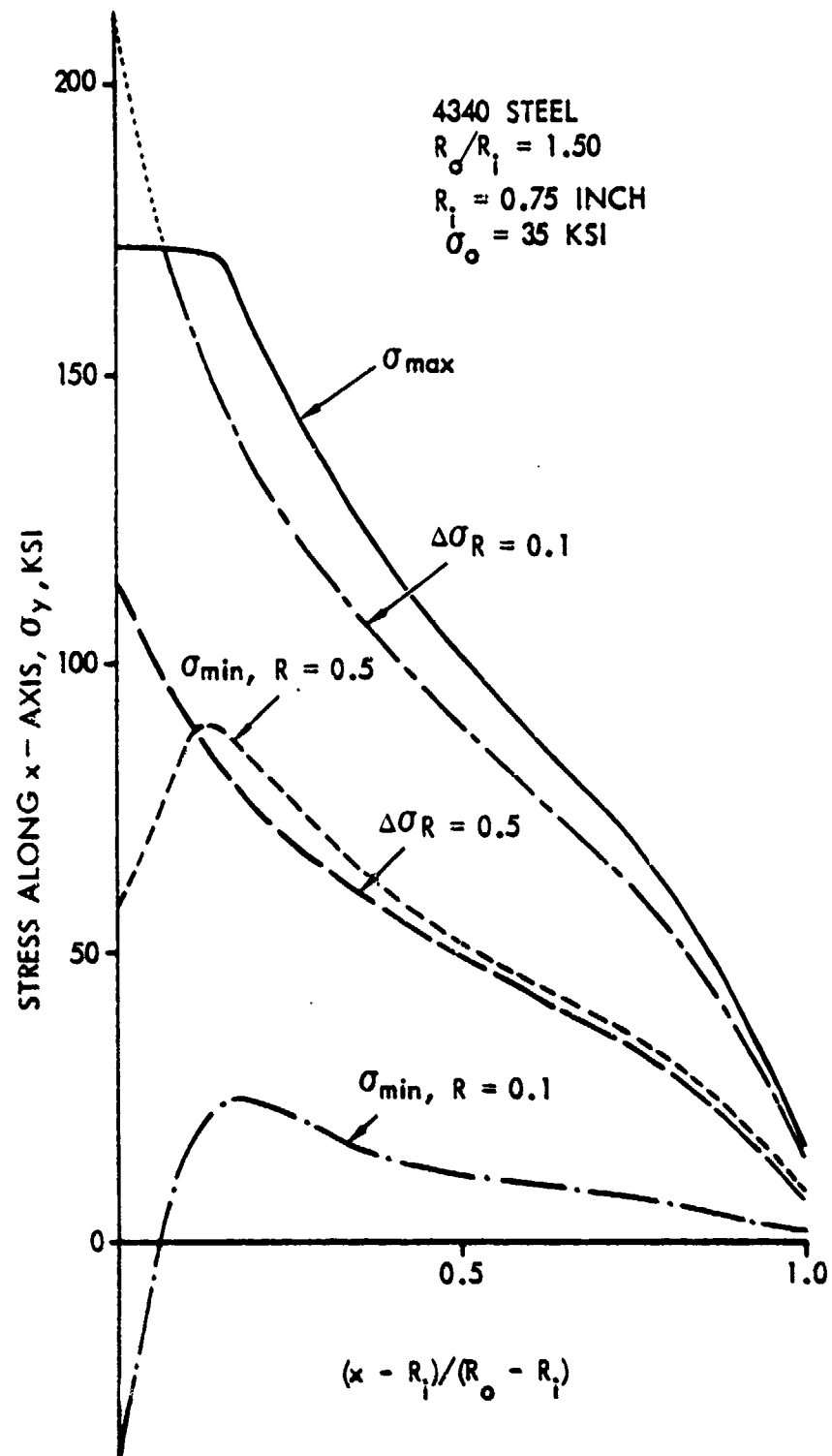
Figure 3-53. Stress Distribution Along x-Axis
for a Steel Lug with $R_o/R_i = 1.50$
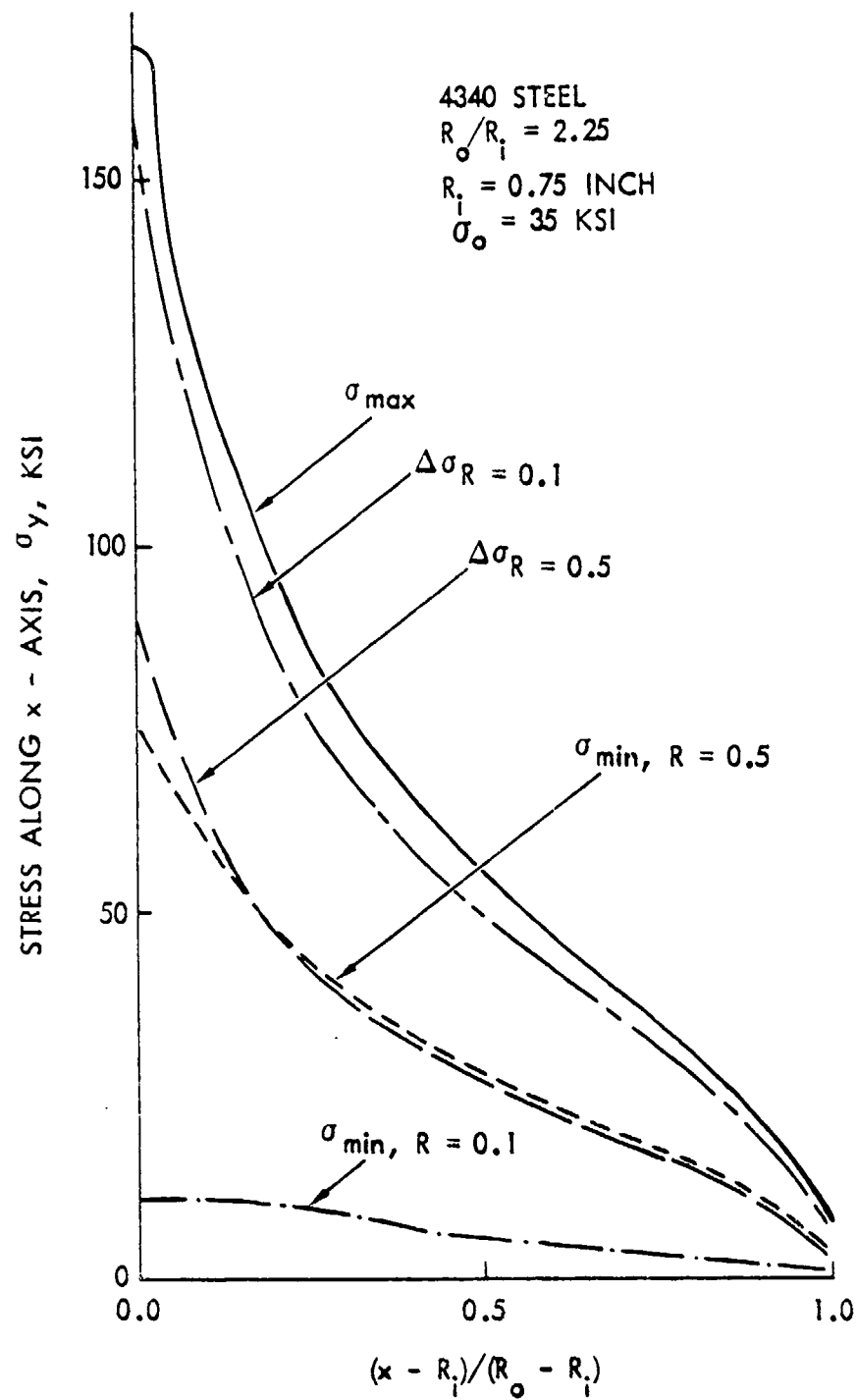
Figure 3-54. Stress Distribution Along x-Axis
for a Steel Lug with $R_o/R_i = 2.25$
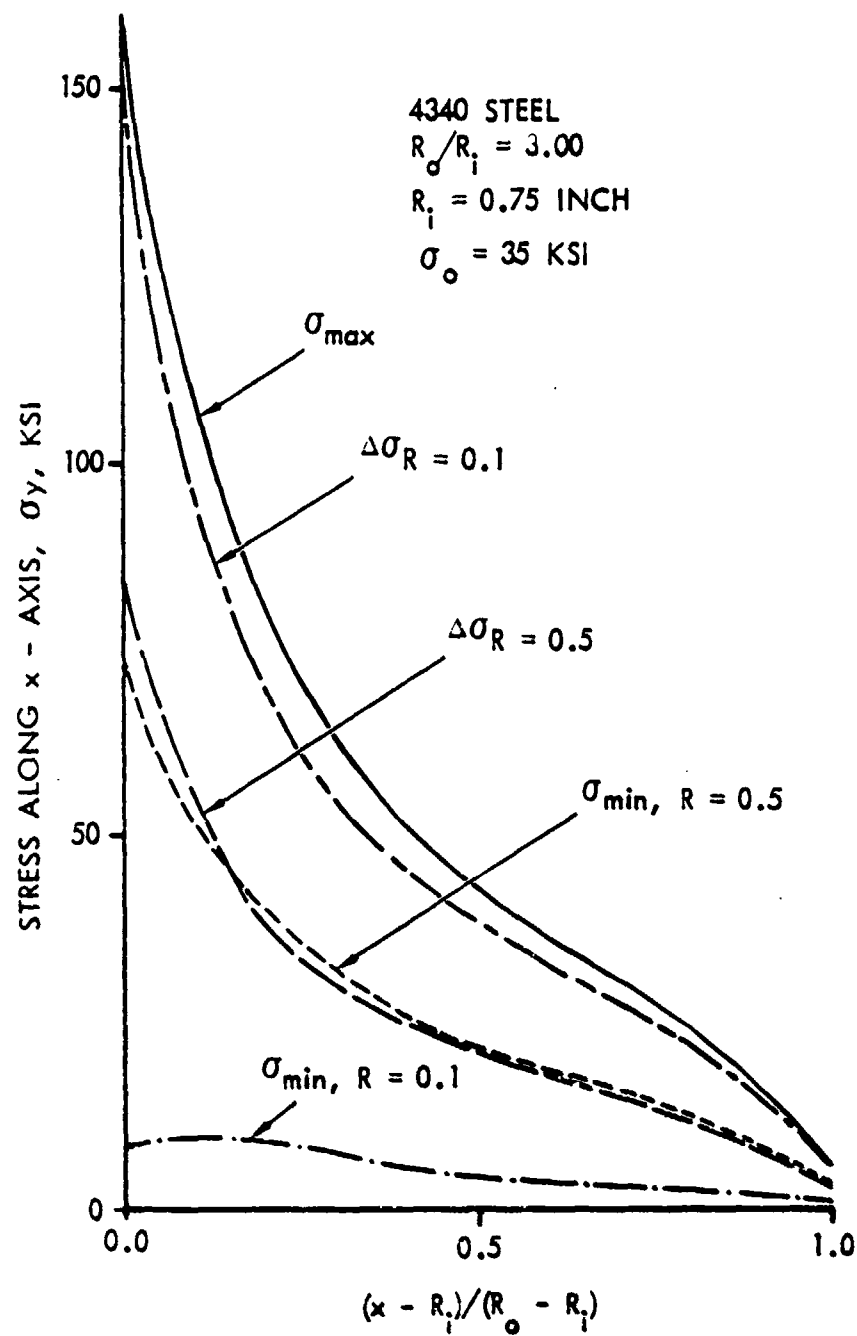
Figure 3-55. Stress Distribution Along x-Axis
for a Steel Lug with $R_o/R_i = 3.00$
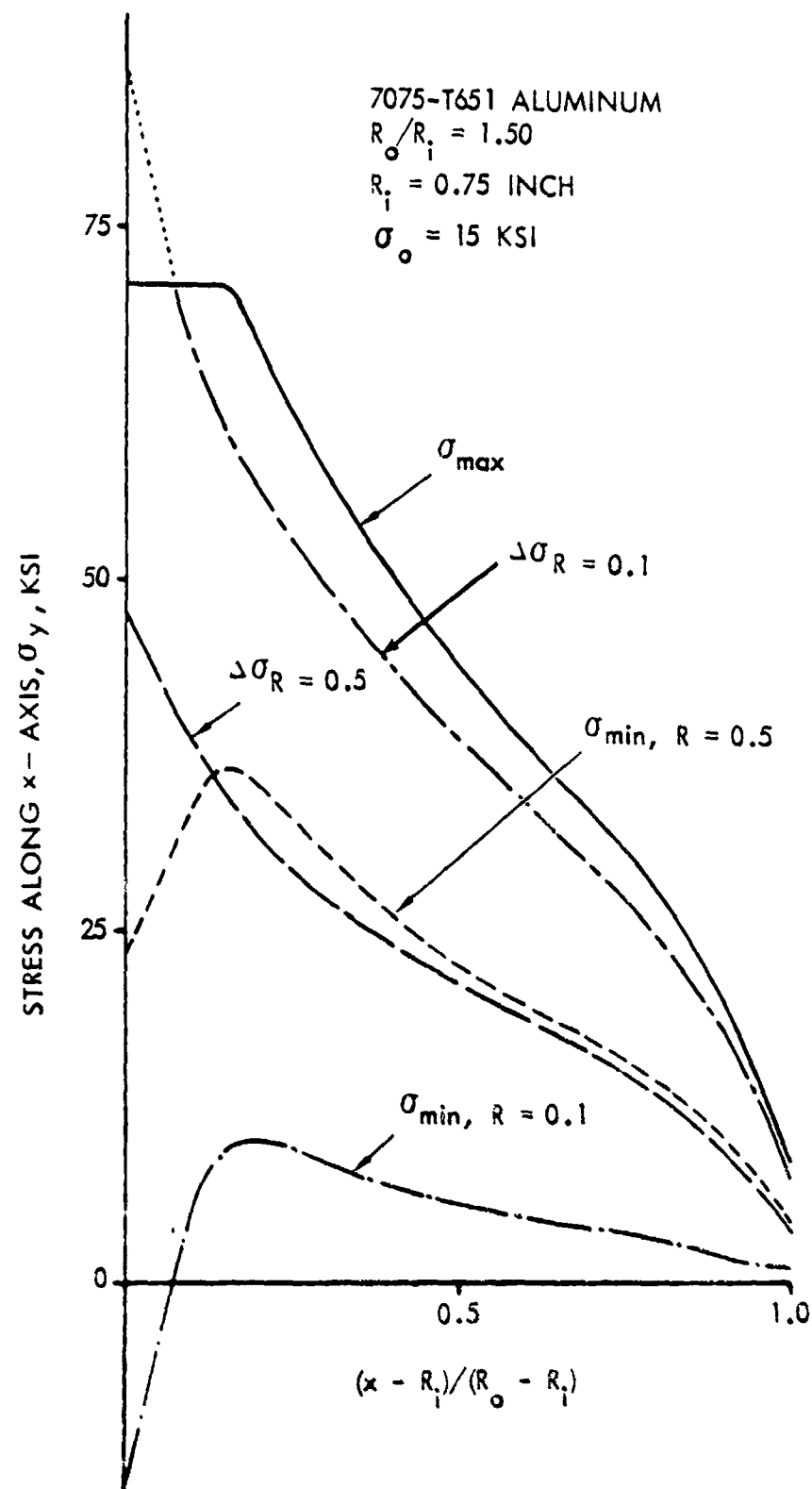
Figure 3-56. Stress Distribution Along x-Axis for an Aluminum Lug with $R_o/R_i = 1.50$

7075-T651 ALUMINUM
$R_o/R_i = 2.25$
$R_i = 0.75$ INCH
$\sigma_o = 15$ KSI

STRESS ALONG x - AXIS, σ_y, KSI

σ_{max}

$\Delta\sigma_R = 0.1$

$\Delta\sigma_R = 0.5$

$\sigma_{min}, R = 0.5$

$\sigma_{min}, R = 0.1$

$(x - R_i)/(R_o - R_i)$
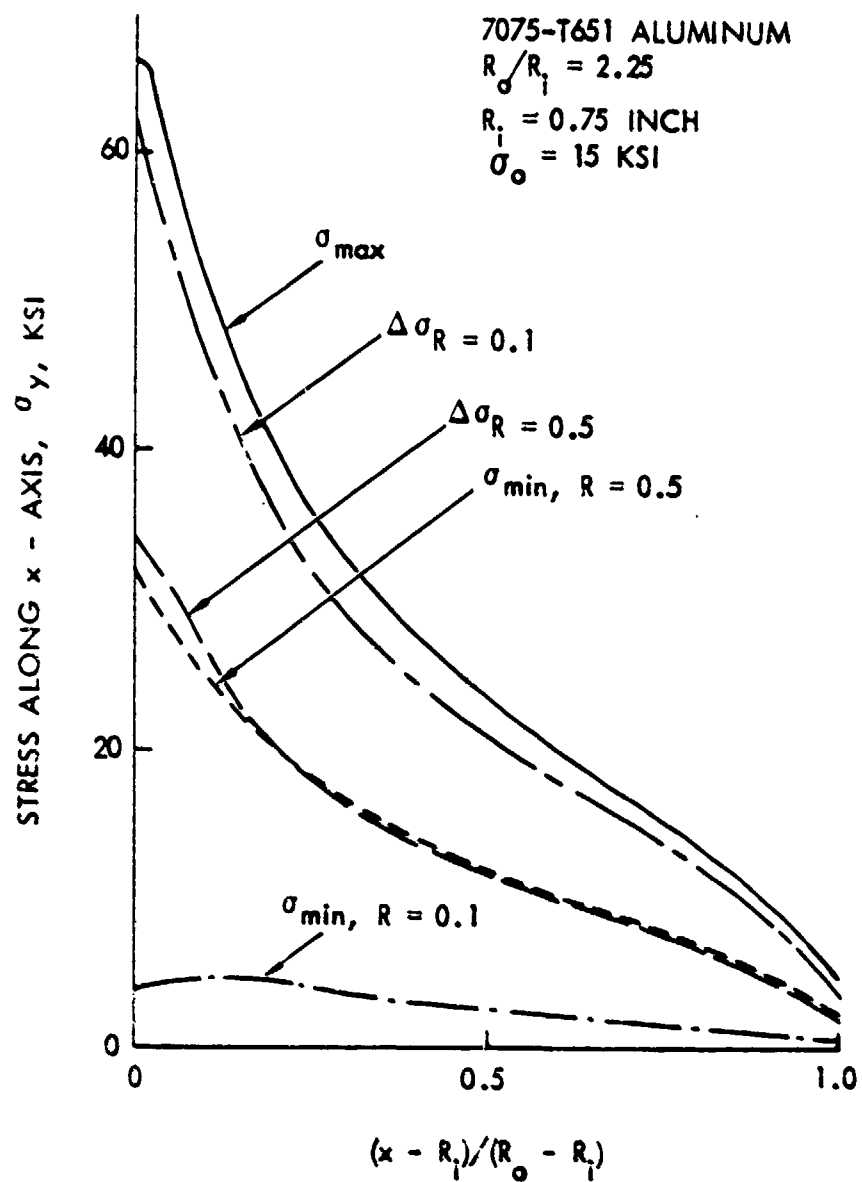
Figure 3-57. Stress Distribution Along x-Axis
for an Aluminum Lug with $R_o/R_i = 2.25$
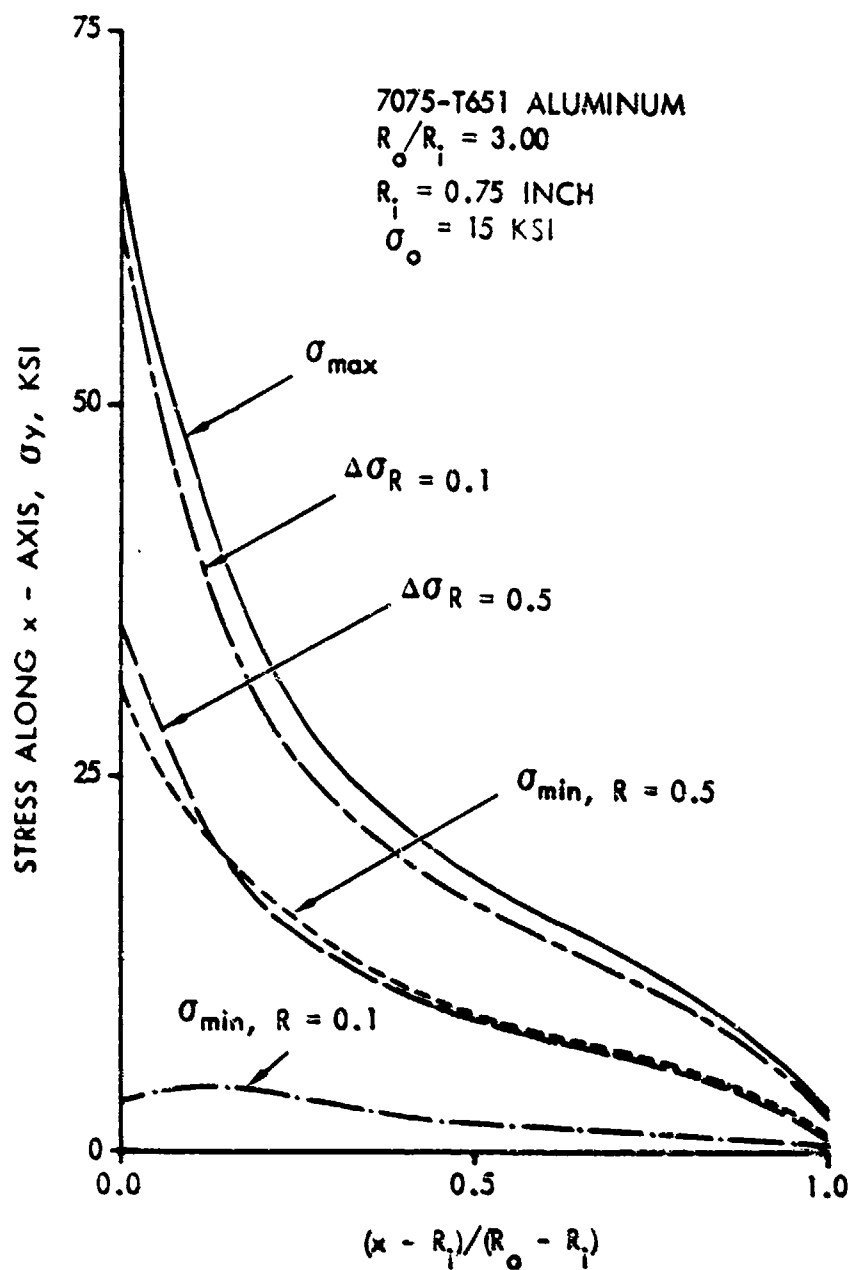
Figure 3-58. Stress Distribution Along x-Axis for an Aluminum Lug with R_o/R_i = 3.00

that is, about 5 percent of the lug ligament. Also, for R=0.1, the minimum stress near the lug hole does not become negative for this lug configuration. Thus, $\Delta\sigma_{R=0.5}$ and $\Delta\sigma_{R=0.1}$ presented are the actual differences in the stresses. Results for steel and aluminum lugs with a R_o/R_i value of 3.00 are presented in Figures 3-55 and 3-58, respectively. In this case, the lugs barely yield, and very small plastic strains were calculated by the elasto-plastic analysis.

The above stress ranges, computed from the elasto-plastic analysis, are then integrated with the Green's function to compute the stress intensity factors for through-the-thickness cracks in lugs that are loaded above yield.

The stress intensity factors can be calculated using the Green's function method by the following equation:

$$K(c) = \sigma_o \sqrt{\pi c} \int_0^1 G(\textbf{c},\xi)\, \bar{\sigma}\,(\xi)\, d\xi \qquad (44)$$

The stress intensity factor range for through-the-thickness cracks can be computed from the above equation by either inputting the maximum and minimum stresses and subtracting the values, or more directly, by using the stress range. However, in the cases where the stresses corresponding to minimum load become negative, the stress range should not be used. Rather the direct input of maximum and minimum stresses should be used and care must be exercised to neglect the negative stress intensity factors corresponding to minimum load while computing the ranges. The computed values of stress intensity factor ranges for steel and aluminum lugs are presented in Figures 3-59 and 3-60, respectively. The results are given for R_o/R_i ratios of 1.50, 2.25 and 3.00 and far-field stress ratios of 0.5 and 0.1 Since this was a nonlinear analysis, the far-field stress ratio (ratio of minimum to maximum far-field stress) differs from the crack-tip stress ratio (ratio of minimum to maximum stress intensity factor). Furthermore, because of the nonlinearity, no effort was made to normalize the stress intensity factor ranges in Figures 3-59 and 3-60. However, the crack length in the presentation has been normalized by the net ligament of each lug.

For normalized crack lengths less than about 0.35, the stress intensity factor ranges are lower for an R_o/R_i ratio of 1.50 and higher for increasing
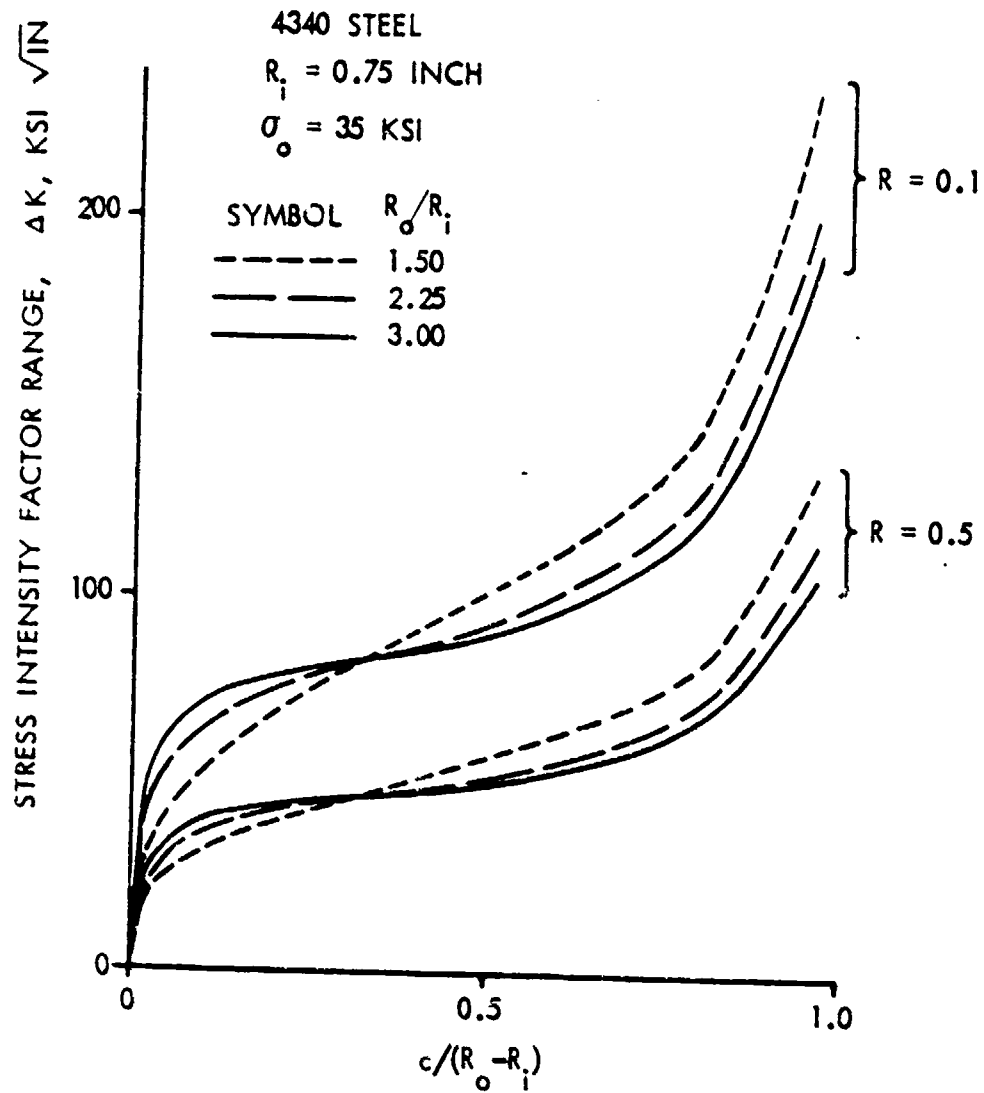
Figure 3-53. Stress Intensity Factor Ranges for Steel Lugs
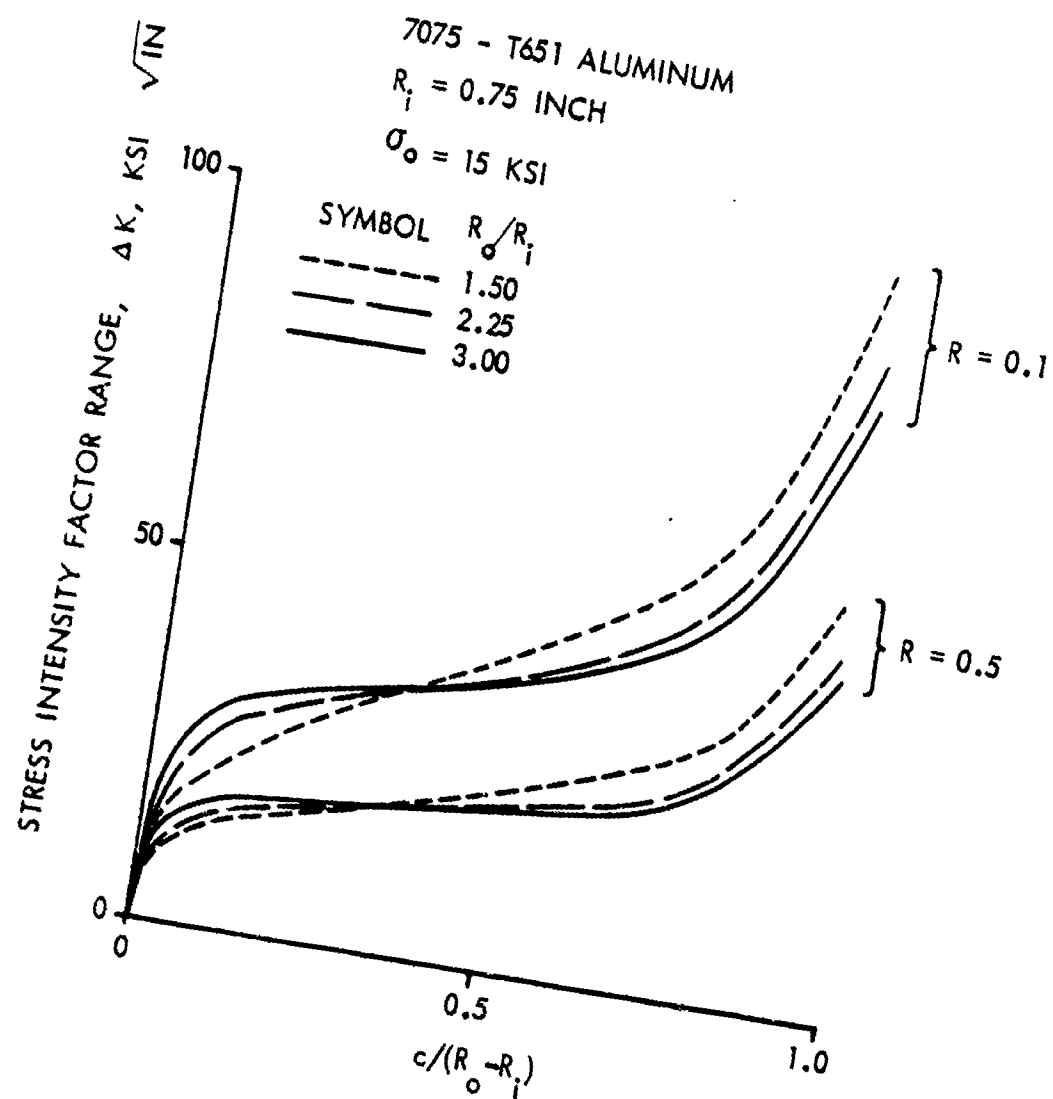
Figure 3-10. Stress Intensity Factor Ranges for Aluminum Lugs

R_o/R_i ratios. For normalized crack lengths above 0.35, the trend changes to higher stress intensity factor ranges for lower R_o/R_i ratios. However, expressed in terms of unnormalized physical crack length, c, the stress intensity factor for any given crack length is always higher for a lower R_o/R_i ratio.

To assess and to have a feel for the effects of plastic yielding by comparing with linear analysis, the stress intensity factor ranges are normalized by $\Delta\sigma_o\sqrt{\pi c}$, where $\Delta\sigma_o$ is the corresponding far-field stress range. These normalized values given in Table 3-13 have limited significance in the sense that these values are applicable to the specific material and loading condition. The values can be directly compared with the normalized stress intensity factor ranges given in Table 3-3 (applicable for R=0.1 and R=0.5), which correspond to linear analysis, to evaluate the effect of plasticity. Table 3-3 can be assumed to be applicable for both materials, since the differences were less than 3 percent.

Comparison of these two tables indicates that the normalized values of ΔK for the elasto-plastic analysis are lower for smaller $c/(R_o-R_i)$ ratios and become higher as the crack grows through the lug ligament. This is because of the stress redistribution in the lug due to yielding. In the yield zone and its neighborhood, the stresses will be lower when compared with the elastic stresses. Away from the plastic zone, the stresses will be higher than elastic stresses, to satisfy the equilibrium. The above behavior is true, in general; however, for an R_o/R_i ratio of 1.50 and a stress ratio of 0.1, the nonlinear values are consistently lower than the linear values for almost all $c/(R_o-R_i)$ values. The reason for this behavioral change can be explained as follows. For this particular lug configuration and stress ratio, there is more plastic yielding as well as compressive residual stresses near the lug hole at the minimum load. These negative stresses are truncated in the stress intensity computation. Also, the net ligament length is the smallest. For these two reasons, i.e., truncation of negative stresses and smaller ligament size, the normalized values of stress intensity factor range never become higher than those of the linear analysis. Also, note that due to plastic yielding while loading and subsequent linear unloading, the normalized values of R = 0.5 for lower $c/(R_o/R_i)$ ratios are greater than the corresponding values of R = 0.1 and closer to linear elastic values given in Table 3-3.

114

TABLE 3-13.   NORMALIZED STRESS INTENSITY FACTOR RANGES FROM PLASTIC ANALYSIS – $\Delta K/(\Delta\sigma_0 \sqrt{\pi c})$

$c/(R_0-R_1)$ $\diagdown$ R_0/R_1	4340 STEEL						7075-T651 ALUMINUM					
	R = 0.1			R = 0.5			R = 0.1			R = 0.5		
	1.50	2.25	3.00	1.50	2.25	3.00	1.50	2.25	3.00	1.50	2.25	3.00
0.00	6.124	5.564	5.404	7.360	5.776	5.376	5.890	5.227	5.123	7.153	5.182	5.092
0.10	4.890	3.805	3.319	5.278	3.902	3.370	4.720	3.711	3.278	5.167	3.751	3.321
0.20	4.471	3.114	2.578	4.688	3.166	2.600	4.348	3.047	2.546	4.591	3.071	2.564
0.30	4.306	2.785	2.235	4.462	2.814	2.241	4.201	2.732	2.208	4.378	2.743	2.212
0.40	4.195	2.558	2.010	4.326	2.577	2.011	4.103	2.514	1.987	4.252	2.518	1.986
0.50	4.197	2.459	1.901	4.310	2.472	1.900	4.117	2.423	1.883	4.246	2.424	1.881
0.60	4.266	2.427	1.854	4.364	2.438	1.854	4.197	2.399	1.841	4.311	2.401	1.839
0.70	4.425	2.492	1.885	4.518	2.500	1.883	4.366	2.467	1.873	4.474	2.466	1.870
0.80	4.799	2.684	2.006	4.889	2.692	2.003	4.749	2.663	1.995	4.853	2.660	1.990
0.90	6.071	3.356	2.478	6.618	3.362	2.473	6.037	3.345	2.469	6.151	3.338	2.463

115

The elasto-plastic method can also be used to calculate the stress intensity factor solutions for corner cracks emanating from attachment lugs that are subjected to loadings above yield. The above through-the-thickless solution can be modified with front-free surface, curvature correction, etc. for corner crack problems, as in Equations (34) and (35) of subsection 3.

SECTION IV

STRESS INTENSITY FACTORS FOR TAPERED ATTACHMENT LUGS

Tapered attachment lugs have been used frequently in aircraft struc-
tural fittings to provide strength against off-axis loading.   To
determine the critical location and direction where a fatigue crack may
initiate and subsequently grow, it is necessary to determine the stress dis-
tribution of the unflawed lug and the stress intensity factors of the cracked
lug.   This section describes the development of stress distribution and
stress intensity factors for tapered attachment lugs subjected to symmetric,
off-axis and transverse loadings.

1.   STRESS ANALYSIS

Because of the complexity of the lug geometry and off-axis loading,
the finite element method was used to determine the tangential stress dis-
tributions along the edge of the hole in the unflawed lug.   This analysis
was conducted for a pin load applied at 0°, 90°, 135°, 180°, 270°, and 315°
measured in the clockwise direction from the axis of the lug.   Figure 4-1
depicts the geometry and typical two-dimensional finite element model used
in the stress analysis of the unflawed lug.   The angle between the two edge
surfaces of the tapered head, β, is 45 degrees.   The finite element model
shown in Figure 4-1 consists of 429 nodes, 72 triangular elements, 348 quad-
rilateral elements, 28 spring elements, and a total of 850 degrees of free-
dom.   A concentrated force was applied at the center of the pin to simulate
pin loading and was reacted at the base of the lug.   The analysis was
carried out to determine the stresses in the lug and the pin-bearing pres-
sure distributions at the pin-lug contact area for the six loading direc-
tions mentioned above.   Three outer-to-inner radius ratios of the tapered
head, i.e., R_o/R_i - 1.50, 2.25 and 3.00, were evaluated.   In all cases of
the analysis, the rigidity of the pin was assumed to be three times the
rigidity of the lug, which simulates an aluminum lug loaded by a steel pin.

For the conventional finite-element analysis using constant strain
elements, the values of stress and strain obtained for a given element
were assigned to the centroid location of that element.   To determine
the stress at the edge of the hole, the stresses at the centroids of a
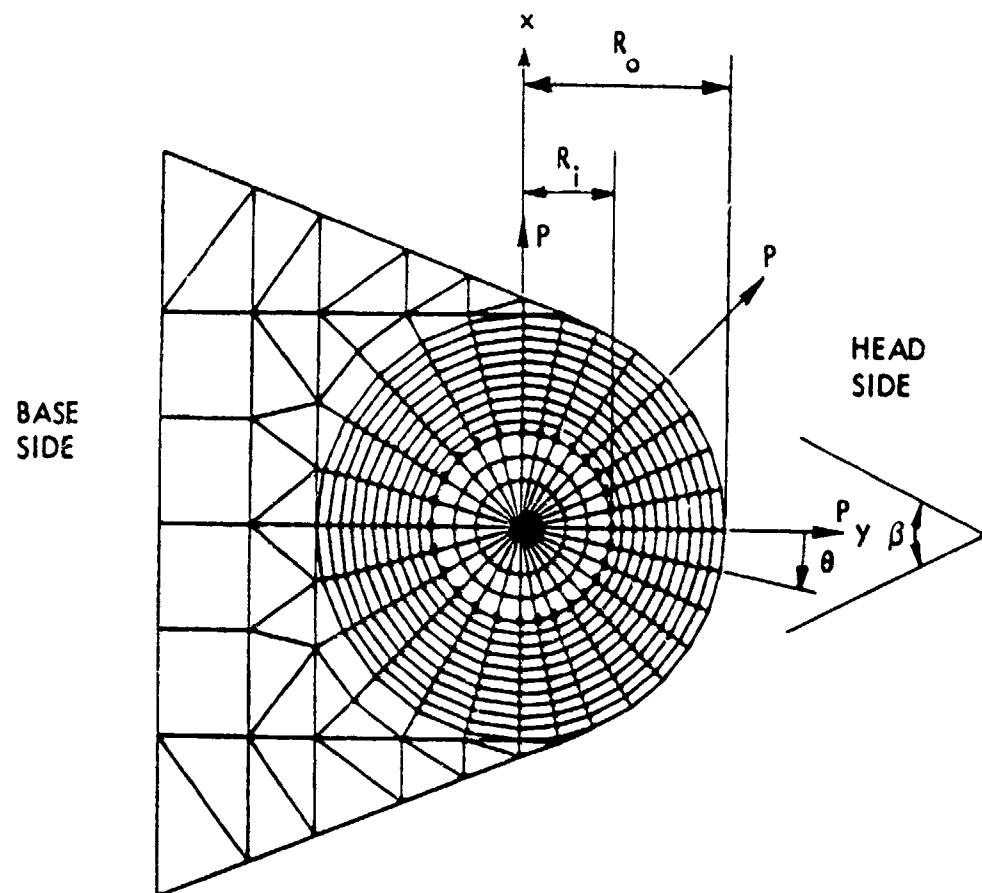
Figure 4-1. Finite Element Model for a Tapered Attachment Lug Having a R_o/R_i Ratio of 2.25

series of elements located in the same radial direction were used to extrap-
olate to the edge location. This procedure was used to determine the tan-
gential stresses along the edge of the hole of tapered lugs having R_o/R_i
ratios of 1.50, 2.25 and 3.00. The results are shown in Figures, 4-2, 4-3,
and 4-4 for pin loadings applied in three principal directions, i.e., 0°,
-45° (315°), and -90° (270°), respectively. In each case, the tangential
stresses were normalized with the average pin bearing pressure, σ_{br}, which
is defined as $P/(2R_iB)$, where B is the thickness of the lug.

As can be seen from these figures, for each loading direction, there
are two local maximum tangential stresses located at each side of the load-
ing direction. The locations of these maximum stresses depend upon the
loading direction and R_o/R_i ratio. For a pin loading applied in the axial
direction of the lug, as shown in Figure 4-2, the maximum stress locations
are found at about ±85 to $\pm90^o$ away from the loading direction. The maximum
stress locations do not change significantly with the change of the R_o/R_i
ratio. When the pin loading is applied in the -45° direction (see Figure
4-3), for $R_o/R_i = 1.50$, the absolute maximum stress occurs at about 65°
measured from the axis of the lug (or 110° away from the load direction)
with the other local maximum stress located about 180° from the first. When
the R_o/R_i ratio increases, the locations of the maximum stresses change
only slightly. However, the absolute maximum stress location switches from
the head side of the lug to the base side of the lug. When the pin loading
is applied in the direction perpendicular to the axis of the lug (see Figure
4-4), for all R_o/R_i ratios, the maximum stress occurs at the location in
the base of the lug at a θ value of about 200° to 210°. Figure 4-5 summa-
rizes the locations of the local maximum tangential stresses at the edge of
the hole for each loading direction. These are the most critical locations,
where one would anticipate that a fatigue crack would initiate. For each
lug geometry and loading condition, Numbers 1 and 2 shown in Figure 4-5
indicate the probable order of crack initiation. They are chosen based upon
the relative magnitude of the two computed local maximum stresses. Stress
distributions along the x-axis for tapered lugs with R_o/R_i ranging from 1.5 to
3.0 subjected to symmetric loading are presented in Figure 4-6 and Table 4-1.

Larsson [47, 48] conducted fatigue testing of axially and transversely
loaded aluminum lugs having a R_o/R_i ratio of 2.2. He observed and tabu-
lated the locations of fretting and crack initiation for three different lug

119
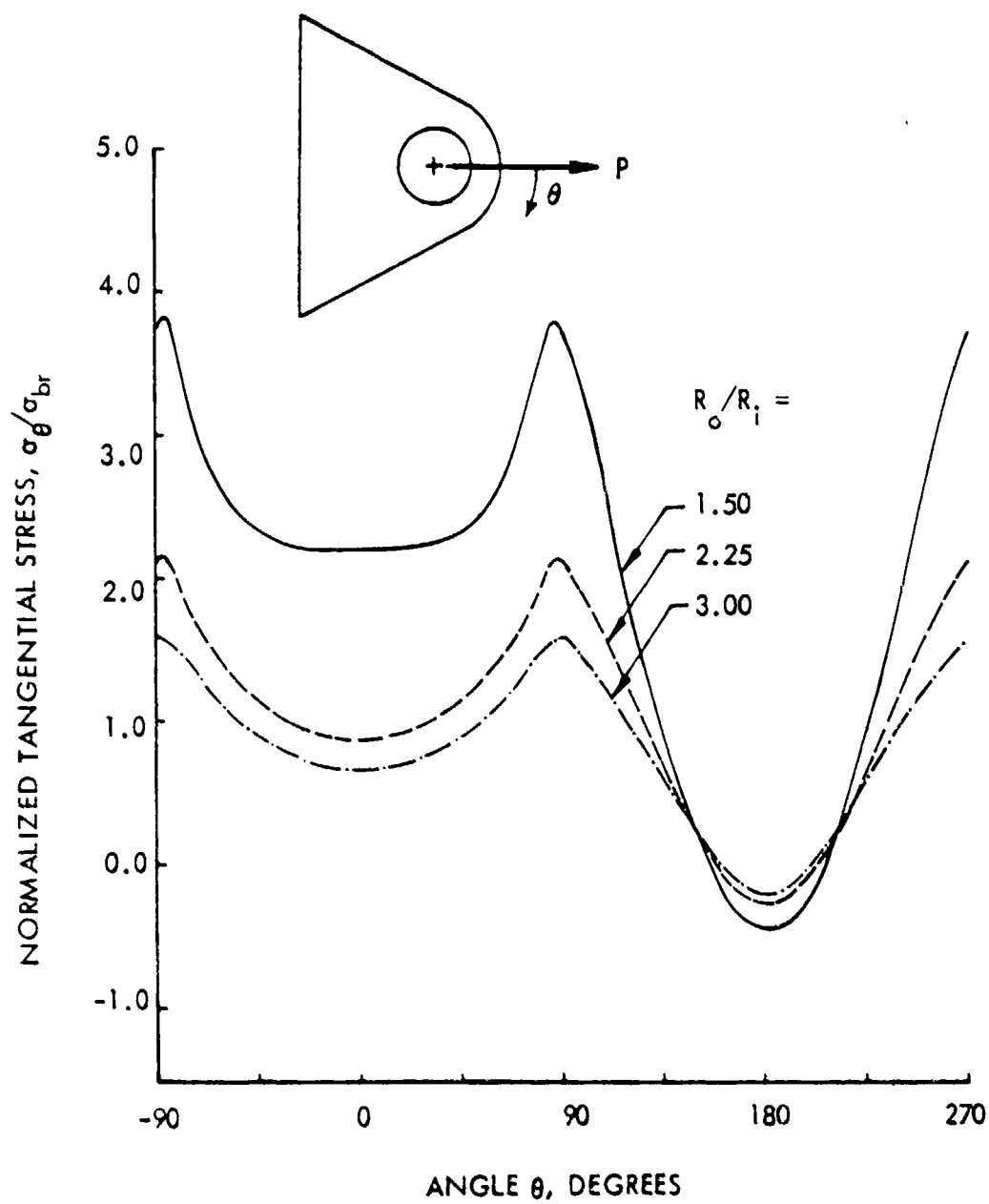
Figure 4-2. Normalized Tangential Stress Distributions Along the Edge of the Hole for Tapered Lugs Subjected to a Pin Loading Applied in $0°$ Direction

120
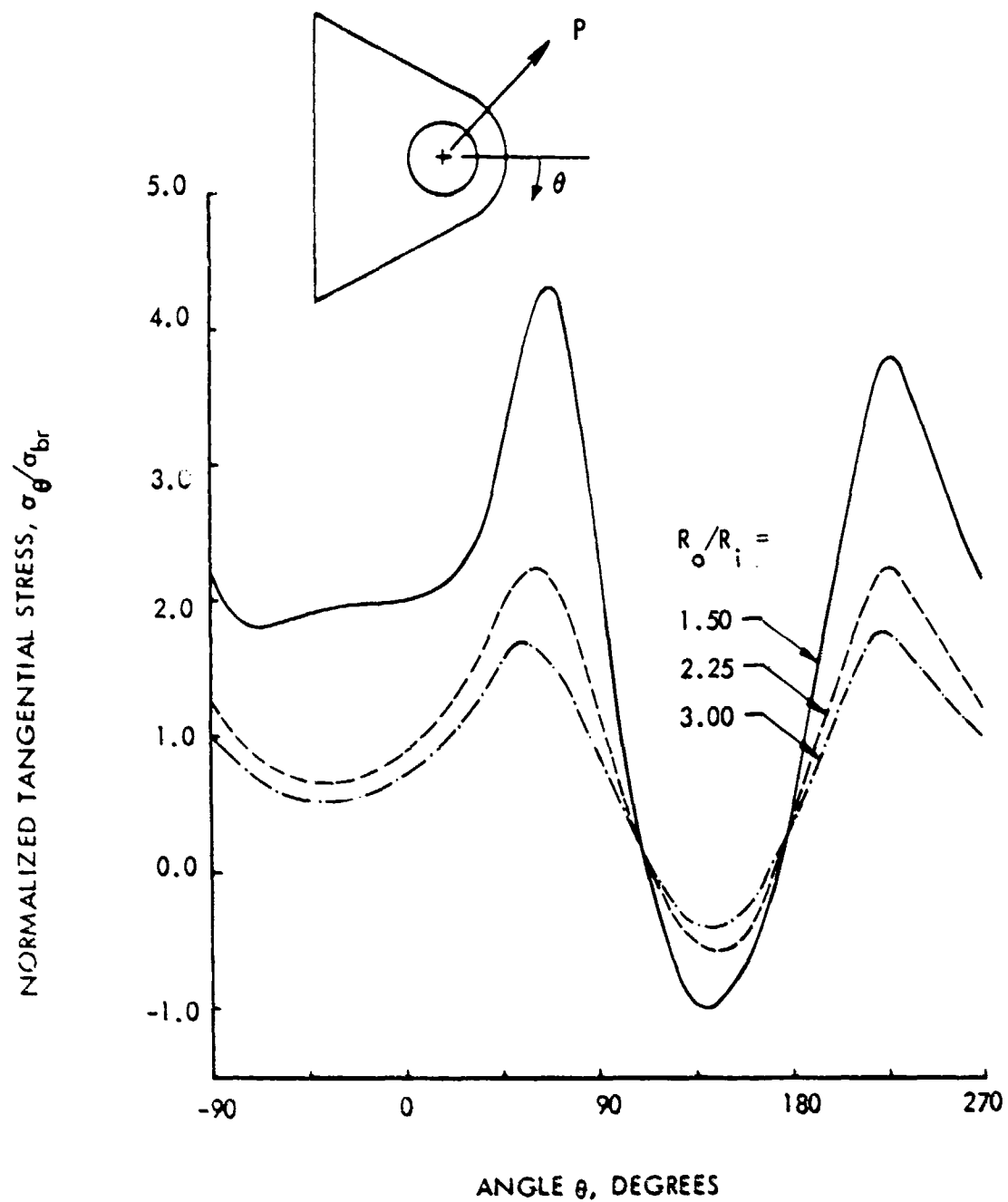
Figure 4-3. Normalized Tangential Stress Distributions Along the Edge of the Hole for Tapered Lugs Subjected to a Pin Loading Applied in –45° Direction

121
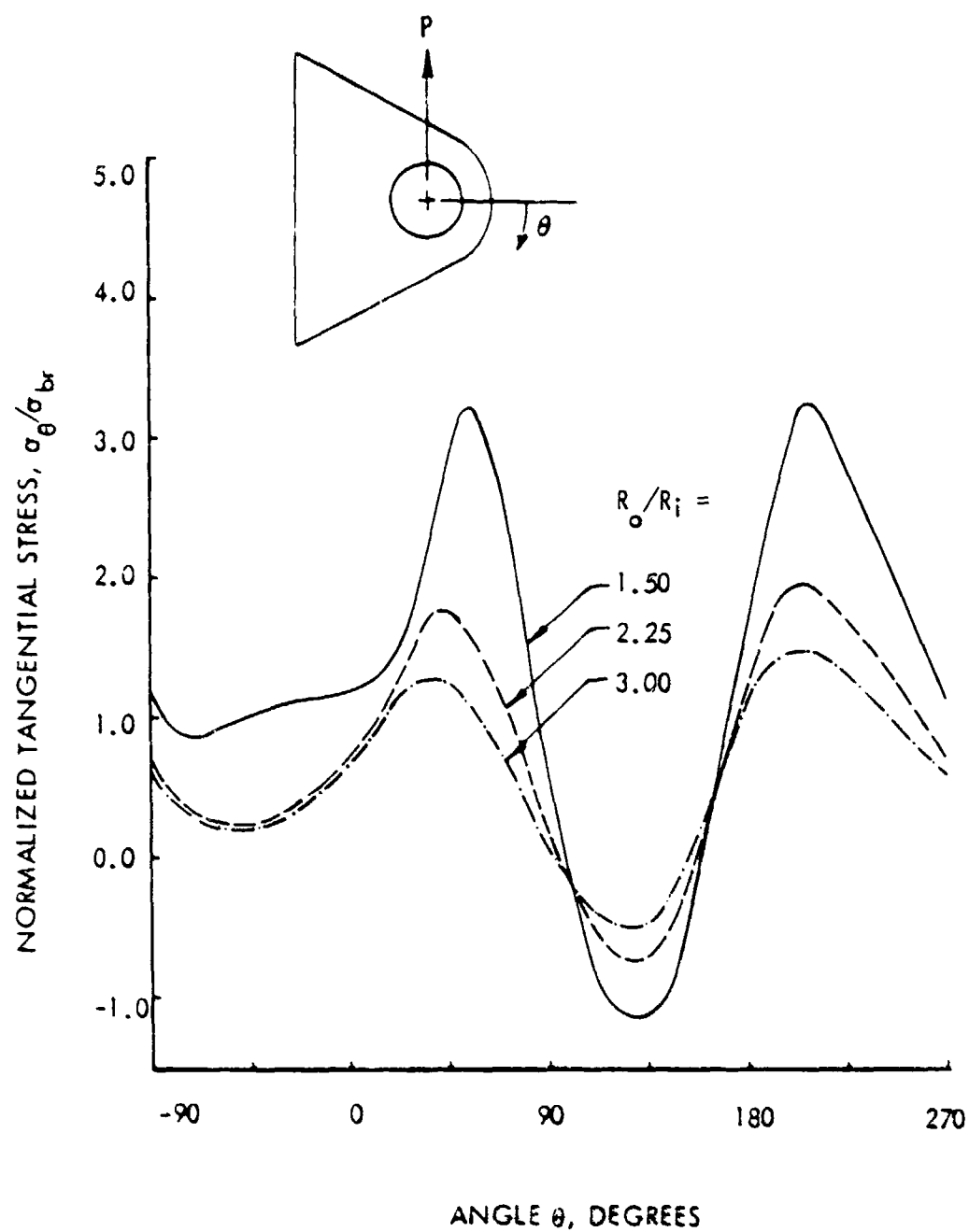
Figure 4-4. Normalized Tangential Stress Distributions Along the Edge of the Hole for Tapered Lugs Subjected to a Pin Loading Applied in $-90°$ Direction

SYMBOL	LOAD DIRECTION
--O--	$0°$
—△—	$-45°$
·—□—·	$-90°$
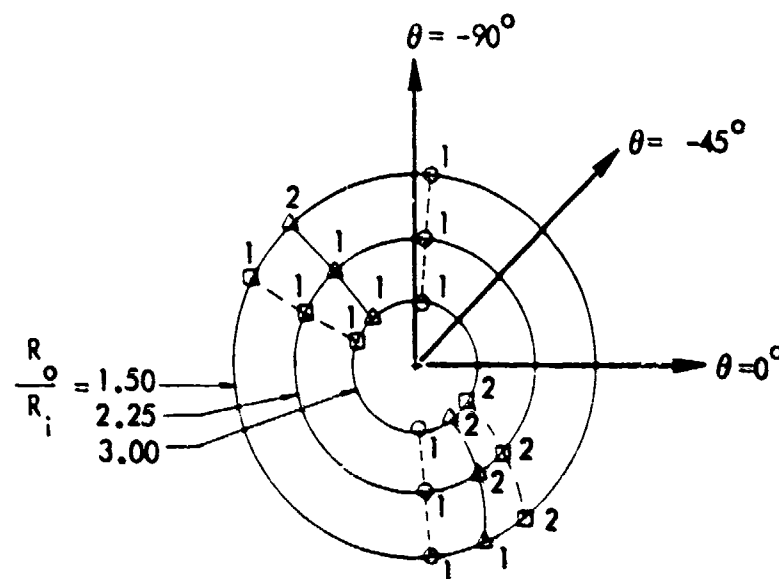
Figure 4-5. Fatigue Critical Locations of Tapered Lugs
Subjected to Various Load Orientations
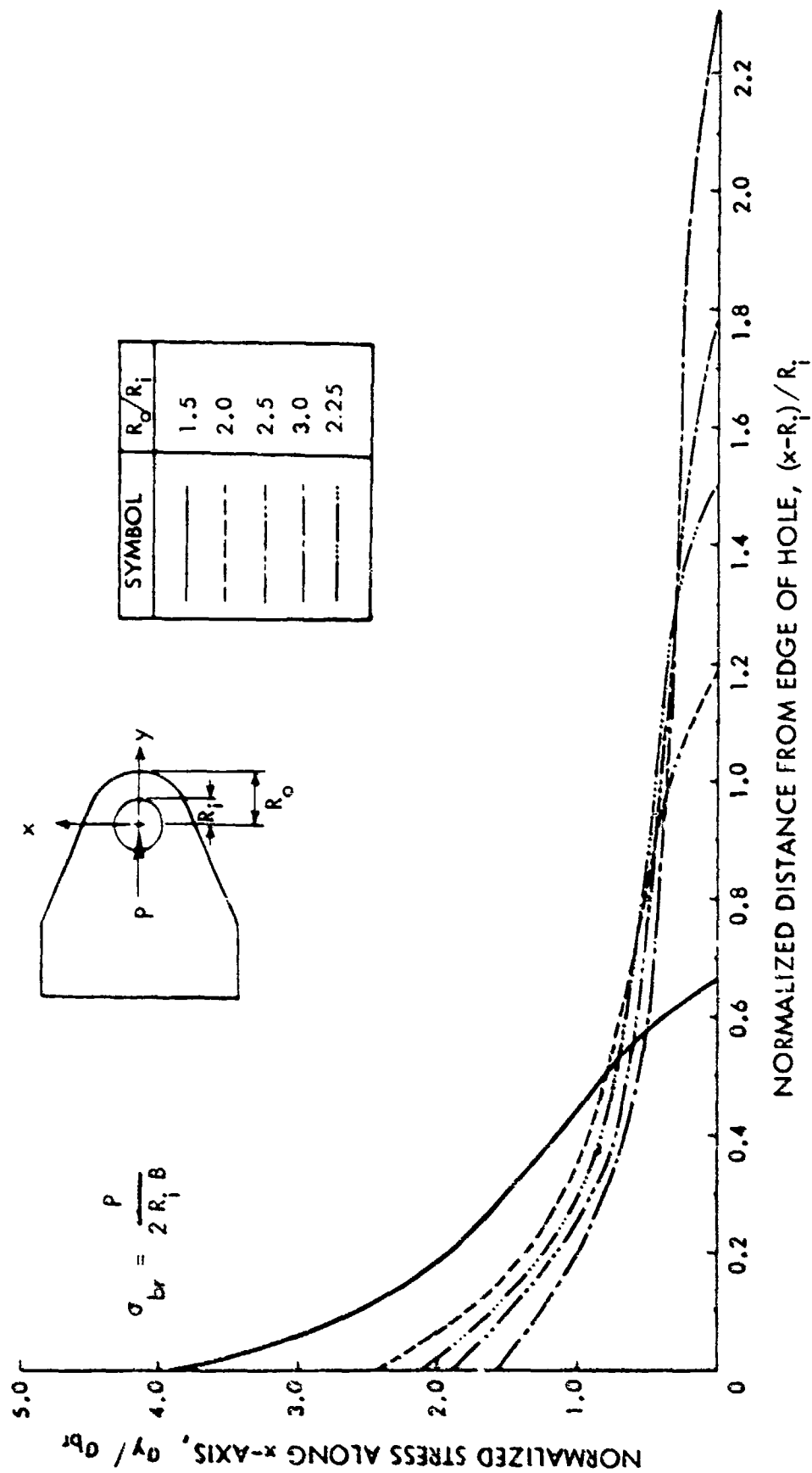
Figure 4-6. Unflawed Stress Distributions at Tapered Attachment Lugs Having Various R_o/R_i Ratios

SYMBOL	R_o/R_i
———	1.5
— —	2.0
—·—	2.5
— —	3.0
·····	2.25

$$\sigma_{br} = \frac{P}{2 R_i B}$$

NORMALIZED DISTANCE FROM EDGE OF HOLE, $(x-R_i)/R_i$

NORMALIZED STRESS ALONG x-AXIS, σ_y/σ_{br}

TABLE 4-1. NORMALIZED UNFLAWED STRESS DISTRIBUTION ALONG x-AXIS FOR TAPERED ATTACHMENT LUGS

$(x-R_i)/(R_o-R_i)$ \ R_o/R_i	σ_y/σ_{br}					σ_y/σ_o				
	1.50	2.00	2.25	2.50	3.00	1.50	2.00	2.25	2.50	3.00
0.00*	3.768	2.405	2.104	1.878	1.562	5.652	4.810	4.734	4.695	4.686
0.05	3.393	2.109	1.783	1.593	1.260	5.090	4.218	4.012	3.983	3.780
0.15	2.770	1.540	1.292	1.057	0.799	4.155	3.080	2.907	2.643	2.397
0.25	2.320	1.190	0.945	0.762	0.563	3.480	2.380	2.126	1.905	1.689
0.35	2.034	0.998	0.793	0.632	0.458	3.051	1.996	1.784	1.580	1.374
0.45	1.778	0.854	0.681	0.538	0.388	2.667	1.708	1.532	1.345	1.154
0.55	1.588	0.747	0.592	0.470	0.339	2.382	1.494	1.332	1.175	1.017
0.65	1.396	0.647	0.521	0.408	0.297	2.094	1.294	1.172	1.020	0.891
0.75	1.246	0.564	0.452	0.355	0.263	1.869	1.128	1.017	0.888	0.789
0.85	1.080	0.475	0.391	0.298	0.230	1.620	0.950	0.880	0.745	0.690
0.95	0.882	0.408	0.332	0.252	0.209	1.323	0.816	0.747	0.630	0.627

*Extrapolated Values

125

configurations. His results of crack initiation locations are summarized in Figures 4-7 and 4-8 for a pin loading applied in the 0° and 90° directions, respectively. As seen from these figures, the current predicted fatigue critical locations as well as the possible sequence of crack initiation agree well with these experimental data. These predicted critical locations will be used in the modeling of the cracked lugs in the subsequent fracture analysis.

The fatigue critical area of an attachment lug for a given loading direction is not necessarily subjected to compression when the loading direction is reversed. Thus, for some load orientations, the reversed fatigue loading might have a significant effect on crack growth behavior. Figures 4-9 through 4-11 show the tangential stress distributions along the edge of the hole for a pin loading applied in the reversed direction of the three primary load orientations presented in Figures 4-2 through 4-4, respectively. As seen from the figures, in most cases, the reversed loading stretches the critical area in tension, but the magnitude is reduced. Note that the result in Figure 4-11 is essentially the same as that in Figure 4-4 except for the definition of the angle θ . Plots of the stress concentration factors at the edge of the hole in logarithmic scales, as shown in Figure 4-12 for symmetrically loaded tapered attachment lugs, reveal that a simple empirical formula can be derived and the relationship is given by the equation

$$K_{tb} = \frac{\sigma_{max}}{\sigma_{br}} = (2.75 - \frac{\beta^o}{135}) \; (\frac{R_o}{R_i} - 1)^{-(0.675 - \frac{\beta^o}{1000})} \qquad (45)$$

where β^o is the taper angle of the attachment lug in degrees. Note that for straight lugs ($\beta = 0^o$) the above equation reduces to that given in Figure 3-5.

The stress concentration factors were obtained by normalizing the peak tangential stresses with the average pin bearing pressure, σ_{br}. The equation of the logarithmic straight lines shown in Figure 4-12 compares with the finite element solution within 0.8 percent for tapered lugs. The values computed by the above equation and the finite element method are also listed in tabular form in Figure 4-12 for comparison. This simple empirical equation may be used for interpolating for taper angles less than 45° or extrapolating for R_o/R_i values outside the range of 1.5 and 3.0. The values of
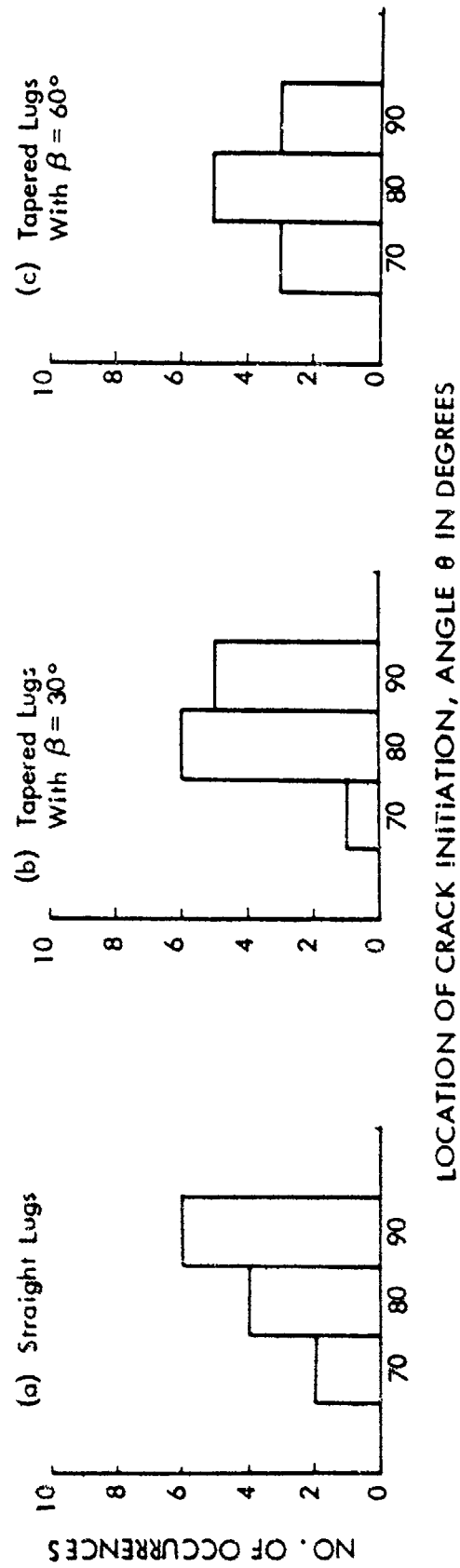
Figure 4—7. Locations of Crack Initiation for Various Attachment Lugs Subjected to a Pin Loading Applied in 0° Direction

127

NO. OF OCCURRENCES

(a) Straight Lugs

(b) Tapered Lugs
With $\beta = 30°$

(c) Tapered Lugs
With $\beta = 60°$
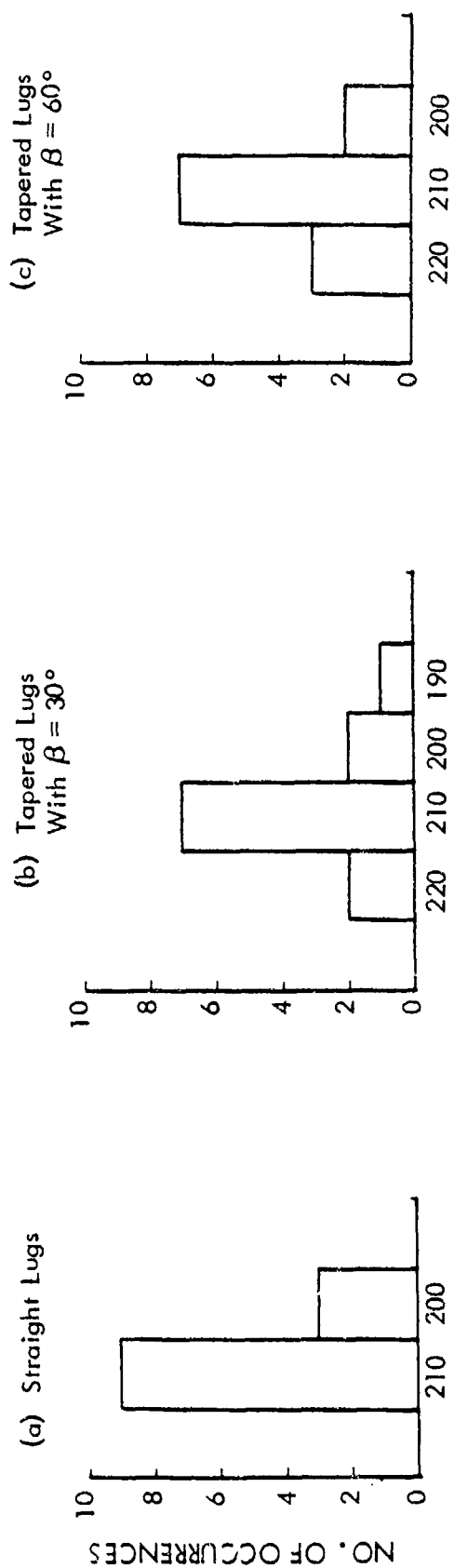
LOCATION OF CRACK INITIATION, ANGLE θ IN DEGREES

Figure 4-8. Locations of Crack Initiation for Various Attachment Lugs Subjected to a Pin Loading Applied in -90° Direction

128
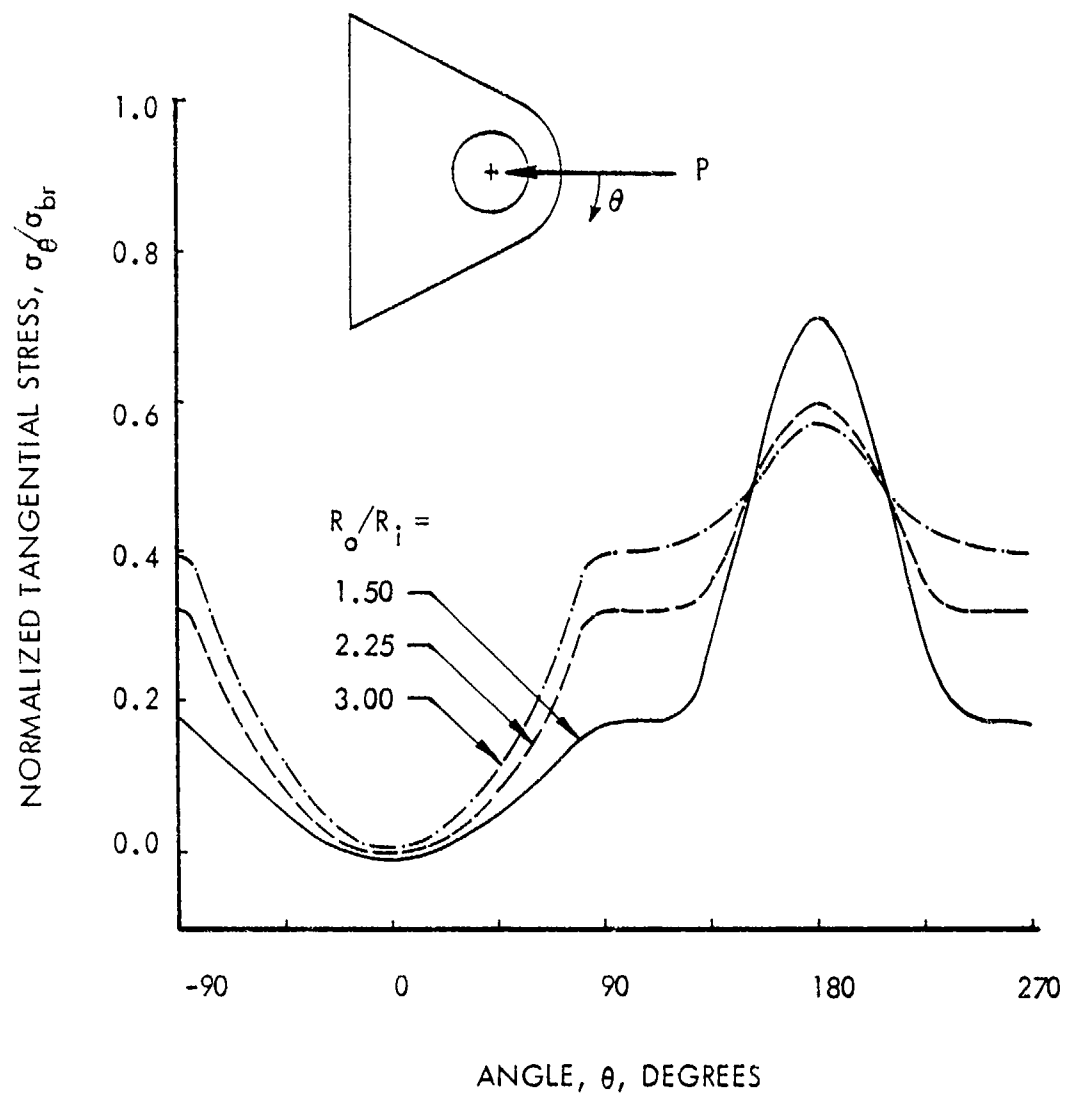
Figure 4-9. Normalized Tangential Stress Distributions Along the Edge of the Hole for Tapered Lugs Subjected to a Pin Loading Applied in 180° Direction

129
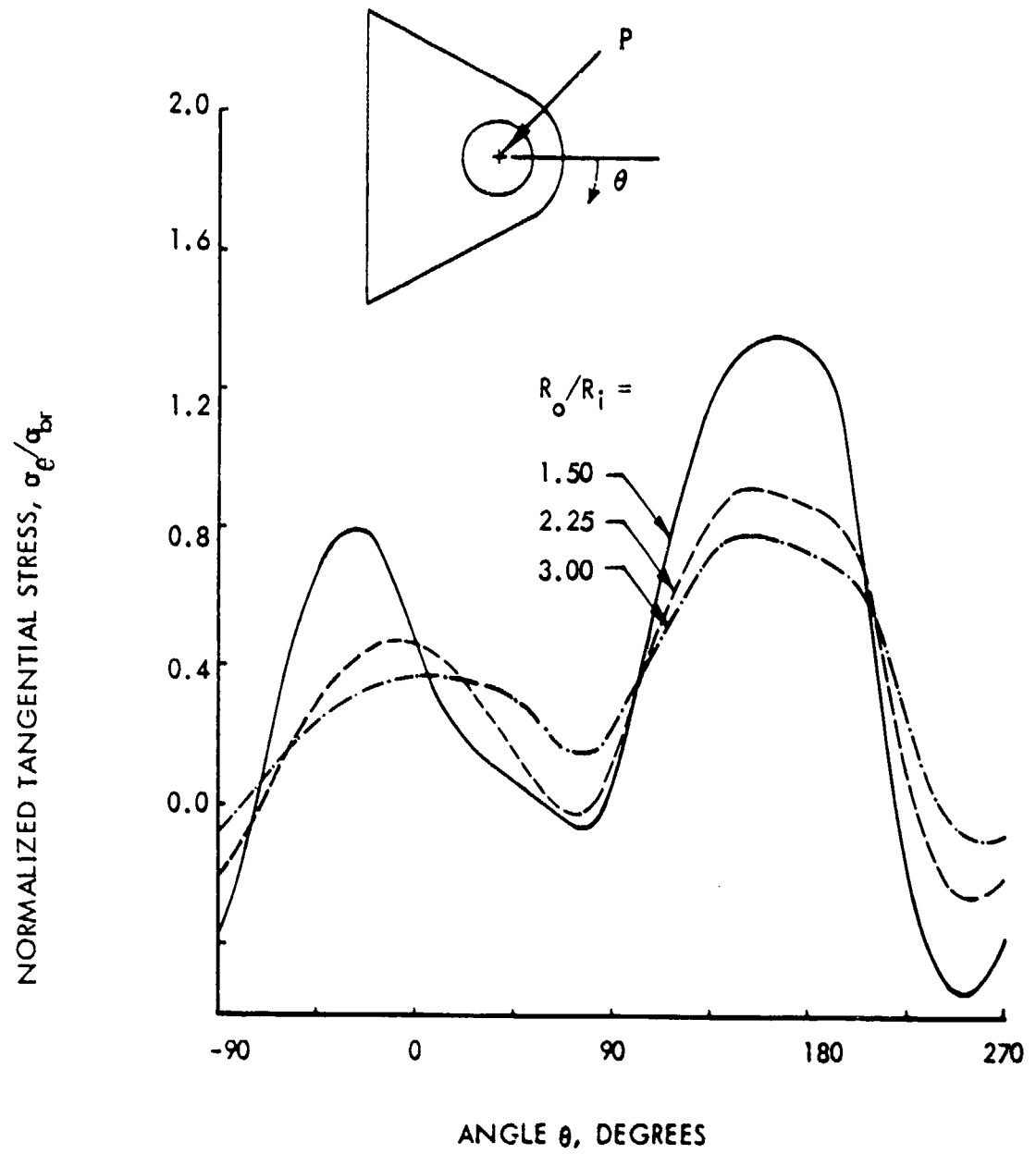
Figure 4-10. Normalized Tangential Stress Distributions Along the Edge of the Hole for Tapered Lugs Subjected to a Pin Loading Applied in 135° Direction

130
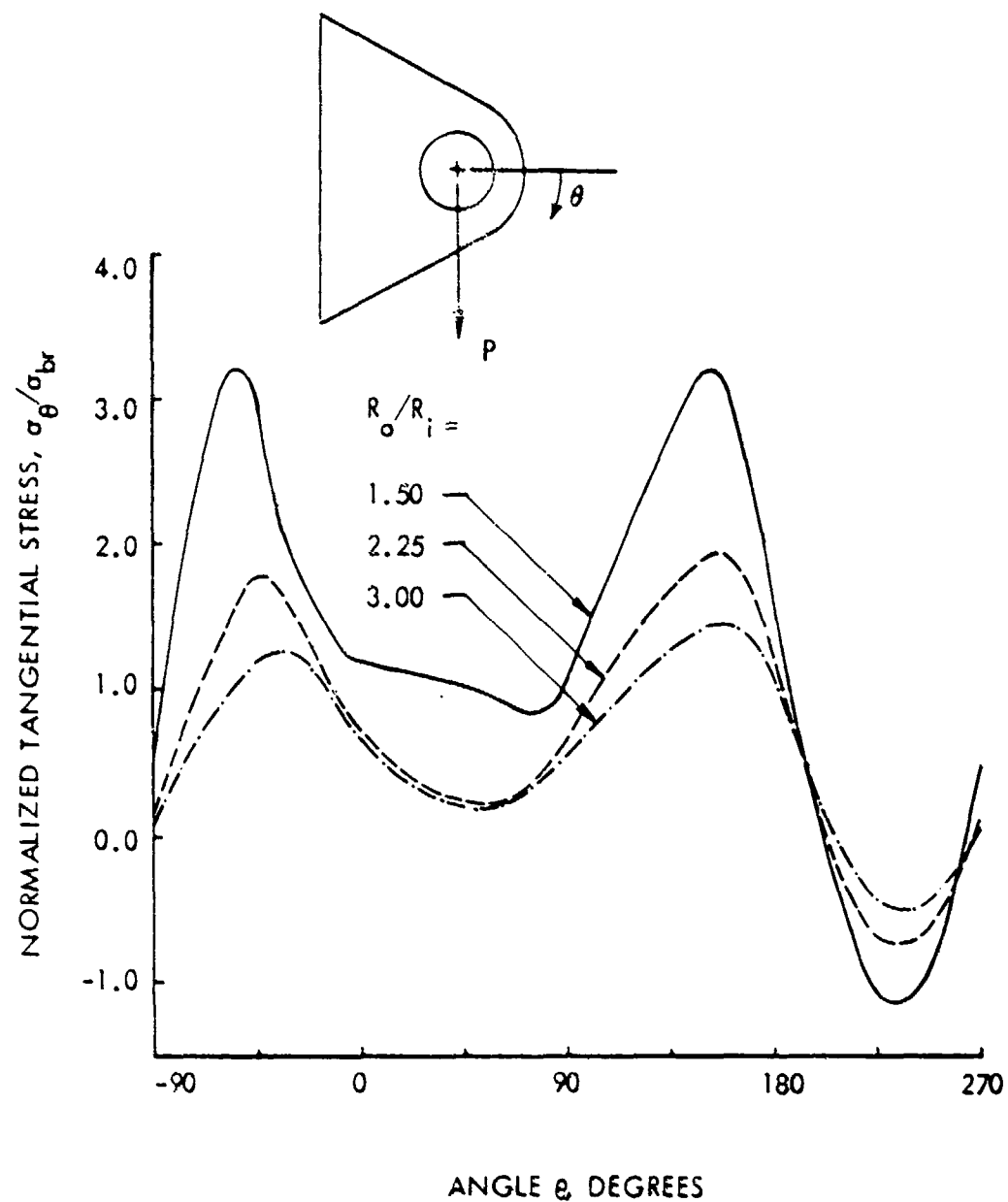
Figure 4-11. Normalized Tangential Stress Distributions Along the Edge of the Hole for Tapered Lugs Subjected to a Pin Loading Applied in 90^θ Direction

$$K_{tb} = \left(2.75 - \frac{\beta^\circ}{135}\right)\left[\left(\frac{R_o}{R_i} - 1\right)\right]^{-\left(0.675 - \frac{\beta^\circ}{1000}\right)}$$

R_o / R_i	$\sigma_{max} / \sigma_{br}$	
	FEM	EQUN
1.50	3.768	3.740
2.00	2.405	2.417
2.25	2.104	2.100
2.50	1.878	1.872
3.00	1.562	1.562
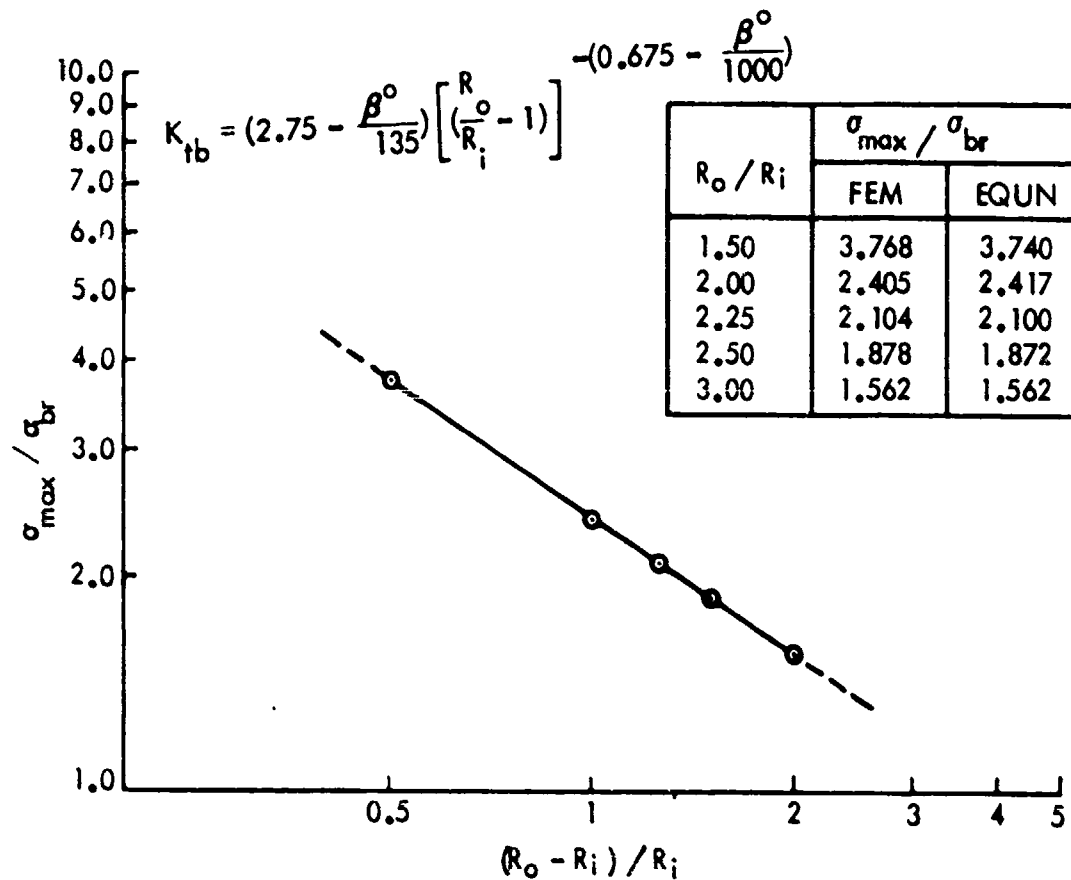
Figure 4-12. Elastic Stress Concentration Factors
for Tapered Attachment Lugs

132

the stress concentration factors presented in Figure 4-12 correspond to the $\theta = \pm 90^\circ$ locations. The actual maximum tangential stress location is between $\pm 85^\circ$ and $\pm 90^\circ$. From a knowledge of the stress distributions, it is anticipated that there will be no appreciable difference in the solutions. Also, in the fracture analysis of tapered lugs subjected to a pin loading in the axial direction, the crack surface will be assumed to be in the plane perpendicular to the loading direction. However, for off-axis loadings of $\pm 45^\circ$ and $\pm 90^\circ$, the crack surface will be assumed to be in the critical location as predicted by the stress analysis.

The computed pin bearing pressure distributions along the contact surfaces with no cracks present are presented in Figures 4-13 through 4-15 for pin loadings applied in the three primary directions, i.e., 0°, -45°, and 90°, respectively. Similar results obtained for the reversed loadings of 180° and 135° are presented in Figures 4-16 and 4-17, respectively. For the reversed loading of 90°, the contact pressure can be obtained from Figure 4-15 by redefining the angle θ as previously discussed.

2.   STRESS INTENSITY FACTOR ANALYSIS

Based on the stress analysis of unflawed tapered attachment lugs, the most critical locations were selected for the fracture analysis to obtain the stress intensity factors for various crack lengths. The special high-order crack tip singularity element [8] was again used in the present analysis to calculate the stress intensity factors. In the analysis, it is assumed that, for a given tapered lug subjected to a specific direction of pin loading, the crack will initiate from the maximum tangential stress location at the hole and propagate radially. Figure 4-18 shows a typical finite element model which was used for a single through-the-thickness crack emanating from a tapered attachment lug subjected to a pin-loading applied in the 0° and 180° directions. The crack surface is assumed to be in the plane perpendicular to the loading direction. The finite element breakdown consists of 366 nodes, 150 triangular elements, 228 quadrilateral elements, 32 spring elements, 1 crack-tip element and a total of 724 degrees of freedom. The computed normalized opening mode stress intensity factors, as a function of normalized crack length, for single through-the-thickness cracks in tapered attachment lugs having R_o/R_i ratios ranging from 1.5 to 3.0 are presented in Figure 4-19 and Table 4-2. The normalized stress

133
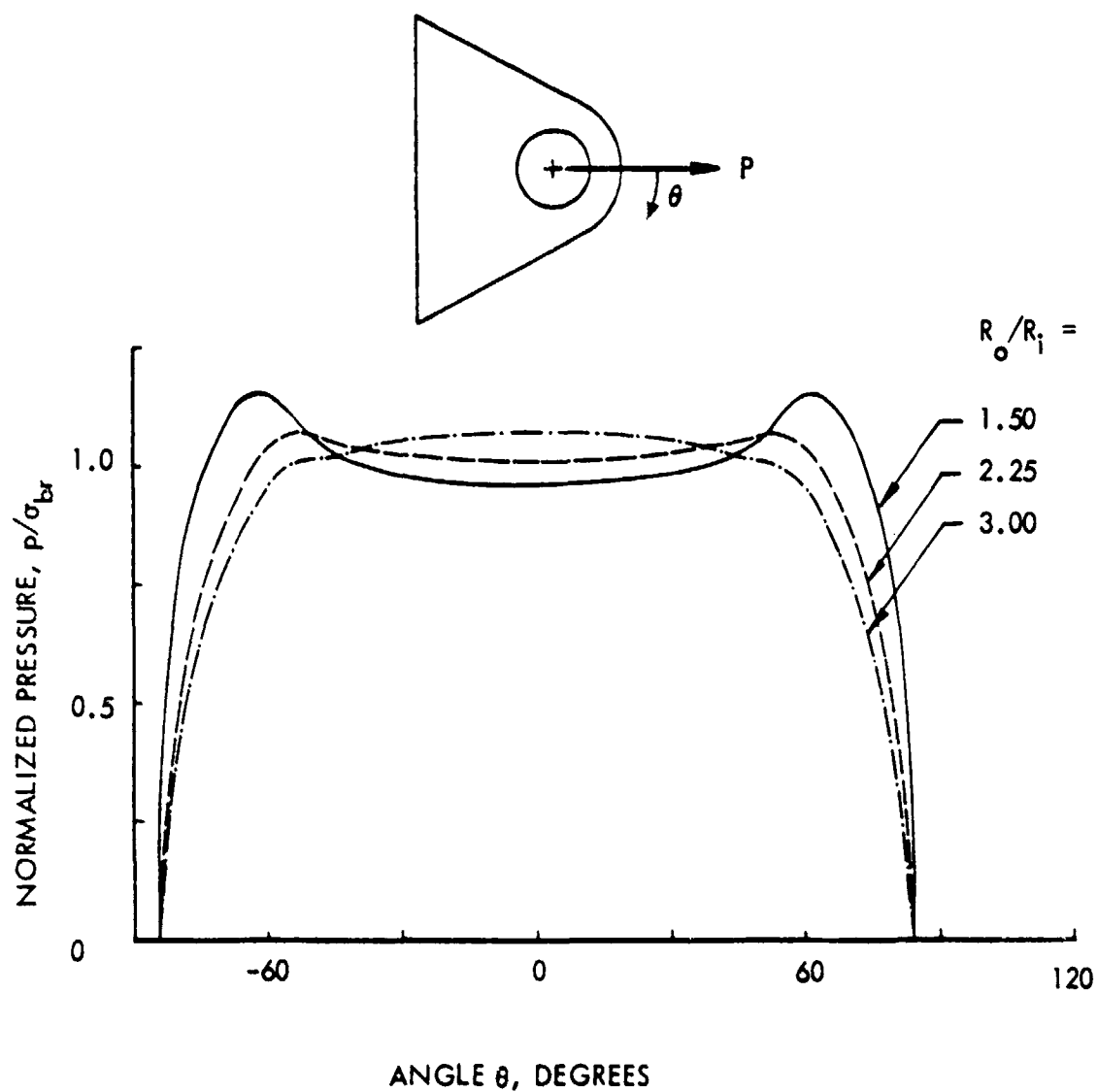
Figure 4-13. Pin-Bearing Pressure Distributions Along the
Contact Surface of Tapered Lugs Subjected to a
Pin Loading Applied in 0° Direction
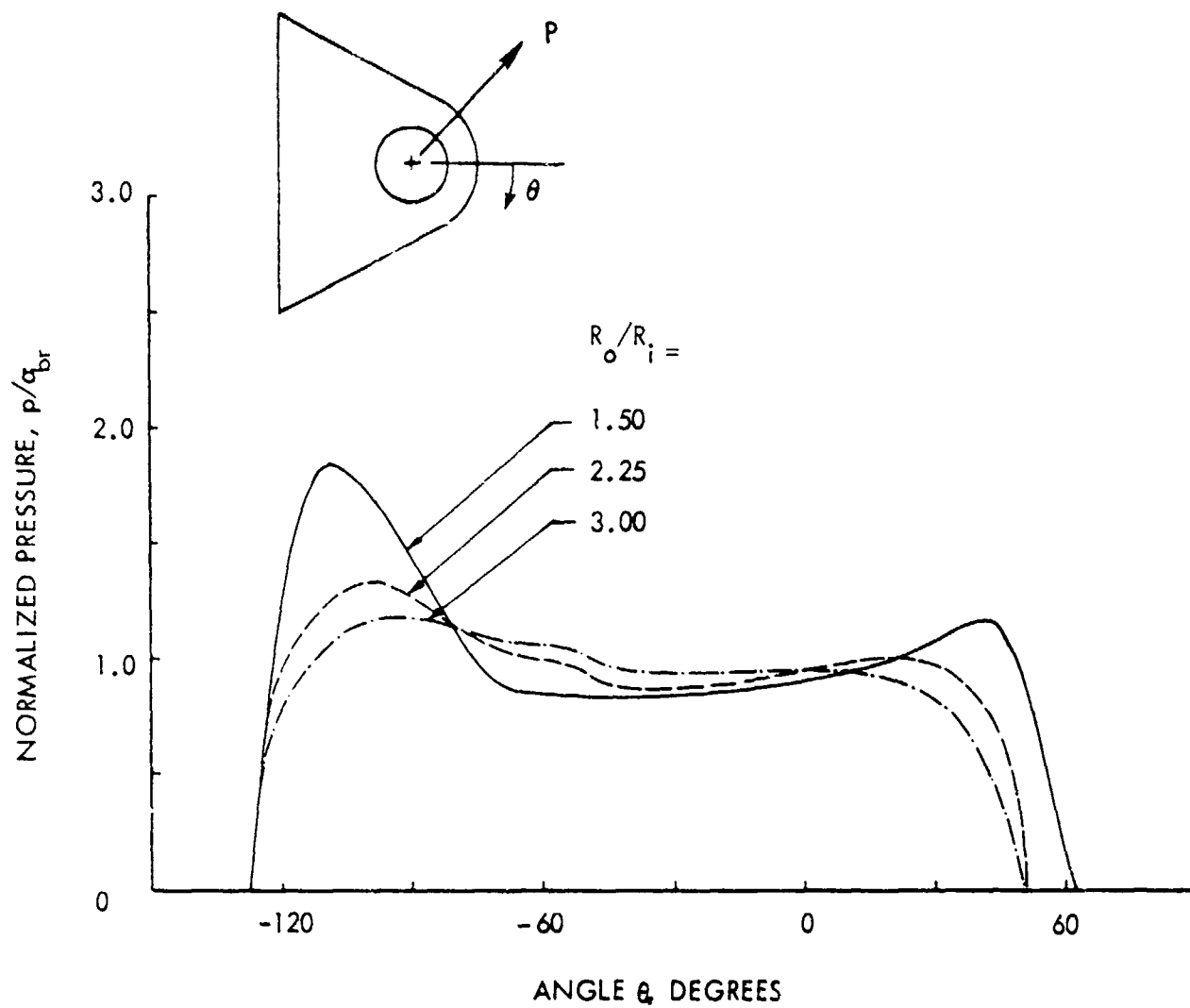
Figure 4-14. Pin-Bearing Pressure Distributions Along the Contact Surface of Tapered Lugs Subjected to a Pin Loading Applied in -45° Direction
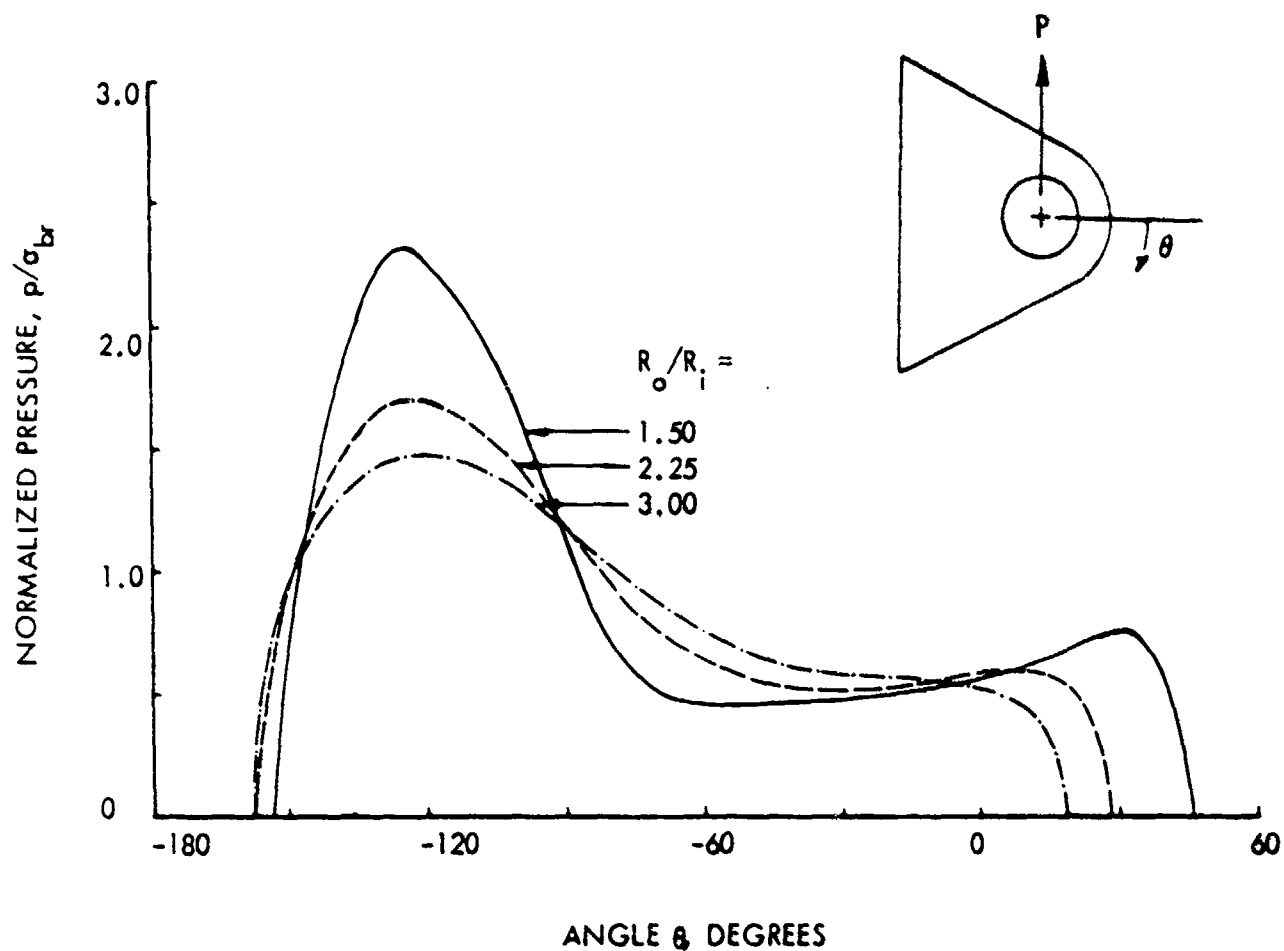
Figure 4-15. Pin-Bearing Pressure Distributions Along the Contact Surface of Tapered Lugs Subjected to a Pin Loading Applied in -90° Direction

136
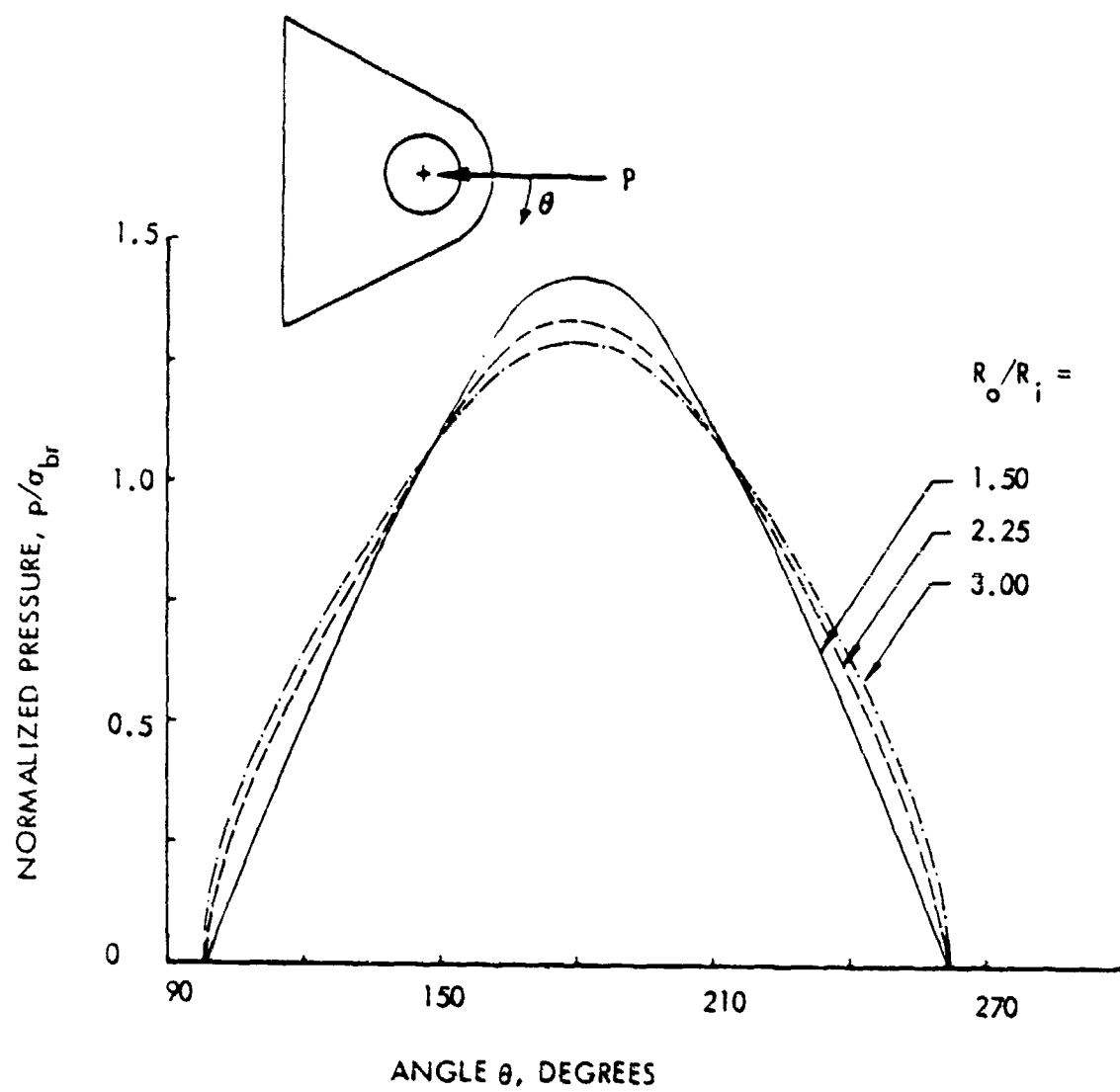
Figure 4-16.   Pin-Bearing Pressure Distributions Along the Contact Surface of Tapered Lugs Subjected to a Pin Loading Applied in 180° Direction

137
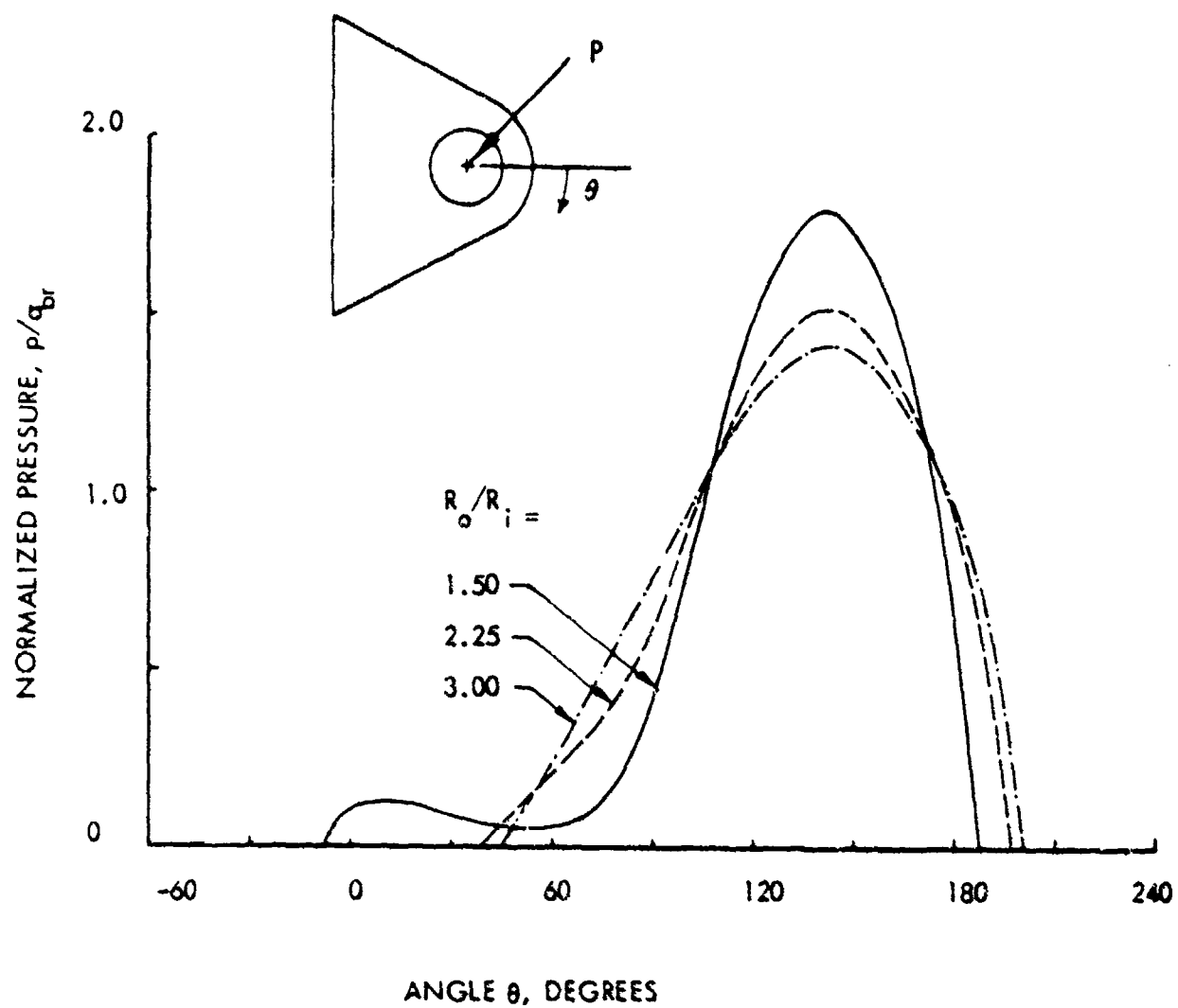
Figure 4-17. Pin-Bearing Pressure Distributions Along the Contact Surface of Tapered Lugs Subjected to a Pin Loading Applied in 135° Direction
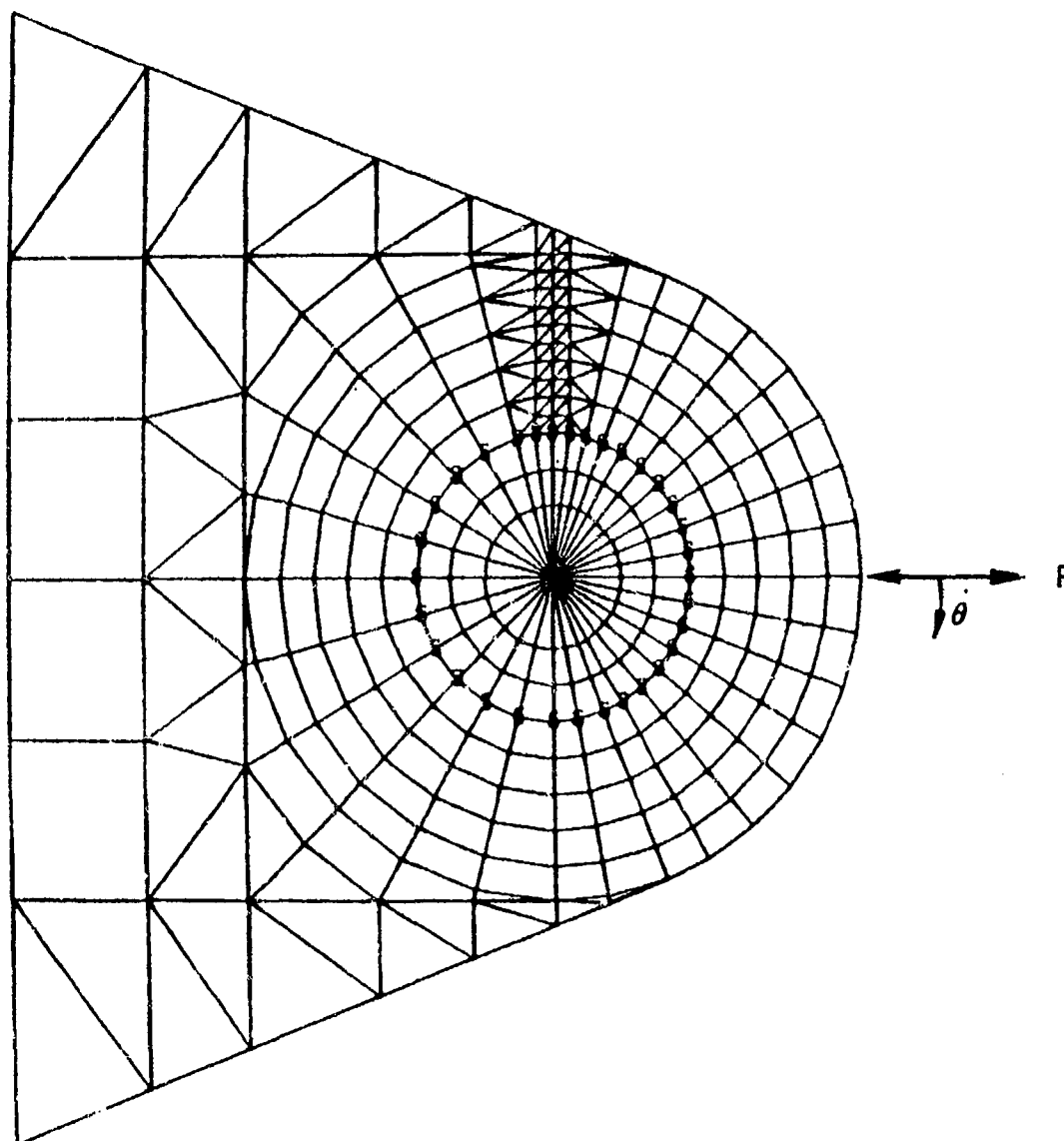
Figure 4-18.   Finite Element Model for a Cracked Tapered Lug
Subjected to a Pin Loading Applied in
0° and 180° Directions

139

Figure 4-19. Normalized Stress Intensity Factors for Single Through-the-Thickness Cracks Emanating from Tapered Attachment Lugs Subjected to a Pin Loading Applied in 0° Loading Direction

140

TABLE 4-2. NORMALIZED STRESS INTENSITY FACTORS FOR SINGLE THROUGH-THE-THICKNESS CRACKS AT TAPERED ATTACHMENT LUGS

$\dfrac{c}{(R_o-R_i)}$ \ R_o/R_i	$K/(\sigma_{br}\sqrt{\pi c})$					$K/(\sigma_o\sqrt{\pi c})$				
	1.50	2.00	2.25	2.50	3.00	1.50	2.00	2.25	2.50	3.00
0.0	4.220	2.694	2.356	2.103	1.749	6.330	5.388	5.301	5.258	5.247
0.1	3.319	1.968	1.588	1.409	1.078	4.979	3.936	3.573	3.523	3.234
0.2	2.867	1.556	1.255	1.052	0.799	4.301	3.112	2.824	2.630	2.397
0.3	2.672	1.408	1.115	0.928	0.685	4.008	2.816	2.509	2.320	2.055
0.4	2.500	1.276	0.988	0.827	0.602	3.750	2.552	2.223	2.068	1.806
0.5	2.433	1.224	0.943	0.782	0.564	3.650	2.448	2.122	1.955	1.692
0.6	2.363	1.173	0.903	0.745	0.535	3.545	2.346	2.032	1.863	1.605
0.7	2.385	1.179	0.912	0.745	0.534	3.579	2.358	2.052	1.863	1.602
0.8	2.410	1.188	0.932	0.746	0.545	3.615	2.376	2.097	1.865	1.635
0.9	2.479	1.273	1.017	0.794	0.585	3.719	2.546	2.288	1.985	1.755

141

intensity factor values at the lug hole, i.e., $c/R_i = 0$, were obtained by multiplying the concentration factors determined from the unflawed stress analysis by 1.12, which was derived by Gross et al [21] for a straight edge crack in a large plate subjected to remote tension. The trends of the above tapered lug solutions are very similar to those obtained for straight lugs. Similar solutions of normalized stress intensity factors as a function of normalized crack length for tapered attachment lugs subjected to pin load- ings applied in the 180° direction are presented in Figure 4-20.

The analysis was then extended to tapered attachment lugs subjected to off-axis loadings of -45°, 135°, -90° and 90°. A R_o/R_i ratio of 2.25 was considered for the off-axis loading fracture analysis. Figure 4-21 shows the finite element model used for analyzing a single through-the-thickness crack emanating from a tapered lug subjected to a pin loading applied in -45° and its reversed (135°) direction. The model contains 401 nodes, 224 triangular elements, 218 quadrilateral elements, 34 spring elements, 1 crack- tip element and a total of 794 degrees of freedom. Note that although there are two critical locations modeled, 58° and 227° measured from the axis of the lug, only one crack was analyzed at a time. The computed normalized stress intensity factors are shown in Figure 4-22 as a function of the normalized crack length. This figure shows that when the crack length is small, say $c/R_i < 0.15$, the stress intensity factor for a crack located closer to the base of the lug is higher than the one located at the head side of the lug. When the crack length increases ($c/R_i > 0.15$), the stress inten- sity factor for a crack located at the head side becomes larger than the one located at the opposite side of the hole. The difference between the two computed K-values increases as the crack length increases. For the case when the direction of the applied pin loading is reversed, the stress intensity factors are also computed and included in the figure for a crack located at the head side of the lug. The surfaces of a crack located closer to the base of the lug are completely closed during the reversed loading. The computed K-values corresponding to the reversed loading are much smaller than the corresponding ones obtained under the primary tensile loading. In the above analysis, only one crack was assumed to exist at a time. However, in reality, both cracks may exist and grow at the same time. In such a case, the influ- ence of one crack on the stress intensity factor of the other crack may be significant. This can be accounted for by developing a matrix of stress

142

Figure 4-20. Normalized Stress Intensity Factors for Single
Through-the-Thickness Cracks Emanating from
Tapered Attachment Lugs Subjected to a Pin
Loading Applied in 180° Loading Direction

143
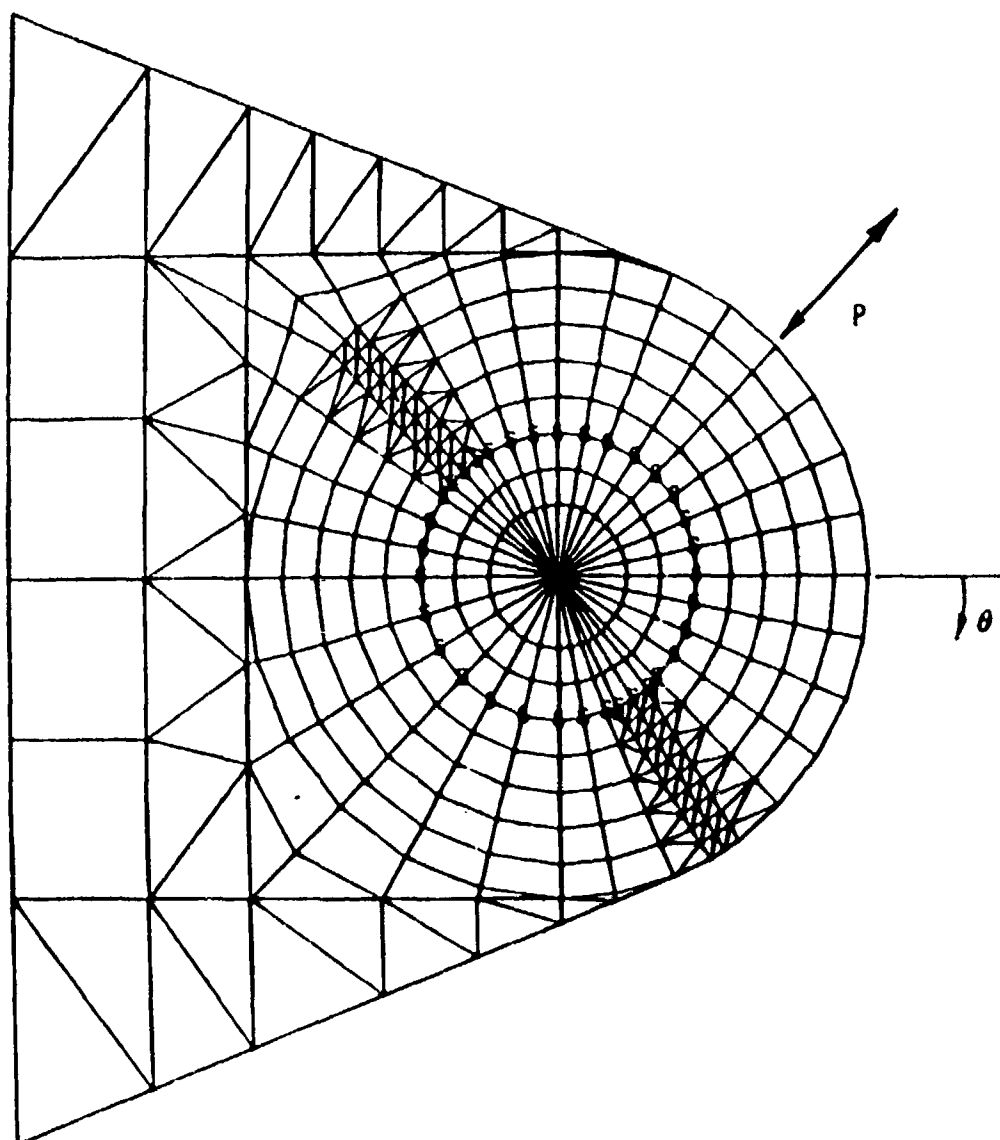
Figure 4-21. Finite Element Model for a Cracked Tapered Lug
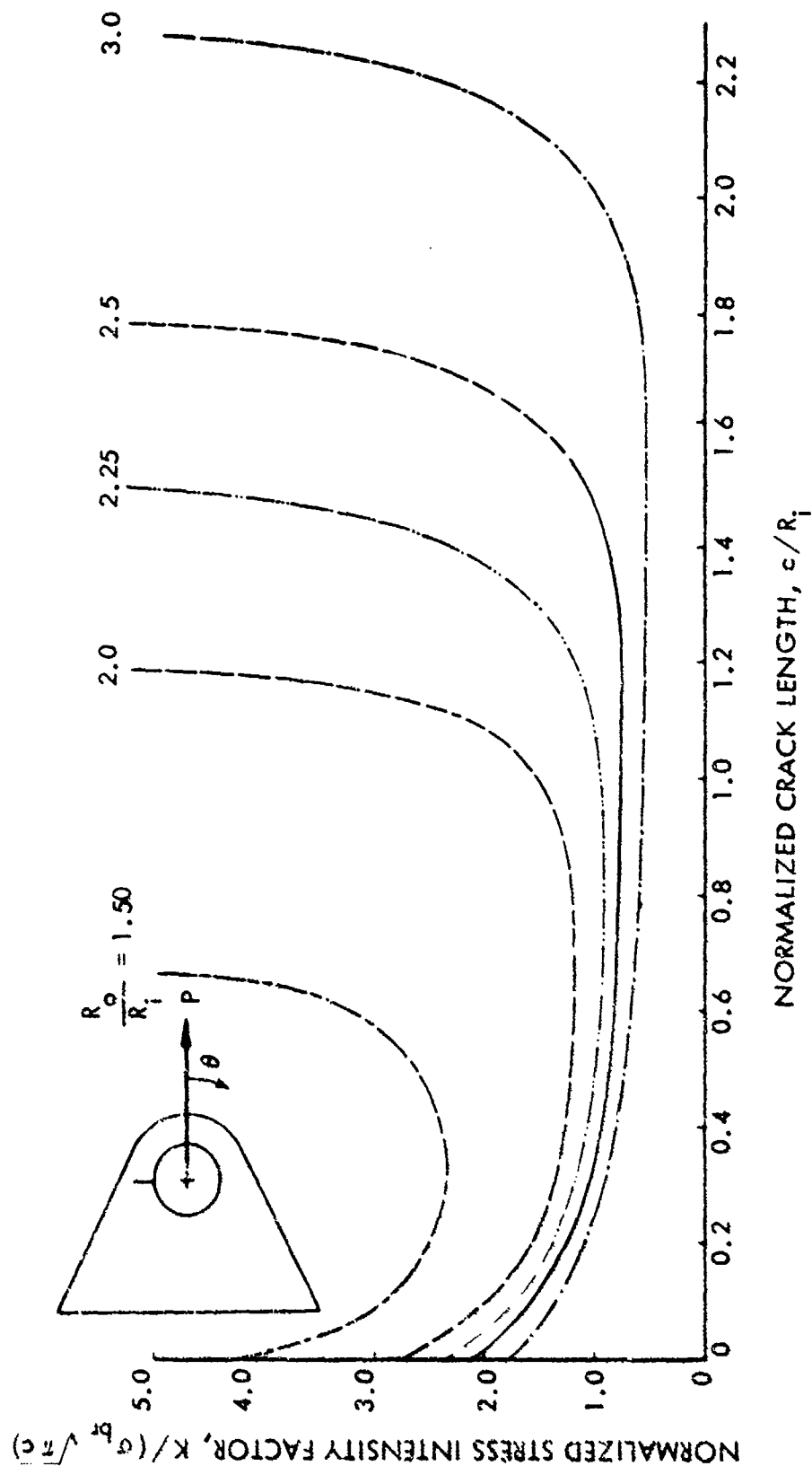Subjected to a Pin Loading Applied in
-45° and 135° Directions
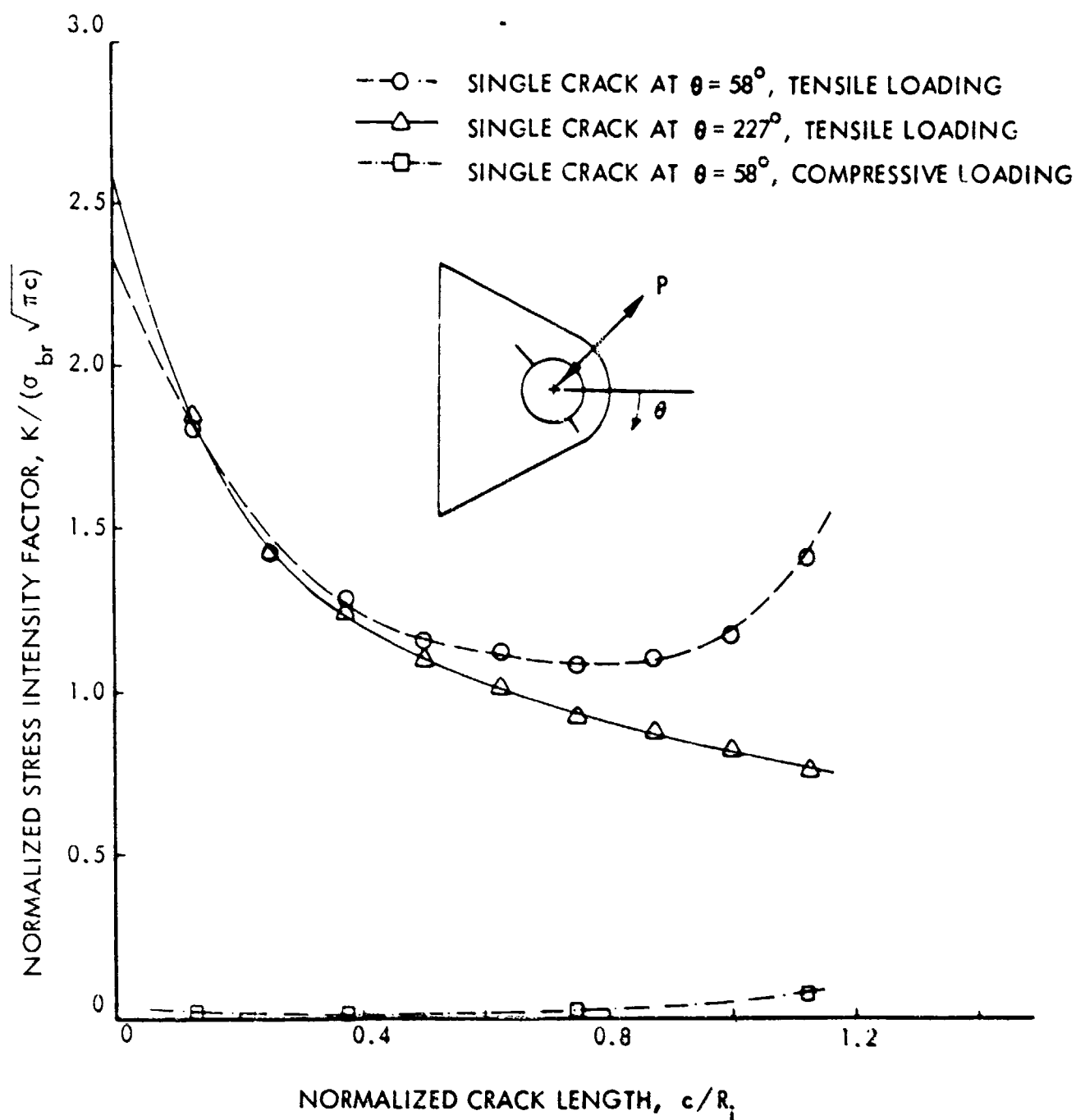
Figure 4-22. Normalized Stress Intensity Factors for Single Through-the-Thickness Cracks Emanating from a Tapered Lug Subjected to a Pin Loading Applied in -45° and its Reversed Directions ($R_o/R_i = 2.25$)

intensity factor solutions for various crack lengths of both cracks. This matrix of solutions may then be used to accurately estimate the stress intensity factor for either crack. However, such an effort is not made in the present analysis.

A similar finite element model to the one shown in Figure 4-21 was used for a tapered lug subjected to a pin-loading applied in the $\pm 90^{\circ}$ directions. Two critical locations, 43° and 205° measured from the axis of the lug, were determined from the results of the stress analysis of an unflawed tapered lug subjected to a pin loading applied in the -90° direction. Similar to the -45° loading case, only one crack was analyzed at a time, though two critical locations were modeled. The computed normalized stress intensity factors are shown in Figure 4-23 as a function of the normalized crack length. The figure shows that when the crack length is smaller than 0.85 R_i, the stress intensity factor for a crack located closer to the base of the lug is higher than the one located at the head side of the lug. When the crack length increases ($c/R_i > 0.85$), the stress intensity factor for a crack located at the head side becomes larger than the one located at the opposite side of the hole. For the case when the direction of the applied pin loading is reversed, the stress intensity factors are also computed and included in the figure for a crack located at the head side of the lug. The surfaces of a crack located closer to the base of the lug are completely closed during the reversed loading. The K-values corresponding to the reversed loading are smaller than the corresponding ones obtained under primary tensile loading. However, these magnitudes are significantly larger than the corresponding ones obtained for a case where the pin loading was applied in the 135° direction.

Based on the current unflawed stress and stress intensity factor analysis, one may conclude that, among the principal pin loading directions of 0°, -45° and -90°, the loading of -45° is the most severe loading case from the point of view of fatigue crack initiation and fatigue crack propagation. Also, when a tapered lug having a R_o/R_i ratio of 2.25 is subjected to cyclic fatigue pin loading in -45° and -90° directions, a crack will probably initiate at the critical location closer to the base of the lug first. When this crack propagates, a second crack will initiate at the head side of the lug. Eventually, the growth of the base-side crack will slow down while the growth rate of the head-side crack will increase and exceed that of the base-side crack. The
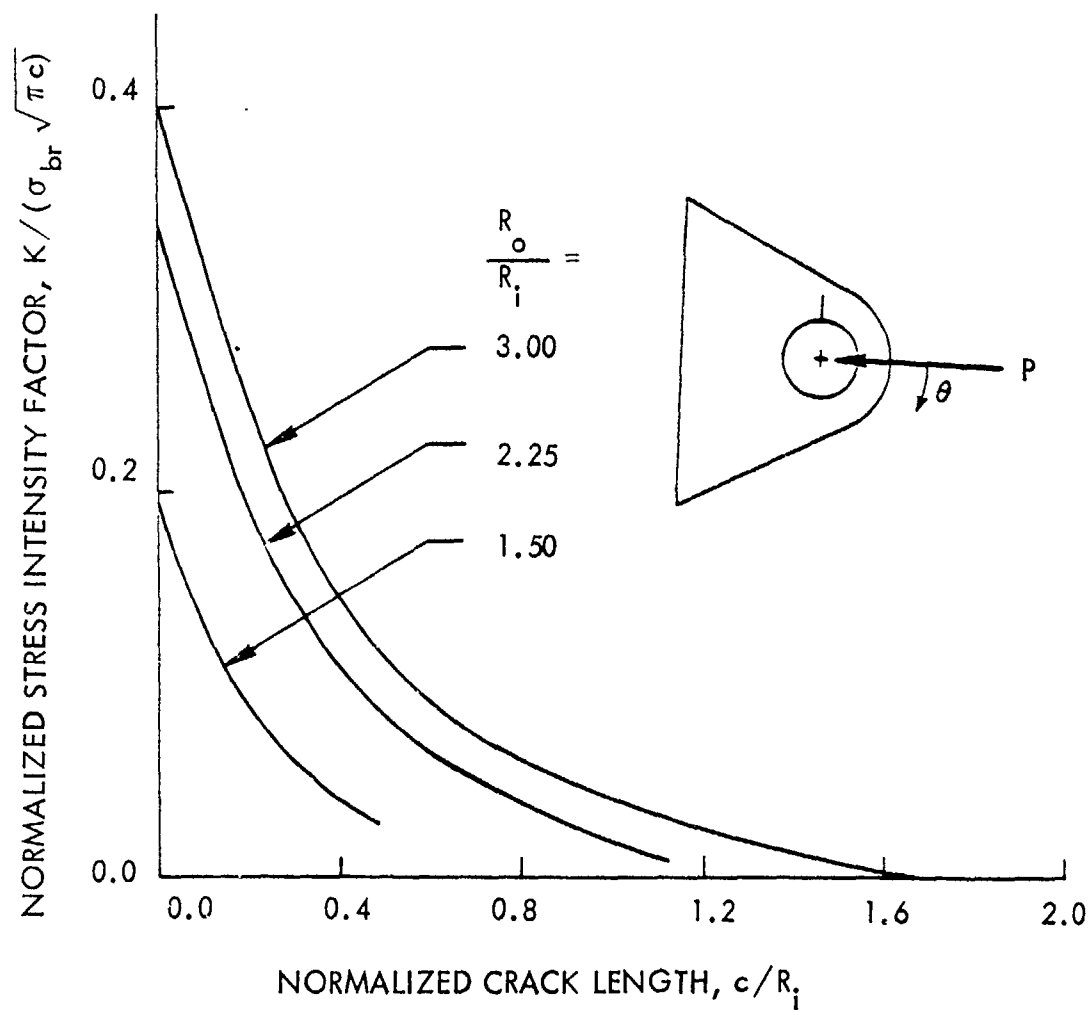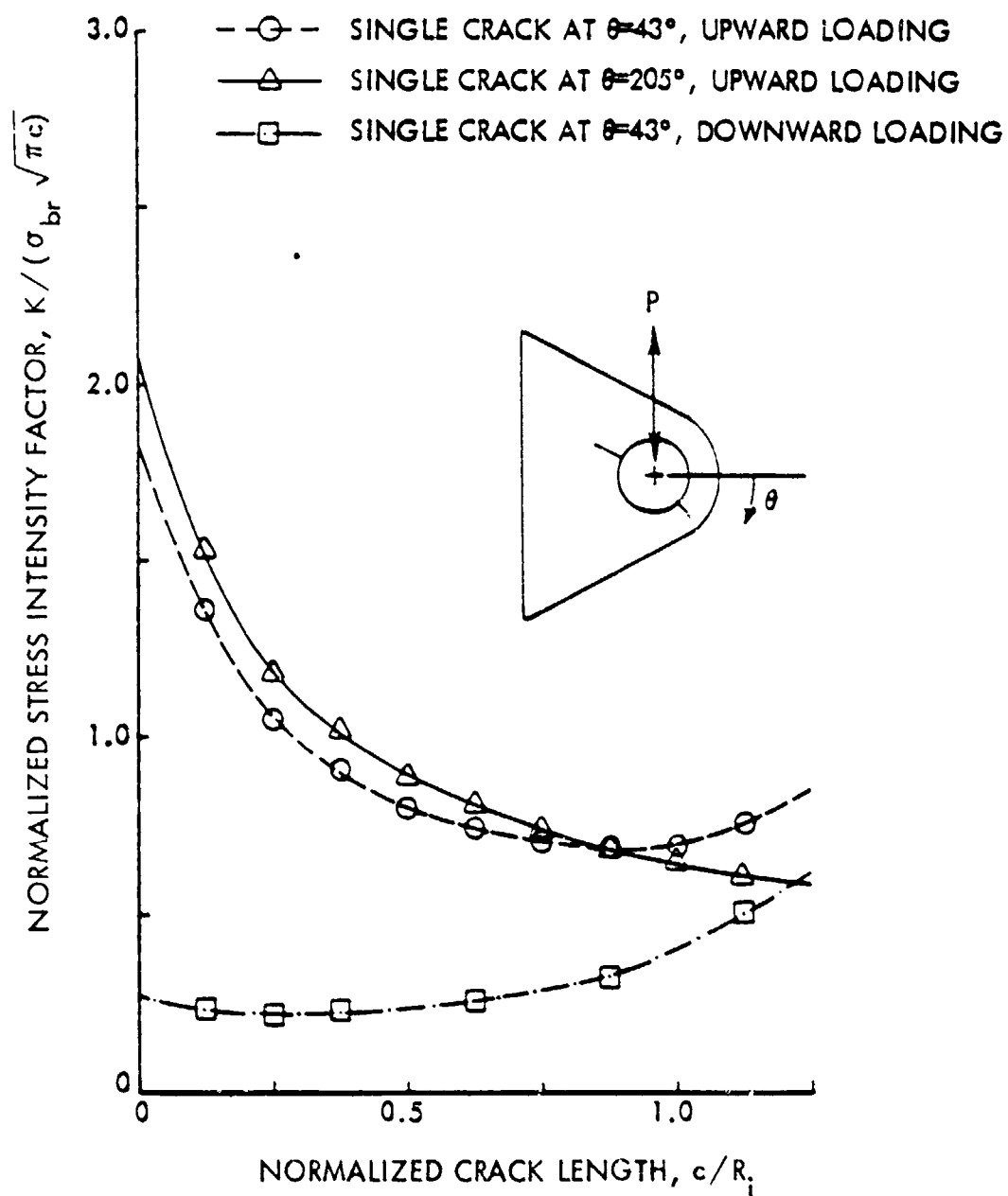
Figure 4-23. Normalized Stress Intensity Factors for Single Through-the-Thickness Cracks Emanating from a Tapered Lug Subjected to a Pin Loading Applied in -90° and its Reversed Directions (R_o/R_i = 2.25)

lug will finally fail from the head side.   Failure modes experimentally studied by Larsson [46] for tapered lugs loaded in the $-90°$ direction are very similar to those discussed above.

SECTION V

CRACK GROWTH ANALYSIS METHOD

Linear elastic fracture mechanics methodology is discussed in this
section to predict crack growth in damaged attachment lugs. An accurate and
efficient prediction of crack growth from an initial crack length to a criti-
cal or final crack length, when subjected to a prescribed load history, de-
pends on a damage accumulation package containing the following four basic
elements:

o   Applied load spectrum

o   Stress intensity factor solution

o   Baseline crack growth rate data or crack growth rate equation

o   Spectrum load interaction model.

The applied load spectrum is the loading sequence or history the attach-
ment lug is subjected to for which the crack growth prediction is to be made,
and is therefore basically an input for the problem.

It is generally accepted that the stress intensity factor controls the
rate of propagation of a fatigue crack in structural components. Any cracked
structure can be expected to respond in a predictable manner to a given
applied load spectrum if its associated stress intensity factor solution is
available. The development of such stress intensity factor solutions was pre-
sented in the previous two sections for straight and tapered attachment lugs
for various configuration, design and loading complexities.

The response of the crack is usually given in the form of constant
amplitude fatigue crack propagation rate, da/dN, as a function of stress
intensity factor range, ΔK. These baseline material property data are
obtained experimentally and can be expressed in either tabular or equation
form, i.e.,

$$\frac{da}{dN} = f\ (\Delta K,\ \ldots\ldots)$$ (46)

Paris' [49], Forman's [50] and Walker's [51] equations are some of the
typical representative crack growth-rate equations which will be discussed
in this section.

The normal crack growth rate under constant amplitude loading changes
if the load cycle is preceded by a different amplitude load cycle. As ex-
amples, a tensile overload causes permanent plastic deformation at the crack
tip which in turn delays the crack growth at subsequent low-load cycles,
while the compressive underload may accelerate the normal crack growth.
To account for such spectrum load-interaction effects, several crack-
growth retardation models have been proposed. Models such as Wheeler [52],
Willenborg [53], Generalized Willenborg [54] and Hsu [55] will be discussed
in this section.

1. CRACK GROWTH RATE EQUATIONS

A large and growing volume of crack growth data are available. Most of the
data are expressed in terms of ΔK versus da/dN. In this relationship,
there is a threshold value of K , say K_{th}, below which a flawed structure
can be cycled without measurable crack extension. At the other extreme is
K_c , called fracture toughness, a value of K at which a flaw will propa-
gate unstably. Therefore, fatigue crack growth must occur in the range
K_{th} to K_c. All crack growth rate data available for establishing the
da/dN versus ΔK relationship fall within this range. Normally, data
show some experimental scatter, and the least-square mean line representa-
tion of all test data is used to establish the ΔK versus da/dN relation-
ship.

Several methods of using the mean data to describe crack growth rates
have been proposed. Of these methods,   three well established
crack propagation equations are used most. They are proposed
by Paris et al [49], Forman et al [50], and Walker [51]. Paris' equation is
limited to cases where a constant stress ratio, R, is applied. Forman and
Walker's equations are more general and applicable to cases where variable
loads exist in the load spectrum.

Accuracy of the predicted crack growth life, using any crack growth
equation, depends upon accurate values of da/dN versus ΔK and correct
stress intensity factor values for a particular geometry.

1.1 Paris' Equation

The crack growth rate equation proposed by Paris, et al. is of the
following form:

$$da/dN = c_p \quad (\Delta K)^{n_p} \tag{47}$$

where:

da/dN = rate of crack growth (inch/cycle)

c_p and n_p are constants for a particular stress ratio

ΔK = stress intensity factor range ($K_{max} - K_{min}$).

Paris' equation has been an effective regression equation for crack propagation rate in unreinforced flat specimens under constant amplitude loading. However, it is not successful in pooling such data for more than one value of stress ratio R, ($\sigma_{min}/\sigma_{max}$).

1.2 Forman's Equation

In an effort to extend Paris' equation to cover various stress ratios, and to take into account the instability of the crack growth when the stress intensity factor approaches its critical value for a given material, Forman, et al, modified Paris' equation as follows:

$$da/dN = \frac{c_f (\Delta K)^{n_f}}{(1-R)K_c - \Delta K} \tag{48}$$

where:

c_f and n_f = material constants

K_c critical stress intensity factor

Because of crack-tip blunting which is produced by cyclic strains in the material ahead of the advancing crack, it is important to select the appropriate K_c value. The choice of a K_c value larger than the fracture toughness of the material normally will give a better result in establishing K versus da/dN relationships. If the available data includes more than one R-ratio, K_c should be used as a curve fitting parameter to force the best fit for all available data.

151

1.3 Walker's Equation

Roberts and Erdogan [56] proposed that stress ratio effects in the power law region of the crack growth rate curve could be described using

$$da/dN = c \ (K_{max}^{P_1} \cdot \Delta K^{P_2}) \tag{49}$$

Walker [51] reformulated the equation so that the stress ratio would be explicit and it had the form

$$da/dN = c \left[K_{max} \ (1 - R)^m \right]^P \tag{50}$$

where c, m and p are material constants.

1.4 Determination of Constants in Paris' and Forman's Equations

Taking logarithms of both sides of Paris' and Forman's equations and re-arranging terms, they become, respectively,

$$\log \ (da/dN) = \log c_p + n_p \ \log \ (\Delta K) \tag{51}$$

and

$$\log \left\{ \left[(1 - R) \ K_c - \Delta K \right] da/dN \right\} = \log c_f + n_f \ \log \ (\Delta K) \tag{52}$$

For any two given coordinate points, say ΔK_i, da/dN_i and ΔK_{i+1}, da/dN_{i+1} which represent a segment of the growth rate curve, one can solve the two simultaneous equations for the unkowns c and n.

2. SPECTRUM LOAD INTERACTION MODELS

The majority of crack growth studies have been carried out for constant stress amplitude because of the simplicity in testing and because the data can be presented in a straightforward manner. In actual practice, engineering components are subjected to loads which are often irregular and vary in a random manner. Fluctuating loads due to atmospheric turbulence on aircraft are typical examples of random loadings. The difference between the conventional fatigue experiments and the actual loading of the components has led to the development of various crack analysis approaches. As discussed in a previous section, normal crack growth rate under constant amplitude loading changes if the load application is preceded by a loading cycle of a different

amplitude. The tensile overload causes permanent plastic deformation at the crack tip which in turn delays the crack growth at subsequent low load cycles, while the compressive overload may accelerate the normal crack growth. The importance of delay in the rate of fatigue crack growth, as produced by tensile overloads, on the accurate prediction of fatigue lives of structures has been recognized, and quite a few investigations have been stimulated in this area.

Several models have been suggested to account for the effects of delay on the prediction of fatigue crack growth. Those models use the plastic-zone size (for either plane stress or plane strain) associated with the applied load levels to characterize the load-interaction effect. These models assume that if the size of the plastic zone, r_p, developed due to application of the current load cycle at crack length a extends to or past the extremities of a previously developed load-interaction zone, a_p, (i.e., $(a + r_p) \geq a_p$), there will be no load interaction and the growth rate associated with the current load cycle is the same as the one generated under constant-amplitude loading. Conversely, the crack-growth rate would be reduced (retarded) if $r_p < (a_p - a)$. Some of the most often referenced retardation models are described below.

2.1 Wheeler Model

The first retardation model proposed was that of Wheeler [52] who suggested the use of a reduction factor on the constant amplitude crack growth rate:

$$\frac{da}{dN} = c_p \ f \ (\Delta K) \tag{53}$$

where c_p is a retardation parameter defined as

$$c_p = \left(\frac{R_y}{a_p - a} \right)^m \qquad \text{for} \quad a_p - a > R_y$$

$$c_p = 1 \qquad \text{for} \quad a_p - a \leq R_y$$

and m   = shaping exponent

R_y = extent of the current yield zone

a_p - a = the distance from crack tip to elastic-plastic interface

This model requires previous spectrum growth data to derive an empirical "shaping exponent," m. Although it is a substantial improvement over the linear cumulative damage rule, this model is more of a data fitting technique than it is a predictive technique. Besides, the exponent in Wheeler's retardation parameter is dependent not only upon the material, but also upon the manner in which spectrum loads were applied. For any design spectrum different from the ones used to generate the test data, the exponent m may be very different.

2.2 Willenborg Model

As mentioned earlier, the rate of propagation of a fatigue crack is controlled by the stress-intensity factor at the crack tip. Therefore, the magnitude of the stress-intensity factor is a good indicator of the extent of crack tip deformation. Since the cyclic crack tip deformation is reduced due to prior overloads, the model of Willenborg et al [53], which uses an "effective stress" concept to reduce the applied stress, and hence the crack tip stress-intensity factor, seems more appealing. The model is described as

$$\frac{da}{dN} = f\left[(\Delta K)_{eff}, \; (K_{max})_{eff}\right] \tag{54}$$

where

$$(\Delta K)_{eff} = (K_{max})_{eff} - (K_{min})_{eff}$$

$$(K_{max})_{eff} = (\sigma_{max})_{eff} \sqrt{\pi a_c} \; \beta_T$$
$$(K_{min})_{eff} = (\sigma_{min})_{eff} \sqrt{\pi a_c} \; \beta_T$$

$$(\sigma_{max})_{eff} = \sigma_{max} - \sigma_{red}$$
$$(\sigma_{min})_{eff} = \sigma_{min} - \sigma_{red}$$
$$\sigma_{red} = \sigma_{ap} - \sigma_{max}, \text{ or zero whichever is larger}$$

$$\sigma_{ap} = \frac{F_{ty}}{\beta_T} \sqrt{\frac{2(a_p - a_c)}{a_c}} \tag{55}$$

and

a_c = the crack length at the beginning of the load cycle after the overload

$a_p - a_c$ = current plastic zone caused by the overload

F_{ty} = tensile yield strength of the material

β_T = total geometric correction factor

This model can be used to predict the fatigue crack growth under spectrum loading without the assistance of empirical factors or data. Although the model gives fairly good predictions for crack growth under moderate spectra, it tends not to give good correlations for spectrum loading with high overloads, especially overloads exceeding 150 percent of the maximum of the low load.

2.3 Generalized Willenborg Model

According to the Willenborg et al model, if the overload ratio, K_{max}^{OL}/K_{max}, is greater than or equal to 2.0, a zero effective stress-intensity factor will be predicted and the crack will stop growing. However, experimental data contradicts such a prediction. Gallagher [54] modified the Willenborg equation for effective stress intensity factors as follows:

$$(K_{max})_{eff} = K_{max} - \phi\left[K_{max}^{OL} \left(1 - \frac{\Delta a}{r_{OL}}\right)^{1/2} - K_{max}\right]$$

and $\tag{56}$

$$(K_{min})_{eff} = K_{min} - \phi\left[K_{max}^{OL} \left(1 - \frac{\Delta a}{r_{OL}}\right)^{1/2} - K_{max}\right]$$

or zero, whichever is larger.

The factor ϕ is defined as

$$\phi = \frac{1 - (K_{max})_{Th} / K_{max}}{S_{SO} - 1} \tag{57}$$

in which $(K_{max})_{Th}$ is the maximum threshold stress intensity factor, and S_{SO} is the "overload shut-off ratio." When $K_{max}^{OL} / K_{max} \geq S_{SO}$, crack arrest occurs. Note that the original Willenborg model is recovered by setting $\phi = 1$.

2.4 Hsu Model

The Hsu model [55] developed at the Lockheed-Georgia Company utilizes an effective stress and closure concept. It assumes that the stress singularity does not exist if the crack surface is closed and that the crack propagates only during that portion of the load cycle in which the crack surface is fully open. Let σ_o be the crack-opening stress, i.e., the corresponding far-field stress at the onset of crack opening. Then the effective stress range of the load cycle during crack propagation can be defined as

$$\Delta\sigma_{eff} = \sigma_{max} - \sigma_o \tag{58}$$

When the opening stress is less than the minimum stress of the applied load cycle, the effective stress range is given by

$$\Delta\sigma_{eff} = \sigma_{max} - \sigma_{min} \tag{59}$$

If the maximum stress of the applied load cycle is less than the crack opening stress due to prior loads, the crack surface will be fully closed. Hence, the fatigue crack will not propagate.

However, experimental evidence indicated that below the closure K, strain concentration at the vicinity of the crack tip still exists. Since fatigue damage is normally related to the cyclic strain range, the effective K_{min} is likely to be somewhat lower than the level at the onset of closure and higher than K_{min} under steady state (constant amplitude) conditions. The effective stress range and the effective load ratio can then be re-written as

$$\Delta\sigma_{eff} = \sigma_{max} - (\sigma_{min})_{eff} \qquad (60)$$

$$R_{eff} = (\sigma_{min})_{eff}/\sigma_{max} \qquad (61)$$

respectively, where $\sigma_{min} \leq (\sigma_{min})_{eff} \leq \sigma_o$.

For any given load cycle, the effective stress-intensity factor can then be calculated from the equation

$$\Delta K_{eff} = \Delta\sigma_{eff} \cdot \sqrt{\pi a} \cdot \beta_T \qquad (62)$$

The crack growth rate associated with this applied load cycle is computed from the growth rate equation

$$\frac{da}{dN} = f\ (\Delta K_{eff},\ R_{eff},\ ---) \qquad (63)$$

For a given loading spectrum, if one can determine the effective minimum stress corresponding to each load cycle, the fatigue crack propagation life can be predicted.

3. CRACK GROWTH ANALYSIS PROGRAM

A computer program has been developed using the state-of-the-art methodologies including the stress intensity factors developed under this program for the prediction of fatigue crack growth behaviors of single through-the-thickness cracks and single corner cracks at attachment lugs under cyclic loading. All the data presented in Sections III and IV, such as stress analysis, fracture analysis, Green's function, interference-fit bushing analysis, etc., have been embedded in the computer program to make it as automatic and simple as possible. This computer program contains the three crack growth rate equations discussed above. There are five different options to input each individual mission load profile from which a mission mix spectrum can be generated. The program predicts the crack growth using a block-by-block integration technique. Crack growth may be analyzed with or without load-interaction using any of the models described above.

For through-the-thickness cracks, either the compounding solution or the Green's function solution can be used in the prediction. In predicting the growth behavior of a single corner crack, the crack may be analyzed by either the one-parameter (i.e., constant a/c ratio) or two-parameter method. For one-parameter analysis, the prediction is straightforward and is similar to through-the-thickness crack prediction. For two-parameter analysis, it is assumed that for a given number of applied load cycles, the extension of the quarter elliptical crack border is controlled by the stress intensity factors at the intersection of the crack periphery at the hole wall and the lug surface, i.e., K_A and K_C, respectively. In general, the stress intensity factors at these two locations are different, resulting in different crack growth rates. Therefore, the new flaw shape aspect ratio after each crack growth increment will be different from the preceding one. The new crack aspect ratio is computed using the new crack lengths on both the hole wall and lug surface. The process will be repeated until the crack length along the hole wall is equal to the lug thickness. At that time the transitional crack growth criteria as discussed in Section III are used until the crack has achieved a uniform format. After that, if the failure has not occurred, a one-dimensional through-the-thickness crack analysis is used to continuously predict the subsequent crack growth life. The analysis is considered to be complete when fracture occurs or when the desired final crack length or the maximum usage time is reached.

A detailed description of the computer program along with the input instructions is provided in Reference [57].

SECTION VI

SUMMARY OF RESULTS

Analytical methods have been presented to predict both fatigue crack growth and residual strength of cracked attachment lugs. Each crack growth analysis includes the following elements:

- o Stress intensity factor solution
- o Baseline crack growth rate relationship
- o Applied load sequence
- o Spectrum load interaction model.

Of these, the emphasis in this report has been upon the calculation of stress intensity factors, covered in Sections III and IV. These sections have been followed by a discussion in Section V of the alternative constant amplitude fatigue crack growth rate relationships and spectrum load interaction models.

The following summary paragraphs are intended to provide an overview and to tie together the content of this report and aid the reader in using the analytical methods and results that have been presented.

1. SUMMARY OF STRESS INTENSITY FACTORS FOR STRAIGHT LUGS (SECTION III)

Section III has covered the calculation of stress intensity factors for straight attachment lugs subjected to axial loading. Several alternative methods have been discussed, including the simple compounding, two-dimensional cracked finite element, weighting function, and three-dimensional cracked finite element method. Parameters and complexities covered in the stress intensity factor solutions presented in this section are outer-to-inner radius ratio (1.50 to 3.0), crack geometry (single corner crack, through-the-thickness crack, and the intermediate transition), crack length (measured on lug face and along bore of hole), change in distribution of pin bearing pressure due to crack length change, ratio of pin modulus to lug modulus (1.0 or 3.0), interference-fit bushings, and elastoplastic analysis when the peak stress at the hole exceeds the material tensile yield strength.

A two-dimensional finite element analysis has been used to compute the stress distribution in the uncracked lug for lugs of various R_o/R_i ratios. The major useful results of this analysis are the stress distribution along the potential crack path (Table 3-1) and the stress concentration factor (Figure 3-5).

The compounding method combines known solutions to obtain an engineering approximation for the stress intensity factor, Equation (10). Stress intensity factor values calculated by this method have been listed in Table 3-2.

The two-dimensional cracked finite element method properly models the crack tip stress singularity and the distribution of pin bearing pressure, which changes drastically with crack length (Figures 3-14 through 3-16). The stress intensity factor results from this method have been shown in Figure 3-18 and listed in Table 3-3.

The weighting function method calculates the stress intensity factor as the integral of the product of the stress in the uncracked lug times the Green's function for the lug; Equation (14). The Green's functions for straight lugs, developed using two-dimensional cracked finite element analyses with point loads applied on the crack surface, have been listed in Tables 3-4 through 3-6. However, these "original" Green's functions, when used with the stress distribution in the uncracked lug from Table 3-1, obtain K_I results at variance with those of the two-dimensional cracked finite element analysis. The discrepancy arises because the Green's function method fails to account for the change in the distribution of pin bearing pressure. To correct the discrepancy, the original Green's functions have been modified such that the cracked finite element results are exactly duplicated when these "modified" Green's functions (Tables 3-7 through 3-9) are used.

Figure 3-29 compares the stress intensity factors for through-the-thickness cracks computed by the various methods. Reasonable agreement among all methods is obtained at R_o/R_i ratios of 2.25 and 3.0, but not at $R_o/R_i = 1.50$. Thus, any method could be used for larger R_o/R_i ratios, but the more rigorous

160

two-dimensional cracked finite element method (or equivalently, the Modified Green's function method) is preferred for $R_o/R_i < 2.0$.

The weighting function method can be applied to account for residual stresses caused by a shrink-fit bushing. Assuming the lug and bushing remain in intimate contact during loading, the stress intensity factor is calculated by Equation (24) from the sum of the residual stress caused by bushing installation plus the distribution of stress caused by the applied load. The residual stress is estimated from the closed-form solution for two concentric cylinders, Equation (30). The applied stress is obtained from two-dimensional finite element analysis of an uncracked lug in intimate contact with a neat-fit bushing. If the bushing and lug are of the same material, then the applied stress distribution can be obtained from Table 3-1. Sample applied stress distributions for various bushing/lug modulus ratios are shown in Figures 3-33 and 3-34. It is to be noted here that this method can give unconservative results when separation occurs between the bushing and lug. In such instances, an improved methodology has been developed and is presented in Volume III of this report.

The solution methods for through-the-thickness cracks can be modified to analyze a corner crack, utilizing a corner crack correction factor, along with a method to account for the transitional behavior as the corner crack becomes a through-the-thickness crack. Two alternative correction factor approaches have been suggested, a one-parameter and a two-parameter method.

In the one-parameter method the flaw shape is assumed to be constant (e.g., $a/c = 1.33$) and the stress intensity factor at the lug surface point (Point C) is calculated using Equations (31) and (32). These equations apply to the crack throughout its growth from a corner crack, through transition, to a through-the-thickness crack.

In the two-parameter method, Equations (33) through (36) (in conjunction with Figures 175, 176 and 178 of Reference [36]) are used to compute stress intensity factors at the lug surface and hole wall (Points C and A). During the transition to a through-the-thickness crack, Equations (37) through (40)

are used to compute stress intensity factors at the front and back surface.

A three-dimensional cracked finite element method, although too expensive for general application, has been used to check the accuracy of the one and two-parameter corner crack solutions. Comparisons of stress intensity factors are shown in Figures 3-46 through 3-50 and comparisons of corner crack correction factors are shown in Figure 3-51.

An elastoplastic analysis has been described for use when the peak stress in the uncracked lug exceeds the material tensile yield strength. Using the stress-strain curves of Figure 3-52, an iterative finite element analysis with incremental loading and unloading is used to calculate the stress distributions in the uncracked lug for the maximum and minimum loads of the fatigue cycle. These stress distributions are used with the modified Green's function to estimate K_{max} and K_{min} for a lug with a through-the-thickness crack. Sample results for ΔK have been given in Figures 3-59 and 3-60 and Table 3-13. This nonlinear method is inexact and only an approximation, because strictly speaking the validity of the Green's function method requires linearity between load and stress.

2. SUMMARY OF STRESS INTENSITY FACTORS FOR TAPERED LUGS (SECTION IV)

Section IV covers the calculation of stress intensity factors for tapered attachment lugs subjected to either axial or off-axis loading. Only unbushed lugs with a 45-degree included taper angle are analyzed.

A two-dimensional finite element analysis has been used to calculate the stress distribution in an uncracked lug. For axial loading, the peak tangential stress is located at approximately 90 degrees to the lug axis (Figure 4-5), and the stresses along the 90-degree line are listed in Table 4-1 for five values of R_o/R_i. Equation (45) is an equation for stress concentration factor for axial loading of a tapered lug with a taper angle between 0 and 45 degrees. For off-axis as well as axial loading, the angular locations of peak stresses are given in Figure 4-5.

Stress intensity factors for tapered lugs have been calculated by two-dimensional cracked finite element analysis. Stress intensity factor results

are listed in Table 4-2 for axial tension loading (and plotted in Figure 4-20 for axial compressive loading) of tapered lugs having R_o/R_i ratios from 1.5 to 3.0. Off-axis loading solutions for stress intensity factors are plotted. in Figures 4-22 and 4-23 for a tapered lug with $R_o/R_i = 2.25$, loaded in the -45 and -90 degree directions, with a crack at either of the two most critical locations.

For corner cracks in tapered lugs, the corner crack correction factors presented in Section III can be used in conjunction with the appropriate through-the-thickness stress intensity factors. For problems involving bushings or stresses above the material yield strength, the weighting function would be needed for tapered lugs for each new loading direction and crack orientation. As an approximation, the Green's function for the axially-loaded straight lug with the same R_o/R_i ratio may be used although the accuracy of this approximation is questionable, particularly for off-axis loading.

3. SUMMARY OF FATIGUE CRACK GROWTH ANALYSIS METHODS (SECTION V)

Crack growth analysis methodology has been briefly summarized in Section V. Alternative constant amplitude fatigue crack growth rate equations described include those of Paris [49], Forman [50], and Walker [51]. Alternative spectrum load interaction models summarized are the Wheeler [52], Willenborg [53], Generalized Willenborg [54] and Hsu [55] models. The selection of a rate equation and retardation model is left to the discretion of the analyst who is conducting the crack growth analysis.

REFERENCES

1. Anon., "Airplane Damage Tolerance Requirements, "MIL-A-83444, Air Force Aeronautical Systems Division, July 1974.

2. Schijve, J., and Hoeymakers, A.H.W., "Fatigue Crack Growth in Lugs and the Stress Intensity Factor," Report LR-273, Delft University of Technology, Delft, the Netherlands, July 1978.

3. Wanhill, R.J.H., and Lof, C.F., "Calculation of Stress Intensity Factors for Corner Cracking in a Lug," Fracture Mechanics Design Methodology, ARGARD CP221, February 1977, Paper No. 8.

4. James, L. A., and Anderson, W. E., "A Simple Experimental Procedure for Stress Intensity Factor Calibration," Engineering Fracture Mechanics, Vol. 1, 1969, pp. 565-568.

5. Liu, A. F., and Kan, H. P., "Test and Analysis of Cracked Lug," Fracture 1977, Vol. 3, ICF4, Waterloo, Canada, June 19-24, 1977, pp. 657-664.

6. Kirkby, W. T., and Rooke, D. P., "A Fracture Mechanics Study of Residual Strength of Pin-Lug Specimens," Fracture Mechanics in Engineering Practice, Applied Scientific Publication, London, 1977, p. 339.

7. Cartwright, D. J., and Rooke, D. P., "Approximate Stress Intensity Factors Compounded from Known Solutions," Engineering Fracture Mechanics, Vol. 6, 1974, pp. 563-571.

8. Aberson, J. A., and Anderson, J. M., "Cracked Finite-Elements Proposed for NASTRAN," Third NASTRAN Users' Colloquium, NASA TMX-2893, 1973, pp. 531-550.

9. Pian, T.H.H., Mar, J. W., Orringer, O., and Stalk, G., "Numerical Computation of Stress Intensity Factors for Aircraft Structural Details by the Finite Element Method," AFFDL-TR-76-12, Air Force Flight Dynamics Laboratory, May 1976.

10. Impellizzeri, L. F., and Rich, D. L., "Spectrum Fatigue Crack Growth in Lugs," Fatigue Crack Growth Under Spectrum Loads, ASTM STP 595, 1976, pp. 320-336.

11. Bueckner, H. F., "Weight Functions for the Notched Bar," Zeitschrift fur Angewandte Mathematik und Mechanik, Vol. 51, 1971, pp. 97-109.

12. Hsu, T. M., "Analysis of Cracks at Attachment Lugs," Proceedings of the AIAA/ASME 21st Structures, Structural Dynamics, and Materials Conference, May 12-14, 1980, Seattle, Washington.

13. Hsu, T. M., and Kathiresan, K., "Analysis of Cracks at an Attachment Lug Having an Interference-Fit Bushing," Fracture Mechanics, ASTM STP 791, J.C. Lewis and George Sines, Eds., ASTM, 1982.

14. Brussat, T. R., Chiu, S. T., Rudd, J. L., and Creager, M., "Fatigue Crack Growth in Reinforced Panels with Initial Corner Cracks," Engineering Fracture Mechanics, Vol. 14, No. 4, 1981, pp. 665-683.

15. Tweed, J., and Rooke, D. P., "The Distribution of Stress Near the Tip
    of a Radial Crack at the Edge of a Circular Hole," _International
    Journal of Engineering Sciences_, Vol. 11, 1973, pp. 1185-1195.

16. Brussat, T. R., "Mode I Stress Intensity for a Radial Crack at a Hole
    With Arbitrary Pressure Distribution," _Engineering Fracture Mechanics_,
    Vol. 14, No. 1, 1981, pp. 233-235.

17. Irwin, G. R., "Analysis of Stresses and Strains Near the End of a Crack
    Traversing a Plate," _Trans. ASME: Journal of Applied Mechanics_,
    Vol. 24, 1957, pp. 361-364.

18. Tada, H., Paris, P. C., and Irwin, G. R., "The Stress Analysis of Cracks
    Handbook," Del Research Corporation, Hellertown, Pa., 1973.

19. Isida, M., "Stress Intensity Factors for the Tension of an Eccentrically
    Cracked Strip," _Trans. ASME: Journal of Applied Mechanics_, Vol. 33,
    1966, pp. 674-675.

20. Peterson, R. E., "Stress Concentration Factors," Wiley, New York, 1974.

21. Gross, B., Srawley, J. W., and Brown, W. F., "Stress Intensity Factors
    for a Single-Edge-Notch Tension Specimen by Boundary Collocation of
    a Stress Function," NASA TN D-2395, August 1964.

22. Bueckner, H. F., "A Novel Principle for the Computation of Stress
    Intensity Factors," _Zeitschrift fur Angewandte Mathematik und
    Mechanik_, Vol. 50, 1970, pp. 529-545.

23. Rice, J. R., "Some Remarks on Elastic Crack-Tip Stress Fields," _Inter-
    national Journal of Solids and Structures_, Vol. 8, 1972, pp. 751-
    758.

24. Emery, A. F., Walker, G. E., Jr., and Williams, J. A., "A Green's
    Function for the Stress Intensity Factors of Edge Cracks and Its
    Application to Thermal Stresses," _Journal of Basic Engineering_,
    Vol. 91, 1969, pp. 618-624.

25. Paris, P. C., and Sih, G. C., "Stress Analysis of Cracks," _Fracture
    Toughness Testing and Its Applications_, ASTM STP 381, 1965, pp. 30-
    81.

26. Bueckner, H. F., "The Weight Functions of the Configuration of Collinear
    Cracks," _International Journal of Fracture_, Vol. 11, 1975, pp. 71-
    83.

27. Crews, J. R., and White, N. H., "Fatigue Crack Growth From a Circular
    Hole With and Without High Prior Loading," NASA TN D-6899,
    September 1972.

28. Schmidt, R. A., "An Approximate Technique for Obtaining Stress Intensity
    Factors for Some Difficult Planar Problems," ASME, ASM 13th Annual
    Symposium on Fracture and Flaws, Albuquerque, New Mexico, 1973.

REFERENCES (Continued)

29. Shah, R. C., "Stress Intensity Factors for Through and Part-Through Cracks Originating at Fastener Holes," ASTM STP 590, 1976, pp. 429-459.

30. Grandt, A. F., "Stress Intensity Factors for Some Through-Cracked Fastener Holes," International Journal of Fracture, Vol. 11, 1975, pp. 283-294.

31. Bowie, O. L., "Analysis of an Infinite Plate Containing Radial Cracks Originating from the Boundary of an Internal Circular Hole," Journal of Mathematics and Physics, Vol. 35, 1956, pp. 60-71.

32. Hsu, T. M., and Rudd, J. L., "Green's Function for Thru-Cracks Emanating from Fastener Holes," Proceedings of the Fourth International Conference on Fracture, Vol. 3, Waterloo, Ontario, Canada, June 1977, pp. 139-148.

33. Zienkiewicz, O. C., "The Finite Element Method," Third Edition, McGraw-Hill Book Company (UK) Limited, England, 1977.

34. Rudd, J. L., Hsu, T. M. and Aberson, J. A., "Analysis and Correlation of Crack Growth from Interference-Fit Fastener Holes," Numerical Methods in Fracture Mechanics, Proceedings of the First International Conference held at University College of Swansea, West Glamorgan, U. K., January 9-13, 1980.

35. Seely, F. B., and Smith, J. O., Advanced Mechanics of Materials, Second Edition, John Wiley and Sons, Inc., New York, December 1960.

36. Hsu, T. M., McGee, W. M., and Aberson, J. A., "Extended Study of Flaw Growth at Fastener Holes," AFFDL-TR-77-83, Air Force Flight Dynamics Laboratory, April 1978.

37. Collipriest, J. E., Jr., and Ehret, R. M., "Computer Modeling of Part-Through Crack Growth," SD 72-CE-0915B, Space Division, Rockwell International Corporation, Downey, California, October 1973.

38. Fujimoto, W. T., "Determination of Crack Growth and Fracture Toughness Parameters for Surface Flaws Emanating from Fastener Holes, Proceedings of AIAA/ASME/SAE 17th Structures,Structural Dynamics, and Materials Conference, King of Prussia, Pennsylvania, May 5-7, 1976.

39. Tracey, D. M., "3-D Elastic Singular Element for Evaluation of K Along an Arbitrary Crack Front," International Journal of Fracture, Vol. 9, 1973.

40. Cruse, T. A., and Meyers, C. J., "Three-Dimensional Fracture Mechanics Analysis," Journal of the Structural Division, Transactions of ASCE, February 1977.

41. Smith, F. W., and Kullgren, T. E., "Theoretical and Experimental Analysis of Surface Cracks Emanating from Fastener Holes," AFFDL-TR-75-104, Air Force Flight Dynamics Laboratory, February 1977.

REFERENCES (Continued)

42. Kathiresan, K., "Three-Dimensional Linear Elastic Fracture Mechanics Analysis By a Displacement Hybrid Finite Element Model," Ph.D. Dissertation, Georgia Institute of Technology, Atlanta, Georgia, September 1976.

43. Atluri, S. N., and Kathiresan, K., "Stress Analysis of Typical Flaws in Aerospace Structural Component Using 3-D Hybrid Displacement Finite Element Method," Proceedings of the AIAA/ASME 19th Structures, Structural Dynamics and Materials Conference, Bethesda, Maryland, April 1978, pp. 340-350.

44. Atluri, S. N., and Kathiresan, K., "Stress Intensity Factor Solutions for Arbitrarily Shaped Surface Flaws in Reactor Pressure Vessel Nozzle Corners," The International Journal of Pressure Vessels and Piping, Vol. 8, No. 4, July-August 1980, pp. 313-322.

45. Atluri, S. N., et al, "Hybrid Finite Element Models for Linear and Non-linear Analysis," Proceedings of the International Conference on Numerical Methods in Fracture, Swansea, England, January 1978, pp. 52-66.

46. Raju, I. S., and Newman, J. C., Jr., "Improved Stress-Intensity Factors fr Semi-Elliptical Surface Cracks in Finite Thickness Plates," T   ictions of the 4th International Conference on Structural Mecnanics in Reactor Technology, San Francisco, California, August 1977, Paper No. G-5/8.

47. Larsson, Nils, "Fatigue Testing of Transversely Loaded Aluminum Lugs," Technical Note FFA HU-1673, the Aeronautical Research Institute of Sweden, Stockholm, Sweden, October 1977.

48. Larsson, Nils, "Fatigue of Transversely Loaded Aluminum Lugs, Sequence II," Technical Note FFA HU-1848, the Aeronautical Research Institute of Sweden, Stockholm, Sweden, April 1978.

49. Paris, P. C., and Erdogan, F., "A Critical Analysis of Crack Propagation Laws," Journal of Basic Engineering, December 1963, pp. 528-534.

50. Forman, R. G., Kearney, V. E., and Engle, R. M., "Numerical Analysis of Crack Propagation in Cyclic Loaded Structures," Journal of Basic Engineering, September 1967, pp. 459-464.

51. Walker, K., "The Effect of Stress Ratio During Crack Propagation and Fatigue for 2024-T3 and 7075-T6 Aluminum," ASTM STP 462, 1970, p. 1

52. Wheeler, O. E., "Crack Growth Under Spectrum Loading," Journal of Basic Engineering, March 1972, pp. 181-186.

53. Willenborg, J., Engle, R. M., and Wood, H. A., "A Crack Growth Retardation Model Using an Effective Stress Concept," AFFDL-TM-71-1-FBR, Air Force Flight Dynamics Laboratory, January 1971.

54.   Gallagher, J. P., and Hughes, T. F., "Influence of Yield Strength on
      Overload Affected Fatigue Crack Growth Behavior in 4340 Steel,"
      AFFDL-TR-74-27, Air Force Flight Dynamics Laboratory, July 1974.

55.   Hsu, T. M., "Development of Load-Interaction Model," Lockheed-Georgia
      Report SMN 390, February 1976.

56.   Roberts, R., and Erdogan, F., "The Effect of Mean Stress on Fatigue
      Crack Propagation in Plates Under Extension and Bending,"
      Journal of Basic Engineering, 1967, p. 885.

57.   Kathiresan, K., and Brussat, T. R., "User's Manual for 'LUGRO' Computer
      Program to Predict Crack Growth in Attachment Lugs", AFWAL-TR-84-3080,
      Vol. VI, Air Force Wright Aeronautical Laboratories, September 1984.

58.   Shah, R.C., and Kobayashi, A.S., "On the Surface Flaw Problem," The
      Surface Crack: Physical Problems and Computational Solutions,
      Proceedings of the Winter Annual Meeting, ASME, NY, November 1972,
      pp. 79-124.

APPENDIX A

MODE I STRESS INTENSITY FORMULAS
RELATED TO CRACKED LUGS

LINE CRACKS IN DOUBLY INFINITE PLATES

CASE 11. Uniform Tensile Stress
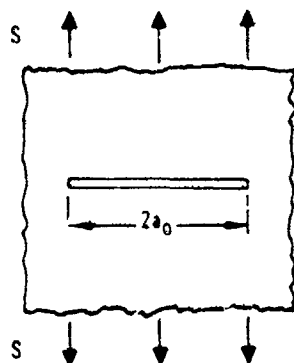
$$K_{11} = S\sqrt{\pi a_0}$$

Numerical Example: $S = 1$, $a_0 = 3$: $K_{11} = 3.06998$

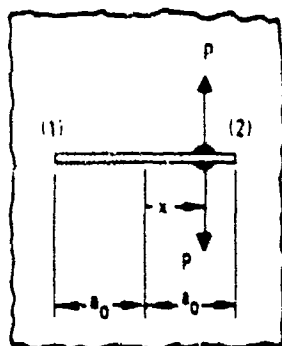CASE 12. Central Splitting Forces on Crack Surfaces
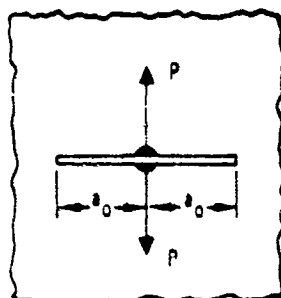
$$K_{12} = \frac{P}{t\sqrt{\pi a_0}}$$

where $t =$ thickness

Numerical Example: $a_0 = 3$, $P = 1$, $t = 0.6$: $K_{12} = 0.54289$

CASE 13. Arbitrary Splitting Forces on Crack Surfaces

$$K_{13}^{(1)} = K_{12}\sqrt{\frac{a_0 - x}{a_0 + x}}$$

$$K_{13}^{(2)} = K_{12}\sqrt{\frac{a_0 + x}{a_0 - x}}$$

NOTE. x is negative if force is applied closer to crack tip (1).

Numerical Example: $a_0 = 3$, $x = 1$, $P = 1$, $t = 0.6$: $K_{13}^{(1)} = 0.76776$, $K_{13}^{(2)} = 0.38388$

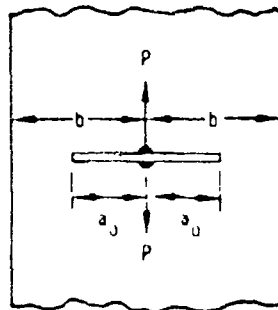CASE 21. Symmetric Crack, Uniform Tension
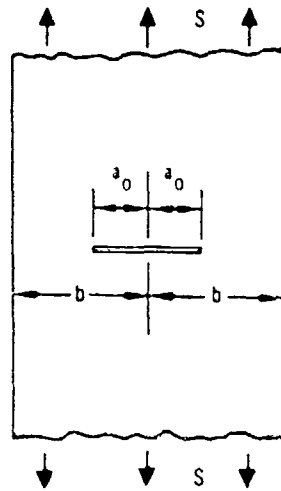
$$K_{21} = K_{11} \, \Phi_{21}\left(\frac{\pi a_0}{2b}\right)$$

$$\Phi_{21}(\lambda_0) = \sqrt{\sec(\lambda_0)}$$

Numerical Example.

$a_0 = 3, b = 8, S = 1. \quad K_{21} = 3.3668$

CASE 22. Symmetric Crack. Central Splitting Forces on Crack Surfaces

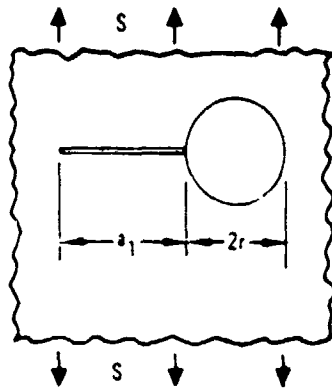$$K_{22} = K_{12} \, \Phi_{21}\left(\frac{\pi a_0}{2b}\right) u_{22}\left(\frac{\pi a_0}{2b}\right)$$

$$u_{22}(\lambda_0) = \frac{\lambda_0}{\sin(\lambda_0)}$$

Numerical Example

$a_0 = 3, b = 8, P = 1, t = 0.6 \quad K_{22} = 0.63125$

173

CASE 31. Single Crack, Tension Normal to Crack
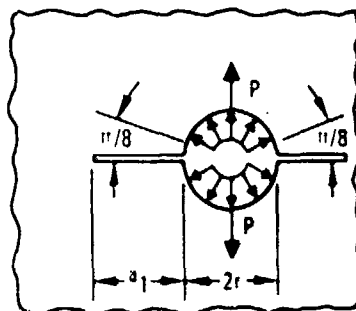

$$K_{31} = S\sqrt{\pi a_1}\, u_{31}\left(\frac{a_1}{a_1 + r}\right)$$

$$u_{31}(\rho_1) = \exp\left(1.2133 - 2.205\,\rho_1 + 0.6451\,\rho_1^2\right)$$

Numerical Example:

$a_1 = 2, r = 1, S = 1: K_{31} = 2.583$

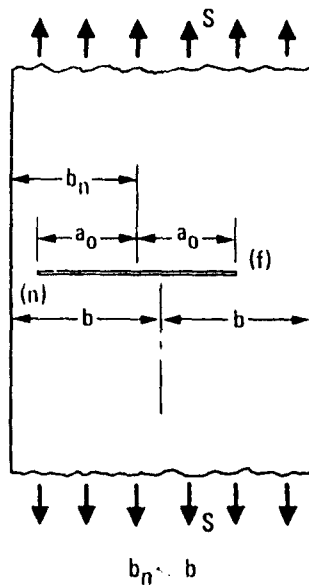CASE 35. Single Crack, Distributed Splitting Forces at Hole

$$K_{35} = K_{13}^{(1)}\,\Phi_{31}(\rho_1)\,u_{35}(\rho_1)$$

$$u_{35}(\rho_1) = \exp\left[0.15\,(\rho_1^2 - 1)\right]$$

$$x = a_1/2, a_0 = r + x$$

Limitation: Total load P results from uniform radial pressure from $\pi/8$ to $7\pi/8$ and $-\pi/8$ to $-7\pi/8$. (K drops drastically if pressure is applied between $-\pi/8$ and $\pi/8$).

174

CASE 26. Unsymmetric Crack, Uniform Tension ($b_n \leq b_f$)

At (f): $K_{26}^{(f)} = K_{11} \Phi_{26}^{(f)} \left(\lambda_f, \lambda_n \right)$

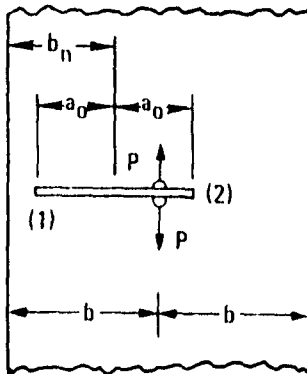At (n): $K_{26}^{(n)} = K_{11} \Phi_{26}^{(n)} \left(\lambda_f, \lambda_n \right)$

$$\Phi_{26}^{(f)} = 1 + \left[\frac{\sqrt{\sec(\lambda_{nf})} - 1}{1 + 0.21 \sin\left\{ 8 \arctan\left[\left(\dfrac{\lambda_n - \lambda_f}{\lambda_n + \lambda_f} \right)^{0.9} \right] \right\}} \right]$$

$$\Phi_{26}^{(n)} = \left[u_{26} + \left(\frac{1 - u_{26}}{4} \right) \left(1 + \frac{1}{4\sqrt{\sec \lambda_n}} \right)^2 \right] \sqrt{\sec \lambda_n}$$

$$u_{26} = \sin\left[\frac{\pi \lambda_f}{\lambda_n + \lambda_f} \right]$$

$$\lambda_f = \frac{\pi a_0}{4b - 2b_n} \qquad \lambda_n = \frac{\pi a_0}{2b_n} \qquad \lambda_{nf} = \frac{4}{7}\lambda_n + \frac{3}{7}\lambda_f$$

CASE 27. Unsymmetric Crack, Central Splitting Forces on Crack Surfaces

$$K_{27}^{(1)} = K_{13}^{(1)} \Phi_{26}^{(n)} (\lambda_f, \lambda_n) \, u_{22} (\lambda_n)$$

$$K_{27}^{(2)} = K_{13}^{(2)} \Phi_{26}^{(f)} (\lambda_f, \lambda_n) \, u_{22} (\lambda_{nf})$$
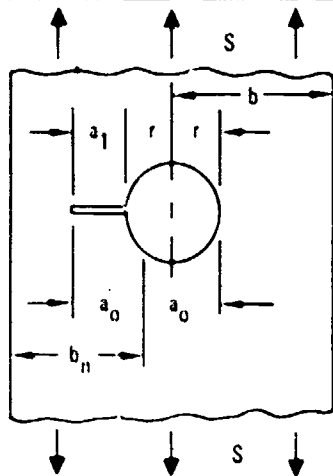
$x = b - b_n$

Combining of Cases 12, 13, 21 22 and 26.

$$u_\nu = \begin{cases} 1 + \nu & : \text{P. Stress} \\ 1/(1-\nu) & : \text{P. Strain} \end{cases}$$

CASE 41. Single Crack, Uniform Tension

$$K_{41} = K_{31} \, \Phi_{26}^{(n)} \, (\lambda_f, \lambda_n) \, \Phi_{21} \, (\lambda_r)$$

$b_n = b - \dfrac{a_1}{2}$	Combining of Cases 11, 21, 26 and 31
$a_0 = r + \dfrac{a_1}{2}$	
$b_f = b + \dfrac{a_1}{2}$	

CASE 44. Single Crack, Distributed Splitting Forces at Hole
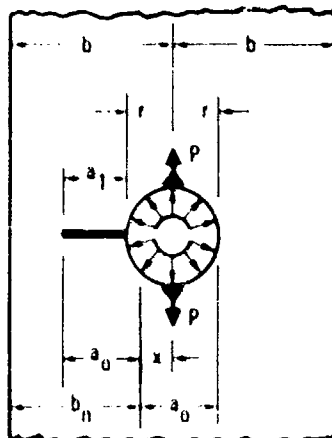
$$K_{44} = K_{27}^{(1)} \, \Phi_{31}(\rho_1) \, \Phi_{21}(\lambda_r) \, u_{35}(\rho_1)$$

Limitation: Same load distribution as Case 35.	Combining of Cases 13, 21, 27, 31 and 35

Dependent Variables:

$x = a_1/2$, $b_n = b - x$ and $a_0 = r + a_1/2$

CASE 71. Quarter-Circular Corner Crack Which Becomes Through-Thickness

Section B-B
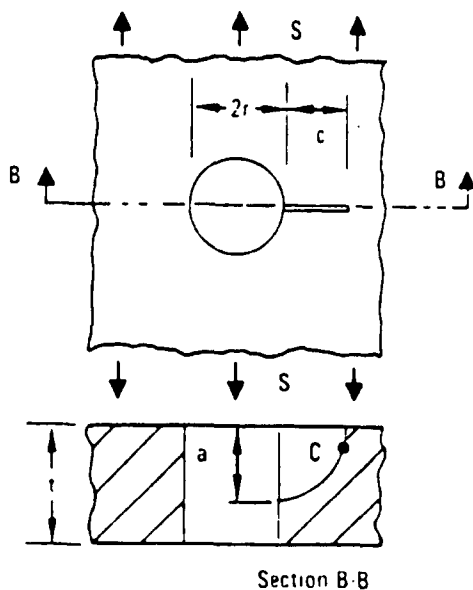
$$K_{71}^{(C)} = S\sqrt{\pi c} \; u_{31}\left(\frac{c}{c+r}\right)\Phi_{71}^{(C)}$$

$$\Phi_{71}^{(C)} = 1.0 - \frac{0.2886}{1 + 2\,(a_{/t})^2}$$

NOTE: For cracks beginning as quarter-circular corner cracks in configurations 32 through 70, multiply the through-crack solution by $\Phi_{71}^{(C)}$

Limitations:
  No plate bending
  a = c

Numerical Example
  $a = c = 2$, $r = 1$, $t = 3$, $S = 1$: $K_{71}^{(C)} = 2.18834$